

UNCLASSIFIED



ODTÜ Very Light Aircraft Project Preliminary Design Report

ABSTRACT: This report covers the conceptual and preliminary design and trade-off studies of VLA project.

AUTHOR(s): ODTÜ VLA TEAM

APPROVER(s): [Manager]

AUTHORIZER(s): [Status]

PUBLISH DATE: [Publish Date]

This page intentionally left blank.

UNCLASSIFIED

UNCLASSIFIED

UNCLASSIFIED

UNCLASSIFIED

APPROVAL & AUTHORIZATION of CHAPTER 1

Responsible	Name-Title	Date	Sign
Author	ODTÜ VLA TEAM		
Contributor	Ömer Tunahan Liman		
Contributor	Veysel Burhan		
Contributor	Rüştü Görkem Yılmaz		
Contributor	Mustafa Özdemir		
Contributor	Kaan Yenipazar		
Contributor	Berk Sarıkaya		
Contributor	Murat Alper Sayıcı		
Contributor	Fatma Çağla Dağ		
Contributor	Mert Ali Andırın		
Contributor	Özgür Zafer		
Contributor	Nilay Kirci		
Contributor	Sima Demir		
Contributor	Eren Dönertaş		
Contributor	Alaaddin Furkan Uzunkaya		
Contributor	Murat Yıldırım		
Contributor	Hüseyin Coskun		
Contributor	Onur Ali Batmaz		
Contributor	Eren Çalış		

UNCLASSIFIED

UNCLASSIFIED

Contributor	Selçuk Güzel		
Contributor	Alper Faruk Yiğit		
Contributor	Güngör Yurttav		
Contributor	Sefa Tak		
Contributor	Metehan Akinci		
Contributor	Uğur Polat		
Contributor	Hakan Doğan		
Contributor	Utku Zengin		
Contributor	Furkan Kaynar		
Contributor	Cem Semerci		
Contributor	Mehmet Şahin		
Contributor	Mert Ozan Taş		
Contributor	Haktan Bozkurt		
Contributor	Salih Toker		
Contributor	Ata Urun		
Contributor	Çağlar Sevinç		
Contributor	Batur Zafer		
Contributor	Hasan Gençarslan		
Contributor	Mehmet Kepenekçi		
Contributor	Mehmet Canpolat		

UNCLASSIFIED

UNCLASSIFIED

Contributor	Can Erdogan		
Approver	[Manager]		
Authorizer	[Status]		

Table 3.1-1 Approval & Authorization

UNCLASSIFIED

UNCLASSIFIED

DOCUMENT ID

Document No	XXXXXXXXXX
Document Title	Preliminary Design Report
Project Name	ODTÜ Very Light Aircraft Project
Document Type	PP
Issue	1
Version	1
Keywords	An index term, subject term, subject heading, or descriptor, in information retrieval, is a term that captures the essence of the topic of a document.
Baseline	N/A.
CDRL/SVİL NO (if have)	N/A.
Publish Date	[Publish Date]
Abstract	This report covers the conceptual and preliminary design and trade-off studies of VLA project.
Applicability	Applicability describes the Model(s) or the Type Version(s) this document is applicable or can/shall/must be applied to.

Table 3.1-2 Document Id

DOCUMENT ID (PROJECT)

ATA	N/A.
SUB ATA	N/A.
System	N/A.
Other System (impacted)	N/A.
Target Milestone	N/A.

Table 3.1-1 Document Id (Project)

UNCLASSIFIED

UNCLASSIFIED

CONTENTS

<u>APPROVAL & AUTHORIZATION of CHAPTER 1</u>	3
<u>DOCUMENT ID (PROJECT)</u>	6
<u>CONTENTS</u>	7
<u>TABLES</u>	14
<u>FIGURES</u>	15
<u>1. PURPOSE</u>	19
<u>2. SCOPE</u>	19
<u>3. CONCEPTUAL DESIGN STUDIES</u>	19
<u> 3.1. Air Vehicle</u>	19
<u> 3.1.1. Aerodynamics</u>	19
<u> 3.1.1.1. Airfoil Selection</u>	19
<u> 3.1.1.1.1. Literature Research and First Elimination Stage</u>	19
<u> 3.1.1.1.2. 2D Analysis and Second Elimination Stage</u>	20
<u> 3.1.1.1.3. 2D Analysis and Third Elimination Stage</u>	25
<u> 3.1.1.1.4. Detailed Analysis of SD7062 Airfoil</u>	27
<u> 3.1.1.2. Flap Configuration Selection</u>	44
<u> 3.1.1.2.1. Literature Research</u>	44
<u> 3.1.1.2.2. 2D Analysis and Flap Configuration Selection</u>	45
<u> 3.1.1.2.3. Set up and Results</u>	48
<u> 3.1.1.3. Wing Analysis</u>	56
<u> 3.1.1.3.1. Cruise Condition</u>	56
<u> 3.1.1.3.2. Takeoff and Landing Conditions</u>	60
<u> 3.1.2. Flight Mechanics</u>	64
<u> 3.1.2.1. Design Requirements</u>	65
<u> 3.1.2.1.1. Weight Fraction</u>	65
<u> 3.1.2.1.2. Sizing</u>	70
<u> 3.1.2.1.3. Design of Control Surfaces</u>	88
<u> 3.1.3. Performance</u>	93
<u> 3.1.3.1. Inertia Calculations</u>	93
<u> 3.1.3.2. Performance Calculations</u>	94
<u> 3.1.3.3. DATCOM Method</u>	94
<u> 3.1.3.4. Performance Parameters</u>	96
<u> 3.1.4. Loads</u>	97
<u> 3.1.4.1. PURPOSE</u>	97
<u> 3.1.4.2. APPLICABILITY</u>	97
<u> 3.1.4.3. NOMENCLATURE</u>	97
<u> 3.1.4.4. GENERAL</u>	97
<u> 3.1.4.4.1. Flight Envelope</u>	98

UNCLASSIFIED

UNCLASSIFIED

3.1.4.5.	CRITICAL LOADS ANALYSIS	100
3.1.4.5.1.	WING	100
3.1.4.5.2.	HORIZONTAL TAIL	113
3.1.4.5.3.	VERTICAL TAIL	116
3.1.5.	Weight and Balance	120
3.1.5.1.	PURPOSE	120
3.1.5.2.	NOMENCLATURE	120
3.1.5.3.	DEFINITIONS	121
3.1.5.4.	INPUTS	123
3.1.5.5.	WEIGHT BREAKDOWNS	125
3.1.5.6.	C.G. CALCULATIONS	126
3.1.5.7.	REFERENCES	129
3.1.6.	Cockpit Design & Human Factor	131
3.1.6.1.	INTRODUCTION	131
3.1.6.2.	CHAPTER 1:	132
3.1.6.3.	CHAPTER 2	133
3.1.6.4.	CHAPTER 3	135
3.1.6.5.	CHAPTER 4	137
3.1.6.6.	APPENDIX	137
3.2.	Airframe	138
3.2.1.	Structural Design	138
3.2.1.1.	Fuselage Configuration	138
3.2.1.1.1.	Tuss type construction	138
3.2.1.1.2.	Monocoque type construction	139
3.2.1.1.3.	Semi-monocoque type construction	140
3.2.1.2.	Competitors' Fuselage Configuration	141
3.2.1.3.	Configuration Choice	142
3.2.1.4.	REFERENCES	143
3.2.1.5.	TYPICAL CONFIGURATIONS OF A VLA TAIL	143
3.2.1.5.1.	Conventional Tail Configuration	143
3.2.1.5.2.	Horizontal Tail	143
3.2.1.5.3.	Vertical Tail	145
3.2.1.5.4.	T-Tail Configuration	145
3.3.	Propulsion & Fuel Systems	146
3.3.1.	Propulsion	146
3.3.1.1.	Introduction	146
3.3.1.2.	Discussion	147
3.3.1.2.1.	Engine	147
3.3.1.3.	Propeller	157

UNCLASSIFIED

UNCLASSIFIED

3.3.1.4.	Conclusion	0
3.3.1.5.	References	1
3.3.2.	Fuel System	2
3.3.2.1.1.	Chapter 1: Fuel Tank Trade-Off Study.....	2
3.3.2.1.2.	Fuel Tank Type Selection.....	3
3.3.2.1.3.	Fuel Tank Locations	4
3.3.2.1.4.	Fuel Tank Location Selection.....	4
3.3.2.1.5.	Result of Fuel Tank Trade-Off Study	5
3.3.2.2.	Chapter 2: Conceptual Fuel System Architecture	6
3.3.2.2.1.	Fuel System Schematic.....	6
3.3.2.2.2.	Fuel System Description.....	7
3.3.2.2.3.	Fuel System Components.....	7
3.3.2.3.	CONCLUSION.....	10
3.3.2.4.	REFERENCES	11
3.4.	Air Vehicle Systems	11
3.4.1.	Flight Control.....	11
3.4.1.1.	Purpose	11
3.4.1.2.	Trade-Off Study	11
3.4.1.2.1.	Cable-Push Rod Selection	11
3.4.1.2.2.	Primary Control Mechanisms.....	12
3.4.1.2.3.	Secondary Control Mechanisms	12
3.4.1.3.	Conceptual Designs	13
3.4.1.3.1.	Primary Control Mechanisms.....	13
3.4.1.4.	Conceptual Design Assembly	15
3.4.2.	Landing Gear System.....	16
3.4.2.1.	Fork Design.....	16
3.4.2.2.	Main Landing.....	17
3.4.2.3.	Sample Drawing and Procedure of Design.....	18
3.5.	Avionics, Missions & Electrical System	19
3.5.1.	Avionics and BFI	19
3.5.1.1.	Choosing the Avionics	19
3.5.1.2.	Avionics	22
3.5.1.2.1.	Garmin G500 TXI	22
3.5.1.2.2.	Garmin GTN750	25
3.5.1.2.3.	Garmin GMA345	26
3.5.1.2.4.	Garmin GTX345	26
3.5.1.2.5.	Garmin G5	26
3.5.1.3.	Proposed Avionic Architecture	27
3.5.2.	Choosing the Necessary Lighting Equipments	31

UNCLASSIFIED

UNCLASSIFIED

3.5.3. Preliminary Electrical Architecture	32
4. APPENDIX (AERODYNAMICS, FLIGHT MECHANICS, FLIGHT PERFORMANCE)	33
 4.1. APPENDIX A	33
 4.2. APPENDIX B	34
 4.3. APPENDIX C	35
 4.4. APPENDIX D	35
 4.5. APPENDIX E	36
 4.6. APPENDIX F	36
 4.7. APPENDIX G	37
 4.8. APPENDIX H	38
 4.9. APPENDIX I	38
 4.10. APPENDIX J	38
 4.11. APPENDIX K	39
 4.12. APPENDIX L	41
 4.13. APPENDIX M	42
 4.14. APPENDIX N	43
5. APPENDIX (LOADS)	44
 5.1. APPENDIX A– HORIZONTAL TAIL SHEAR AND MOMENT DIAGRAMS FOR EACH CRITICAL CASE	44
 5.2. APPENDIX B – VERTICAL TAIL SHEAR AND MOMENT DIAGRAMS FOR EACH CRITICAL CASE	49

APPROVAL & AUTHORIZATION of CHAPTER 1 _____ 3

UNCLASSIFIED

UNCLASSIFIED

TABLES

Table 3.1-1 Approval & Authorization	5
Table 3.1-2 Document Id.....	6
Table 3.1-1 Document Id (Project).....	6
Table 3.1-1. Grid refinement with NACA4415 values at 5 degrees AOA	<u>Hatalı Yer işareteti tanımlanmamış.</u> ¹⁸
Table 3.1-2. Grid refinement with Rhodes St. Genesee 32 Airfoil with slotted flaps deflected 15 degrees at 5 degrees AOA	<u>Hata!</u> <u>Yer işareteti tanımlanmamış.</u> ⁴⁵
Table 3.1-3. Coefficients of the wing at 3 degrees of angle of attack.....	<u>Hatalı Yer işareteti tanımlanmamış.</u> ⁵⁷
Table 3.1-4. Coefficients and generated force of the half wing at 13 degrees of angle of attack with 10 degrees of flap deflection	<u>Hatalı Yer işareteti tanımlanmamış.</u> ⁵⁹
Table 3.1-5. Coefficients and generated force of the half wing at 13 degrees of angle of attack with 13 degrees of flap deflection	<u>Hatalı Yer işareteti tanımlanmamış.</u> ⁶⁰
Table 3.1-6. Propeller Specific Fuel Consumption	<u>Hatalı Yer işareteti tanımlanmamış.</u> ⁶⁴
Table 3.1-7. Lift to Drag Ratio for Different Missions	<u>Hatalı Yer işareteti tanımlanmamış.</u> ⁶⁵
Table 3.1-8. Weight fraction Outputs	<u>Hatalı Yer işareteti tanımlanmamış.</u> ⁶⁶
Table 3.1-9. Altitude – Power required trade off	<u>Hatalı Yer işareteti tanımlanmamış.</u> ⁶⁶
Table 3.1-10. Air Specifications at Cruise Altitude.....	<u>Hatalı Yer işareteti tanımlanmamış.</u> ⁶⁸
Table 3.1-11. Range and Endurance Formulas for Different Conditions	<u>Hatalı Yer işareteti tanımlanmamış.</u> ⁷²
Table 3.1-12. Outputs Of Performance Parameter.....	<u>Hatalı Yer işareteti tanımlanmamış.</u> ⁷²
Table 3.1-13. Wing Loadings for different conditions.....	<u>Hatalı Yer işareteti tanımlanmamış.</u> ⁷⁴
Table 3.1-14. Equivalent Skin Friction Coefficient	<u>Hatalı Yer işareteti tanımlanmamış.</u> ⁷⁴
Table 3.1-15. DATCOM 3D Wing Analysis	<u>Hatalı Yer işareteti tanımlanmamış.</u> ⁸¹
Table 3.1-16. 3D Wing Outputs From Different Software	<u>Hatalı Yer işareteti tanımlanmamış.</u> ⁸¹
Table 3.1-17. Fuselage Length vs W_0.....	<u>Hatalı Yer işareteti tanımlanmamış.</u> ⁸¹
Table 3.1-18. Tail Volume Coefficient	<u>Hatalı Yer işareteti tanımlanmamış.</u> ⁸²
Table 3.1-19. Tail Aspect Ratio and Taper Ratio	<u>Hatalı Yer işareteti tanımlanmamış.</u> ⁸²
Table 3.1-20. Geometric Outputs	<u>Hatalı Yer işareteti tanımlanmamış.</u> ⁸³
Table 3.1-21. Geometric Outputs in Both Units.....	<u>Hatalı Yer işareteti tanımlanmamış.</u> ⁸³
Table 3.1-22. Performance Output From Design Process.....	<u>Hatalı Yer işareteti tanımlanmamış.</u> ⁸⁴
Table 3.1-23. Definition of Fundamental Terms	<u>Hatalı Yer işareteti tanımlanmamış.</u> ⁸⁵
Table 3.1-24. Typical Values for Geometry of Control Surfaces	<u>Hatalı Yer işareteti tanımlanmamış.</u> ⁸⁶
Table 3.1-25. Aircraft Classes	<u>Hatalı Yer işareteti tanımlanmamış.</u> ⁸⁶
Table 3.1-26. Flight Phase Categories	<u>Hatalı Yer işareteti tanımlanmamış.</u> ⁸⁷
Table 3.1-27. Level of Acceptability	<u>Hatalı Yer işareteti tanımlanmamış.</u> ⁸⁷
Table 3.1-28. Level Of Acceptability And Pilot Comfort.....	<u>Hatalı Yer işareteti tanımlanmamış.</u> ⁸⁷
Table 3.1-29. Control Surface Sizes.....	<u>Hatalı Yer işareteti tanımlanmamış.</u> ⁸⁹
Table 3.1-30. Main Properties of the Aircraft used in the Analyses	<u>Hatalı Yer işareteti tanımlanmamış.</u> ⁹⁴
Table 3.1-32. Critical Load Cases for the Wing	<u>102</u> ⁹⁸
Table 3.1-33. Case 122 – STALL +N	<u>103</u> ⁹⁹
Table 3.1-34. Case 205 – MAN D.....	<u>104</u> ¹⁰⁰
Table 3.1-35. Case 130 – GUST +C	<u>105</u> ¹⁰¹
Table 3.1-36. Case 153 – GUST -C	<u>106</u> ¹⁰²
Table 3.1-37. Case 220 – AC ROLL	<u>107</u> ¹⁰³
Table 3.1-38. Case 18 – ST ROL C	<u>108</u> ¹⁰⁴
Table 3.1-39. Shear Forces [N] at Spanwise Locations.....	<u>120</u> ¹¹⁶
Table 3.1-40. Moments [Nm] at Spanwise Locations	<u>120</u> ¹¹⁶
Table 3.1-41: Iterated Input Values for Empirical Weight Methods	<u>124</u> ¹²⁰
Table 3.1-42: Weight Breakdown of the Components and Subsystems of the VLA	<u>125</u> ¹²¹
Table 3.1-43: Historical Components' Weight Ratio to MTOW	<u>125</u> ¹²¹
Table 3.1-44: Most Forward C.G.	<u>126</u> ¹²²
Table 3.1-45: Most Aft C.G.	<u>127</u> ¹²²
Table 3.1-46: C.G without fuel	<u>128</u> ¹²⁴
Table 3.2-1. Competitors' fuselage configuration type	<u>141</u> ¹³⁷
Table 3.2-2. Percentage of competitors' fuselage configuration type	<u>141</u> ¹³⁷

UNCLASSIFIED

UNCLASSIFIED

Table 3.3-1 Competitors and their engines	148 144
Table 3.3-2 Candidate Engines and Fuel Consumption Data and Grading.....	152 148
Table 3.3-3 The table is put to show the comments about the selected five engines compared to each other.....	154 150
Table 3.3-4 Bill of Materials.....	155 151
Table 3.3-5 Showing Trade-off for Number of Blades.....	157 153
Table 3.3-6 Trade-off for Pitch mechanism	159 155
Table 3.3-7 Material trade-off.....	160 156
Table 3.3-8 Candidate Propellers.....	163 159
Table 3.3-9. Fuel Tank Type Trade-Off Study.....	3
Table 3.3-10. Fuel Tank Location Trade-Off Study.....	5
Table 3.5-1 Corresponding Requirements for Avionics	33 22

FIGURES

Figure 3.1-1. Fluid domain with airfoil geometry created in ICEM CFD.....	20 16
Figure 3.1-2. 2D structured meshed domain	21 17
Figure 3.1-3. 2D structured mesh around the airfoil	21 17
Figure 3.1-4. Experimental Values of NACA4415 Airfoil	22 18
Figure 3.1-5. Change of Cl Values of thirteen airfoils with respect to angle of attack.....	23 19
Figure 3.1-6. Change of Cd Values of thirteen airfoils with respect to angle of attack	23 19
Figure 3.1-7. Change of Cm Values around c/4 of thirteen airfoils with respect to angle of attack.....	24 20
Figure 3.1-8. NACA4415.....	24 20
Figure 3.1-9. GOE 387	24 20
Figure 3.1-10. Rhodes St. Genesee 32	24 20
Figure 3.1-11. SD 7062	25 21
Figure 3.1-12. Change of Cl values of four airfoils with respect to AOA and zero lift AOA.....	25 21
Figure 3.1-13. Change of Cd values of four airfoils with respect to AOA.....	25 21
Figure 3.1-14. Change of Cm values of four airfoils with respect to AOA.....	26 22
Figure 3.1-15. Rhodes St. Genese 32 with %12 Thickness	26 22
Figure 3.1-16. SD 7062 with %14 thickness	26 22
Figure 3.1-17. Structured mesh for SD7062 with blunt TE	28 24
Figure 3.1-18. Close-up of the structured mesh with blunt TE	28 25
Figure 3.1-19. Structured mesh for SD7062 with sharp TE.....	29 25
Figure 3.1-20. Close-up of the structured mesh with sharp TE	29 26
Figure 3.1-21. The figure above shows the lift coefficient predictions of XFOIL, SU2 and Fluent for various angles of attack.....	30 26
Figure 3.1-22. The figure above shows the lift coefficient predictions of XFOIL, SU2 and Fluent for various angles of attack.....	30 27
Figure 3.1-23. The figure above shows the moment coefficient predictions of XFOIL, SU2 and Fluent for various angles of attack.	31 27
Figure 3.1-24. The figure above shows the lift coefficient vs. drag coefficient predictions of XFOIL, SU2 and Fluent for various angles of attack.....	32 28
Figure 3.1-25. The figure above shows the lift coefficient divided by drag coefficient predictions of XFOIL, SU2 and Fluent for various angles of attack.....	32 28
Figure 3.1-26. The figure above shows the lift coefficient to the power 3/2 over drag coefficient predictions of XFOIL, SU2 and Fluent for various angles of attack.....	33 29
Figure 3.1-27. The figure above shows the lift coefficient predictions of SU2 for both sharp and blunt trailing edges	34 30
Figure 3.1-28. The figure above shows the drag coefficient predictions of SU2 for both sharp and blunt trailing edges	34 30
Figure 3.1-29. Lift coefficient over drag coefficient vs. angle of attack and lift coefficient versus drag coefficient plots, predicted by SU2.....	35 31
Figure 3.1-30. Pitching moment coefficient vs. angle of attack plot, predicted by SU2.....	35 31
Figure 3.1-31. The figure above shows lift coefficient predictions of SU2 and Fluent, both with sharp TE	36 32
Figure 3.1-32. The figure above shows drag coefficient predictions of SU2 and Fluent, both with sharp TE	36 32
Figure 3.1-33. The figure above shows lift coefficient divided by drag coefficient predictions of SU2 and Fluent, both with sharp TE	37 33
Figure 3.1-34. The figure above shows moment coefficient predictions of SU2 and Fluent, both with sharp TE	37 33
Figure 3.1-35. The figure above shows the lift coefficient versus drag coefficient values predicted by SU2 and Fluent.....	38 34
Figure 3.1-36. Contours of pressure coefficient for SD7062 at 3 degrees of angle of attack.....	38 34
Figure 3.1-37. Contours of Mach number for SD7062 at 3 degrees of angle of attack	39 35

UNCLASSIFIED

UNCLASSIFIED

Figure 3.1-38. Contours of pressure coefficient for SD7062 at 6 degrees of angle of attack.....	3935
Figure 3.1-39. Contours of Mach number for SD7062 at 6 degrees of angle of attack.....	4036
Figure 3.1-40. Contours of pressure coefficient for SD7062 at 9 degrees of angle of attack.....	4036
Figure 3.1-41. Contours of Mach number for SD7062 at 9 degrees of angle of attack.....	4137
Figure 3.1-42. Contours of pressure coefficient for SD7062 at 12 degrees of angle of attack.....	4137
Figure 3.1-43. Contours of Mach number for SD7062 at 12 degrees of angle of attack.....	4238
Figure 3.1-44. Contours of pressure coefficient for SD7062 at 15 degrees of angle of attack.....	4238
Figure 3.1-45. Contours of Mach number for SD7062 at 15 degrees of angle of attack.....	4339
Figure 3.1-46. Streamlines and separation bubble for SD7062 at 15 degrees of angle of attack.....	4339
Figure 3.1-47. Velocity profile near trailing edge between 0.55c and 0.75c.....	4440
Figure 3.1-48. General Aviation Aircrafts and Flap Types used	4440
Figure 3.1-49. Airflow around an airfoil with Plain Flaps and Slotted Flaps	4541
Figure 3.1-50. Geometry of SD 7062 Airfoil with Plain Flaps Deflected 15 Degrees at %30 Chord	4541
Figure 3.1-51. Geometry of SD 7062 Airfoil with Slotted Flaps Deflected 15 Degrees at %30 Chord	4642
Figure 3.1-52. Cessna 172 with deflected flaps	4642
Figure 3.1-53. Close up of slotted flaps of Cessna 172	4642
Figure 3.1-54. Fluid domain around the airfoil with flaps.....	4743
Figure 3.1-55. Meshing Around the Slotted Flapped Airfoil with deflection 15 degrees	4743
Figure 3.1-56. Close up to meshing at crucial parts	4743
Figure 3.1-57. Refined mesh through the ANSYS Fluent	4844
Figure 3.1-58. Coupled Solution Procedure.....	4945
Figure 3.1-59. Change of lift coefficient of SD 7062 Airfoil Plain Flapped with Different deflections w.r.t. AOA.....	4945
Figure 3.1-60. Change of drag coefficient of SD 7062 Airfoil Plain Flapped with Different deflections w.r.t. AOA.....	5046
Figure 3.1-61. Change of lift coefficient of SD 7062 Airfoil Slotted Flapped with Different deflections w.r.t. AOA.....	5046
Figure 3.1-62. Change of drag coefficient of SD 7062 Airfoil Slotted Flapped with Different deflections w.r.t. AOA	5147
Figure 3.1-63. Comparison of lift coefficient values of SD 7062 Airfoil with Plain and Slotted Flaps at 15 degrees of deflection	5147
Figure 3.1-64. Comparison of lift coefficient values of SD 7062 Airfoil with Plain and Slotted Flaps at 15 degrees of deflection	5248
Figure 3.1-65. Comparison of drag coefficient values of SD 7062 Airfoil with Plain and Slotted Flaps at 15 degrees of deflection	5248
Figure 3.1-66. Comparison of drag coefficient values of SD 7062 Airfoil with Plain and Slotted Flaps at 30 degrees of deflection	5349
Figure 3.1-67. Comparison of moment coefficient values of SD 7062 Airfoil with Plain and Slotted Flaps at 15 degrees of deflection	5400
Figure 3.1-68. Comparison of moment coefficient values of SD 7062 Airfoil with Plain and Slotted Flaps at 30 degrees of deflection	5400
Figure 3.1-69. Velocity Distribution over SD 7062 Airfoil with 15 degrees deflected slotted flap at AOA=0	5554
Figure 3.1-70. Pressure Distribution over SD 7062 Airfoil with 15 degrees deflected slotted flap at AOA=0	5554
Figure 3.1-71. Velocity Distribution over SD 7062 Airfoil with 30 degrees deflected slotted flap at AOA=0	5554
Figure 3.1-72. Pressure Distribution over SD 7062 Airfoil with 30 degrees deflected slotted flap at AOA=0	5652
Figure 3.1-73. In trim condition generated lift force will be equal to the total weight	5652
Figure 3.1-74. Top view of wing geometry	5753
Figure 3.1-75. Fluid domain around the wing and sizing box	5753
Figure 3.1-76. Mesh sizing around the wing at the symmetry view	5854
Figure 3.1-77. Surface mesh on the wing	5854
Figure 3.1-78. Change of lift coefficient with Angle of Attack for 3D Wing and 2D airfoil	5955
Figure 3.1-79. Tip vortices obtained from CFD Results	5955
Figure 3.1-80. Pressure counters on the wing at 3 degrees of angle of attack	6056
Figure 3.1-81. Top view of the wing and flap geometry	6056
Figure 3.1-82. Isometric view of the wing and flap geometry with 15 degrees of deflection	6157
Figure 3.1-83. Surface mesh on the 15 degrees flap deflected wing	6157
Figure 3.1-84. Lift coefficient of the wing vs Angle of attack with different flap deflections	6258
Figure 3.1-85. Isometric view of the pressure counters on the wing with 15 degrees of flap deflections	6358
Figure 3.1-86. Velocity counters on the 15 degrees flap deflected wing for three different sections	6369
Figure 3.1-87. Pressure counters on the 15 degrees flap deflected wing for three different sections	6460
Figure 3.1-88. Simple Cruise Mission Sketch	6460
Figure 3.1-89. Constants for empty weight fractions	6662
Figure 3.1-90. Wetted Area Ratios.....	6763
Figure 3.1-91. Maximum L/D Trends	6864

UNCLASSIFIED

UNCLASSIFIED

Figure 3.1-92. Range – Weight trade off.....	<u>7066</u>
Figure 3.1-93. Endurance – Weight trade off	<u>7066</u>
Figure 3.1-94. Aerodynamic Forces	<u>7268</u>
Figure 3.1-95. Drag Force Components	<u>7268</u>
Figure 3.1-96. Maximum L/D for Cambered and Zero Camber Wing	<u>7369</u>
Figure 3.1-97. Min Power Required and Maximum Lift To Drag Ratio Point.....	<u>7370</u>
Figure 3.1-98. Available And Required Power Versus Velocity.....	<u>7470</u>
Figure 3.1-99. Power Required versus Flight Speed	<u>7470</u>
Figure 3.1-100. SD7062 airfoil XFLR5 analysis	<u>7874</u>
Figure 3.1-101. XFLR5 analysis of different wing Platforms.....	<u>7975</u>
Figure 3.1-102. OpenVSP CL vs Alpha Graph	<u>7975</u>
Figure 3.1-103. XFLR5 CL vs Alpha Graph	<u>8076</u>
Figure 3.1-104. OpenVSP CDO vs Alpha Graph	<u>8076</u>
Figure 3.1-105. XFLR5 CD0 vs Alpha Graph.....	<u>8177</u>
Figure 3.1-106. OpenVSP CD vs Alpha Graph.....	<u>8177</u>
Figure 3.1-107. XFLR5 CD vs Alpha Graph.....	<u>8278</u>
Figure 3.1-108. OpenVSP (L/D) vs Alpha Graph	<u>8278</u>
Figure 3.1-109. XFLR5 (L/D) vs Alpha Graph	<u>8379</u>
Figure 3.1-110. XFLR5 3D Wing Analysis VLM method	<u>8379</u>
Figure 3.1-111. Top and Isometric View	<u>8783</u>
Figure 3.1-112. Front View.....	<u>8883</u>
Figure 3.1-113. Left View	<u>8884</u>
Figure 3.1-114. Classification of Conventional Control Surfaces	<u>8985</u>
Figure 3.1-115. Geometry of Aileron (a) Top View of The Wing and Aileron (b) Side View of the Wing and Aileron	<u>9187</u>
Figure 3.1-116. Horizontal Tail and Elevator Geometry	<u>9288</u>
Figure 3.1-117. Directional Control via Rudder Deflection Top View	<u>9288</u>
Figure 3.1-118. Layout of the Aircraft.....	<u>9389</u>
Figure 3.1-119. CD vs AOA	<u>9490</u>
Figure 3.1-120. CL vs AOA	<u>9590</u>
Figure 3.1-121. CM vs AOA	<u>9594</u>
Figure 3.1-122. L/D vs AOA	<u>9694</u>
Figure 3.1-123. Combined Flight Envelope	<u>10095</u>
Figure 3.1-124. Half-Wing Geometry used in FAR23 Loads	<u>10196</u>
Figure 3.1-125. Shear Forces in z-dir. along Half Span.....	<u>109104</u>
Figure 3.1-126. Shear Forces in x-dir. along Half Span.....	<u>109104</u>
Figure 3.1-127. Moments about x-axis along Half Span	<u>110105</u>
Figure 3.1-128. Moments about y-axis along Half Span	<u>110105</u>
Figure 3.1-129. Moments about z-axis along Half Span	<u>111106</u>
Figure 3.1-130. Force Resultants in z-dir. along Half Span.....	<u>111106</u>
Figure 3.1-131. Force Resultants in z-dir. along Half Span.....	<u>112107</u>
Figure 3.1-132. The Horizontal Tail Geometry along Half Span	<u>113108</u>
Figure 3.1-133. Back-View Illustration of the Left Half of The Tail of an Aircraft	<u>114109</u>
Figure 3.1-134. V-y for all 13 Cases.....	<u>115110</u>
Figure 3.1-135. M-y for all 13 Cases.....	<u>116111</u>
Figure 3.1-136. Vertical Tail Geometry	<u>117112</u>
Figure 3.1-137. Sample Force Distribution on the Vertical Tail Shown on the Back-View Illustration of an Aircraft	<u>118113</u>
Figure 3.1-138. V-z far all Four Cases.....	<u>119114</u>
Figure 3.1-139. M-z for all Four Cases	<u>119114</u>
Figure 3.2-1. Truss type construction	<u>138133</u>
Figure 3.2-2. Pratt truss type construction	<u>138133</u>
Figure 3.2-3. Warren truss type construction	<u>139134</u>
Figure 3.2-4. Monocoque type construction	<u>139134</u>
Figure 3.2-5. Semi-monocoque type construction	<u>140135</u>
Figure 3.2-6 Conventional Tail	<u>143138</u>

UNCLASSIFIED

UNCLASSIFIED

Figure 3.2-7. Permanently fixed mount	<u>143</u> <u>138</u>
Figure 3.2-8. Jackscrew mechanism	<u>144</u> <u>139</u>
Figure 3.2-9. Taileron movement	<u>144</u> <u>139</u>
Figure 3.2-10. Flying tail of Aero AT-3	<u>144</u> <u>139</u>
Figure 3.2-11. Fixed vertical tail	<u>145</u> <u>140</u>
Figure 3.2-12 T-Tail Configuration	<u>145</u> <u>140</u>
Figure 3.2-13. A comparison of the vertical fin stiffness requirement between a low tail and a T-tail design	<u>146</u> <u>141</u>
Figure 3.3-1. Piston- Propeller Engine	<u>147</u> <u>142</u>
Figure 3.3-2. Change of available power with altitude	<u>149</u> <u>144</u>
Figure 3.3-3. Thrust to Weight ratio vs Wing Loading	<u>150</u> <u>145</u>
Figure 3.3-4. Power vs Wing Loading	<u>151</u> <u>146</u>
Figure 3.3-5. Engines and their overall grading	<u>153</u> <u>148</u>
Figure 3.3-6. Rotax 912 iSc Sport	<u>154</u> <u>149</u>
Figure 3.3-7. Engine System Architecture for Rotax 912 iSc Sport	<u>156</u> <u>151</u>
Figure 3.3-8.2 and 3-blade propellers	<u>157</u> <u>152</u>
Figure 3.3-9. Showing how constant speed propeller Works	<u>158</u> <u>153</u>
Figure 3.3-10. Showing the difference between fixed propeller and constant speed propeller [2]	<u>159</u> <u>154</u>
Figure 3.3-11. Showing tip speed limits for different materials[2]	<u>160</u> <u>155</u>
Figure 3.3-12: Fuel Tank Types2
Figure 3.3-13. Rigid Removable Tank2
Figure 3.3-14. Bladder Tank2
Figure 3.3-15. Fuel Tank Locations4
Figure 3.3-16. Fuel Tank Locations on an Aircraft4
Figure 3.3-17. Fuel System Schematic6
Figure 3.3-18. Electrical Fuel Pump Set8
Figure 3.3-19. Selector Valve8
Figure 3.4-1: Isometric View of the Stick13
Figure 3.4-2: Isometric View of the Pedal14
Figure 3.4-3: Isometric View of Flap System14
Figure 3.4-4: Final Assembly15
Figure 3.5-1 : The crude electrical architecture	<u>29</u> <u>20</u>
Figure 3.5-2 : The proposed avionic architecture. Notice the legend	<u>30</u> <u>21</u>
Figure 3.5-3 Anti-collision LED light – Red or White	<u>31</u> <u>22</u>
Figure 3.5-4 Navigation / Position / Strobe LED light	<u>31</u> <u>22</u>

UNCLASSIFIED

UNCLASSIFIED

1. PURPOSE

Purpose of this report is to show the preliminary design and trade off studies of VLA project.

2. SCOPE

3. CONCEPTUAL DESIGN STUDIES

3.1. Air Vehicle

3.1.1. Aerodynamics

Aim of this section is to briefly introduce the procedures of CFD analysis of 2-D airfoils and 2-D airfoils with flaps and select the appropriate airfoil and flap configuration for the very light aircraft. Computational tools like ANSYS Fluent, ICEM CFD, and SU2 were used to gather the necessary data to compare the different cases and choose the best options eventually. Approximately 30 airfoil types will be considered during the airfoil selection process, in general. To achieve the most efficient airfoil for our very light aircraft, airfoils will be eliminated one by one according to some of the needs. To achieve the best option for the flap configuration, there will be a competitor study and then analyze the configurations one by one to see the advantages and disadvantages of them.

First, the selection of the right airfoil for the aircraft has been made and then skipped to the subject of choosing the right configuration of flaps. To begin the selection of the most suitable airfoil, approximately 30 airfoils were chosen from competitors and literature. Half of the airfoils has been eliminated before the analysis due to the restrictions of the technical requirements, limitations of the manufacturing processes and obvious poor performances. When only four airfoil options were left, a detailed analysis has been hold to see the advantages and disadvantages of these four. Then, according to our needs and avoids the best airfoil option will be selected for the very light aircraft.

Second, the selection of the right flap configuration the aircraft has been made. A competitor study was held to see which kind of flaps that the previously made very light aircrafts has used and started the analysis with three type of flaps. A detailed analysis was hold to see the required data of the different configurations and best option to hold the needs of our aircraft was made.

3.1.1.1. Airfoil Selection

3.1.1.1.1. Literature Research and First Elimination Stage

Different aircrafts in the category of very light aircrafts has been examined and some of the airfoils has been taken to the list of options to analyze later. Competitor study started with most commonly used airfoils like NACA4415, 2415, 24012 and 24015. Although these are the most commonly used airfoils at the previous aircrafts, studies were not limited here and further researches has been made to gather more airfoil data and maybe find one better airfoil. So, the not-very-detailed elimination process has approximately begin with 30 airfoils. Due to the technical requirements and limitations of the manufacturing processes, almost half of the airfoils has been eliminated at the first stage. Here are the list of remaining airfoils, later to be analyzed:

- **NACA4412**
- **NACA4415**
- **NACA23012**
- **NACA23015**
- **Eppler 1210**
- **SD 7062**
- **GOE222**
- **GOE366**
- **GOE387**
- **GOE646**
- **GOE702**
- **GOE769**
- **Rhodes St. Genesee 32**
- **Rhodes St. Genesee 34**

UNCLASSIFIED

UNCLASSIFIED

3.1.1.2. 2D Analysis and Second Elimination Stage

In order to be more specific about which airfoil would be best option for the very light aircraft, remaining thirteen airfoils have been analyzed using CFD tools.

Grid Refinement

Meshing part is the most demanding part of the CFD analysis, choosing the right mesh type according to the flow type is really important. In our case to choose the airfoil, we aren't really interested in the angle of attacks where the flow becomes highly turbulent. That's why, while choosing the airfoil type structured mesh that was created in ICEM CFD which is a meshing tool of ANSYS has been used to create the mesh and also the geometries (Figure 3.1-1).

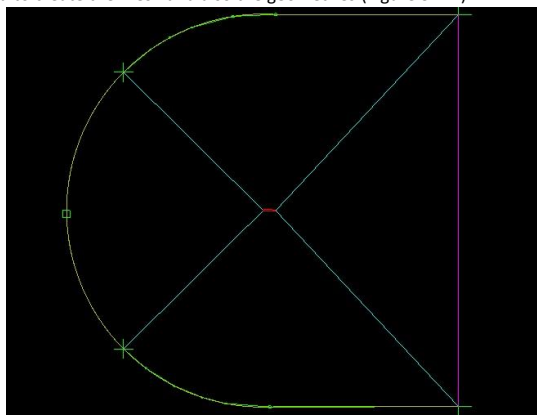


Figure 3.1-1. Fluid domain with airfoil geometry created in ICEM CFD

C-Grid type is used with enough element numbers, element numbers to be used was determined by a grid refinement, and Y+ value of 1 to better predict the flow around the airfoil (Figure 3.1-2, Figure 3.1-3).

UNCLASSIFIED

UNCLASSIFIED

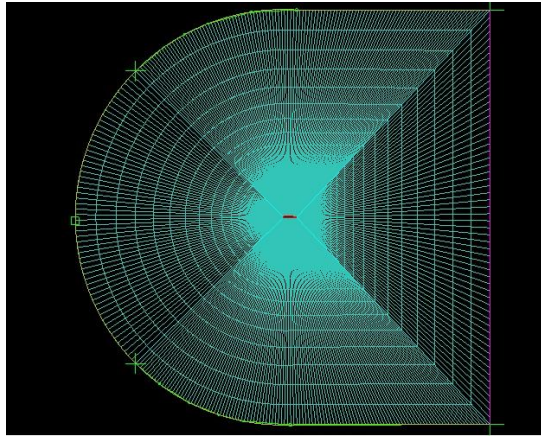


Figure 3.1-2. 2D structured meshed domain

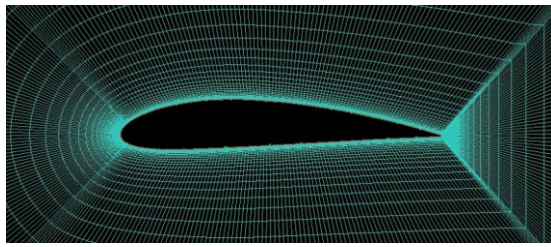


Figure 3.1-3. 2D structured mesh around the airfoil

Grid refinement has been done in two different ways. First of all, NACA4415 airfoil was chosen to perform the grid refinement study since it is a widely used airfoil and there are many data on the internet that can be compared with our data. Started with a low number of elements, as the number of elements increased, the error between finer C_l , C_d values and previous coarser C_l , C_d values have been calculated (Table 3.1-1). Calculations has been made for the flow conditions at 7500 ft and 5 degree AOA..

Table 3.1-1. Grid refinement study with NACA4415 at 5 degree AOA

	Number of Elements	C_l	C_d	C_l Error %	C_d Error %
Mesh 1	3000	0.4543	0.0036		
Mesh 2	5000	0.5801	0.0044	21.68%	19.09%
Mesh 3	8000	0.7446	0.0164	22.09%	73.14%
Mesh 4	14000	0.8782	0.0221	15.22%	25.79%
Mesh 5	25000	0.8896	0.0225	1.28%	1.98%
Mesh 6	52000	0.8903	0.0228	0.08%	1.27%

The mesh sizing of Mesh 5 has been used for the following analysis. Second check that has been done was the compare the C_l , C_d and C_m values of NACA4415 that were obtained at the iteration 5 was compared with the experimental value of NACA4415 in the [Theory of Wing Sections: Including Summary of Airfoil Data book](#) (Figure 3.1-4).

UNCLASSIFIED

UNCLASSIFIED

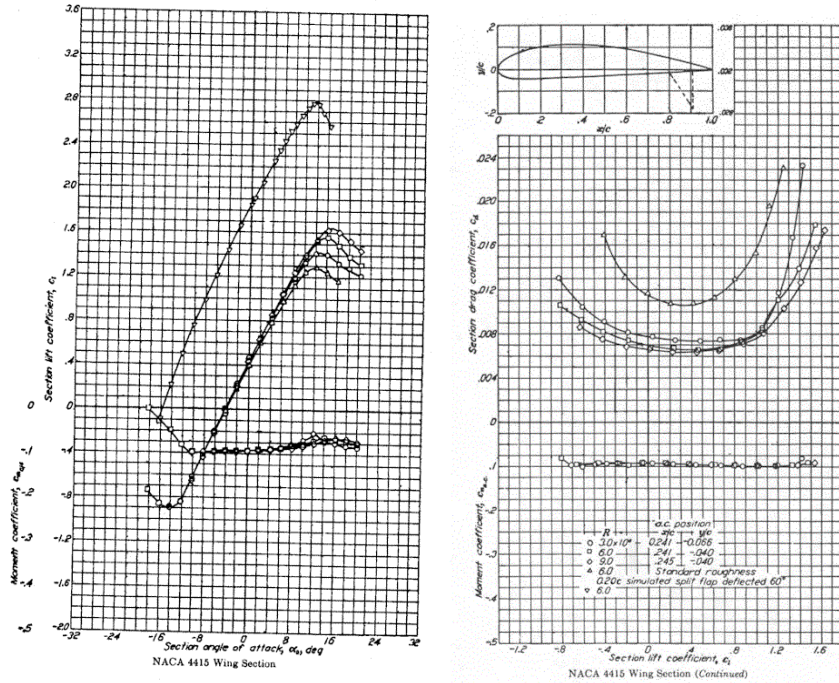


Figure 3.1-4. Experimental Values of NACA4415 Airfoil

Get Data Graph Digitizer software was used to extract the data from the graphics and compared with CFD values, the error was around %5 and counted it acceptable since there might always be some difference between CFD and experimental data.

Set Up and Results

All calculations were made with the atmospheric conditions of 7500 ft altitude, 81 Knots Speed. The governing equations are solved by k-omega (k-w) turbulence model. Since at this stage there are yet many airfoils to be eliminated, it was a bit challenging to get to the next stage. The mesh type and element numbers that were obtained in the grid refinement study has been used for all the airfoils. The comparison of the aerodynamic coefficients for 13 airfoils investigated are given in Figure 3.1-5 -Figure 3.1-7.

UNCLASSIFIED

UNCLASSIFIED

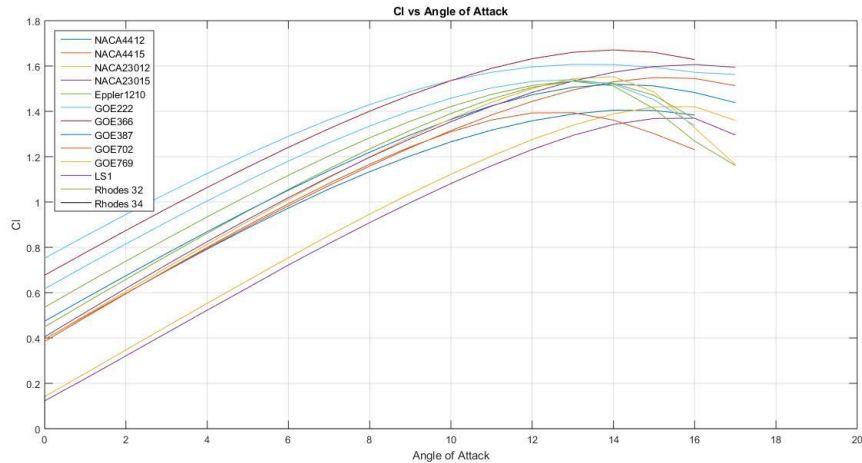


Figure 3.1-5. $f C_l$ versus angle of attack for thirteen airfoils investigated

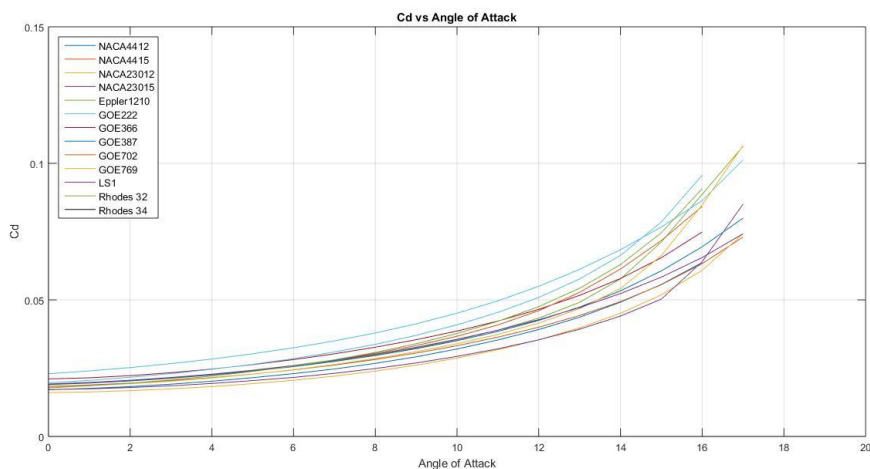


Figure 3.1-6. C_d versus angle of attack for thirteen airfoils investigated

UNCLASSIFIED

UNCLASSIFIED

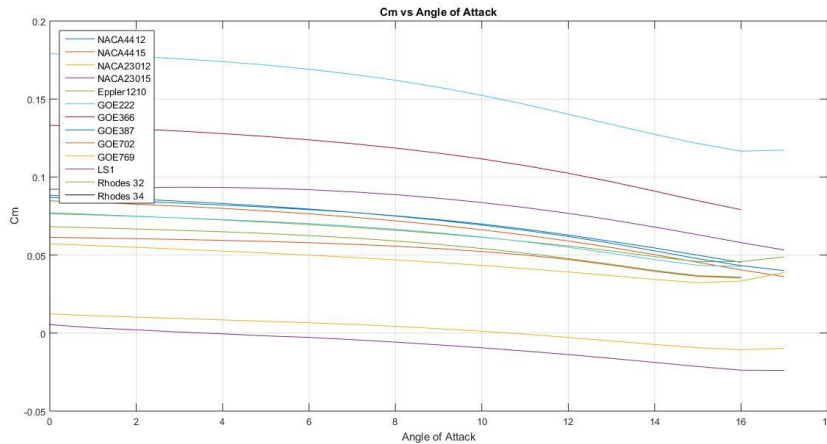


Figure 3.1-7. Change of C_m Values around $c/4$ of thirteen airfoils with respect to angle of attack

Checking all the data further elimination was made according to some criteria. Although some of the airfoils like GOE222 are giving very high C_l values, since also their C_m and C_d values being very high they were eliminated during the process.

5 digit NACA Airfoils like 23012 and 23015 were eliminated during this process although they are giving the best values of C_d and especially C_m since they cannot reach the required maximum C_l values for our VLA.

With some optimization of remaining airfoils according to the C_l , C_d , C_m values and manufacturing limitations, number of airfoil candidates has been reduced to only four. These are to be; NACA4415, GOE 387, Rhodes St. Genesee 32 and SD 7062 (Figure 3.1-11).



Figure 3.1-8. NACA4415

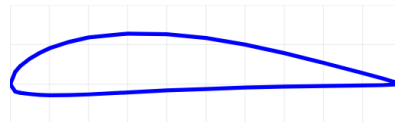


Figure 3.1-9. GOE 387



Figure 3.1-10. Rhodes St. Genesee 32

UNCLASSIFIED

UNCLASSIFIED



Figure 3.1-11. SD 7062

3.1.1.3. 2D Analysis and Third Elimination Stage

During this process remaining four airfoils has been analyzed even with further details by checking the zero lift angle of attacks, lift curve slopes, efficiencies and endurances (Figure 3.1-12-Figure 3.1-14).

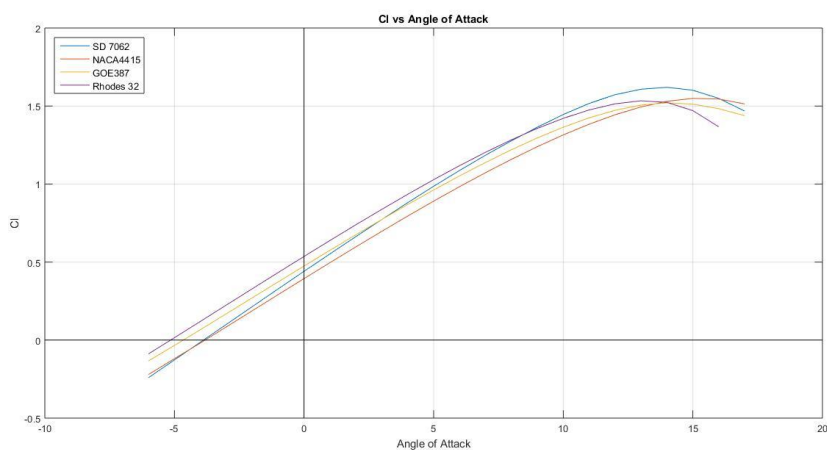


Figure 3.1-12. C_l versus α for four airfoils and zero lift AOA

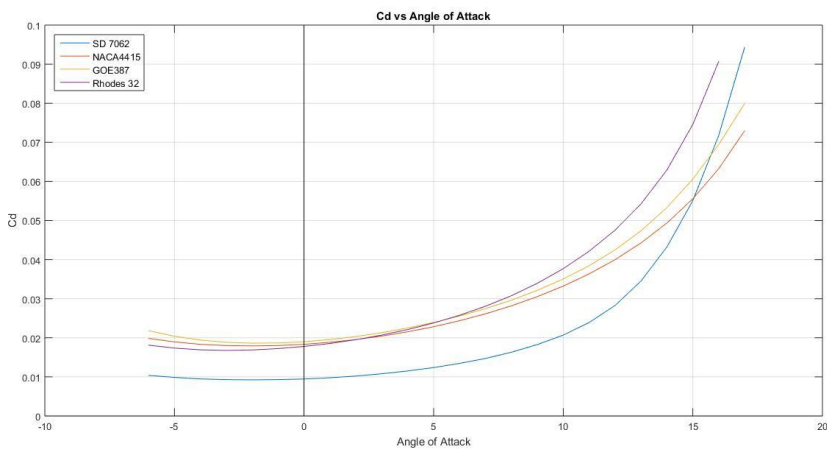


Figure 3.1-13. C_d versus α for four airfoils

UNCLASSIFIED

UNCLASSIFIED

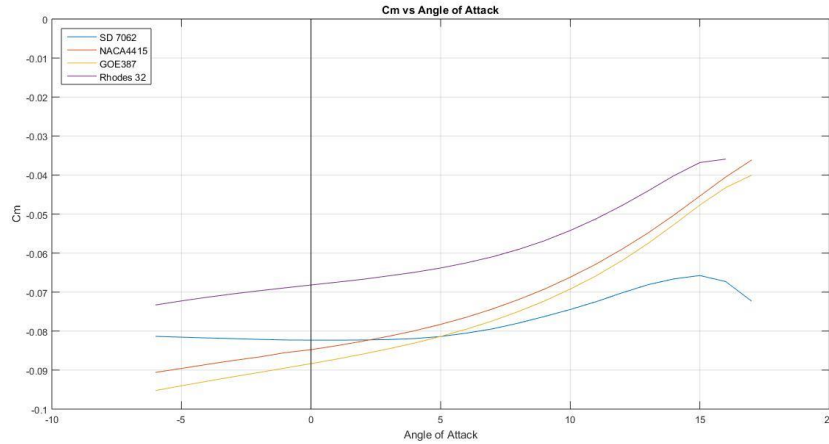


Figure 3.1-14. C_m versus α for four airfoils

Although SD 7062 airfoil is one step ahead than other three airfoils, their stall angles differs a little bit. Among them NACA4415 having the best stall characteristics, Rhodes St. Genesee 32 has the highest C_l value along the linear interval of the C_l graph. At slow angle of attacks Rhodes St. Genesee 32, GOE 387 and NACA4415 almost having the same C_d values at lower AOA's, SD 7062 has the BEST C_d characteristics. Comparing the moment coefficients, Rhodes St. Genesee 32 undisputed has the best values. Considering our VLA will cruise in trim with low AOA's, checking the efficiencies by C_l/C_d values, SD 7062 also have the best values.

Rhodes St. Genesee airfoil having the flat bottom surface also results an easy manufacturing procedure. Some airfoils have better characteristics for some parameters and some of them have better for some other parameters. Optimizing between the airfoils, [Rhodes St. Genesee 32](#) (Figure 3.1-15) or [SD 7062](#) (Figure 3.1-16) would likely to be the best option for our VLA. Rhodes St. Genesee 32 having the thickness of 12% chord gives it some disadvantages with the perspective of structural design, and SD 7062 has the maximum thickness of 14% chord. That's why in this stage it is wise to keep up with both of them.



Figure 3.1-15. Rhodes St. Genesee 32 with 12% Thickness



Figure 3.1-16. SD 7062 with 14% thickness

UNCLASSIFIED

UNCLASSIFIED

Finally SD 7062 was chosen as airfoil type because it was the only airfoil which fulfills the requirement of C_{lmax} . However, it wasn't really clear to go with either of the airfoils. So, the flap analyses have been done with Rhodes St. Genese 32 airfoil.

3.1.1.4. Detailed Analysis of SD7062 Airfoil

Since we have chosen SD7062 for the aircraft, detailed analyses are required. In this case, it is good practice to use various CFD codes. We are required to check the CFD and panel code performance difference of the aforementioned airfoil. For CFD analyses ANSYS Fluent V19.1 and **SU2** (Stanford University Unstructured), which is an **open-source code**, are put to test. Since we also plan to use SU2 in TAI and also in the project this will also be a good comparison in 2D. SU2 has many capabilities but many of them are of academic interest (Hybrid DES, DDES etc.). However, turbulence models provided are verified. To name a few, Spalart-Allmaras (SA), its variants (SA_NEG, SA_E, SA_COMP, and SA_E_COMP) and Menter's Shear Stress Transport (SST) turbulence models are available. All the results provided are obtained using SST turbulence model.

In order to use SST model, having a $y+$ (non-dimensional wall distance) value around 0.5 will give good results, if not excellent. If unable to do so, the user will not resolve the near wall effects. However, if the first layer of the grid is not in the viscous sublayer ($y+$ around 30) one can get away using wall functions in Fluent but it is not possible yet in SU2. Thus, SU2 grids are more 'computationally expensive' if wall functions on Fluent are used (Palacios et al., 2014).

Also, since SD7062 is a sharp trailing edged airfoil, creating a blunt trailing edge is essential since sharp trailing edges are not easy to manufacture.

Table 3.1-2. Trailing Edge Type

Type(s) of TE	FLUENT	SU2	XFOIL
Sharp	Sharp	Sharp & Blunt	Sharp

From Table 3.1-2, one can see that it is possible to compare:

- Sharp TE vs. Blunt TE using SU2
- Sharp TE analysis using SU2, Fluent, XFOIL

Figure 3.1-17 shows the whole grid domain of SD7062 airfoil with blunt trailing edge and Figure 3.1-18 shows a zoomed view of the mesh around the airfoil. Similarly, Figure 3.1-19 shows the mesh for the SD7062 airfoil with sharp trailing edge and Figure 3.1-20 is close view to the grid around the airfoil. Both meshes have $y+$ values of 0.5 (roughly).

UNCLASSIFIED

UNCLASSIFIED

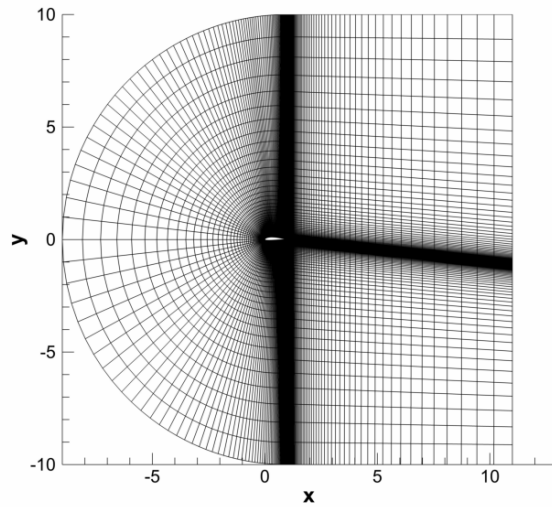


Figure 3.1-17. Structured mesh for SD7062 with blunt TE.

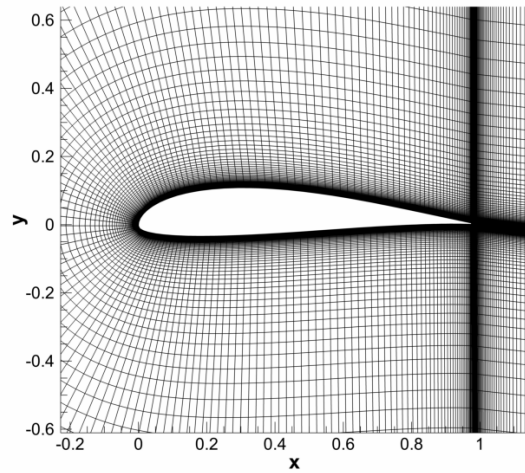


Figure 3.1-18. Close-up of the structured mesh with blunt TE.

UNCLASSIFIED

UNCLASSIFIED

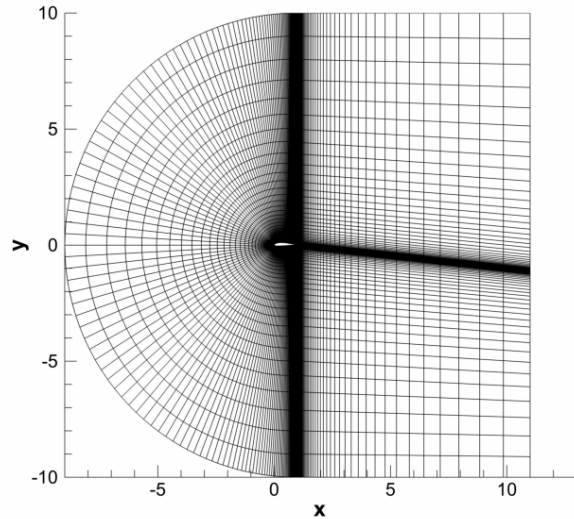


Figure 3.1-19. Structured mesh for SD7062 with sharp TE.

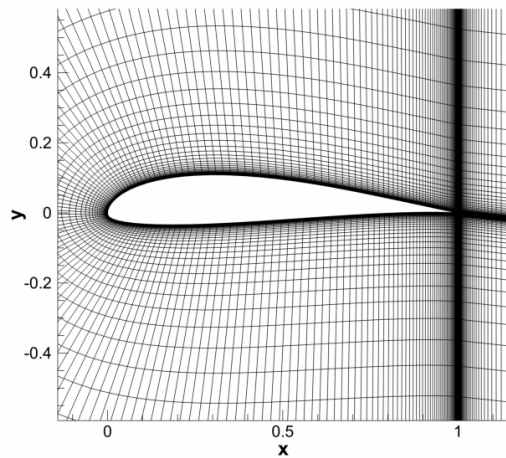


Figure 3.1-20. Close-up of the structured mesh with sharp TE.

Case 1: Comparisons of the solvers

UNCLASSIFIED

UNCLASSIFIED

Figure 3.1-21 shows the lift coefficient versus angle of attack curve of SD 7062 airfoil obtained from analysis of XFOIL, SU2 and Fluent. The drag coefficient versus angle of attack curve is given in Figure 3.1-22.

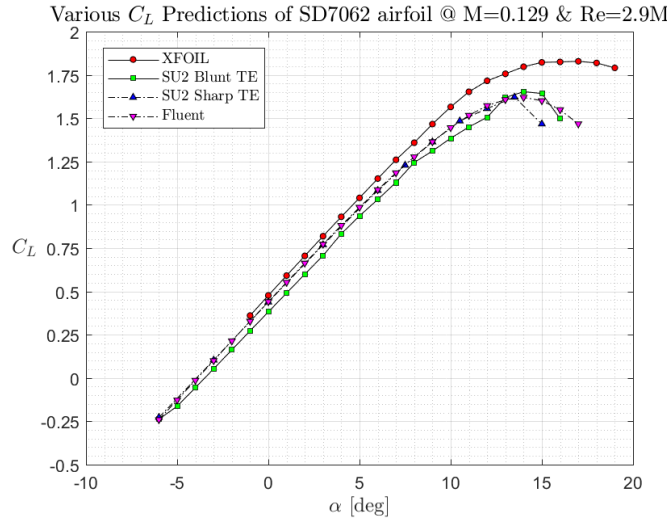


Figure 3.1-21. C_L versus α curves obtained from XFOIL, SU2 and Fluent analyses.

From Figure 3.1-21, we can see that Fluent and SU2 sharp TE are in perfect agreement. However, the more realistic case, blunt TE case has the same lift curve slope but lower zero lift angle of attack which makes sense. XFOIL gives acceptable results for this case.

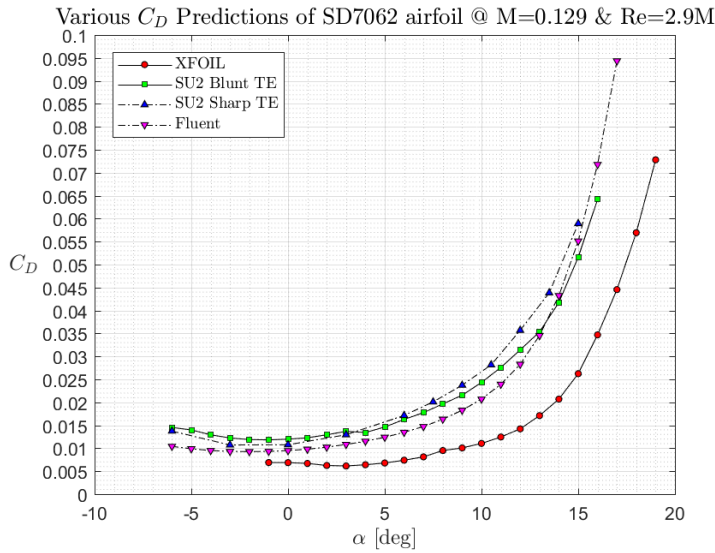


Figure 3.1-22. C_D versus α curves obtained from XFOIL, SU2 and Fluent analyses.

UNCLASSIFIED

UNCLASSIFIED

From Figure 3.1-22, again, SU2 and Fluent are in agreement. We can conclude that SU2 may be over predicting the drag. Since drag is hard to predict on CFD, the results are more than acceptable with small margins of error. Parasitic drag is around 0.01 and drag coefficient increases quadratically. However, this is where XFOIL starts to fail. Since XFOIL is a panel code, the drag prediction is not that great.

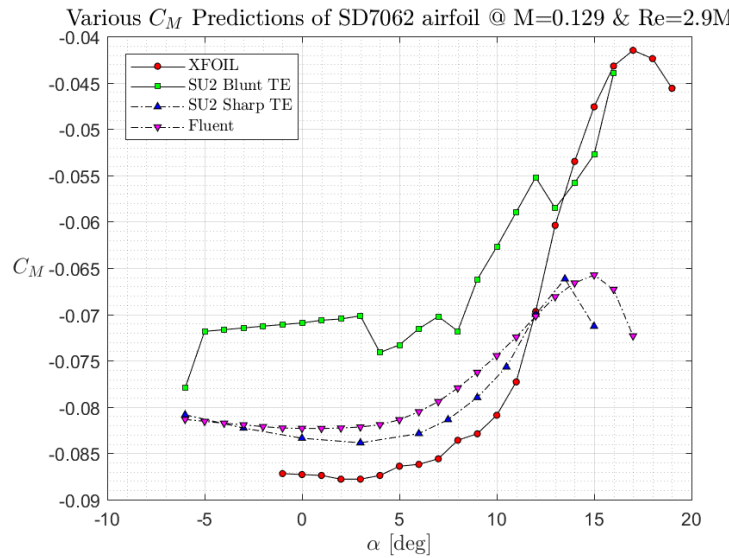


Figure 3.1-23. C_m versus α curves obtained from XFOIL, SU2 and Fluent analysis.

Again, SU2 sharp TE and Fluent give similar results for the pitching moment. One can also see the impact of having a blunter trailing edge in pitching moment coefficients. This behavior is expected. Why? Because trailing edge sharpness and TE 'direction' are crucial for pitching moment coefficient values. Theoretically, it is possible to have an airfoil/wing with zero pitching moment: 'reflexed airfoil'. However, this is beyond the scope of this report and will not be discussed.

UNCLASSIFIED

UNCLASSIFIED

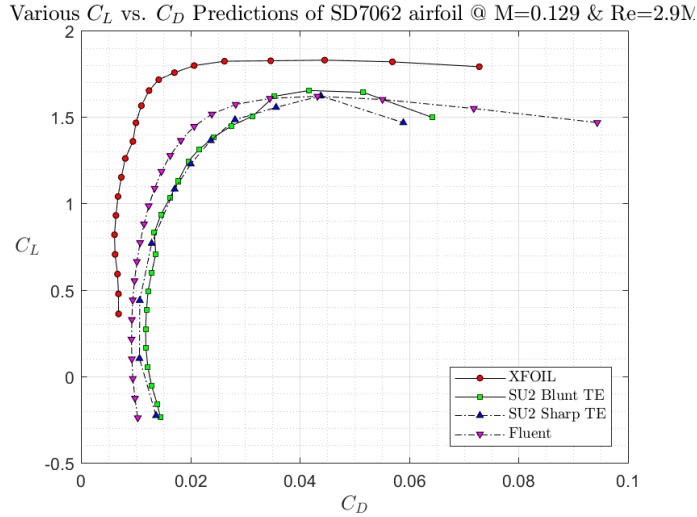


Figure 3.1-24. Lift coefficient vs. drag coefficient predictions of XFOIL, SU2 and Fluent for various angles of attack.

Results are fairly close in SU2 and Fluent side, but not on XFOIL side. We can also see the quadratic behavior of drag. Not much to say, since it's similar to drag coefficient vs. angle of attack figure.

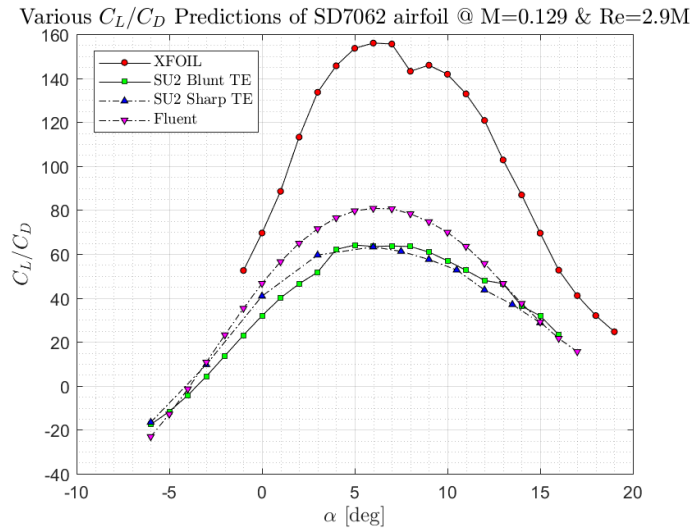


Figure 3.1-25. Cl/Cd ratio predictions of XFOIL, SU2 and Fluent for various angles of attack.

For this case, again XFOIL is off by miles. SU2 and Fluent results are very close, with both peaking around 6 degrees and having values 60 and 80, respectively. Since we plan to have 3 degrees of incidence in the wing; 3 degrees of angle of attack in order to get maximum range is not bad.

UNCLASSIFIED

UNCLASSIFIED

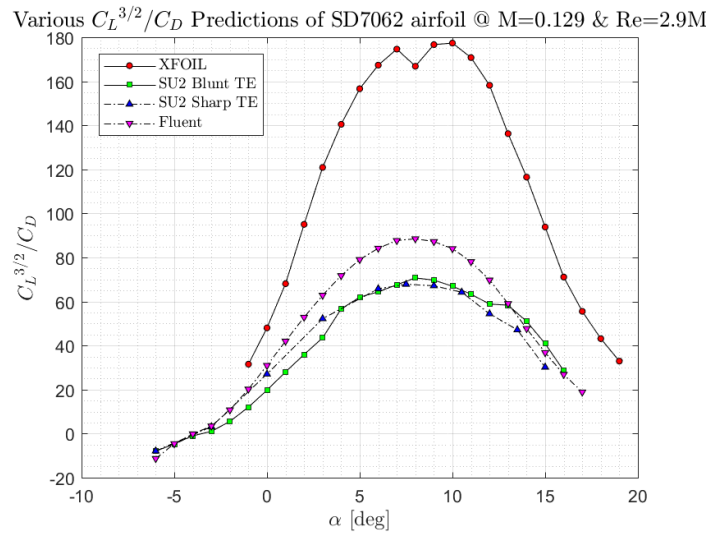


Figure 3.1-26. $C_L^{3/2}/C_D$ predictions of XFOIL, SU2 and Fluent for various angles of attack.

In order to maximize the range, we need to check the plot above and fly with the alpha where we have a peak. Fluent and SU2 are again close. Both peaking at 8 degrees, SU2 and Fluent gives 60 and 80, respectively. This means, with 3 degrees of incidence, we have to fly with 5 degrees of alpha in order to maximize the endurance.

Conclusion for case 1: Fluent and SU2 gives similar results in 2D. We should also compare them for 3D cases. XFOIL gives reasonable results for back of the envelope calculations but should not be relied on too much.

Case 2: Sharp Trailing Edge versus Blunt Trailing Edge

UNCLASSIFIED

UNCLASSIFIED

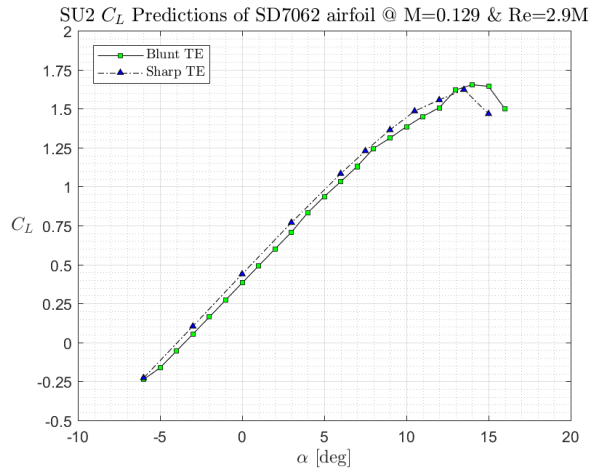


Figure 3.1-27. The figure above shows the lift coefficient predictions of SU2 for both sharp and blunt trailing edges.

Both cases yield similar lift curve slopes, similar maximum lift coefficients.

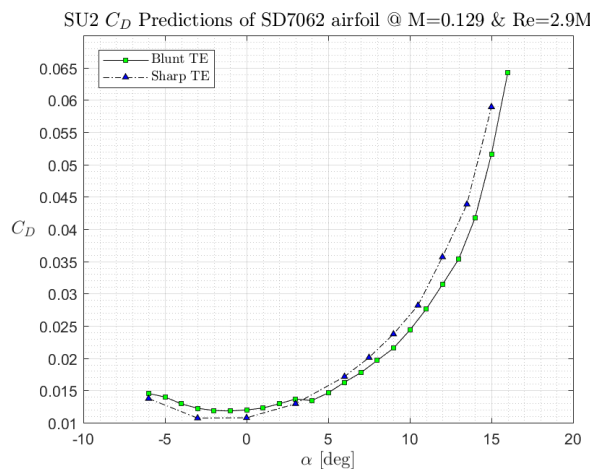


Figure 3.1-28. The figure above shows the drag coefficient predictions of SU2 for both sharp and blunt trailing edges.

Very similar results in terms of drag when both cases are considered, note the quadratic behavior of the drag.

UNCLASSIFIED

UNCLASSIFIED

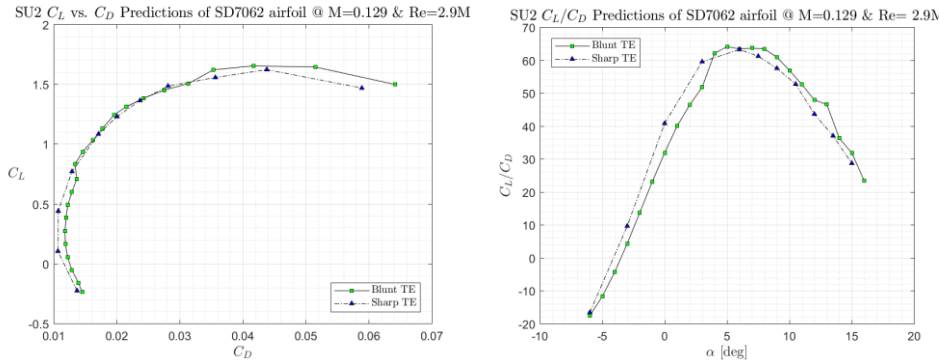


Figure 3.1-29. Lift coefficient over drag coefficient vs. angle of attack and lift coefficient versus drag coefficient plots, predicted by SU2.

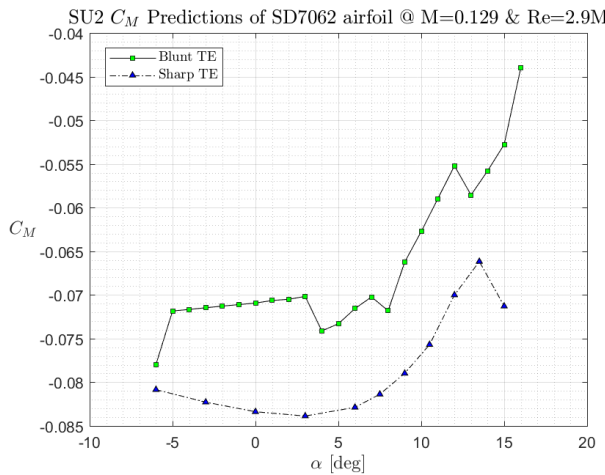


Figure 3.1-30. Pitching moment coefficient vs. angle of attack plot, predicted by SU2.

From the figure above, we can see that bluntness is beneficial for the VLA since we need to have smaller pitching moment to act on the aircraft. Having a greater amount of pitching moment requires having a greater moment arm (since moment is counteracted by the horizontal tail), hence the added weight.

UNCLASSIFIED

UNCLASSIFIED

Case 3: Fluent vs SU2

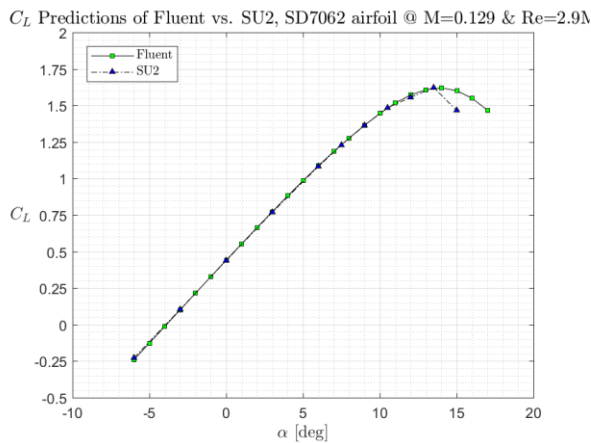


Figure 3.1-31. The figure above shows lift coefficient predictions of SU2 and Fluent, both with sharp TE.

It seems that SU2 starts stalling a bit early, apart from that the lift curves predicted are identical.

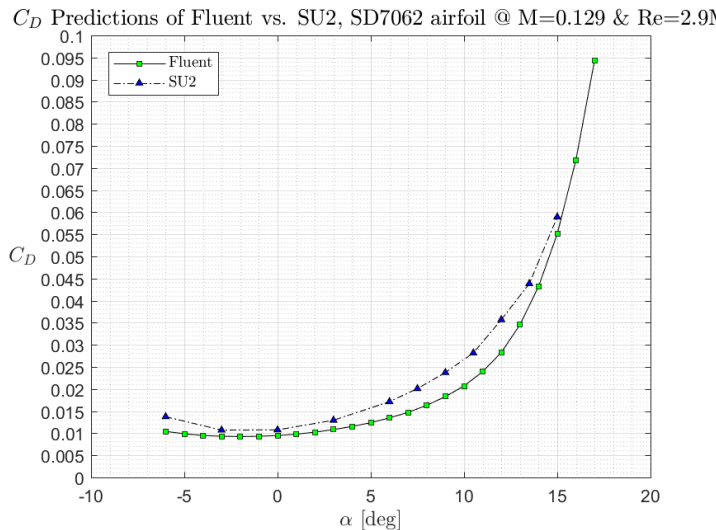


Figure 3.1-32. The figure above shows drag coefficient predictions of SU2 and Fluent, both with sharp TE.

From the figure above, SU2 can be said to be over predicting the drag coefficient. However, it is not much of an over prediction and can be considered acceptable.

UNCLASSIFIED

UNCLASSIFIED

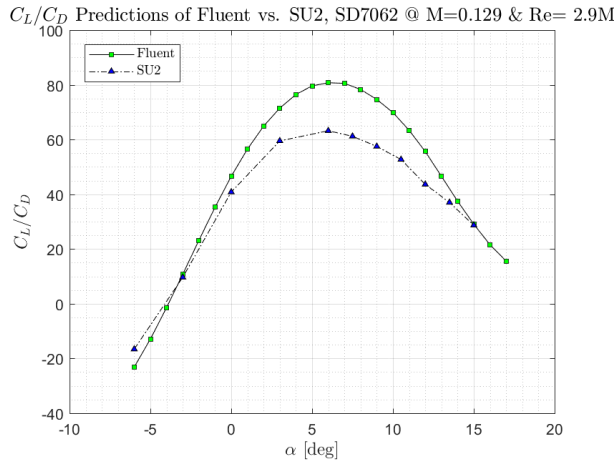


Figure 3.1-33. The figure above shows lift coefficient divided by drag coefficient predictions of SU2 and Fluent, both with sharp TE.

The figure above shows that this is where SU2 and Fluent differ a bit. Since there is a bit of an over prediction on SU2 side, consequently having a greater denominator in the plot above, it results in lower peak values.

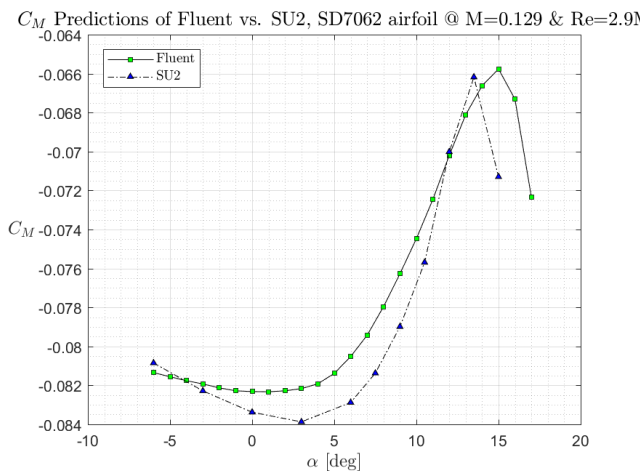


Figure 3.1-34. The figure above shows moment coefficient predictions of SU2 and Fluent, both with sharp TE.

The results are in good agreement. Taking fluent results as the baseline reference, SU2 over predicts again, but not too much. We may need to investigate stall and post-stall behavior in the future.

UNCLASSIFIED

UNCLASSIFIED

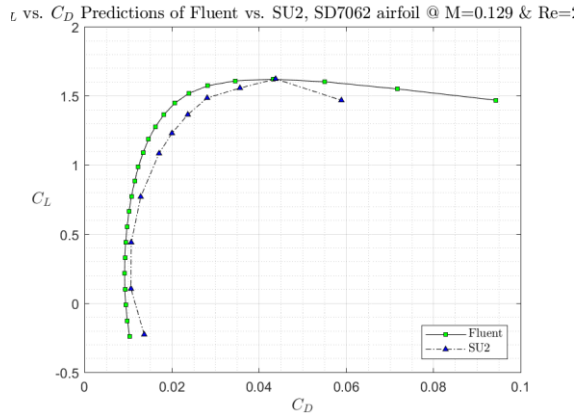


Figure 3.1-35. The figure above shows the lift coefficient versus drag coefficient values predicted by SU2 and Fluent.

Conclusion: SU2 results are fairly accurate, if we consider Fluent as a reference. The over prediction issue might be solved by changing the solver settings.

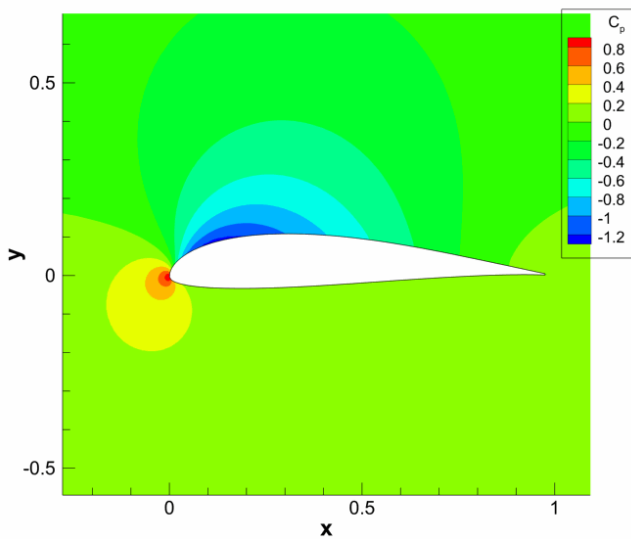


Figure 3.1-36. Contours of pressure coefficient for SD7062 at $\alpha=3^\circ$.

UNCLASSIFIED

UNCLASSIFIED

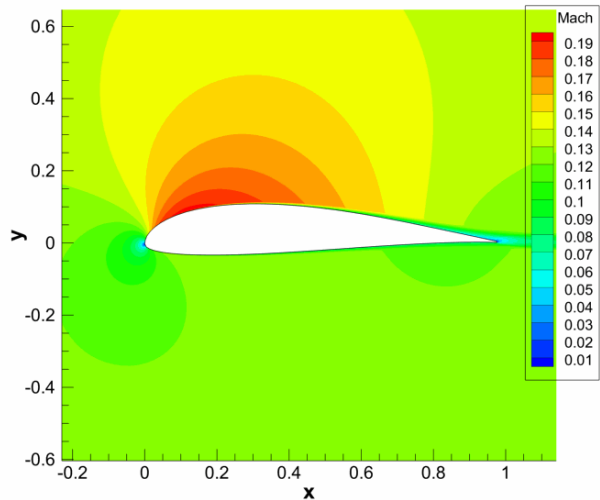


Figure 3.1-37. Contours of Mach number for SD7062 at $\alpha=3^\circ$.

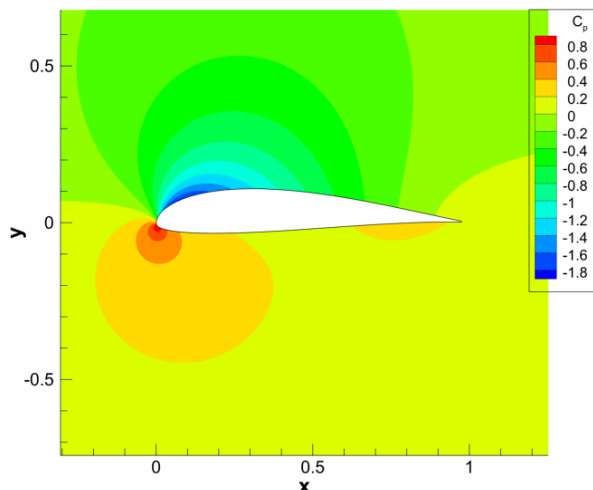


Figure 3.1-38. Contours of pressure coefficient for SD7062 at $\alpha=6^\circ$.

UNCLASSIFIED

UNCLASSIFIED

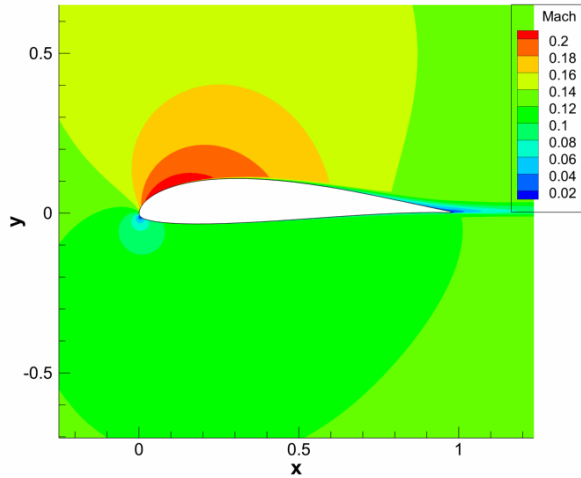


Figure 3.1-39. Contours of Mach number for SD7062 at $\alpha=6^\circ$.

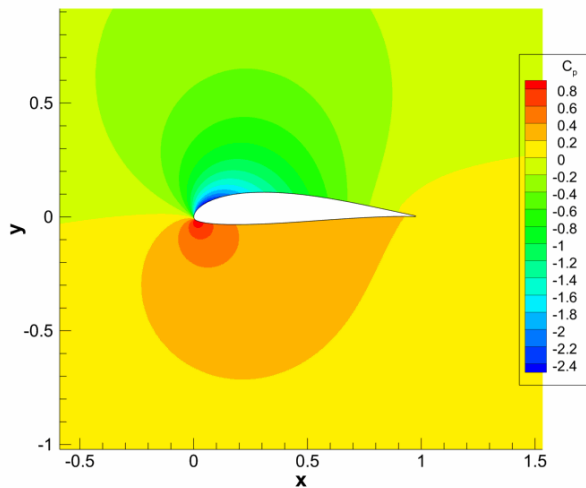


Figure 3.1-40. Contours of pressure coefficient for SD7062 at $\alpha=9^\circ$.

UNCLASSIFIED

UNCLASSIFIED

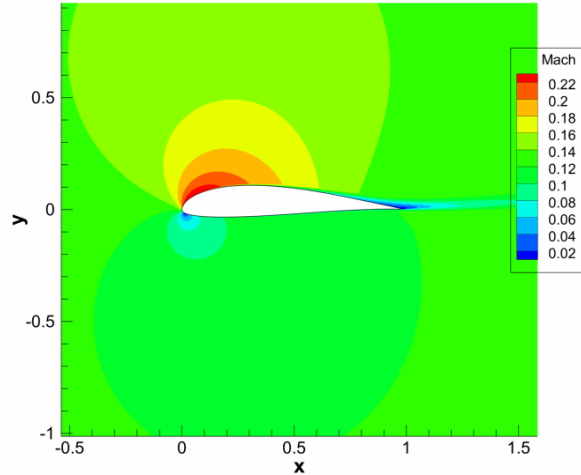


Figure 3.1-41. Contours of Mach number for SD7062 at $\alpha=9^\circ$.

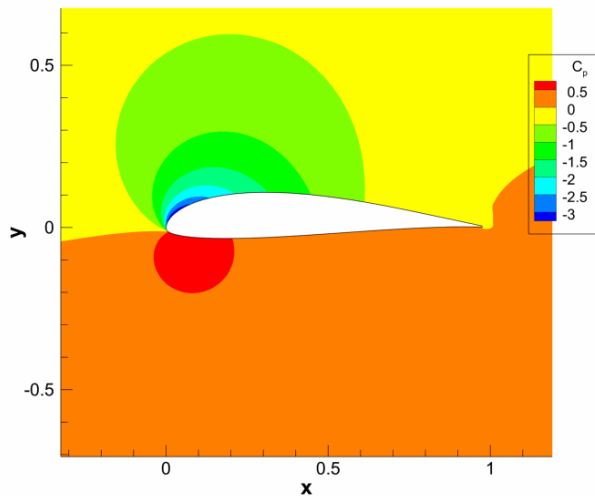


Figure 3.1-42. Contours of pressure coefficient for SD7062 at $\alpha=12^\circ$.

UNCLASSIFIED

UNCLASSIFIED

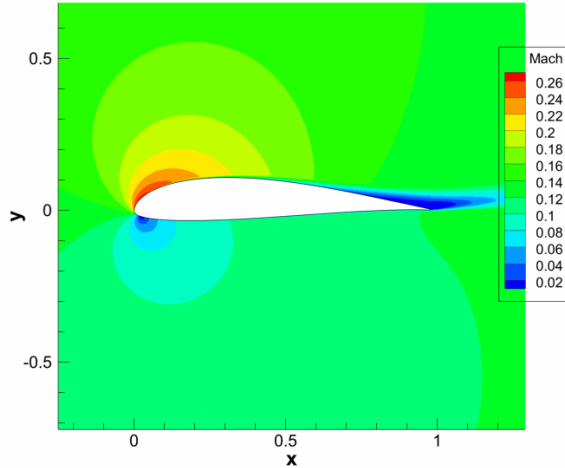


Figure 3.1-43. Contours of Mach number for SD7062 at $\alpha=12^\circ$.

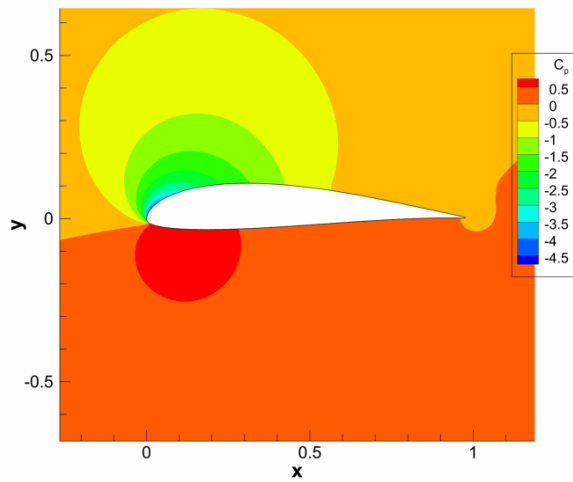


Figure 3.1-44. Contours of pressure coefficient for SD7062 at $\alpha=15^\circ$.

UNCLASSIFIED

UNCLASSIFIED

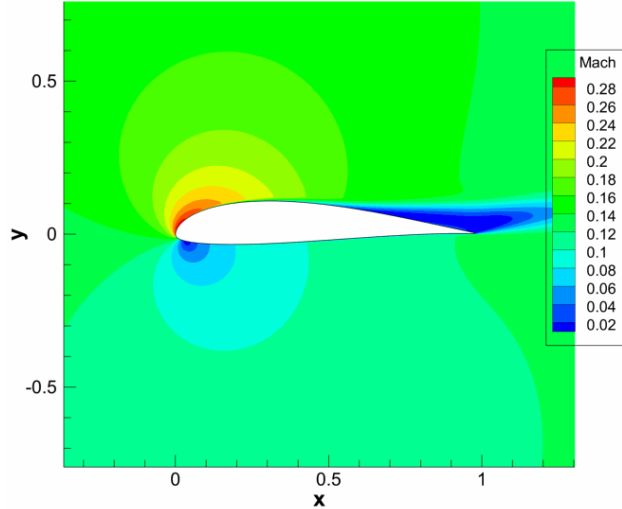


Figure 3.1-45. Contours of Mach number for SD7062 at $\alpha=15^\circ$.

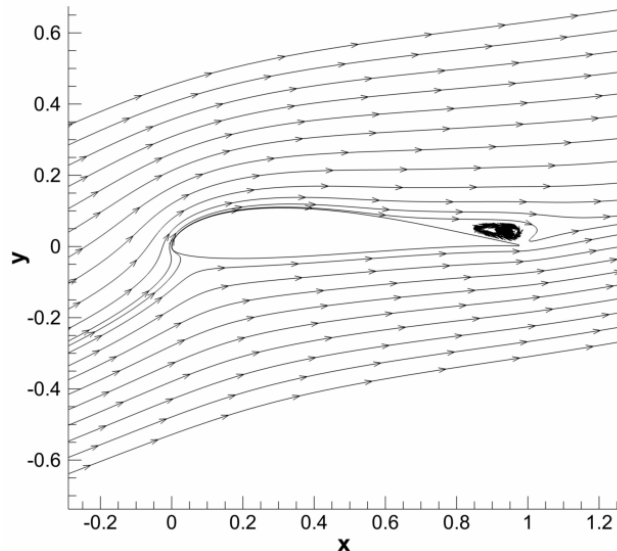


Figure 3.1-46. Streamlines and separation bubble for SD7062 at $\alpha=15^\circ$.

UNCLASSIFIED

UNCLASSIFIED

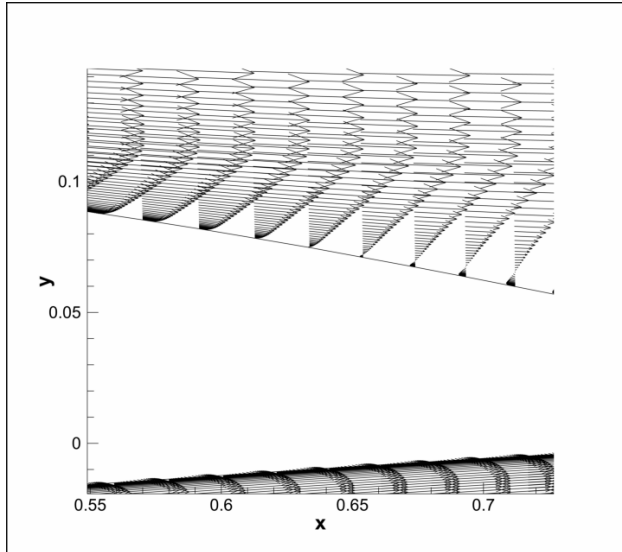


Figure 3.1-47. Velocity profile near trailing edge between $0.55c$ and $0.75c$.

With increasing angle of attack, by figures, pressure coefficient on upper surface decreases, which is what we want. This results in a higher lift. However, since we predict the stall to be around 15 degrees, we need to check flow field at 15 degrees of angle of attack. We have a separation bubble which moves upstream with increasing angle of attack, this results in stall. This separation bubble is caused by flow separation at $x = 0.65c$, which can be seen in the figure above.

3.1.1.2. Flap Configuration Selection

3.1.1.2.1. Literature Research

Relatively high wing loading leads to increase in fuel efficient in commercial as well as in small general aviation aircraft, but requires sophisticated high lift devices to keep the take-off and landing distances within acceptable limits. High lift devices can in turn have a detrimental effect on cruise performance, and thus fuel efficiency, in the form of additional parasitic drag of the high lift system mechanism fairings under the wing. In addition, the weight and complexity of the high lift system increases with its performance.

Panthera 260 HP	Cessna 172S Sky- hawk	Cessna 182 Turbo Skylane JT-A	Cessna TTx	Diamond DA-40 XLT	Cirrus SR22	Cirrus SR20	Piper Cherokee Archer	PA Beechcraft Bonanza
Plain flap	Slotted flap	Slotted flap	Slotted flap	Plain flap	Slotted flap	Slotted flap	Slotted flap	Slotted flap

Figure 3.1-48. General Aviation Aircrafts and Flap Types used

Looking at the literature, most of the smaller general aviation aircrafts have been designed with mostly plain flaps and slotted flaps. The simplest flap is the plain flap. Plain flaps hinge to the back of the wing, and they pivot down when you extend them. However, they're fairly limited in the amount of lift they can create. That's because as air moves over the wing, it loses energy and starts to separate from the wing. By extending flaps, the airflow separation is even more pronounced, creating a large wake behind the wing.

UNCLASSIFIED

UNCLASSIFIED

Slotted flaps are the most commonly used flaps today, and they can be found on both small and large aircraft. What makes them so special? Two things:

- They increase wing camber, like other flaps
- When extended, they open a slot between the wing and the flap

By opening a slot between the wing and the flap, high pressure air from the bottom of the wing flows through the slot into the upper surface. This adds energy to the wing's boundary layer, delays airflow separation, and produces less drag. The result is lots of additional lift, without the excessive drag.

In this part of the report, two configurations will be considered and analyzed with already chosen airfoil geometry. The flaps will be deflected at the %30 chord of the airfoil.

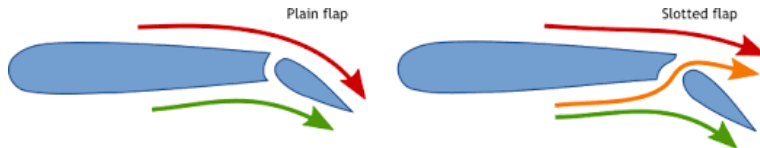


Figure 3.1-49. Airflow around an airfoil with Plain Flaps and Slotted Flaps

3.1.1.2.2. 2D Analysis and Flap Configuration Selection

Grid Refinement

In the previous chapter, we didn't have to deal with very complex flows around the airfoil, so structured mesh with less element numbers were enough to observe the flow around different airfoils. In this chapter, we will be dealing with somehow complex flows due to the high deflections rates of different types of flaps and more complex geometries. That's why, in this case it would be wiser to use unstructured mesh around a bit more complex geometries to observe the flow better. ANSYS meshing tool was used to create the mesh and adapting feature in ANSYS Fluent has been used to refine the important regions a bit further. Geometries were created in ANSYS Design Modeler tool.

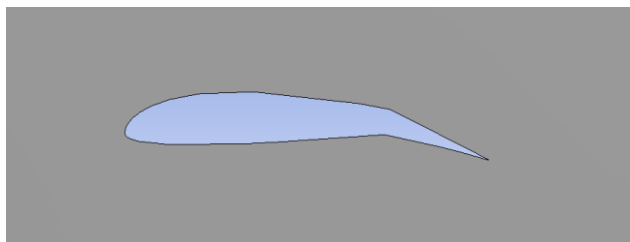


Figure 3.1-50. Geometry of SD 7062 Airfoil with Plain Flaps Deflected 15 Degrees at 30% Chord

UNCLASSIFIED

UNCLASSIFIED

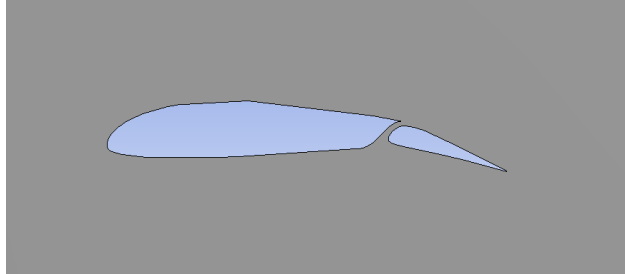


Figure 3.1-51. Geometry of SD 7062 Airfoil with Slotted Flaps Deflected 15 Degrees at 30% Chord

Design of the plain flaps was made simply placing a hinge at the 70% chord of the airfoil and rotating it around the hinge axis. For the design of the slotted flaps it was a bit more challenging since there are many types of slotted flaps that's been used in the literature. To create the geometry of the slotted flaps, the flaps that's been used in Cessna 172 Aircraft was inspired.



Figure 3.1-52. Cessna 172 with deflected flaps



Figure 3.1-53. Close up of slotted flaps of Cessna 172

Rhodes 32 St. Genese Airfoil with slotted flaps deflected 15 degrees was used to do the grid refinement. There are many information and data about the flapped airfoils in literature but almost all of them are unique cases. There was no possibility to compare the CFD solution data with experimental values. Since the flow is somehow complex than before, after the grid refinement grid is refined a bit further using the ANSYS Fluent adapt tool.

UNCLASSIFIED

UNCLASSIFIED

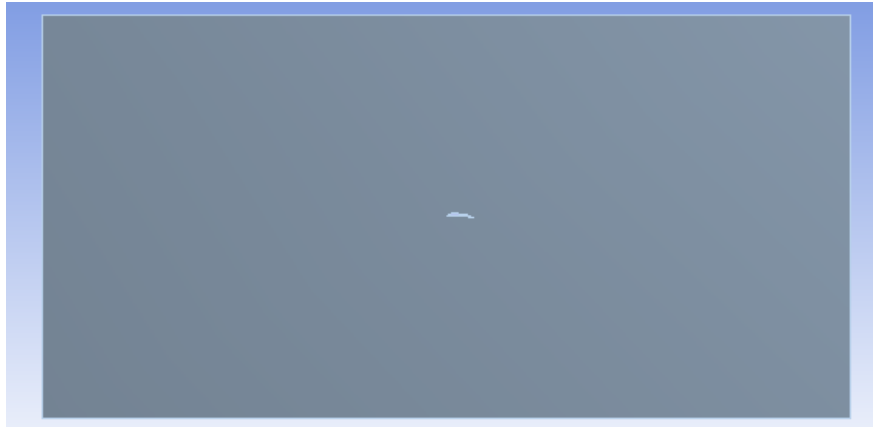


Figure 3.1-54. Fluid domain around the airfoil with flaps

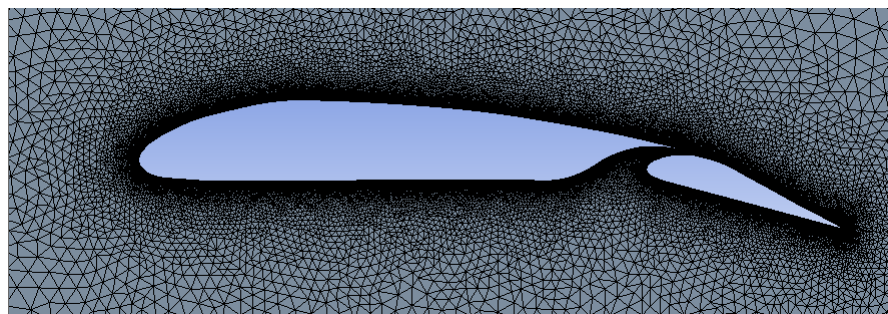


Figure 3.1-55. Meshing Around the Slotted Flapped Airfoil with deflection 15 degrees

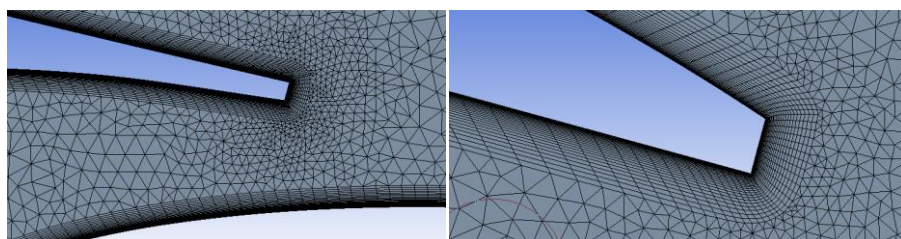


Figure 3.1-56. Close up to meshing at crucial parts

UNCLASSIFIED

UNCLASSIFIED

Table 3.1-32. Grid refinement with Rhodes St. Genesee 32 Airfoil with slotted flaps deflected 15 degrees at $\alpha=5^\circ$

	Number of Elements	Cl	Cd	Cl Error %	Cd Error %
Mesh 1	8000	0.150	0.203		
Mesh 2	15000	0.761	0.101	80.32%	100.74%
Mesh 3	25000	1.253	0.058	39.25%	73.14%
Mesh 4	38000	1.480	0.046	15.35%	25.70%
Mesh 5	57000	1.660	0.040	10.85%	16.23%
Mesh 6	104000	1.680	0.039	1.19%	3.45%
Mesh 7	147000	1.701	0.037	1.28%	3.52%

Since the flow is somehow complex than before, after the grid refinement grid is refined a bit further using the ANSYS Fluent adapt tool. A rectangular shaped around the airfoil was chosen to adapt and iterated in ANSYS Fluent to refine it and element numbers are further increased.

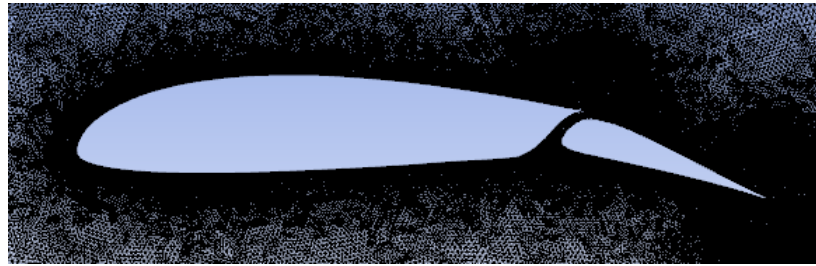


Figure 3.1-57. Refined mesh through the ANSYS Fluent

3.1.1.2.3. Set up and Results

Flaps mostly used when the aircraft is at take-off or landing situation, otherwise the flaps decreases the efficiency. That's the analyzes were held at the atmospheric conditions of 0 ft altitude, again k-w SST turbulence model is used and coupled solver was preferred for this case. Plain and slotted flap cases with 15 and 30 degrees deflection were analyzed by using the same mesh structure obtained in grid refinement part, results and comparisons are shown below.

UNCLASSIFIED

UNCLASSIFIED

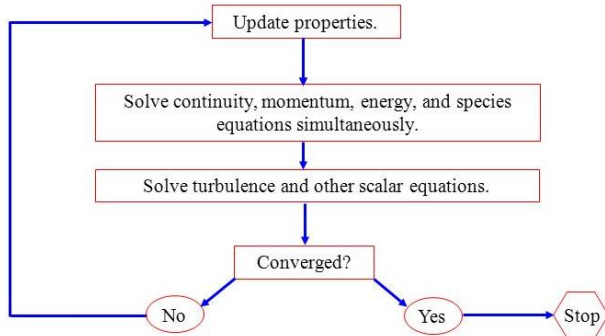


Figure 3.1-58. Coupled Solution Procedure

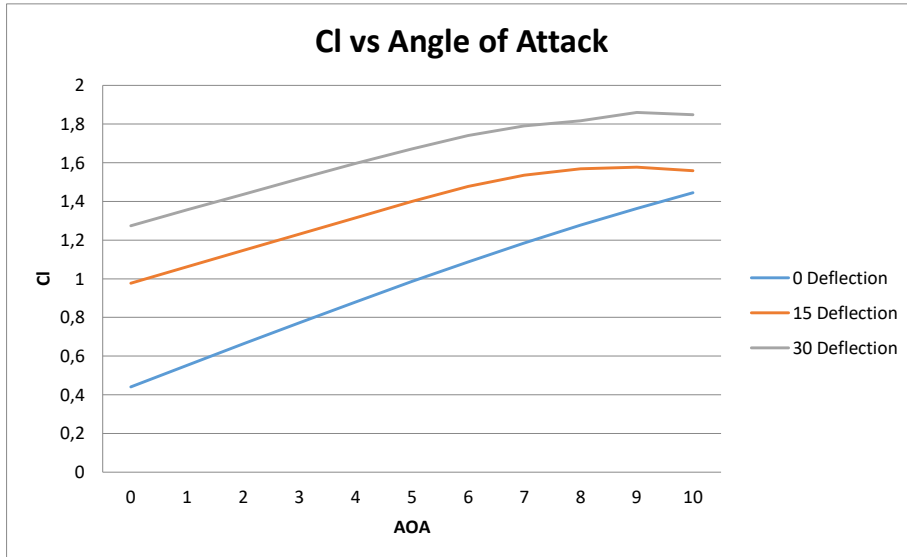


Figure 3.1-59. C_l versus α for Plain Flapped SD 7062 Airfoil with different deflection angles

UNCLASSIFIED

UNCLASSIFIED

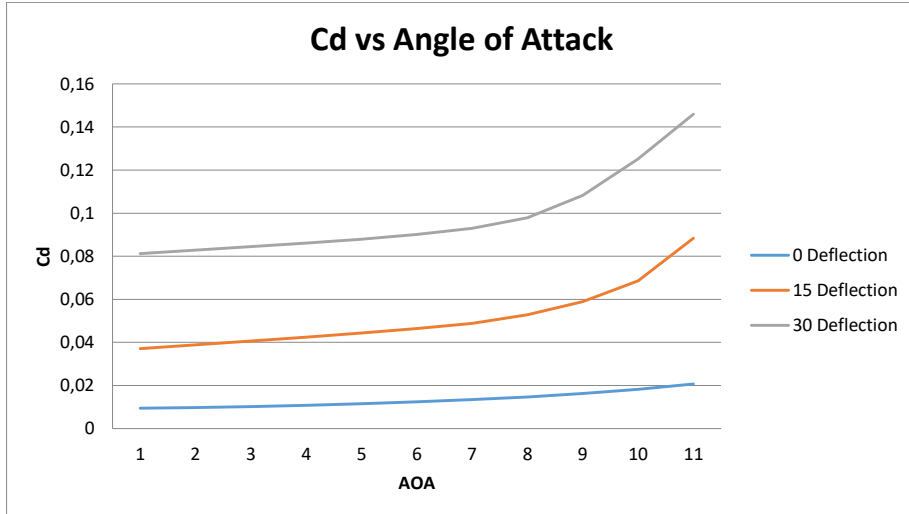


Figure 3.1-60. C_d vs Alpha of SD 7062 Airfoil Plain Flapped with Different deflections

According to the analysis, as the airfoil with plain flaps is deflected more and more both lift and drag coefficients kept increasing, by the time the stall angle decreases as the deflection is increased.

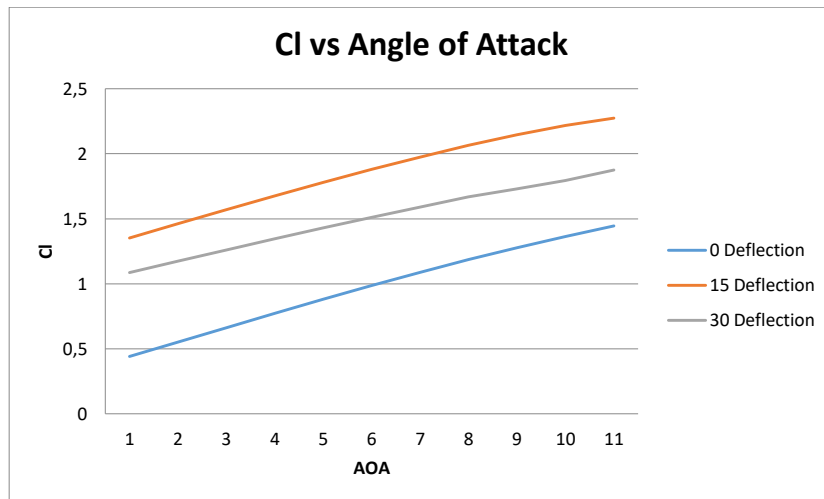


Figure 3.1-61. C_l vs Alpha of SD 7062 Airfoil Slotted Flapped with Different deflections

UNCLASSIFIED

UNCLASSIFIED

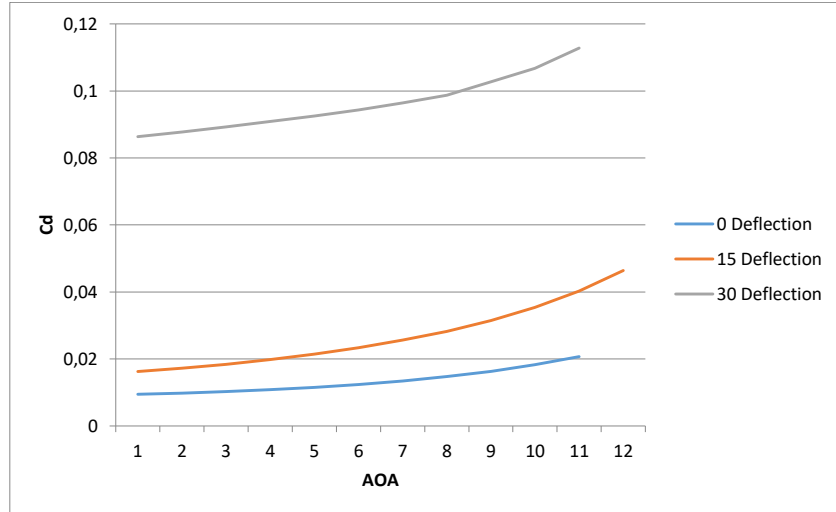


Figure 3.1-62. C_d vs Alpha of SD 7062 Airfoil Slotted Flapped with Different deflections

For the slotted flap case, although the graphs almost have the same attitude with plain flaps ones, values are mostly very different. Lift and drag coefficient for the slotted case also keeps increasing with the increasing deflection angle and the stall angle keeps decreasing while the deflection angle increased. Comparisons between two configurations are shown below.

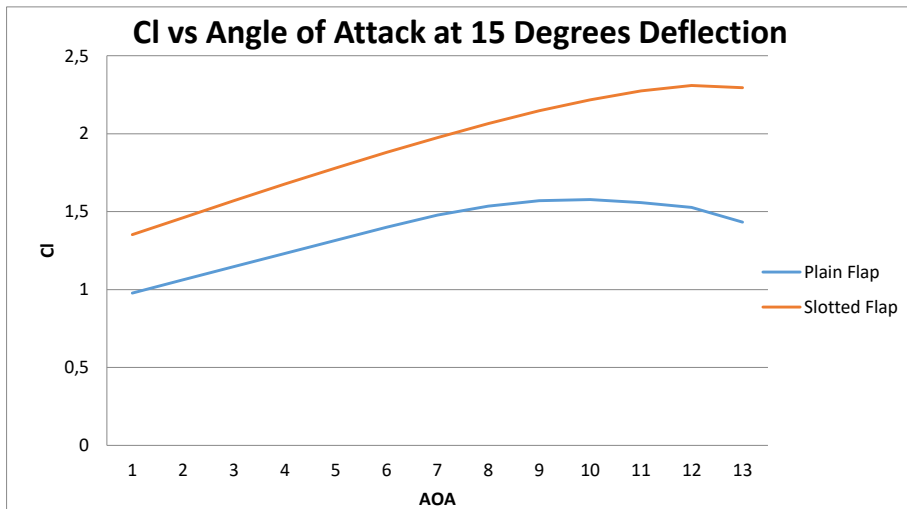


Figure 3.1-63. C_l vs Alpha of SD 7062 Airfoil with Plain and Slotted Flaps at 15 degrees of deflection

UNCLASSIFIED

UNCLASSIFIED

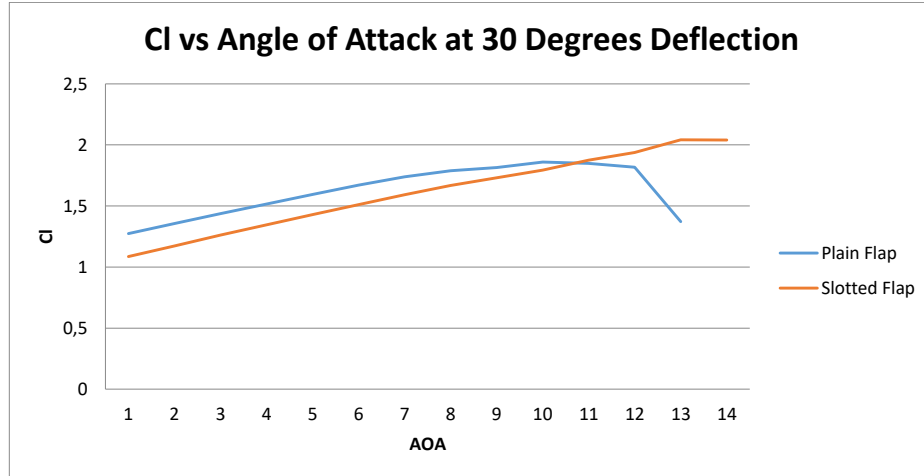


Figure 3.1-64. C_l vs Alpha of SD 7062 Airfoil with Plain and Slotted Flaps at 15 degrees of deflection

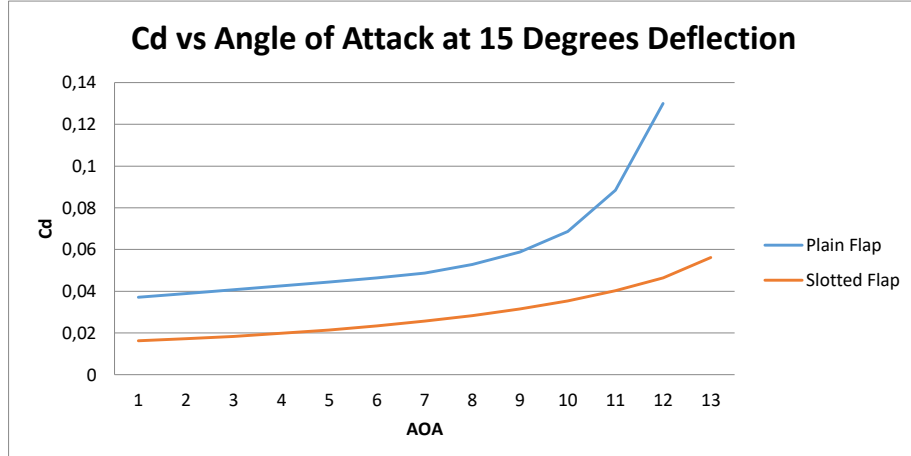


Figure 3.1-65. C_d vs Alpha of SD 7062 Airfoil with Plain and Slotted Flaps at 15 degrees of deflection

UNCLASSIFIED

UNCLASSIFIED

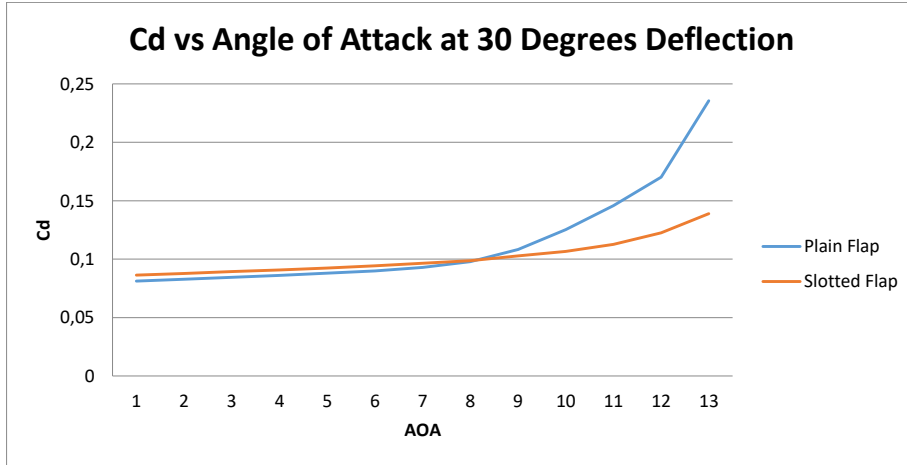


Figure 3.1-66. C_d vs Alpha of SD 7062 Airfoil with Plain and Slotted Flaps at 30 degrees of deflection

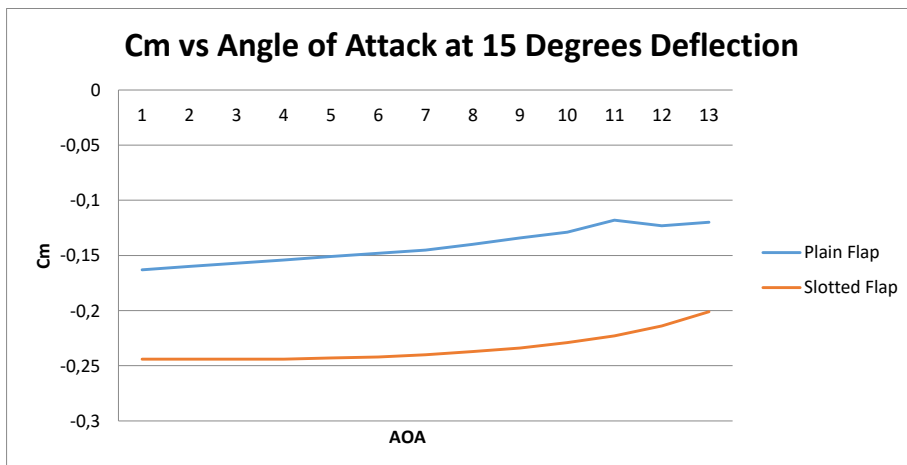


Figure 3.1-67. C_m vs Alpha of SD 7062 Airfoil with Plain and Slotted Flaps at 15 degrees of deflection

UNCLASSIFIED

UNCLASSIFIED

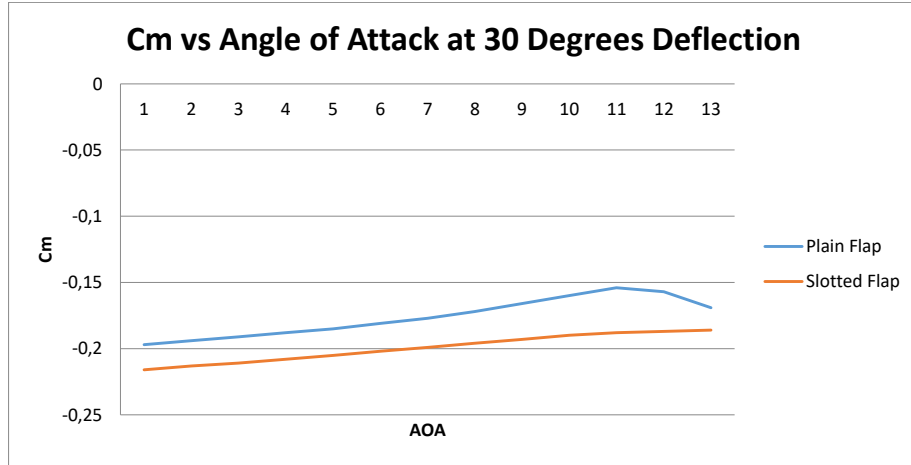


Figure 3.1-68. C_m vs Alpha of SD 7062 Airfoil with Plain and Slotted Flaps at 30 degrees of deflection

Plain flap is one of the simplest high lift devices. It operates as a moving aft part of the airfoil and is widely used as a control device in form of ailerons, elevators and rudders. The main difference is that in case of a high lift device, the flap deflections are much higher than in case of a control device. Pure Fowler motion of the flap means that the flap only translates rearward, extending the effective chord. A slotted flap will in practice almost always have both a Fowler motion and an angular motion. On the other hand it is possible to have a system with Fowler motion and no gap. Some flap mechanisms initially provide predominantly Fowler motion for use during take-off and climb while at larger flap extraction higher angular deflection is provided for use during approach and landing. It is important to recognize that C_l values are based on the clean airfoil chord length, i.e. with flap retracted. Therefore some increase in lift coefficient comes purely from extending the effective chord.

Comparing the lift coefficients between plain and slotted flaps, there is a difference around value of 0.3 between their $C_{l\max}$ values; slotted flaps also have the advantage when it comes to comparison of drag coefficients. Slotted flaps have better characteristics at lift and drag coefficients due to the gap between the airfoil and flap, and the increase in chord length. But, When redesigning the plain flap high lift system into a single-slotted flap system the design of the flap deployment mechanism has an important impact on the overall performance of the aircraft because of its weight and drag, the hinge point location was one of the design variables in the optimization routine where the plain flap has the advantage here rather than slotted flaps. However, looking at the data obtained unfortunately plain flaps configurations are not likely to meet the needs of our VLA's C_l and $C_{l\max}$ values. In this stage, it is decided to go with slotted flaps that the detailed design of them to be decided at later stages.

Flaps analysis also completed again with the new one and data is presented in Appendix A. Pressure and velocity counters of slotted flapped SD 7062 Airfoil is shown below.

UNCLASSIFIED

UNCLASSIFIED

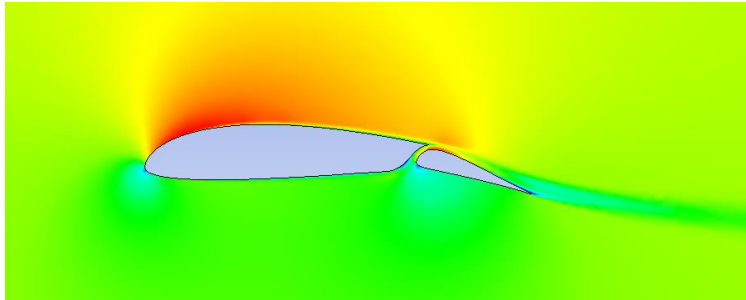


Figure 3.1-69. Velocity Distribution over SD 7062 Airfoil with 15 degrees deflected slotted flap at $AOA=0$

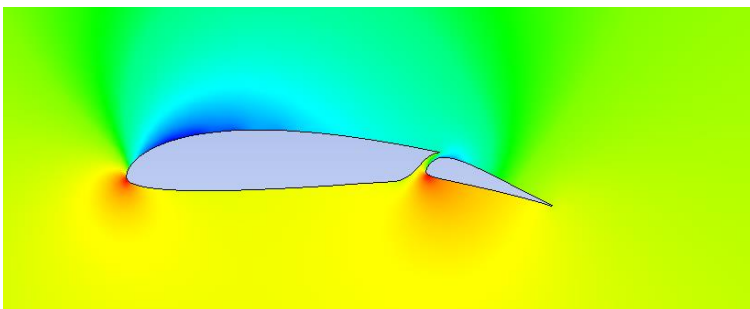


Figure 3.1-70. Pressure Distribution over SD 7062 Airfoil with 15 degrees deflected slotted flap at $AOA=0$

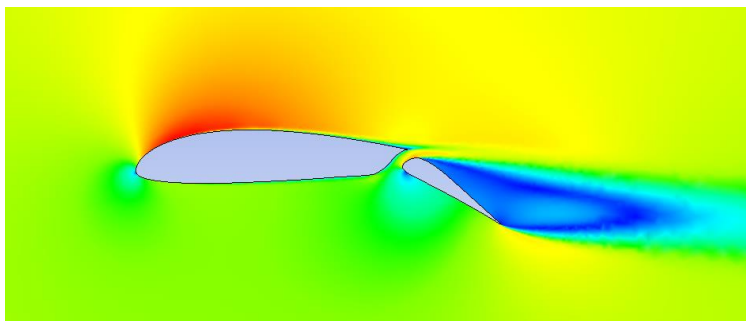


Figure 3.1-71. Velocity Distribution over SD 7062 Airfoil with 30 degrees deflected slotted flap at $AOA=0$

UNCLASSIFIED

UNCLASSIFIED

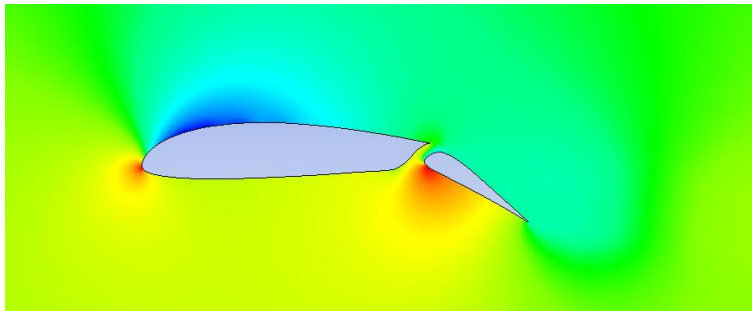


Figure 3.1-72. Pressure Distribution over SD 7062 Airfoil with 30 degrees deflected slotted flap at AOA=0

3.1.1.3. Wing Analysis

Aim of this section is to briefly introduce the procedures of CFD analysis of 3D wings with no flaps and different flap deflections. For three conditions that are cruise, takeoff and landing, required incidence and angle of attacks will be obtained and weight requirements will be observed. Computational tools like ANSYS Fluent, ANSYS Meshing were used to gather the necessary data to compare the different cases and choose the best options eventually. Wing configurations with accurate flap deflections according to flight conditions will be analyzed that are cruise, takeoff and landing respectively. Airfoil section has already been decided in this stage (SD 7062) and with necessary parameters like taper, span that has been already obtained in initial sizing part has been used. Firstly, wing incidence angle will be decided to fulfill the cruise conditions and then flap deflections and angle of attacks to fulfill the takeoff and landing requirements.

First, the geometry for the wing structure has been obtained by using Design Modeler. Required parameters were already obtained at initial sizing part. In this part of the analysis only exterior surfaces of the design were important to obtain the results. Then, fluid domain was created around the wing and it was analyzed by using ANSYS Fluent. Outputs were discussed. Same procedure was held to analyze different flap deflected wing structures as an aerodynamic perspective only. To this point in our aerodynamic discussions, we have been working mainly in a two-dimensional world, from now on the analyses of a finite wings will be carried out.

3.1.1.3.1. Cruise Condition

It is planned that our very light aircraft will be in trim condition at atmospheric conditions of 5000 ft and speed of 160 ft/s. In trim condition we expect the aircraft to accomplish to cruise first and then cruise with maximum efficiency. In this part only half span of the wing is analyzed with these conditions to fulfill the requirements. Due to the absence of vertical location constancy, we expect the generated lift force to be equal to total weight of the aircraft.

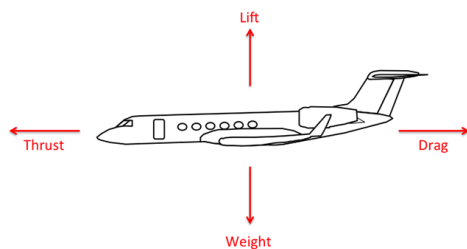


Figure 3.1-73. In trim condition generated lift force will be equal to the total weight

UNCLASSIFIED

UNCLASSIFIED

Geometry and Mesh

As it was mentioned before the wing parameters were already obtained in initial sizing process. In this step the flap deflection is taken to be zero.

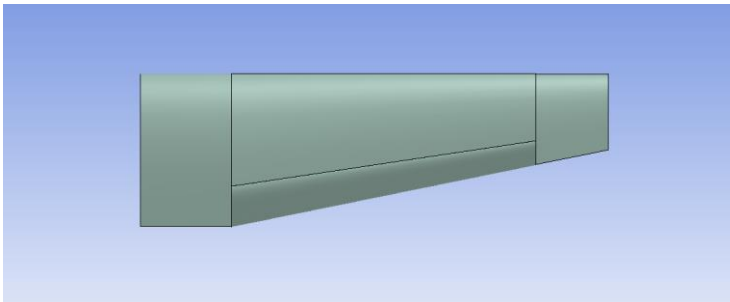


Figure 3.1-74. Top view of wing geometry

Half span of 16.15 ft., Root Chord of 5.32 ft., Tip Chord of 2.66 ft. and %80 of the wing is tapered with the ratio of 0.5.

3D Fluid domain was created around the wing. Fluid domain boundary dimensions were at least 15 times of the chord length to capture the flow better. To intensify the mesh around the wing and use the body of influence option in meshing part a box almost having the similar shape as the wing were created.

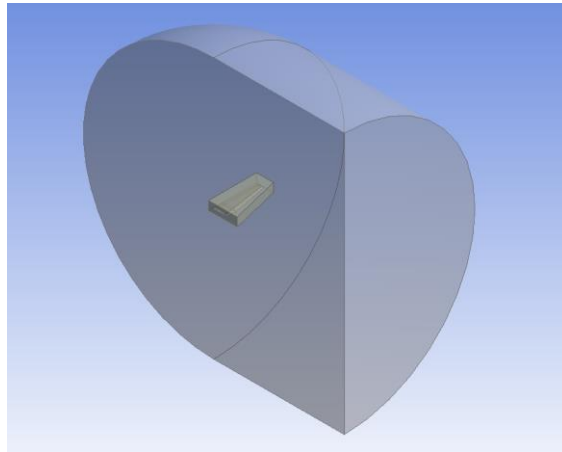


Figure 3.1-75. Fluid domain around the wing and sizing box

Unstructured mesh was created in the fluid domain. To accomplish the accurate mesh sizing around the wing, wing surface were separated in different faces and sized separately. Important parts like leading edge and near the trailing edge were meshed more densely than other parts of the wing. Totally around 4 million elements were created in the domain.

UNCLASSIFIED

UNCLASSIFIED

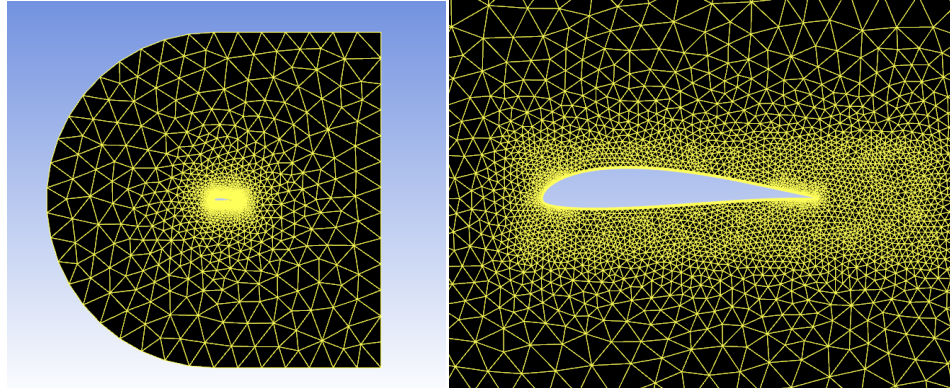


Figure 3.1-76. Mesh sizing around the wing at the symmetry view

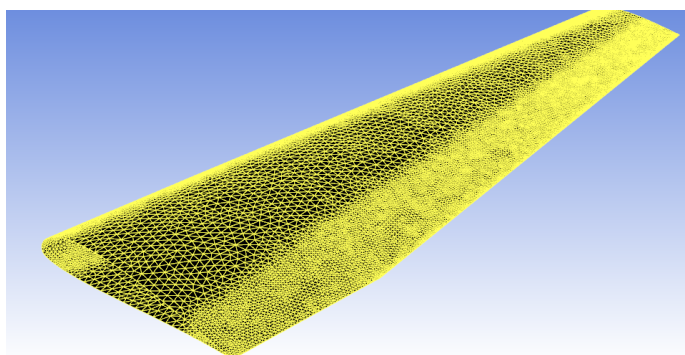


Figure 3.1-77. Surface mesh on the wing

Set Up and Results

All calculations were made with the atmospheric conditions of 5000 ft. altitude, 160 ft./s Speed. The governing equations by solved by a turbulence model called K-omega (k-w). In this part, results were also compared with 2D analysis of the same airfoil SD7062.

UNCLASSIFIED

UNCLASSIFIED

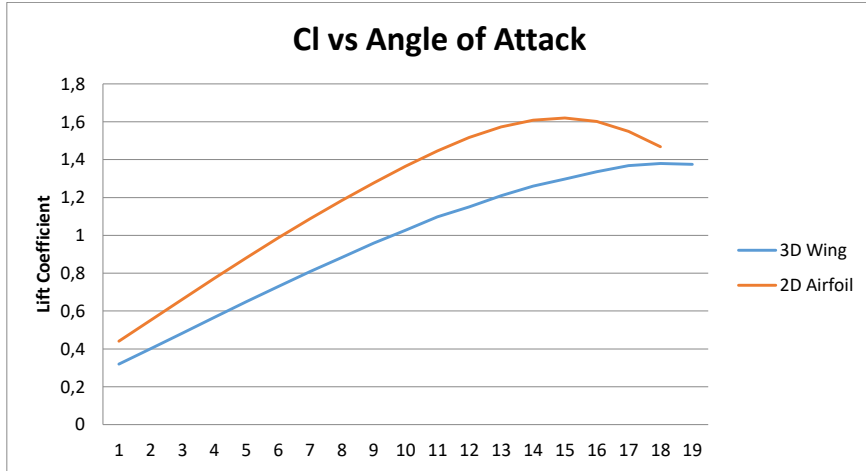


Figure 3.1-78. Change of lift coefficient with Angle of Attack for 3D Wing and 2D airfoil

Aspect ratio is a measure of the slenderness of a wing; a long thin wing has a high aspect ratio compared with a short stubby wing of low aspect ratio. With this in mind, return to the case of the 2D and 3D wings shown in figure 78. The 2D wing is the equivalent of an infinite span wing and, as such, one can say it has an infinite aspect ratio. The 3D wing has a finite aspect ratio. Figure 78 shows the coefficient of lift curves obtained for both wings. Readily evident is the effect that the tip vortices (shown in figure 79) have in creating the additional downwash at the wing. Resulting in less maximum lift coefficient and also resulting in an increase at the stall angle due to the delay of the separation.

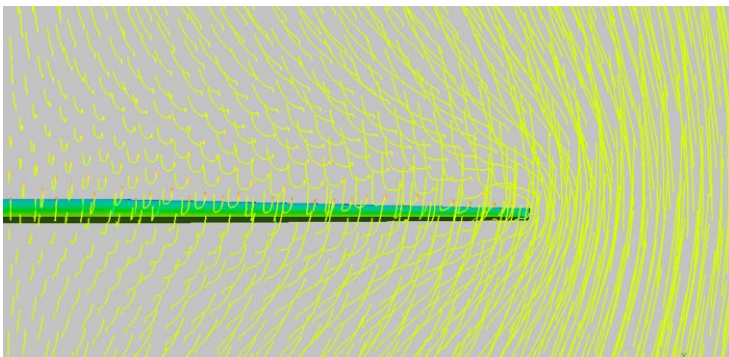


Figure 3.1-79. Tip vortices obtained from CFD Results

CL, CD and CM values are shown at Appendix A, for the first 5 degrees of angle of attack total forces have been calculated. According to the calculations for our aircraft to trim at 0 angle of attack and at 5000 ft. with 160 ft./s speed, wings should have around 3 degrees of incidence angle. At 3 degrees of angle of attack half wing will be generating around 4300 N of force that means wings

UNCLASSIFIED

UNCLASSIFIED

totally will be able to carry around 8600 N of total weight. Considering the aircraft will be around 720-750 Kg and there will be a loss at the total lift force due to the fuselage effect, that results seem accurate.

Table 3.1-43. Coefficients of the wing at 3 degrees of angle of attackAOA	CL	CD	CM	Force
3	0,130	0,0156	0,150	4300 N

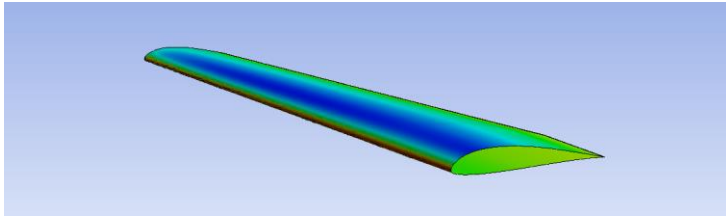


Figure 3.1-80. Pressure counters on the wing at 3 degrees of angle of attack

3.1.1.3.2. Takeoff and Landing Conditions

In the previous stages at airfoil and flap configuration selection part, it was decided to go on with the slotted flap design since the plain flap designs couldn't achieve the desired lift coefficient values. In this stage our 3D wing was analyzed with slotted flap design with 10,15 and 30 degrees of flap deflections for different angle of attacks. Due to the poor performances of the computers with around 10 million elements including meshes, the analyzes mostly held at the angle of attacks where the possible takeoff and landing takes place that are 12 degrees of angle of attack to 17 degrees for the wing and 9 degrees of angle of attack to 14 degrees for the whole aircraft (considering the incidence angle). Since in takeoff and landing conditions the aircraft cannot reach its maximum speed which is in this case almost half of it, the wings should have some flap deflections to increase the lift coefficients to achieve the required lift force generation.

Geometry and Mesh

Geometries were created on the same wing geometry, flaps were deflected around %30 of the chord length and the flap size is the %65 of the span along the span wise. Same fluid domain and similar sizing methods were used as it was described in previous chapter.

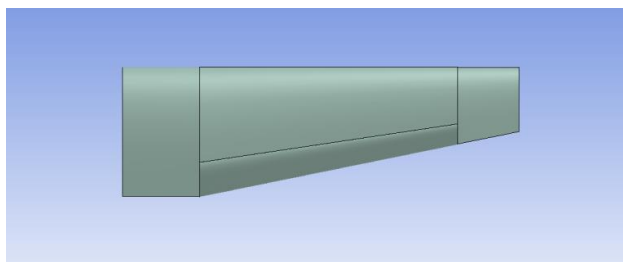


Figure 3.1-81. Top view of the wing and flap geometry

UNCLASSIFIED

UNCLASSIFIED

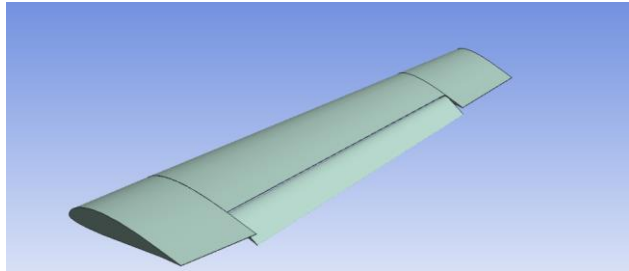


Figure 3.1-82. Isometric view of the wing and flap geometry with 15 degrees of deflection

To capture the complex flows behind the flaps due to high deflection angles, element sizes around the flaps were also increased. Rest of the mesh was almost same as the wing meshing and the flap design was inspired from the very light sport aircraft of Bristell. Flaps only start with the tapered region of the wing and along with the span their size is around %65 of the span of the wing, leaving %15 of the span for the ailerons which will be enough to satisfy the requirements according to the other calculations were done on other parts.

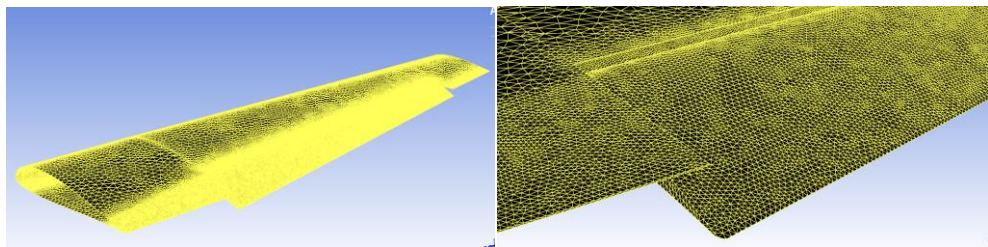


Figure 3.1-83. Surface mesh on the 15 degrees flap deflected wing

Totally 6.4 millions of elements have been created in the domain which made the calculations harder than before and that's why only limited numbers of angle of attacks could have been analyzed.

Set Up and Results

All calculations were made with the atmospheric conditions of 0 ft. altitude, 85 ft./s Speed. The governing equations by solved by a turbulence model called K-omega (k-w).

UNCLASSIFIED

UNCLASSIFIED

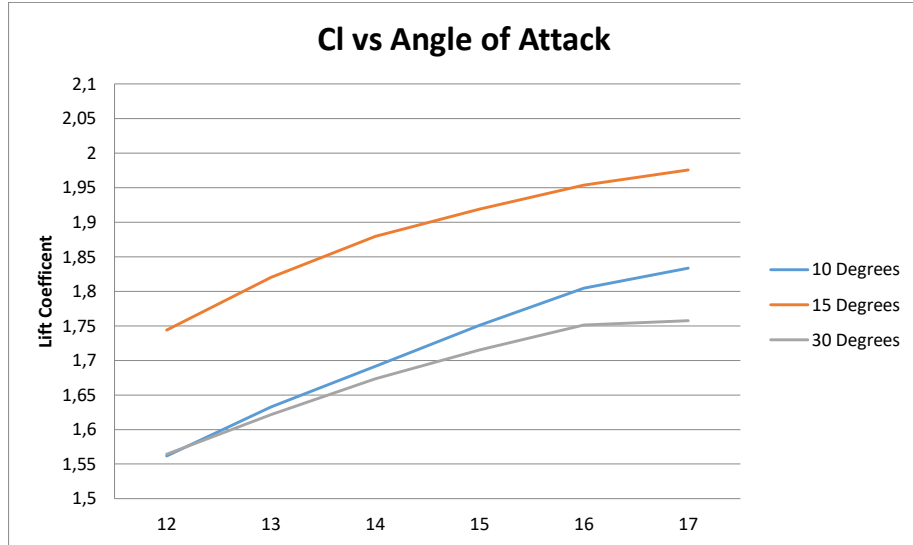


Figure 3.1-84. Lift coefficient of the wing vs Angle of attack with different flap deflections

Observing the results, we conclude that for our case as the flaps were kept deflected until 20 degrees the lift coefficient for the same angle of attack also keeps increasing. However as the flaps were deflected more than 20 degrees the separation begins to have high effects on the lift and resulting in a decrease.

Firstly, considering the take-off conditions what we want is high lift coefficients along with low drag coefficients. Comparing two cases where the flaps are deflected 10 degrees and 15 degrees, in both cases it is possible to achieve takeoff requirements. In literature most of the very light aircrafts takeoff moment occurs at angle of attacks of 10 to 15 degrees. In this case, keeping in mind that we need also lower drag forces, it seems possible to achieve takeoff requirements with 10 degrees of flap deflections and 10 degrees of angle of attack of the aircraft. Wings having 3 degrees of incidence and aircraft is having 10 degrees of angle of attack results in 4139 N of forces for half wing which is enough to carry out the takeoff.

Table 3.1-54. Coefficients and generated force of the half wing at 13 degrees of angle of attack with 10 degrees of flap deflection

AOA	CL	CD	CM	Force
13	1,56	0,127	-0,31	4139 N

UNCLASSIFIED

UNCLASSIFIED

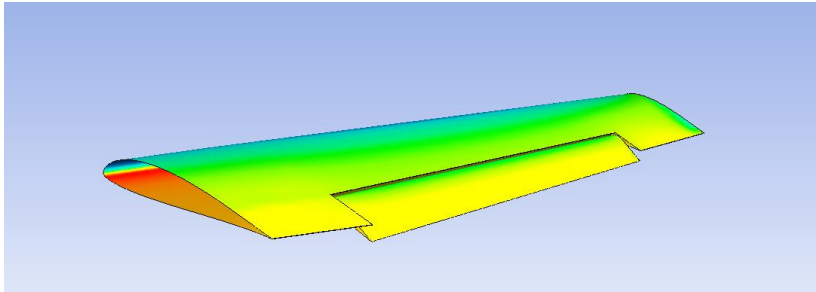


Figure 3.1-85. Isometric view of the pressure counters on the wing with 15 degrees of flap deflections

As it was mentioned before, total lift coefficient of the wing starts to decrease as the flap deflections are kept increasing above 20 degrees. However, this is something that can be turned into our advantage. As the landing occurs aircraft will also need more drag forces to slow down, in this case higher flap deflections for the flaps that are above 20 degrees will act like spoilers and generate required forces, but still the wing should be generating enough forces to carry out the landing. In this case, it seems possible to achieve the landing requirements with 30 degrees of flap deflections and 10 degrees of angle of attack of the aircraft. Wings having 3 degrees of incidence and aircraft is having 10 degrees of angle of attack with 30 degrees of flap deflections results in 4142 N of forces for half wing which is enough to carry out the landing.

Table 3.1-65. Coefficients and generated force of the half wing at 13 degrees of angle of attack with 13 degrees of flap deflection

AOA	CL	CD	CM	Force
13	1.62	0.191	-0.33	4142 N

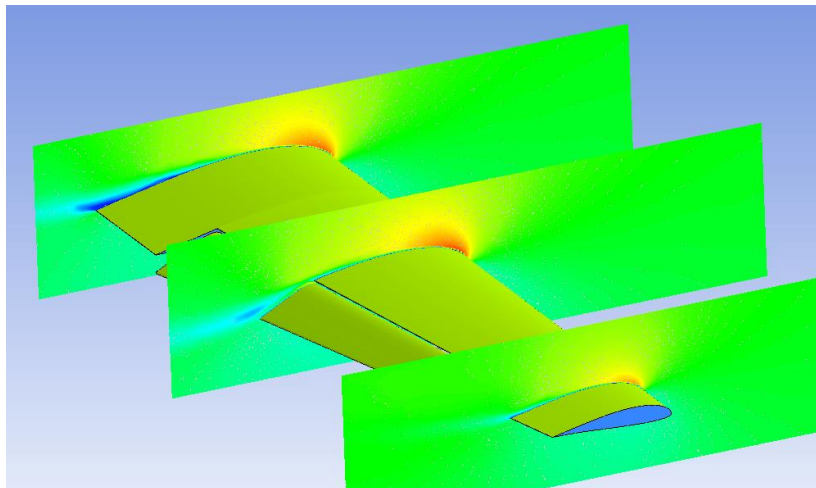


Figure 3.1-86. Velocity counters on the 15 degrees flap deflected wing for three different sections.

UNCLASSIFIED

UNCLASSIFIED

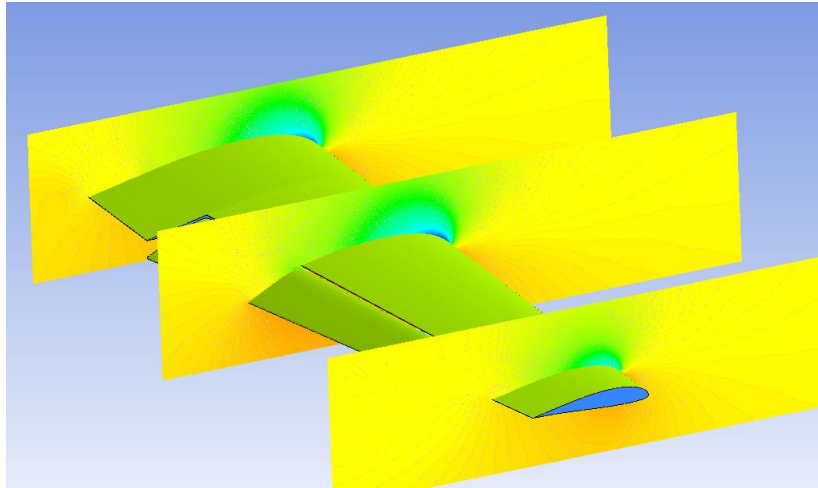


Figure 3.1-87. Pressure counters on the 15 degrees flap deflected wing for three different sections

3.1.2. Flight Mechanics

In this project a geometry is designed by using methods introduced in the aerodynamic design books and different geometric alternatives are analyzed depending on trade off studies. First we try to obtain a database about competitor aircrafts. Then general concept for aircraft is determined.

As a result of feasibility phase, configuration of aircraft is decided as low wing, conventional tail and tricycle landing gear.

As a starting point, mission profile and technical requirements are determined.

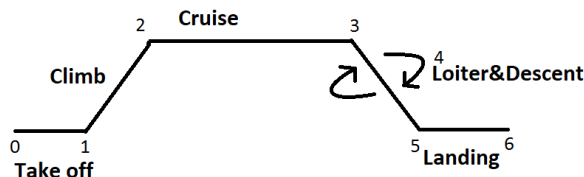


Figure 3.1-88. Simple Cruise Mission Sketch

UNCLASSIFIED

UNCLASSIFIED

3.1.2.1. Design Requirements

- Stalling speed in landing configuration of less than 83 km/h (45 knots).
- Maximum takeoff weight of not more than 750 kg.
- Non aerobatic operation, i.e. maneuvers should not require bank angles more than 60°.
- Number of seats, including the pilot seat not to be more than 2.
- Fixed landing gear
- Payload weight will be 25 kg
- Range will be greater than 500 km (aimed as 1200km)
- Cruise speed: 150 km/h (81 knots) (aimed more than 90 knots)
- Service ceiling will be 7500 ft.
- Maximum endurance to be greater than 2 hours (aimed as 5 hours)
- Takeoff distance not to be more than 500 m at sea level
- Landing distance not to be more than 1000 m at sea level
- G limits: +3.8 / -1.5
- Cruise altitude will be 3000ft (aimed as 5000ft)

3.1.2.1.1. Weight Fraction

As a first estimate, weight is calculated with weight fraction method. In order to calculate take off weight, following formula is used.

$$W_0 = W_{crew} + W_{payload} + W_{fuel} + W_{empty}$$

$W_{payload}$: 25 kg

W_{crew} : 170 kg

Calculation of Empty Weight Fraction

We have a formula to calculate the empty weight to take-off gross weight ratio given in the book (Raymer 1992) as following:

$$\frac{W_e}{W_0} = A * W_0^c * K_{vs}$$

The constants K_{vs} , A and c are selected from the table below:

UNCLASSIFIED

UNCLASSIFIED

$W_e/W_0 = AW_0^C K_{vs}$	<i>A</i>	<i>C</i>
Sailplane—unpowered	0.86	-0.05
Sailplane—powered	0.91	-0.05
Homebuilt—metal/wood	1.19	-0.09
Homebuilt—composite	0.99	-0.09
General aviation—single engine	2.36	-0.18
General aviation—twin engine	1.51	-0.10
Agricultural aircraft	0.74	-0.03
Twin turboprop	0.96	-0.05
Flying boat	1.09	-0.05
Jet trainer	1.59	-0.10
Jet fighter	2.34	-0.13
Military cargo/bomber	0.93	-0.07
Jet transport	1.02	-0.06

K_{vs} = variable sweep constant = 1.04 if variable sweep
= 1.00 if fixed sweep

Figure 3.1-89. Constants for empty weight fractions

The constants taken from the tables is chosen with respect to homebuilt metal/wood type aircraft.

Calculation of Fuel Weight Fraction

Fuel weight fraction of the simple cruise mission can be calculated by these equations:

$$W_6/W_0 = W_6/W_5 * W_5/W_4 * W_4/W_3 * W_3/W_2 * W_2/W_1 * W_1/W_0$$

The numbers in the equation represent the mission points given at the Figure 89. According to this equation we can calculate fuel weight fraction as follows:

$$(W_f/W_0) = 1.06 * (1 - W_6/W_0)$$

By involving (1.06) coefficient, we take account extra 6% reserve or trapped fuel. To calculate mission segment weight fraction we benefit from historical trend and formulations.

Mission segment weight fractions:

- (0-1): Engine start, warmup, taxi and takeoff (historical trend):
 $W_1/W_0 = 0.97$

- (1-2): Climb (historical trend):
 $W_2/W_1 = 0.985$

- (2-3): Cruise (Breguet Range Equation):

$$\frac{W_3}{W_2} = e^{-\frac{RC}{V(L/D)}}$$

C: Power Specific Fuel Consumption --- L/D: Lift to Drag Ratio

- (3-5): Loiter (20 minutes) and descend (historical trend):
 $W_3/W_5 = 0.997$

- (5-6): Landing (historical trend):
 $W_5/W_6 = 0.995$

UNCLASSIFIED

UNCLASSIFIED

Specific fuel consumption:

$$C = \frac{Wf/time}{T} = c_p \frac{V}{\eta_p} = \frac{C_{bhp} * V_\infty}{550\eta_p}$$

According to (Raymer 1992), for a typical aircraft with a propeller efficiency of about 0.8. And C_{bhp} values as following table:

Table 3.1-76. Propeller Specific Fuel Consumption

Propeller: $C = C_{bhp} V / (550\eta_p)$ Typical C_{bhp} and η_p	Cruise	Loiter
Piston-prop (fixed pitch)	0.4/0.8	0.5/0.7
Piston-prop (variable pitch)	0.4/0.8	0.5/0.8
Turboprop	0.5/0.8	0.6/0.8

Lift to Drag Ratio:

Lift-to-drag ratio (L/D) is a measure of aerodynamic efficiency. L/D is a function of the wetted aspect ratio ($\frac{b^2}{S_{wet}}$). That's why we can use historical trend to find wetted aspect ratio. In order to determine wetted aspect ratio, Cessna Skyline RG can be taken as an example from the figure below:

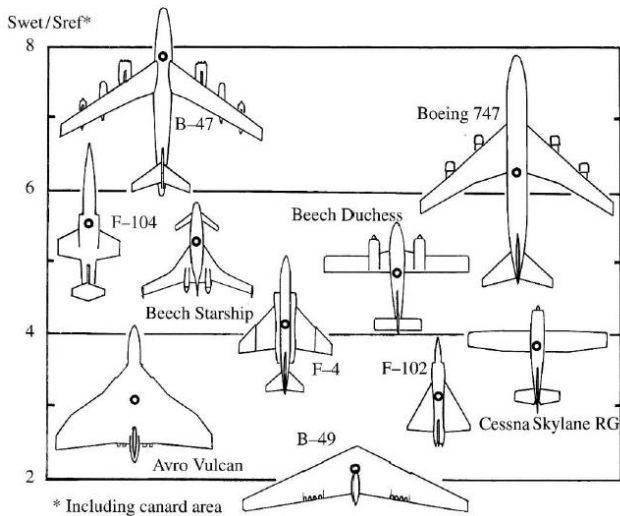


Figure 3.1-90. Wetted Area Ratios

According to this figure we choose the $Swet/Sref$ as 3.85. Also, AR is determined as 7.6 after the general competitor aircrafts research. By using these knowledge, we can find the L/D max from the following figure:

UNCLASSIFIED

UNCLASSIFIED

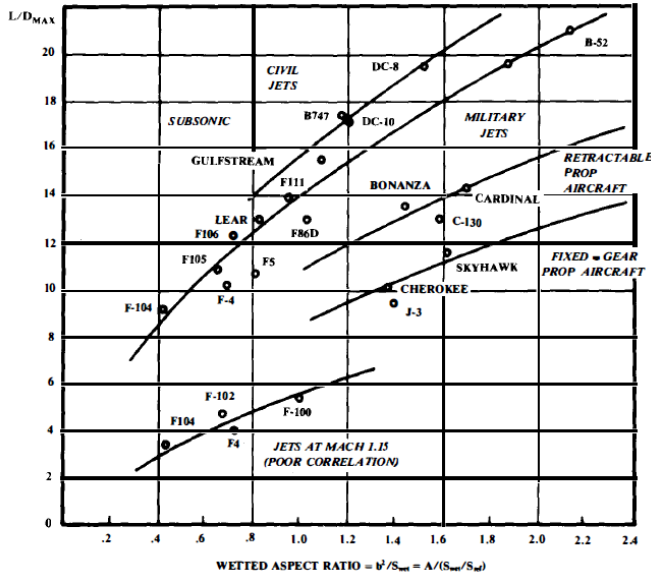


Figure 3.1-91. Maximum L/D Trends

To link between (L/D) and $(L/D)_{\text{max}}$ the figure below can be used. According to (Raymer 1992) for propeller driven aircrafts, to maximize cruise or loiter efficiency the aircraft should fly at approximately the velocity for maximum L/D .

Table 3.1-87. Lift to Drag Ratio for Different Missions

Jet Prop	Cruise		Loiter	
	$0.866 L/D_{\text{max}}$	L/D_{max}	L/D_{max}	$0.866 L/D_{\text{max}}$

UNCLASSIFIED

UNCLASSIFIED

From all these figures and formulations L/D cruise is determined as 12.62 as a first estimate. After necessary iterations, the take-off weight, which is used to begin the sizing of the aircraft, is found as 694 kg. All outputs are tabulated below.

Table 3.1-98. Weight fraction Outputs

	RANGE		SI
	CRUISE	LOITER	
Propeller Efficiency	0.8	0.7	
Cbhp	0.4	0.5	
PSFC(nud)	2.18182E-05	2.7E-05	
Speed(knot)	81	75	
Speed(feet/second) nud	136.7	126.5	
Range	3.94E+06		1200
Endurance		1200	
AR(competitor)	7.6		
Swt/Sref	3.85		
ARwet(nud)	1.97		
L/D max	12.6		
L/D (nud)	12.6	10.9	
Loiter fuel fraction(nud)		0.99	
Cruise fuel fraction(nud)	0.95		
Take off fuel fraction	0.97		
Climb fuel fraction	0.985		
Landing fuel fraction	0.995		
Total Mission Fuel Fraction(nud)	0.90		
Total Fuel Fraction (nud)	0.10		
Wcrew	374.7		
Wpayload	55.1		25
Empty weight fraction	0.56		
Total gross weight old	1653		
Total gross weight new	1288.5		694

Trade off Studies

Table 3.1-109. Altitude – Power required trade off

Altitude(ft/s)	Power required(hp)
6000	93.178
5000	91.76
4000	90.383
3000	89.038
2000	87.71
1000	86.42
0	85.15

UNCLASSIFIED

UNCLASSIFIED

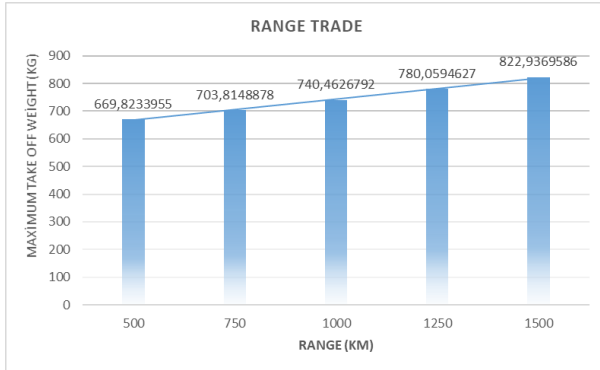


Figure 3.1-92. Range – Weight trade off

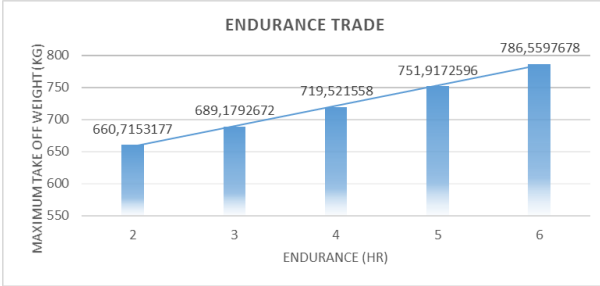


Figure 3.1-93. Endurance – Weight trade off

3.1.2.1.2. Sizing

At the beginning of the sizing part, an altitude condition calculator is coded in British unit system according to formulations below. As a result of these code, temperature, density, pressure and viscosity can change by depending on altitude only.

$$T = T_0(1 + Kh) \quad (1)$$

$$P = P_0(1 + Kh)^{5.2561} \quad (2)$$

$$\rho = \rho_0 (1 + Kh)^{4.2561} \quad (3)$$

$$\mu = 3.1767 * 10^{(-11)} T^{1.5} \frac{734.7}{(T + 216)} \quad (4)$$

$$K = -0.0000068756 \quad (5)$$

UNCLASSIFIED

UNCLASSIFIED

Table 3.1-[1140](#). Air Specifications at Cruise Altitude

	CRUISE
Altitude	5000
T₀	518.67
p₀	2116.23
p₀	0.00237713
kap	-6.8756E-06
T	500.8391627
p	1760.790707
rho	0.002048286
visc	3.64932E-07

Definition of Aspect Ratio

The aspect ratio is the wing span divided by the mean geometric chord. It is a measure of how long and narrow a wing is. A square wing would have an aspect ratio of 1! We can calculate the aspect ratio in several ways:

$$AR = \frac{b}{c_g} = \frac{b^2}{S} \quad (6)$$

$$S = \text{Geometric mean cord} * \text{Wing Span} \quad (7)$$

Geometric Mean Cord

The mean geometric chord is the chord of a rectangular wing having the same span and the same area as the original wing. It can be found for straight tapered wings in the following way:

$$c_g = \frac{c_r}{2}(1 + \lambda) = \frac{S}{b} \quad (8)$$

Aerodynamic Mean Cord

The mean aerodynamic chord is the chord of a rectangular wing with the span that has the same aerodynamic properties with regarding the pitch-moment characteristics as the original wing. It can be found for straight tapered wings in the following way:

$$c_{\text{mean aerodynamic}} = \frac{2}{3} c_r \frac{1 + \lambda + \lambda^2}{1 + \lambda} \quad (9)$$

Performance

For a vehicle in steady, level flight, the thrust force is equal to the drag force, and lift is equal to weight. Any thrust available in excess of that required to overcome the drag can be applied to accelerate the vehicle (increasing kinetic energy) or to cause the vehicle to climb (increasing potential energy).

UNCLASSIFIED

UNCLASSIFIED

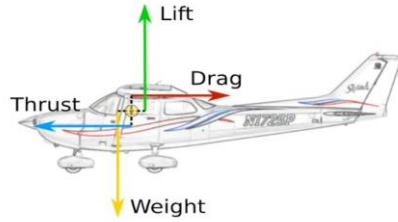


Figure 3.1-94. Aerodynamic Forces

For steady level flight we can link the forces as below:

$$T = D \quad (10)$$

$$L = W \quad (11)$$

$$T = \frac{W}{(L/D)} \quad (12)$$

We know that drag takes the form shown in Figure, being composed of a part termed parasitic drag that increases with the square of the flight velocity, and a part called induced drag, or drag due to lift, that decreases in proportion to the inverse of the flight velocity.

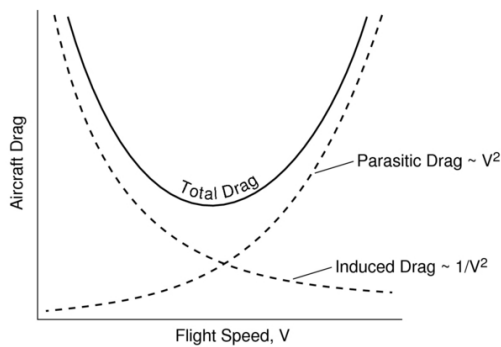


Figure 3.1-95. Drag Force Components

$$C_D = C_{D_0} + KCL^2 \quad (13)$$

$$D = \frac{1}{2}\rho V^2 S C_{D_0} + \frac{W^2}{\frac{1}{2}\rho V^2 S} \left(\frac{1}{\pi e A R} \right) \quad (14)$$

For a given weight, minimum drag condition satisfies the maximum L/D .This means that for the maximum flight efficiency and maximum range, drag should be minimum:

$$D_{min} = \frac{W}{(L/D)_{max}} \quad (15)$$

We can find a relationship for the maximum lift-to-drag ratio by setting:

UNCLASSIFIED

UNCLASSIFIED

$$\frac{d}{dC_L} \left(\frac{C_{D_0} + \frac{C_L^2}{\pi e AR}}{C_L} \right) = 0 \quad (16)$$

From this equality we can find formulas for CL, CD and velocity at minimum drag condition as follows:

$$C_{L,\min drag} = \sqrt{\pi e A R C_{D_0}} \quad (17)$$

$$C_{D,\min drag} = 2C_{D_0} \quad (18)$$

$$\left(\frac{C_L}{C_D}\right)_{\max} = \frac{1}{2} \sqrt{\frac{\pi e A R}{C_{D_0}}} \quad (19)$$

$$V_{\min drag} = \sqrt{\frac{W}{\frac{1}{2} \rho S C_{L,\min drag}}} = \left[4 \left(\frac{W}{S} \right)^2 \frac{1}{\rho^2} \frac{1}{C_{D_0}} \left(\frac{1}{\pi e A R} \right) \right]^{\frac{1}{4}} \quad (20)$$

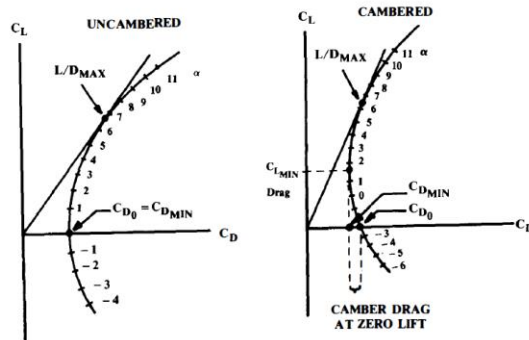


Figure 3.1-96. Maximum L/D for Cambered and Zero Camber Wing

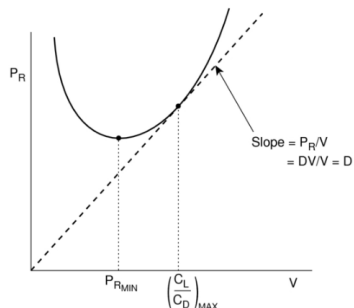


Figure 3.1-97. Min Power Required and Maximum Lift To Drag Ratio Point

UNCLASSIFIED

UNCLASSIFIED

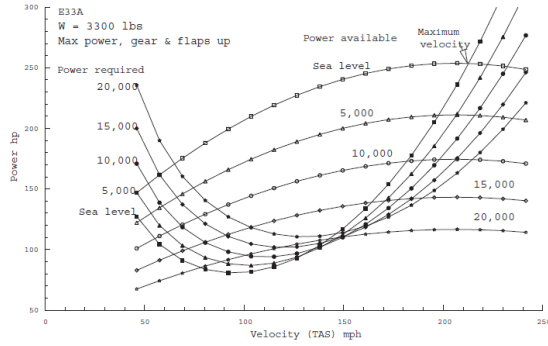


Figure 3.1-98. Available and Required Power Versus Velocity

Now we can look at the propulsion system requirements to maintain steady flight:

$$T_{req} = D \quad (21)$$

$$P_{req} = T_{req}V = DV \quad (22)$$

$$P_{req} = \frac{1}{2} \rho V^3 S C_{D_0} + \frac{W^2}{16 \rho V S} \left(\frac{1}{\pi e A R} \right) \quad (23)$$

$$C_{L,\min \text{ power}} = \sqrt{\frac{3 \pi e A R C_{D_0}}{16}} \quad (24)$$

$$C_{D,\min \text{ power}} = 4 C_{D_0} \quad (25)$$

$$\left(\frac{C_L}{C_D} \right)_{\min \text{ power}} = \sqrt{\frac{3 \pi e A R}{16 C_{D_0}}} \quad (26)$$

Thus the power required (for steady level flight) takes the form of Figure:

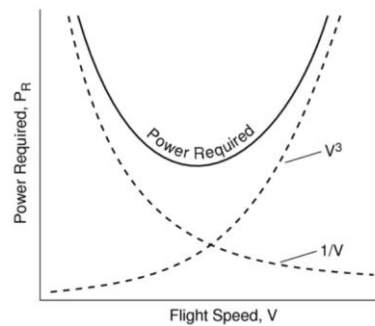


Figure 3.1-99. Power Required versus Flight Speed

The velocity for minimum power is obtained by taking the derivative of the equation for P_{req} with respect to V and setting it equal to zero:

UNCLASSIFIED

UNCLASSIFIED

$$V_{\min power} = \left[\frac{4}{3} \left(\frac{W}{S} \right)^2 \frac{1}{\rho^2} \frac{1}{C_D} \left(\frac{1}{\pi e A R} \right) \right]^{\frac{1}{4}} \quad (27)$$

As we will see shortly, maximum endurance occurs when the minimum power is used to maintain steady level flight. Maximum range is obtained when the aircraft is flown at the most aerodynamically efficient condition (max L/D – min drag).

Thus, the minimum power (maximum endurance) condition occurs at a speed which is 76 % of the minimum drag (maximum range) condition. The corresponding lift-to-drag ratio is 86.6% of the maximum lift-to-drag ratio.

$$\text{Endurance} = \frac{(L/D) \min power}{C \text{ loiter}} \ln \frac{W_0}{W_1} \quad (28)$$

$$\text{Range} = V \max range \frac{(L/D) \max}{C \max range} \ln \frac{W_0}{W_1} \quad (29)$$

Table 3.1-[1244](#). Range and Endurance Formulas for Different Conditions

<u>For constant altitude (ρ) and lift coefficient (C_L):</u> $\text{Range} = \frac{1}{c} \frac{2\sqrt{2}}{\sqrt{\rho S}} \frac{\sqrt{C_L}}{C_D} (\sqrt{W_0} - \sqrt{W_1})$ $\text{Endurance} = \frac{1}{c} \frac{C_L}{C_D} \ln \frac{W_0}{W_1}$	<u>For constant velocity (V) and lift coefficient (C_L):</u> $\text{Range} = \frac{V}{c} \frac{C_L}{C_D} \ln \frac{W_0}{W_1}$ $\text{Endurance} = \frac{1}{c} \frac{C_L}{C_D} \ln \frac{W_0}{W_1}$
<u>For constant velocity (V) and constant altitude (ρ):</u> $\text{Range} = \frac{V}{c\sqrt{k C_{D_0}}} \left[\tan^{-1} \frac{\sqrt{k}}{\frac{1}{2} \rho V^2 S \sqrt{C_{D_0}}} W_0 - \tan^{-1} \frac{\sqrt{k}}{\frac{1}{2} \rho V^2 S \sqrt{C_{D_0}}} W_1 \right]$ $\text{Endurance} = \frac{1}{c} \frac{1}{\sqrt{k C_{D_0}}} \tan^{-1} \left[\frac{1}{\left(\frac{2}{1 - \frac{W_1}{W_0}} - 1 \right)} \right]$	

Where: W_0 = Takeoff Weight W_1 = Landing Weight

To determine cruise speed, we should know also max range speed and Carson speed. Cruise speed is between these two speeds. We already calculated max range speed from above formulations. And according to (Gudmundsson, 2014) Carson speed equal to 1.32 times max range speed. According to 3D wing analysis, 2 degree incidence enable to have $C_L=0.45$. At 5000 ft, we reach this CL with 155 ft/s cruise speed. Depending on this knowledge and competitor study we can choose cruise speed about 1.25 times max range speed as 155 ft/s.

Also, according to (Sadraey, 2013) we can aim maximum cruise speed as 1.3 times cruise speed. That's why we have 194 ft/s aimed maximum cruise speed.

Power Loading

To calculate power required for maximum cruise speed we use the below equations:

$$\left(\frac{T}{W} \right)_{\text{cruise}} = \frac{1}{(L/D)_{\text{cruise}}} \quad (30)$$

UNCLASSIFIED

UNCLASSIFIED

$$\left(\frac{hp}{W}\right)_{take\ off} = \left(\frac{V_{cruise}}{550\eta_p}\right) \left(\frac{1}{(L/D)_{cruise}}\right) \left(\frac{W_{cruise}}{W_{takeoff}}\right) \left(\frac{hp_{takeoff}}{hp_{cruise}}\right) \quad (31)$$

At the above equation, take off to cruise power ratio can be found from engine data.

Together max cruise speed condition, sustained turn condition also has an importance with regard to choosing power required:

$$\frac{T}{W} = \frac{qC_{D_0}}{W/S} + \frac{W}{S} \left(\frac{n^2}{q\pi e AR} \right) \quad (32)$$

Bank angle is maximum 60 degree ($n=2$) for sustained turn condition.

As can be seen in the figure below, sustain turn determined power loading as 17.5 which is required 88 hp:

Table 3.1-[1342](#). Outputs Of Performance Parameter taken from Excel as Screen Shot

Level steady Flight condition at the altitude of	5000
CD = CD0+K*CL^2	0,0366496
CL=W/(q*S)	0,457137861
CL/CD= L/D	12,47320191
D = q*S*CD0+(K*W^2)/(q*S)	123,8670927
P_req = D*V	34,92199666
V_min power required = (K*(4/3)*(W/S)^2/(rho^2*CD0))^(1/4)	94,25740629
V_min Drag estimated (Vcruise)	123,0514442
D = W/(CL/CD)	112,4786313
(L/D) max =min drag condition	
CL min Drag=(3,14*e*AR*CD0)^,5	0,714277907
CD min Drag= 2*CD0	0,052
(CL/CD)max =(CL/CD)min drag	13,7361136
V_min drag= (2*W/(rho*S*CL_min drag))^,5	124,049723
V_min drag = V_max range	
Maximum speed at related altitude	193,8276921
(T/W)cruise = D/W	0,080171876
(hp_take off/hp_cruise) from engine data	1,075268817
Wcruise/Wtake off	0,95545
(hp/W)take off = (T/W)cruise*(Wcruise/Wtake off)*(hp take off/hp cruise)*(V_cruise/(550*propeller efficiency))	0,030961994
Required take off power for cruise = (hp/W) take off*Wtake off	50,06737872
Dynamic pressure for maximum velocity	38,4762117
D_max speed	160,3386404
D/W max cruise	0,103777762
hp/w take off for max cruise	0,050098092
P_req for maximum cruise speed	81,01158323
<hr/>	
Sustained Turn at the altitude of	5000
(T/W)	0,151871792
(hp/W)	0,05708986
Power required	88,20493255
Selected power loading	17,51624554

To calculate wing loading, first we need to know $C_{L_{max}}$ and Stall speed. Because stall condition has minimum wing loading. According to aerodynamic analysis and technical requirements Wing loading can be calculated as 11.78 and required reference area as 137.25 ft² from below equations 33 and 34.

UNCLASSIFIED

UNCLASSIFIED

Table 3.1-[1443](#). Wing Loadings for different conditions taken from Excel as Screen Shot

		S_reference
Wing Loading (Stall)	11,78179621	137,250655
Take off Parameter	159,5	
Wing Loading (Take off distance)	14,07469879	114,8912151
Wing Loading (Landing Distance)	43,4066976	37,25368055
Wing Loading (Cruise)	17,58919065	91,93482964
Wing Loading (Loiter)	30,46537187	53,07859864
Wing Loading(max ceiling)	16,29445387	99,23985543
Selected wing Loading	11,78179621	137,250655

$$W = L = \frac{1}{2} \rho V_{stall}^2 S C_{Lmax} \quad (33)$$

$$W/S = \frac{1}{2} \rho V_{stall}^2 C_{Lmax} \quad (34)$$

According to (Raymer 1992) for a wing of fairly high aspect ratio (over about 5), the maximum lift coefficient will be approximately 90% of the airfoil maximum lift coefficient at the same Reynolds number, provided that the lift distribution is nearly elliptical.

As a crude approximation to CL max for stall condition below Equation can be used.

As a crude approximation for wings of a fairly high aspect ratio is given in the equation below, where Clunflapped is the lift coefficient of the unflapped airfoil at the angle of attack at which the flapped airfoil stalls.

$$C_{Lmax} \cong 0.9 \left\{ (C_{lmax})_{flapped} \frac{S_{flapped}}{S_{ref}} + (C_l)_{unflapped} \frac{S_{unflapped}}{S_{ref}} \right\} \quad (35)$$

Prediction of Drag Coefficient

Equivalent Skin-Friction Method

The method for the prediction of the parasite drag (C_{D0}) enable us to know drag coefficient if we know wetted area of the aircraft. According to (Raymer 1992) for the single engine light aircraft equivalent skin friction coefficient (C_{fe}) can be predicted as 0.0055 from the figure below. To get wetted area of the aircraft OPENVSP software can be used. By having all this knowledge we can find the parasite drag coefficient as 0.0255.

$$C_{D0} = C_{fe} \frac{S_{wet}}{S_{ref}} \quad (36)$$

Table 3.1-[1544](#). Equivalent Skin Friction Coefficient

$C_{D0} = C_{fe} \frac{S_{wet}}{S_{ref}}$	C_{fe} -subsonic
Bomber and civil transport	0.0030
Military cargo (high upsweep fuselage)	0.0035
Air Force fighter	0.0035
Navy fighter	0.0040
Clean supersonic cruise aircraft	0.0025
Light aircraft – single engine	0.0055
Light aircraft – twin engine	0.0045
Prop seaplane	0.0065
Jet seaplane	0.0040

Calculation of Lift to Drag Ratio

UNCLASSIFIED

UNCLASSIFIED

During cruise, the lift equals the weight, so the L/D can be expressed as the inverse of the drag divided by the weight:

$$\frac{L}{D} = \frac{1}{\frac{qC_{D_0}}{W/S} + \frac{1}{S} \frac{1}{q\pi e AR}} \quad (37)$$

According to (Raymer 1992) the Oswald efficiency factor is typically between 0.7 and 0.85. More realistic estimation equations based upon actual aircrafts are presented below:

$$\text{Straight - Wing Aircraft: } e = 1.78(1 - 0.045A^{0.68}) - 0.64 \quad (38)$$

By looking this information, we calculate Lift to drag ratio for the aircraft as 12.473.

Airfoil and Wing Planform Analysis

For the airfoil selection, CFD analyses is completed and SD7062 type airfoil is selected. For the flap configuration, plain flap and slotted flap are analyzed separately. And we see slotted flap is more usable for our concept. Also airfoil is analyzed with XFLR5 program. And the results are plotted as below.

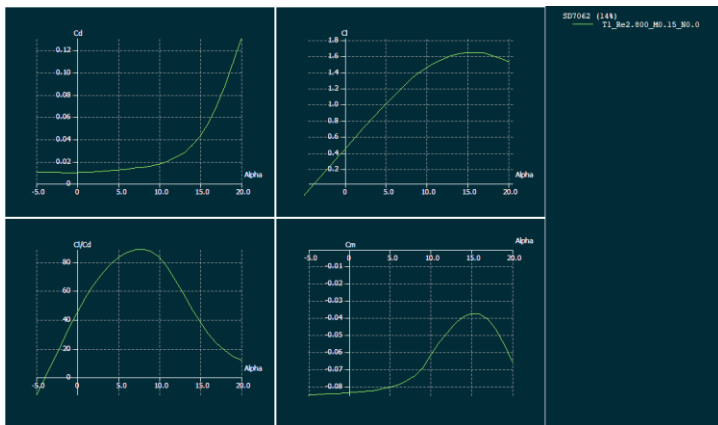


Figure 3.1-100. SD7062 airfoil XFLR5 analysis

$$C_{l_{max}} = 1.64$$

$$C_{l_{\alpha=0}} = 0.445$$

$$C_{d_{\alpha=0}} = 0.01$$

$$C_{m_{\alpha=0}} = 0.083$$

In the low wing configuration, stability of the aircraft reduces and dihedral is needed in the regard of stability to compensate low wing effect. That's why, we determined to use 5o dihedral.

For the most efficient lift distribution on the wing, taper ratio is calculated as 0.47 and selected as 0.5. Since VLA type aircrafts fly at very low speeds with respect to supersonic jets, sweep angle is predicted as zero degree at quarter chord.

To determine the wing planform, different wing geometries is analyzed aerodynamically by using XFLR5 program and tapered wing is selected:

UNCLASSIFIED

UNCLASSIFIED

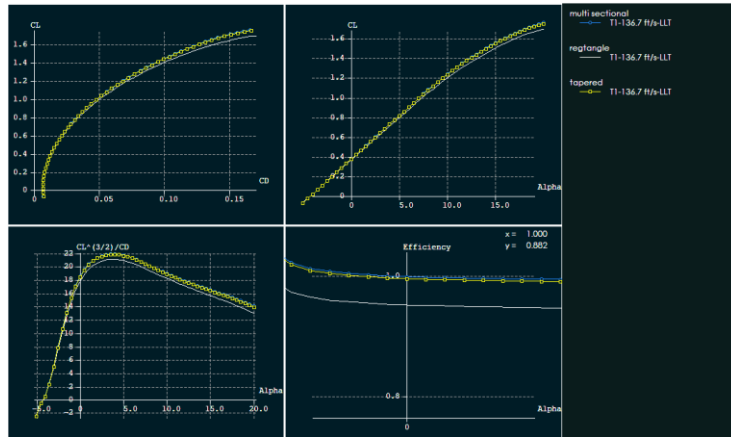


Figure 3.1-101. XFLR5 analysis of different wing Platforms

As can be seen in the figure, tapered and multi sectional wings are more efficient when compared to rectangle. Tapered wing has a few advantage over the multi section with regard to flapped area flexibility and structure. That's why tapered wing is the best choice for this aircraft configuration.

For the determined Wing planform, 3D wing is analyzed with XFLR5, OPENVSP and DATCOM programs:

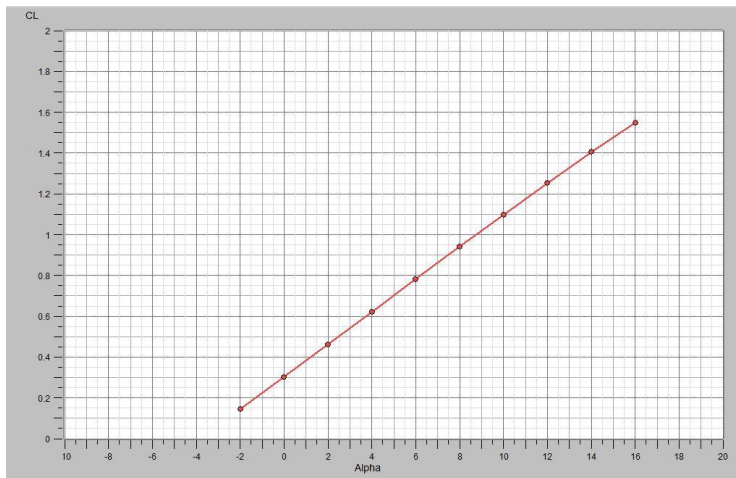


Figure 3.1-102. OpenVSP CL vs Alpha Graph

UNCLASSIFIED

UNCLASSIFIED

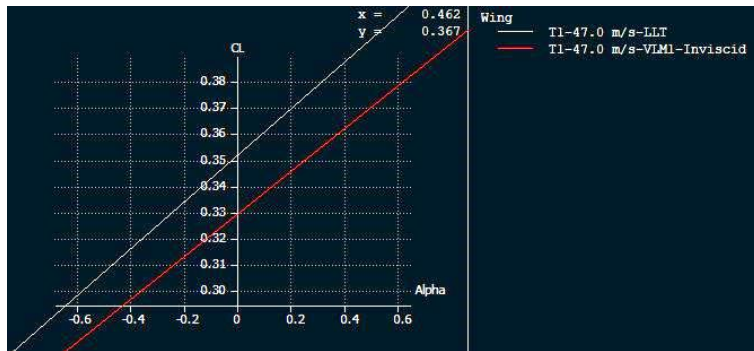


Figure 3.1-103. XFLR5 CL vs Alpha Graph

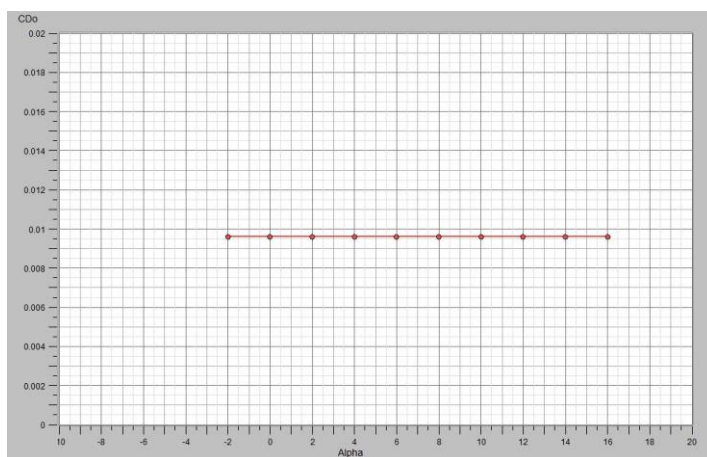


Figure 3.1-104. OpenVSP CD0 vs Alpha Graph

UNCLASSIFIED

UNCLASSIFIED

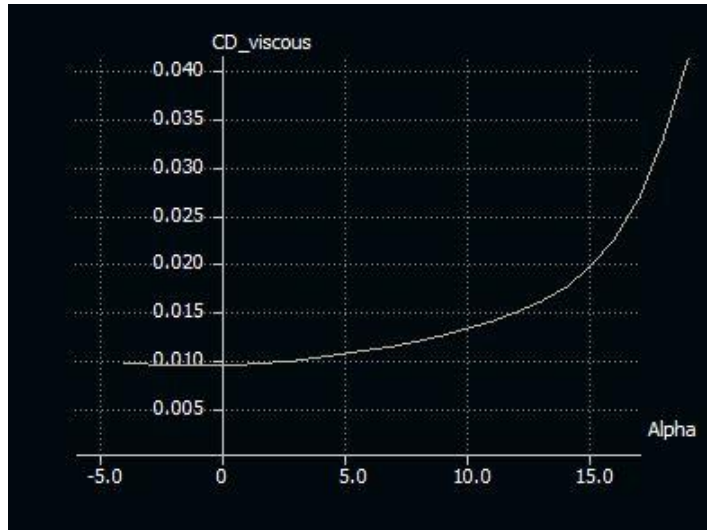


Figure 3.1-105. XFLR5 CD0 vs Alpha Graph

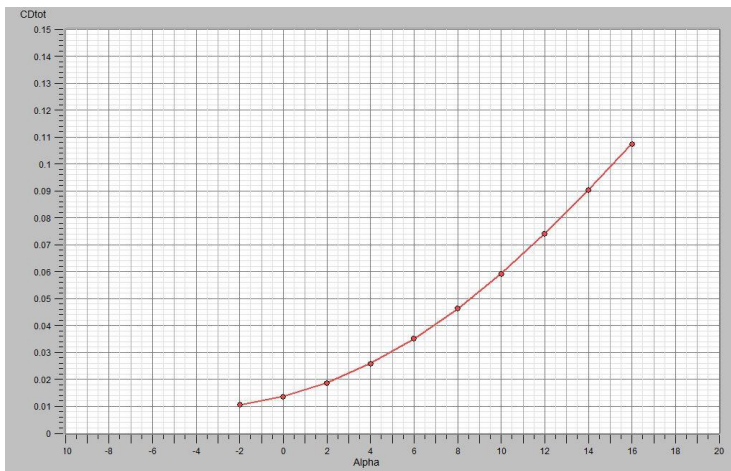


Figure 3.1-106. OpenVSP CD vs Alpha Graph

UNCLASSIFIED

UNCLASSIFIED

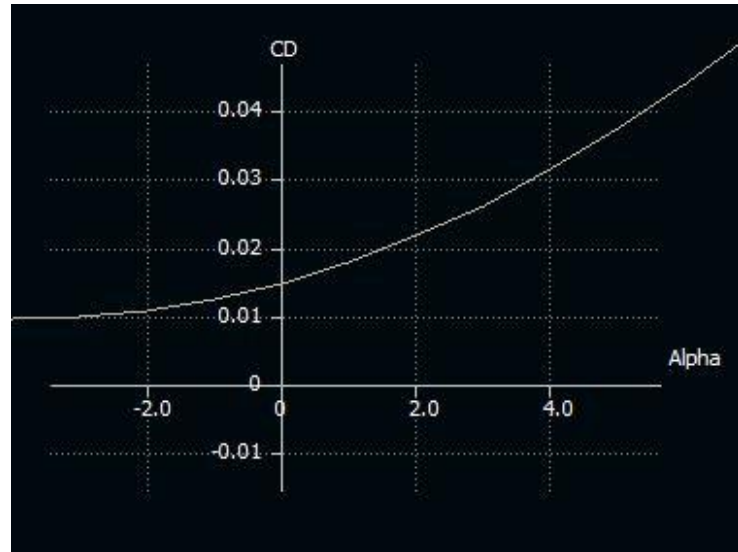


Figure 3.1-107. XFLR5 CD vs Alpha Graph

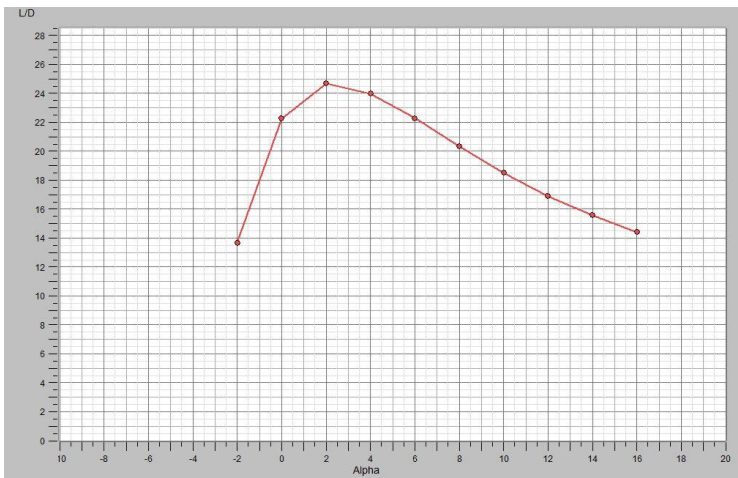


Figure 3.1-108. OpenVSP (L/D) vs Alpha Graph

UNCLASSIFIED

UNCLASSIFIED

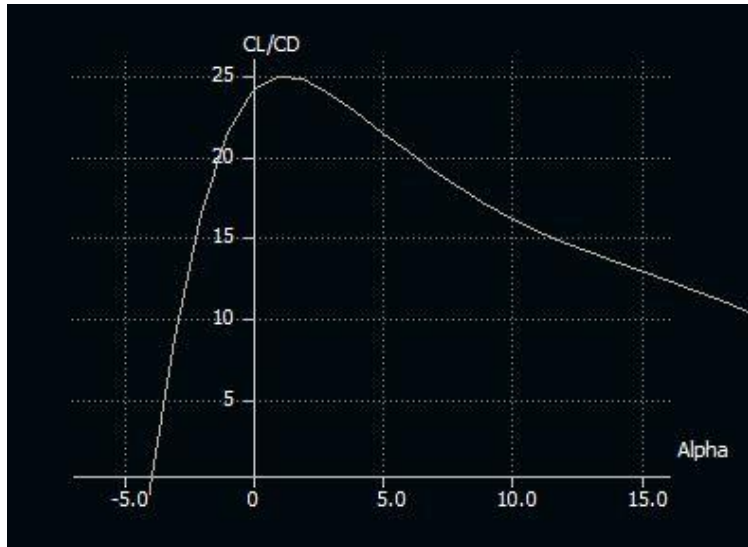


Figure 3.1-109. XFLR5 (L/D) vs Alpha Graph

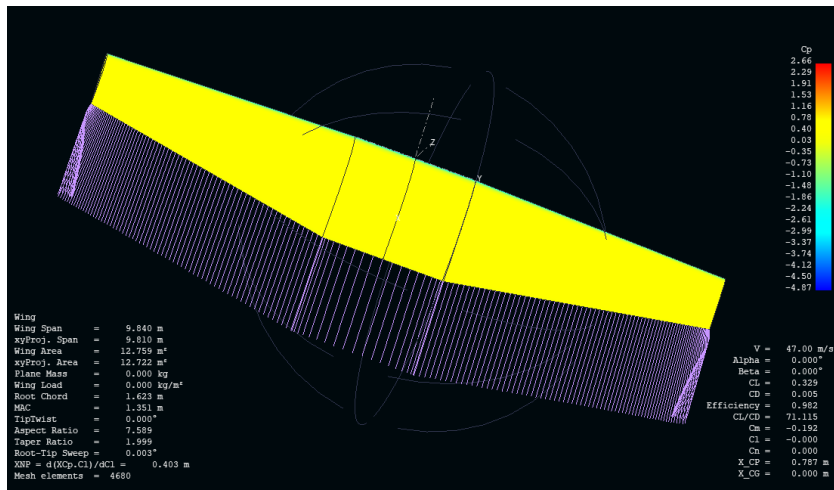


Figure 3.1-110. XFLR5 3D Wing Analysis VLM method

UNCLASSIFIED

UNCLASSIFIED

Table 3.1-[1645](#). DATCOM 3D Wing Analysis

MACH NUMBER	ALTITUDE	VELOCITY	PRESSURE
	FT	FT/SEC	LB/FT**2
0 0.150	5000.00	164.55	1.7609E+03
0			
0 ALPHA	CD	CL	CM CN
0	0.0	0.012	0.320 -0.1782 0.320

Table 3.1-[1746](#). 3D Wing Outputs from Different Softwares

	C _L max	C _L zero AOA	C _D zero AOA	L/D max
XFLR5 LLT	-	0.353	0.015	25
XFLR5 VLM	-	0.329	-	-
OPENVSP VLM	-	0.310	0.014	24.8
DATCOM	1.58	0.320	0.012	-

Fuselage

Fuselage length has a direct connection with take-off weight. According to figure below, coefficient can be taken from homebuilt type aircrafts. But, with regard to approach to real case, in our equation we chose the coefficients which are taken from competitor base curve fitting equation in MATLAB. And as a result fuselage length is calculated as 23.1 feet.

Table 3.1-[1847](#). Fuselage Length vs Empty Weight

Length = aW_0^C	a	C
Sailplane—unpowered	0.86	0.48
Sailplane—powered	0.71	0.48
Homebuilt—metal/wood	3.68	0.23
Homebuilt—composite	3.50	0.23
General aviation—single engine	4.37	0.23
General aviation—twin engine	0.86	0.42
Agricultural aircraft	4.04	0.23
Twin turboprop	0.37	0.51
Flying boat	1.05	0.40
Jet trainer	0.79	0.41
Jet fighter	0.93	0.39
Military cargo/bomber	0.23	0.50
Jet transport	0.67	0.43

According to (Raymer, 1992) for a fixed internal volume the subsonic drag is minimized by a fineness ratio of about 3.0 while supersonic drag is minimized by a fineness ratio of about 14. Most aircraft fall between these values. A historically-derived fuselage fineness ratio can be used, along with the length estimate, to develop the initial fuselage layout. However, "real-world constraints" such as payload envelope must take priority. For most design efforts the realities of packaging the internal components will establish the fuselage length and diameter.

That's why with respect to cabin requirement and competitor study, fineness ratio is chosen as 5 which means that 4.62 feet maximum fuselage diameter.

UNCLASSIFIED

UNCLASSIFIED

Tail

Table 3.1-[1918](#). Tail Volume Coefficient

	Typical values	
	Horizontal c_{HT}	Vertical c_{VT}
Sailplane	0.50	0.02
Homebuilt	0.50	0.04
General aviation—single engine	0.70	0.04
General aviation—twin engine	0.80	0.07
Agricultural	0.50	0.04
Twin turboprop	0.90	0.08
Flying boat	0.70	0.06
Jet trainer	0.70	0.06
Jet fighter	0.40	0.07
Military cargo/bomber	1.00	0.08
Jet transport	1.00	0.09

To decide horizontal and vertical tail surface area, tail volume ratios and moment arm variables are used. We can get the volume ratios from the figure above regarding homebuilt type aircraft data.

And we know that for an aircraft with a front-mounted propeller engine, the tail arm is about 60% of the fuselage length from Raymer.

Note that the moment arm L is commonly approximated as the distance from the tail quarter-chord to the wing quarter-chord.

$$S_{VT} = c_{vt} b_w S_w / L_{vt} \quad (39)$$

$$S_{HT} = c_{ht} C_{w_mean} S_w / L_{HT} \quad (40)$$

Table 3.1-[2019](#). Tail Aspect Ratio and Taper Ratio

	Horizontal tail		Vertical tail	
	A	λ	A	λ
Fighter	3-4	0.2-0.4	0.6-1.4	0.2-0.4
Sail plane	6-10	0.3-0.5	1.5-2.0	0.4-0.6
Others	3-5	0.3-0.6	1.3-2.0	0.3-0.6
T-Tail	—	—	0.7-1.2	0.6-1.0

As a result of competitor study and historical data of (Raymer 1992), tail ratios determined as following:

Table 3.1-[2120](#). Geometric Outputs

HORIZONTAL TAIL	
Aspect Ratio (Competitor)	3.6
Sweep angle (quarter cord),	0
Taper Ratio	1
Twist Angle	0

UNCLASSIFIED

UNCLASSIFIED

Incidence Angle	-1
Dihedral angle	0
Horizontal Tail Ratio	0.5
VERTICAL TAIL	
Aspect Ratio (Competitor)	1.5
Sweep angle (quarter cord)	20
Taper Ratio	0.4
Twist Angle	0
Incidence Angle	0
Dihedral angle	0
Vertical Tail Ratio	0.04
FUSELAGE	
Fuselage Length	23.1 ft
Fuselage Max Diameter	4.6 ft
Tail Moment Arm	14.20 ft
CL_required	0.74
Mach Number	0.14
Mean cord	4.40 ft.
Horizontal tail surface area	21.23 ft ²
Vertical tail surface area	11.20 ft ²

Table 3.1-2224. Geometric Outputs in Both Units

Fuselage Length	23.10 ft.	7.05 m
Max Fuselage Diameter	4.62 ft.	1.40 m
Tail Moment Arm	14.20 ft.	4.33 m
Wing Span	32.2 ft.	9.83 m
Wing root cord	5.66 ft.	1.72 m
Wing tip Cord	2.83 ft.	0.86 m
Wing Sweep	0	0
Wing Twist Angle	0	0
Wing Incidence Angle	2 deg.	2 deg.
Wing Dihedral angle	5 deg.	5 deg.
HT Span	8.74 ft.	2.66 m
HT root cord	2.43 ft.	0.74 m
HT tip Cord	2.43 ft.	0.74 m
HT Sweep	0	0
HT Twist Angle	0	0
HT Incidence Angle	-1 deg.	-1 deg.
HT Dihedral angle	0	0
VT Span	4.1 ft.	1.25 m
VT root cord	3.9 ft.	1.19 m
VT tip Cord	1.56 ft.	0.48 m
VT Sweep	20 deg.	20 deg.
VT Twist Angle	0	0
VT Incidence Angle	0	0
VT Dihedral angle	0	0

Table 3.1-2322. Performance Output From Design Process

L/D cruise	12.47
------------	-------

UNCLASSIFIED

UNCLASSIFIED

L/D max	13.73
Sref	137.0 ft ²
Take off distance	1351.0
Wing loading	11.79 slug/ft ²
Power loading available	16.16 N/W
Takeoff weight	1616.7 lb.
Cruise speed	155.15 ft./s
Maximum cruise speed	214 ft./s
Absolute ceiling	14000 ft.
Bank angle	60 deg.
Cruise altitude	5000 ft.
Max range speed	123.12 ft./s
Max endurance speed	94.31 ft./s
Carson speed	163.8 ft/s
CD0	0.025
Design Lift coefficient	0.714
CL_max	1.4
CL cruise	0.45
CL full flap at sea level	2.2

At the end of the calculation and analysis, geometry is designed roughly as below:

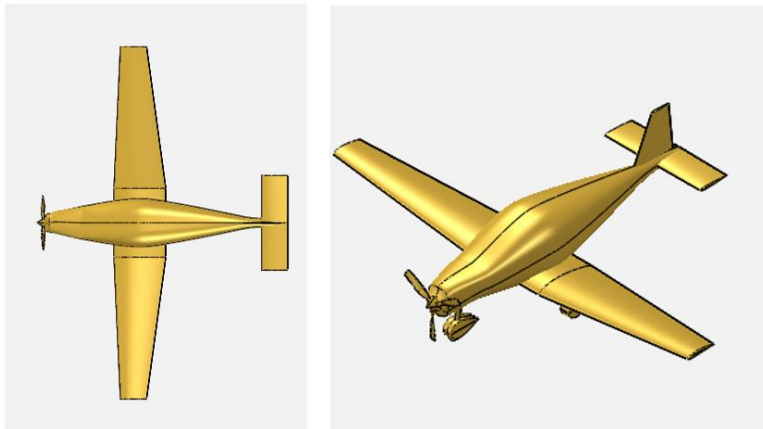


Figure 3.1-111. Top and Isometric View

UNCLASSIFIED

UNCLASSIFIED

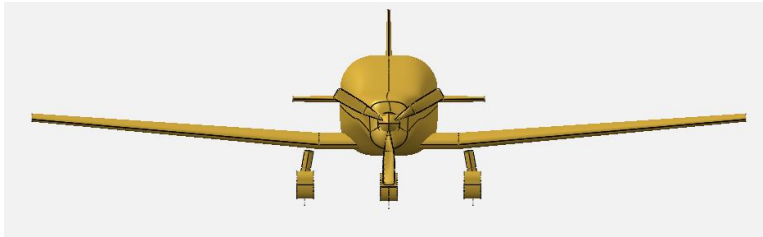


Figure 3.1-112. Front View



Figure 3.1-113. Left View

3.1.2.1.3. Design of Control Surfaces

There are three aircraft design objectives which influence the design of the control surfaces. They are basically 'stability', controllability and handling qualities.

Stability is defined as opposing any perturbation and return back to the original trim condition. When the summation of all forces along each of the three axes, and the summation of all the moments about each of the three axes are zero, an aircraft is said to be in trim or equilibrium. In this case, aircraft will have a constant linear/angular speed.

Control is the process of changing the aircraft flight condition from an initial trim point to a final or new trim point. This is done by pilot through the control surfaces/throttle. Maneuverability is a branch of controllability.

Table 3.1-[2423](#). Definition of Fundamental Terms

UNCLASSIFIED

UNCLASSIFIED

No.	Term	Definition
1	Trim, balance, and equilibrium	When the summation of all forces exerted on an aircraft and the summation of all moments about an aircraft center of gravity are zero, the aircraft is in "trim."
2	Control	A desired change in the aircraft trim condition from an initial trim point to a new trim point with a specified rate.
3	Stability	The tendency of an aircraft to oppose any input and return to the original trim point if disturbed by an undesired force or moment.
4	Static stability	The tendency of an aircraft to oppose any input if disturbed from the trim point.
5	Dynamic stability	The tendency of an aircraft to return to the original trim point if disturbed.

In table above, basic definitions are classified and explained.

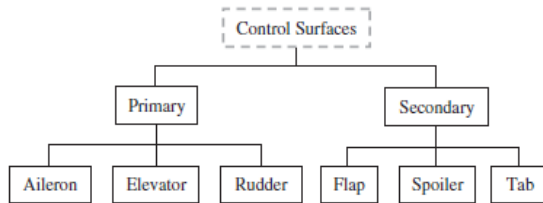


Figure 3.1-114. Classification of Conventional Control Surfaces

In figure 114 basic control surfaces briefly shown.

Table 3.1-2524. Typical Values for Geometry of Control Surfaces

Control surface	Elevator	Aileron	Rudder
Control surface area/lifting surface area	$S_E/S_h = 0.15-0.4$	$S_A/S = 0.03-0.12$	$S_R/S_V = 0.15-0.35$
Control surface span/lifting surface span	$b_E/b_h = 0.8-1$	$b_A/b = 0.2-0.40$	$b_R/b_V = 0.7-1$
Control surface chord/lifting surface chord	$C_E/C_h = 0.2-0.4$	$C_A/C = 0.15-0.3$	$C_R/C_V = 0.15-0.4$
Control surface maximum deflection (negative)	-25 deg (up)	25 deg (up)	-30 deg (right)
Control surface maximum deflection (positive)	+20 deg (down)	20 deg (down)	+30 deg (left)

In table 24, for a typical conventional aircraft parameter estimations are tabulated. Values with its own purpose can be acceptable in sense.

Aircraft Classes

An aircraft is considered to belong to one of the four classes shown in Table stated below. It is seen that classification is based on the weight of an aircraft as well as its maneuverability. The handling qualities of each class differ. According to MIL-F-8785C, for the purpose of handling qualities, aircraft are classified into four classes: I, II, III, and IV.

Table 3.1-2625. Aircraft Classes

UNCLASSIFIED

UNCLASSIFIED

Class	Aircraft characteristics
I	Small, light aircraft (maximum take-off mass less than 6000 kg) with low maneuverability
II	Aircraft of medium weight and low-to-medium maneuverability (maximum take-off mass between 6000 and 30 000 kg)
III	Large, heavy, and low-to-medium maneuverability aircraft (maximum take-off mass more than 30 000 kg)
IV	Highly maneuverable aircraft, no weight limit (e.g., acrobatic, missile, and fighter)

According to Table 25, VLA type of aircraft basically is in CLASS1.

In Class I, small light aircraft such as (i) light utility, (ii) primary trainer, and (iii) light observation aircraft are included. GA aircraft may be considered as Class I air vehicles.

Flight Phase

The flight phase is another parameter which has a significant role in handling qualities. Flying quality requirements vary for the different phases of a mission. Take-off, climb, cruise, descent, and landing are the least operations necessary to have a conventional flight mission.

From this point of view, VLA is a Category B aircraft from following table.

Table 3.1-[2726](#). Flight Phase Categories

Category	Examples of flight operation
A	(i) Air-to-air combat (CO); (ii) ground attack (GA); (iii) weapon delivery/launch (WD); (iv) aerial recovery (AR); (v) reconnaissance (RC); (vi) in-flight refuelling (receiver) (RR); (vii) terrain following (TR); (viii) anti-submarine search (AS); (ix) close formation flying (FF); and (x) low-altitude parachute extraction system (LAPES) delivery.
B	(i) Climb (CL); (ii) cruise (CR); (iii) loiter (LO); (iv) in-flight refueling in which the aircraft acts as a tanker (RT); (v) descent (D); (vi) emergency descent (ED); (vii) emergency deceleration (DE); and (viii) aerial delivery (AD).
C	(i) Take-off (TO); (ii) catapult take-off (CT); (iii) powered approach (PA); (iv) wave-off/go-around (WO); and (v) landing (L).

Levels of Acceptability

The third point a control surface designer should know before considering the issue of handling qualities is levels of acceptability. The requirements for airworthiness and handling qualities are stated in terms of three distinct, specified values of control (or stability) parameters. Each value is a limiting condition necessary to satisfy one of the three levels of acceptability. These levels are related to the ability of the pilot to complete the missions for which the aircraft is intended.

Table 3.1-[2827](#). Level of Acceptability

Level	Definition
1	Flying qualities clearly adequate for the mission flight phase.
2	Flying qualities adequate to accomplish the mission flight phase, but some increase in pilot workload or degradation in mission effectiveness, or both, exists.
3	Flying qualities such that the airplane can be controlled safely, but pilot workload is excessive or mission effectiveness is inadequate, or both. Category A flight phases can be terminated safely, and Category B and C flight phases can be completed.

From Table 28, VLA is a desired to have Level1 level of acceptability.

UNCLASSIFIED

UNCLASSIFIED

Table 3.1-[2928](#). Level Of Acceptability And Pilot Comfort

Level	Meaning	Pilot comfort level	Pilot status
1	Very comfortable	1 – 3	
2	Hardly comfortable	4 – 6	
3	Uncomfortable	7 – 10	

Longitudinal stability, dynamic modes damping ratios, oscillations and lateral & directional stabilities are not the point of view of this conceptual and preliminary design report. They will be handled later in detail.

Aileron Design

The primary function of an aileron is the roll control of the aircraft but it also affect the directional control. Hence, aileron and rudder generally are designed together. Roll control is basically defined as the p (roll rate).

Aileron effectiveness is a measure of how good the deflected aileron is, in producing the desired rolling moment. The generated rolling moment is a function of

- Aileron size
- Aileron deflection
- Aileron moment arm (distance from the fuselage center line)

Unlike rudder and elevator which are displacement control, aileron is the rate control. Any change in the aileron geometry or deflection will change the roll rate, which subsequently varies constantly the roll angle.

In the design process of an aileron, four parameters need to be determined:

1. Aileron planform area
2. Aileron chord/wing span
3. Maximum up/down deflections
4. Location of inner edge of the aileron along wing span

About 5–10% of the wing area is devoted to the aileron, the aileron-to-wing-chord ratio is about 15–25%, the aileron-to-wing-span ratio is about 20–30%, and the inboard aileron span is about 60–80% of the wing span.

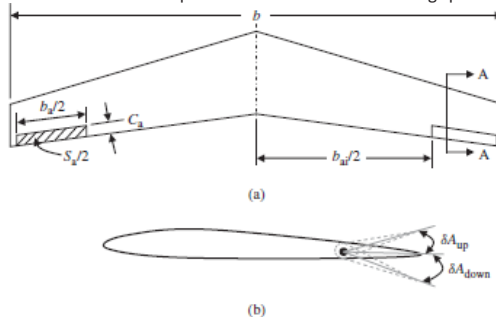


Figure 3.1-115. Geometry of Aileron (a) Top View of The Wing and Aileron (b) Side View of the Wing and Aileron

According to the written a MATLAB script aileron sizing code, mentioned parameters are found there.

Elevator Design

UNCLASSIFIED

UNCLASSIFIED

In a conventional aircraft, the longitudinal control is primarily applied through the deflection of elevator and engine throttle setting. There are two groups of requirements in the aircraft longitudinal controllability: (i) pilot force and (ii) aircraft response to the pilot input. In order to deflect the elevator, the pilot must apply a force to stick/yoke/wheel and hold it (in the case of an aircraft with a stick-fixed control system). In an aircraft with a stick-free control system, the pilot force is amplified through such devices as tab and spring. The pilot force analysis is out of scope of this text.

In the design of the elevator, four parameters should be determined. They are:

- i. Elevator planform area
- ii. Elevator chord
- iii. Elevator span
- iv. Maximum elevator deflection.

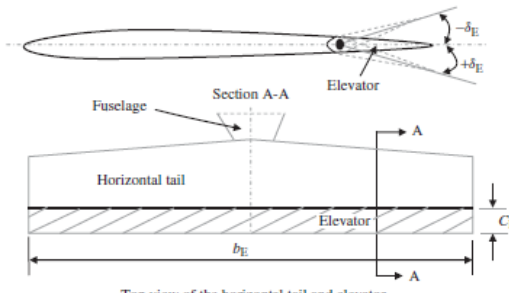


Figure 3.1-116. Horizontal Tail and Elevator Geometry

According to the written a MATLAB script elevator sizing code, mentioned parameters are found there.

Rudder Design

The rudder is a primary control surface and is responsible for the aircraft directional control. The rudder is a movable surface located on the trailing edge of the vertical tail. The rudder is the vertical counterpart to the elevator. When the rudder is rotated (i.e., deflected) lift force (i.e., side force, L_V) is created by the rudder/vertical tail combination. Consequently, a yawing moment (N) about the aircraft center of gravity (about the aircraft z -axis) is generated. Thus, control of the yawing moment about the center of gravity is primarily provided by means of the rudder.

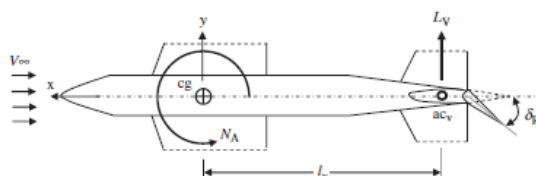


Figure 3.1-117. Directional Control via Rudder Deflection Top View

The aircraft heading angle (ψ) is mainly determined through a directional control process.

According to the written a MATLAB script rudder sizing code, mentioned parameters are found there.

Table 3.1-3029. Control Surface Sizes

AILERON	
b_ail_in/b_half_wing	0.67
b_ail_out/b_half_wing	0.99
C_ail/C_wing	0.3
Maximum Deflection	-30 / +30

UNCLASSIFIED

UNCLASSIFIED

ELEVATOR	
b_elev / b_ht	0.95
C_elev / C_ht	0.3
Maximum Deflection	-25 / +25
RUDDER	
b_r / b_vt	1
C_r / C_vt	0.3
Maximum Deflection	-30 / +30

3.1.3. Performance

3.1.3.1. Inertia Calculations

In order to model the aircraft's handling qualities and stability properly, inertia matrix of the aircraft has to be estimated. At this stage, approximate geometries of the components were created in CATIA V5 and allocated in the aircraft. Appropriate densities were assigned to each component and the skin in order to obtain the correct mass of every component. The following figure illustrates the allocation and shapes of the components in the aircraft.



Figure 3.1-118. Layout of the Aircraft

After this process, inertia matrix of the aircraft was found by the measure inertia tool of CATIA V5. The results are shown below.

Inertia Matrix with respect to CG:

$$I_{xx} = 801.562 \text{ kg}\cdot\text{m}^2$$

$$I_{xy} = -0.005 \text{ kg}\cdot\text{m}^2$$

$$I_{xz} = -58.103 \text{ kg}\cdot\text{m}^2$$

$$I_{yy} = 1104.09 \text{ kg}\cdot\text{m}^2$$

$$I_{yz} = 0.007 \text{ kg}\cdot\text{m}^2$$

$$I_{zz} = 1714.502 \text{ kg}\cdot\text{m}^2$$

UNCLASSIFIED

UNCLASSIFIED

3.1.3.2. Performance Calculations

Performance parameters like range, endurance, lift to drag ratio of the aircraft were found to see if the aircraft performs like intended and fulfills the requirements. Digital DATCOM and the in house performance tool was used to estimate the parameters.

3.1.3.3. DATCOM Method

Parameters like C_L , C_D , C_M , were found using Datcom after inputting the geometry of the aircraft to the software. Following graphs show the related coefficients of the aircraft and regarding outputs were tabulated in the appendix.

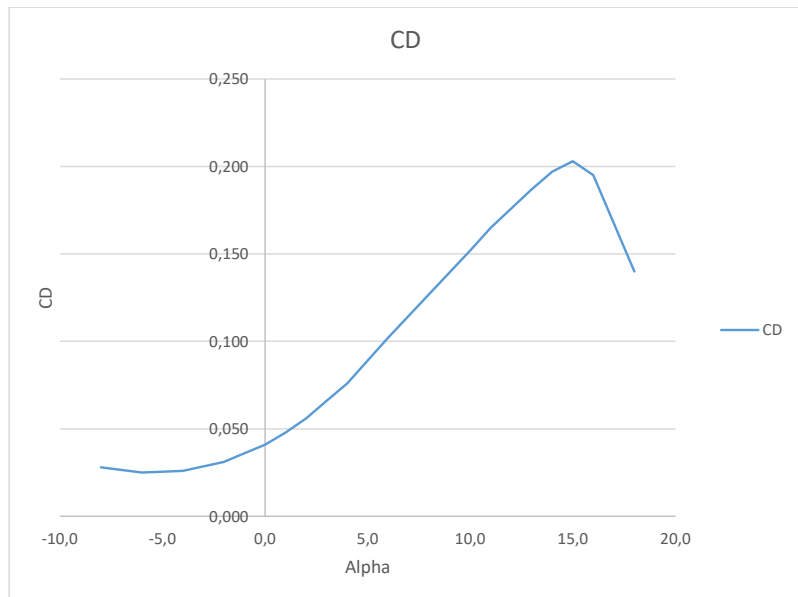


Figure 3.1-119. CD vs AOA

UNCLASSIFIED

UNCLASSIFIED

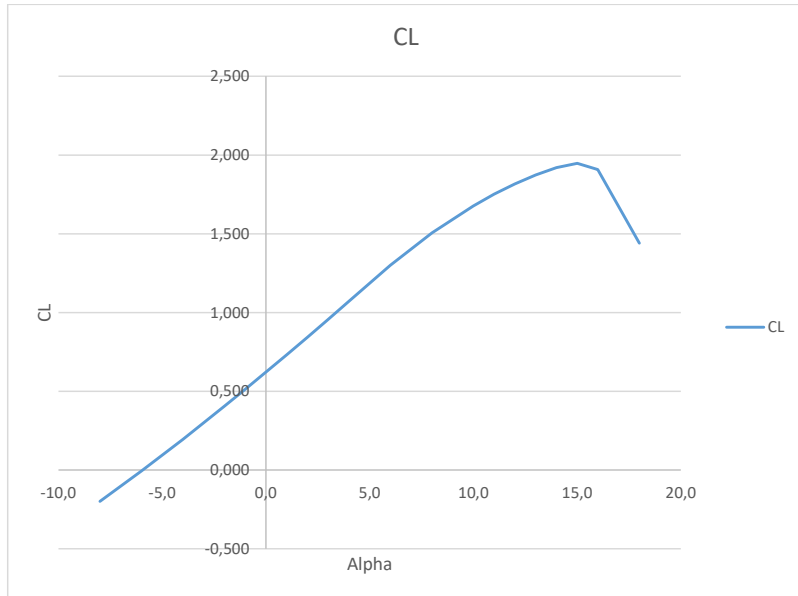


Figure 3.1-120. CL vs AOA

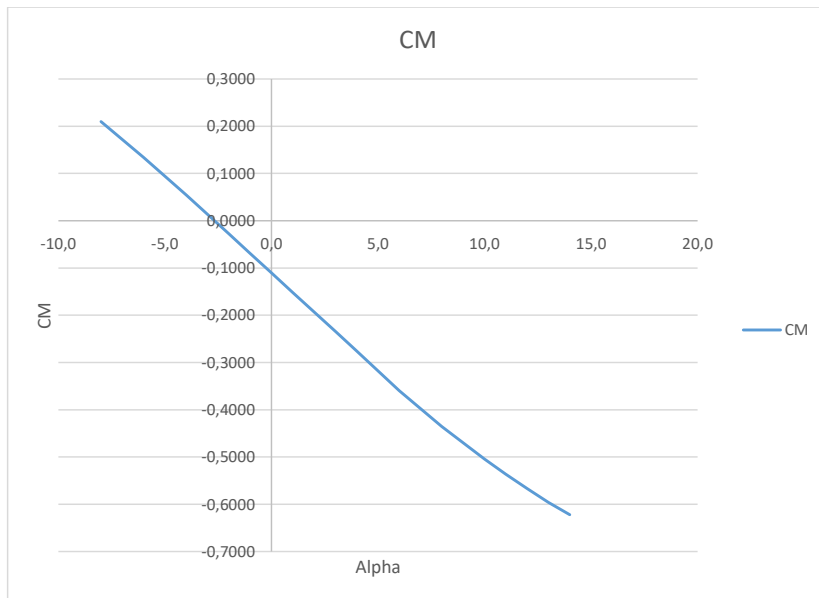


Figure 3.1-121. CM vs AOA

UNCLASSIFIED

UNCLASSIFIED

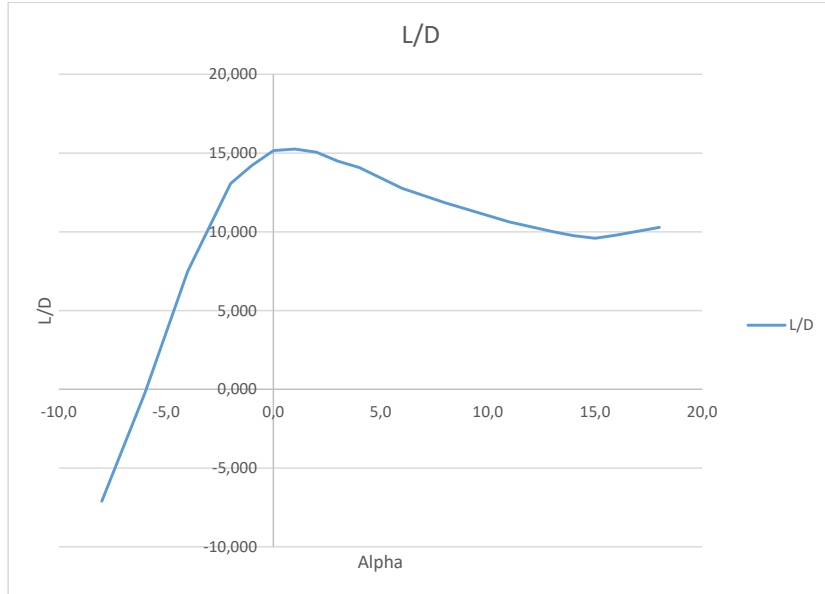


Figure 3.1-122. L/D vs AOA

3.1.3.4. Performance Parameters

Parameters regarding the performance of the aircraft were found by establishing a tool which utilizes empirical correlations like Breguet Range Equation, endurance equation and equations in several design methods like Raymer and Nikolai. After giving the design inputs like taper, fuel weight, wing loading, engine, etc., the code generates the performance outputs like endurance, range, stall speed etc. Performance outputs are as follows.

Stall Speed [KCAS]	39.7
Loiter Speed [KCAS]	55.6
Cruise Speed [KCAS]	71.5
Max Speed [KTAS]	133
Max L/D	15.3
Max Rate of Climb [ft. /min]	1030
Range [nm]	430
Endurance [h]	4.5
Take-off Distance [ft.]	540
Landing Distance [ft.]	755

Loiter speed and cruise speed shown above are the speeds at which the aircraft will perform the most efficiently in loiter and cruise respectively.

UNCLASSIFIED

UNCLASSIFIED

3.1.4. Loads

3.1.4.1. PURPOSE

The aim of this work is to determine critical load cases, to obtain loads for the mentioned cases on wings, horizontal tail and vertical tail of the aircraft that is to be designed within the scope of the contract signed by ODTU and TAI and to document all the findings.

3.1.4.2. APPLICABILITY

The study included in this document adapts the standards put forth by CS-VLA and FAR23(Federal Aviation Regulations) documents. As the work presented in this report is in concordance with the above-mentioned standards, unless there is any evidence present against the results obtained, it is convenient for the results of this study to be used as a baseline in the critical design phase of the aircraft provided the results are re-examined.

3.1.4.3. NOMENCLATURE

x: Negative x of Body Axis Coordinate System (Pointing towards the tail)

y: y of Body Axis Coordinate System

z: Negative z of Body Axis Coordinate System (Pointing against the ground during level flight)

F_x : Force in x-direction

F_z : Force in z-direction

S_x : Shear Force in x-direction

S_y : Shear Force in y-direction

M_x : Moment about x-axis

M_y : Moment about y-axis

M_z : Moment about z-axis

V: Internal Shear Force

q: Distributed Force

P: Pressure

M/S: Wing Loading

g: Gravitational Acceleration

3.1.4.4. GENERAL

A number of properties of the aircraft that define the aircraft in consideration for the load analyses documented in next sections of this report are tabulated in *Table 3.0*. Note that some of the properties listed in the following table are not available in hand definitively are either based on assumptions or data the competitor aircraft manufacturers provide.

Table 3.1-3120. Main Properties of the Aircraft used in the Analyses

GENERAL		VERTICAL TAIL	
Maximum Weight	750 kg	Vertical Tail Area	1.04 m ²

UNCLASSIFIED

UNCLASSIFIED

Gross Weight	584.4 kg	Vertical Tail Span	1.25 m
Length of the Airplane	7.04 m	HORIZONTAL TAIL	
Investigated Altitudes	0-5000-7500 ft	Horizontal Tail Area	0.99 m ²
Investigated Weight Range	750-703-612-571.5 kg	Aspect Ratio of HT	3.6
Wing Loading	57.52 kg/m ²	Horizontal Tail Span	2.67 m
WING		Incidence of Horizontal Tail	-1°
Aspect Ratio of the Wing	7.6	DESIGN SPEEDS	
Wing Area	12.65 m ²	Design cruising speed, V_C^*	111 KIAS
Wing Span	9.85 m	Design dive speed, V_D^*	155 KIAS
Weight of the Wing	174.2 kg	Design Manoeuvring Speed, V_A^{**}	102 KIAS
Wing Profile	Rhode St. Genese 32	Design Flap Speed, V_F^{**}	74.7 KIAS
Wing Sweep	0	Positive Manoeuvring Limit Load Factor	+3.8g
Wing Dihedral Angle	5°	Negative Manoeuvring Limit Load Factor	-1.5g

*: V_C and V_D are calculated taking the formulas given in CS-VLA 335 as a basis, i.e.

$$V_C = 4.7 \sqrt{Mg / S} \quad (41)$$

$$V_D = 1.40 V_C \dots (2)$$

**: V_A and V_F are assigned after examining the values obtained via Appendix A for the sake of the analysis as they are not available at the time of the analyses.

3.1.4.4.1. Flight Envelope

The flight envelope, is formed by following the standards given in CS-VLA 333. The envelope itself consists of limit manoeuvring envelopes, limit gust envelope and the limit combined envelope which is the combination of the foregoing two.

The curve between 0g and 3.8g is a 2nd order quadratic equation obtained via expressing lift in two different ways, equating them to each other and solving for n, the load factor, as follows:

$$L = n \times M \times g = 0.5 \times \rho \times V^2 \times S \times C_L \dots (3)$$

UNCLASSIFIED

UNCLASSIFIED

OR

$$n = \frac{0.5 \times \rho \times V^2 \times S \times C_{L_{max}}}{M \times g} \dots (4)$$

with

n = Load Factor

ρ = Air Density(Taken at Sea Level) = $1.225 \frac{kg}{m^3}$

V = Equivalent Airspeed of the Aircraft($\pm V_C$ and $\pm V_D$)

M = Mass of the Aircraft = 750 kg

g = Gravitational Acceleration = $9.81 \frac{m}{s^2}$

S = Wing Area = $12.65 m^2$

$C_{L_{max}}$ = Maximum Lift Coefficient = 1.5

The curve lying between $0g$ and $-1.5g$ is obtained by applying the same procedure, except with the difference that $C_{L_{max}} = -0.6$ for the airfoil used.

The boundaries limit combined envelope is formed via combining the aforementioned two envelopes by choosing the one that contains the other.

The gust load factors are found via using the following relation

$$n = 1 + \frac{0.5 \times \rho_0 \times V \times a \times K_g \times U_{de}}{M \times g / S} \dots (5)$$

where

$K_g = \frac{0.88\mu_g}{5.3 + \mu_g}$ = Gust Alleviation Factor

$\mu_g = \frac{M/S}{\rho Ca}$ = Aeroplane Mass Ratio

U_{de} = Gust Velocities($15.24 \frac{m}{s}$ for V_C and $7.62 \frac{m}{s}$ for V_D)

ρ_0 = Density of Air at Sea Level = $1.225 \frac{kg}{m^3}$

a = Wing Lift Curve Slope C_L per radian = 5.1486

$\bar{C} = \text{Mean Geometric Chord} = \frac{\text{chord}_{root}}{2} \left(1 + \frac{\text{chord}_{tip}}{\text{chord}_{root}} \right) = 1.3 \text{ m}$

UNCLASSIFIED

UNCLASSIFIED

Finally, $V_{S(+)}$ & $V_{S(-)}$, positive and negative stalling speeds, respectively, are found as 45 and 77.4 knots by solving equation (4) for V with $n = \pm 1g$ and respective stall C_L values. Hence, the flight envelope formed is as shown in *Figure 123*.

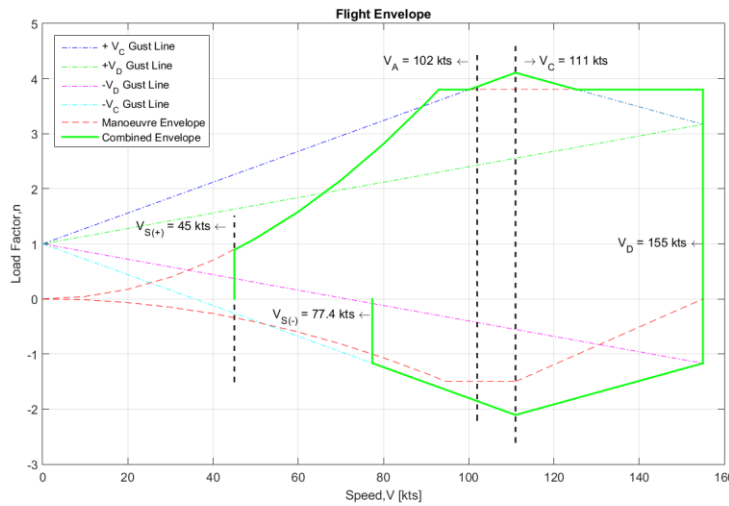


Figure 3.1-123. Combined Flight Envelope

3.1.4.5. CRITICAL LOADS ANALYSIS

3.1.4.5.1. WING

Geometry

UNCLASSIFIED

UNCLASSIFIED

The overall geometry is as the first sizing process provides. It should be noted, however, that the dimensions of the control surfaces on the wing having no geometry data during the preparation of this report, i.e. ailerons and flaps, are determined via scaling the surfaces within the ranges the competitor aircraft use and are as shown in *Figure 124*.

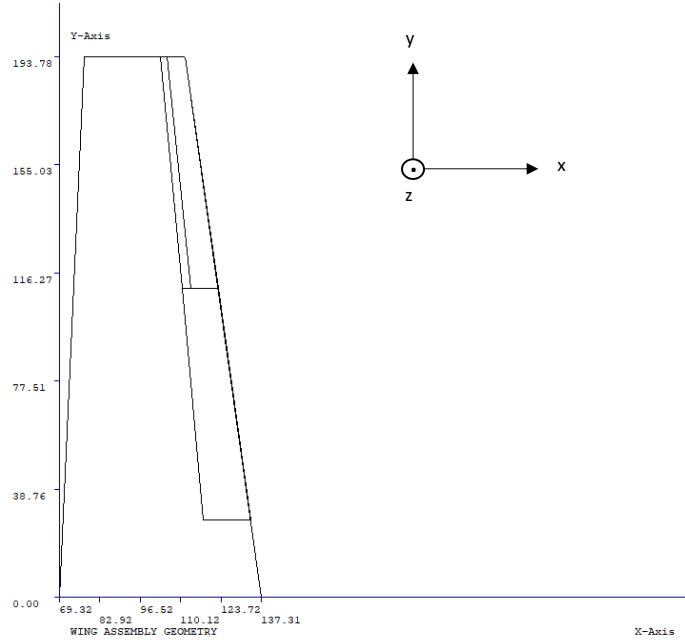


Figure 3.1-124. Half-Wing Geometry used in FAR23 Loads

Critical Load Cases

Critical load cases investigated are as tabulated in *Table 32*.

UNCLASSIFIED

UNCLASSIFIED

CASE	ANGLE	CL	V KEAS	CONFIG	CG	ALT	COND	FAR
122	PHAA	1.553	92.1	CRUISE	1	5000	STALL +N	23.333(b)
205	PLAA	0.63	143.77	CRUISE	1	7500	MAN D	23.333(b)
130	PMAA	1.214	108.53	CRUISE	1	5000	GUST +C	23.333(b)or(c)
153	NAA	-0.65	108.53	CRUISE	2	5000	GUST -C	23.333(b)
220	ACRL	1.351	92.22	CRUISE	1	7500	AC ROLL	23.349(a)
18	TORS	0.705	111	CRUISE	1	0	ST ROL C	23.349(b)

process of loads for the critical *Table 3.1-32. Critical Load Cases for the Wing* cases given above, the commercial software FAR23 is employed. Having calculated the air loads present on the wings, the net load is found by summing up the air loads with the wing inertia, which again is obtained via FAR23.

Results

The resultant forces, F_x and F_z , shear forces, S_x and S_z , and the moments, M_x , M_y and M_z , along with their positions in all three directions measured from the nose of the aircraft, which is taken as the origin, are tabulated as in *Tables 3-8*.

Note that the following distances are in meters, forces are in Newtons and the moments are in Newton meters.

Method

In the calculation

CASE 122 – STALL +N

UNCLASSIFIED

UNCLASSIFIED

X	Y	Z	FX	FZ	SX	SZ	MX	MY	MZ
2.19	4.80	-0.09	-54.39	256.58	-54.39	256.58	0.00	156.33	0.00
2.19	4.55	-0.11	-85.70	325.84	-140.09	582.42	63.14	327.22	13.39
2.19	4.31	-0.13	-108.67	373.35	-248.76	955.77	206.48	512.76	47.86
2.19	4.06	-0.15	-127.41	411.67	-376.18	1367.44	441.70	713.24	109.08
2.19	3.81	-0.17	-143.24	444.48	-519.41	1811.92	778.23	929.00	201.66
2.19	3.57	-0.20	-156.81	473.45	-676.22	2285.38	1224.15	1160.48	329.49
2.19	3.32	-0.22	-168.53	499.49	-844.75	2784.87	1786.59	1408.17	495.91
2.19	3.08	-0.24	-178.68	523.18	-1023.43	3308.05	2471.96	1672.57	703.81
2.19	2.83	-0.26	-187.47	544.89	-1210.89	3852.94	3286.08	1954.25	955.68
2.19	2.58	-0.28	-195.05	564.89	-1405.95	4417.84	4234.30	2253.79	1253.68
2.19	2.34	-0.30	-201.56	583.37	-1607.51	5001.21	5321.55	2571.80	1599.69
2.19	2.09	-0.32	-207.10	600.47	-1814.61	5601.68	6552.36	2908.93	1995.31
2.19	1.85	-0.35	-211.74	616.30	-2026.34	6217.98	7930.96	3265.83	2441.89
2.19	1.60	-0.37	-215.56	630.93	-2186.15	6510.84	9400.94	3641.42	2930.64
2.19	1.35	-0.39	-218.62	644.43	-2349.01	6817.20	10945.66	4039.29	3459.15
2.19	1.11	-0.41	-220.97	656.86	-2458.47	6797.93	12556.44	4458.53	4026.21
2.19	0.86	-0.43	-219.45	648.89	-2677.93	7446.82	14229.43	4913.94	4631.25
2.19	0.62	-0.45	-247.44	822.64	-2925.37	8269.46	16062.12	5326.85	5290.30
2.19	0.37	-0.48	-248.66	836.69	-3174.03	9106.16	18097.27	5759.86	6010.24
2.19	0.12	-0.50	-249.30	849.79	-3423.33	9955.95	20338.32	6213.61	6791.38

Table 3.1-33. Case 122 – STALL +N

CASE 205 – MAN D

UNCLASSIFIED

UNCLASSIFIED

X	Y	Z	FX	FZ	SX	SZ	MX	MY	MZ
2.19	4.80	-0.09	-16.21	255.87	-16.21	255.87	0.00	77.80	0.00
2.19	4.55	-0.11	-28.85	329.81	-45.06	585.67	62.97	163.13	3.99
2.19	4.31	-0.13	-38.08	380.97	-83.14	966.64	207.11	256.12	15.08
2.19	4.06	-0.15	-45.58	422.31	-128.72	1388.94	445.00	356.96	35.54
2.19	3.81	-0.17	-51.87	457.63	-180.58	1846.57	786.82	465.89	67.22
2.19	3.57	-0.20	-57.24	488.69	-237.82	2335.26	1241.27	583.16	111.66
2.19	3.32	-0.22	-61.83	516.47	-299.66	2851.74	1815.99	709.06	170.19
2.19	3.08	-0.24	-65.79	541.60	-365.45	3393.33	2517.81	843.88	243.94
2.19	2.83	-0.26	-69.18	564.47	-434.63	3957.80	3352.92	987.95	333.88
2.19	2.58	-0.28	-72.08	585.39	-506.71	4543.18	4326.95	1141.58	440.84
2.19	2.34	-0.30	-74.53	604.56	-581.24	5147.74	5445.04	1305.12	565.54
2.19	2.09	-0.32	-76.58	622.15	-657.82	5769.90	6711.92	1478.93	708.59
2.19	1.85	-0.35	-78.26	638.30	-736.08	6408.19	8131.91	1663.36	870.48
2.19	1.60	-0.37	-79.61	653.08	-818.01	6723.21	9648.71	1856.00	1052.05
2.19	1.35	-0.39	-80.64	666.59	-900.98	7051.73	11245.69	2059.97	1253.76
2.19	1.11	-0.41	-81.38	678.87	-987.01	7054.48	12914.19	2272.87	1475.95
2.19	0.86	-0.43	-81.98	670.64	-1068.99	7725.11	14650.32	2511.01	1718.86
2.19	0.62	-0.45	-81.07	844.00	-1150.05	8569.11	16551.50	2695.78	1981.94
2.19	0.37	-0.48	-80.99	857.55	-1231.05	9426.66	18660.39	2890.04	2264.97
2.19	0.12	-0.50	-80.69	870.04	-1311.74	10296.70	20980.33	3094.07	2567.94

Table 3.1-34. Case 205 – MAN D

UNCLASSIFIED

UNCLASSIFIED

CASE 130 – GUST +C

X	Y	Z	FX	FZ	SX	SZ	MX	MY	MZ
2.19	4.80	-0.09	-44.96	277.39	-44.96	277.39	0.00	137.93	0.00
2.19	4.55	-0.11	-71.79	355.23	-116.75	632.63	68.27	288.80	11.06
2.19	4.31	-0.13	-91.49	408.80	-208.24	1041.43	223.96	452.72	39.80
2.19	4.06	-0.15	-107.56	452.03	-315.80	1493.46	480.26	629.94	91.05
2.19	3.81	-0.17	-121.12	488.98	-436.92	1982.44	847.81	820.80	168.77
2.19	3.57	-0.20	-132.73	521.52	-569.65	2503.97	1335.69	1025.69	276.29
2.19	3.32	-0.22	-142.76	550.69	-712.41	3054.66	1951.93	1245.06	416.49
2.19	3.08	-0.24	-151.44	577.14	-863.85	3631.80	2703.69	1479.37	591.81
2.19	2.83	-0.26	-158.94	601.29	-1022.78	4233.09	3597.49	1729.12	804.41
2.19	2.58	-0.28	-165.40	623.44	-1188.19	4856.53	4639.27	1994.85	1056.12
2.19	2.34	-0.30	-170.94	643.82	-1359.13	5500.35	5834.48	2277.11	1348.54
2.19	2.09	-0.32	-175.63	662.59	-1534.76	6162.95	7188.13	2576.47	1683.02
2.19	1.85	-0.35	-179.57	679.88	-1714.33	6842.83	8704.86	2893.54	2060.73
2.19	1.60	-0.37	-182.79	695.79	-1858.56	7158.74	10321.16	3226.52	2475.76
2.19	1.35	-0.39	-185.35	710.38	-2005.36	7489.25	12018.21	3579.22	2926.59
2.19	1.11	-0.41	-187.31	723.72	-2115.57	7453.21	13786.09	3949.98	3412.48
2.19	0.86	-0.43	-186.48	714.12	-2302.05	8167.34	15620.36	4356.03	3933.13
2.19	0.62	-0.45	-205.95	908.68	-2508.00	9076.02	17630.37	4708.97	4499.67
2.19	0.37	-0.48	-206.80	923.77	-2714.79	9999.79	19864.01	5079.23	5116.90
2.19	0.12	-0.50	-207.16	937.75	-2921.95	10937.54	22324.99	5467.37	5785.02

Table 3.1-35. Case 130 – GUST +C

CASE 153 – GUST -C

UNCLASSIFIED

UNCLASSIFIED

X	Y	Z	FX	FZ	SX	SZ	MX	MY	MZ
2.19	4.80	-0.09	-2.92	-146.76	-2.92	-146.76	0.00	35.44	0.00
2.19	4.55	-0.11	-10.20	-189.98	-13.12	-336.74	-36.12	74.30	0.72
2.19	4.31	-0.13	-15.40	-219.83	-28.52	-556.57	-118.99	116.55	3.95
2.19	4.06	-0.15	-19.55	-243.90	-48.07	-800.47	-255.96	162.26	10.97
2.19	3.81	-0.17	-22.97	-264.43	-71.03	-1064.89	-452.96	211.48	22.80
2.19	3.57	-0.20	-25.81	-282.46	-96.85	-1347.36	-715.04	264.29	40.28
2.19	3.32	-0.22	-28.19	-298.57	-125.04	-1645.93	-1046.63	320.78	64.11
2.19	3.08	-0.24	-30.18	-313.11	-155.22	-1959.04	-1451.70	381.05	94.89
2.19	2.83	-0.26	-31.81	-326.33	-187.03	-2285.37	-1933.82	445.21	133.09
2.19	2.58	-0.28	-33.14	-338.39	-220.18	-2623.76	-2496.26	513.37	179.12
2.19	2.34	-0.30	-34.20	-349.43	-254.38	-2973.19	-3141.97	585.65	233.30
2.19	2.09	-0.32	-35.01	-359.55	-289.39	-3332.74	-3873.69	662.17	295.91
2.19	1.85	-0.35	-35.59	-368.81	-324.99	-3701.55	-4693.89	743.06	367.13
2.19	1.60	-0.37	-35.97	-377.27	-327.21	-3862.63	-5566.30	830.81	441.09
2.19	1.35	-0.39	-36.15	-384.97	-329.60	-4031.43	-6480.06	923.87	515.86
2.19	1.11	-0.41	-36.14	-391.96	-298.25	-3991.01	-7429.39	1024.83	590.29
2.19	0.86	-0.43	-34.04	-385.89	-332.29	-4376.90	-8411.60	1122.60	663.69
2.19	0.62	-0.45	-50.02	-495.99	-382.30	-4872.90	-9488.77	1267.64	745.47
2.19	0.37	-0.48	-49.99	-503.96	-432.30	-5376.86	10688.00	1419.84	839.56
2.19	0.12	-0.50	-49.83	-511.31	-482.13	-5888.16	12011.27	1579.39	945.95

Table 3.1-36. Case 153 – GUST -C

CASE 220 – AC ROLL

UNCLASSIFIED

UNCLASSIFIED

X	Y	Z	FX	FZ	SX	SZ	MX	MY	MZ
2.19	4.80	-0.09	-40.73	224.30	-40.73	224.30	0.00	120.85	0.00
2.19	4.55	-0.11	-64.64	286.10	-105.37	510.40	55.20	252.99	10.02
2.19	4.31	-0.13	-82.19	328.60	-187.56	839.00	180.81	396.52	35.96
2.19	4.06	-0.15	-96.50	362.90	-284.06	1201.90	387.29	551.64	82.11
2.19	3.81	-0.17	-108.59	392.25	-392.65	1594.15	683.08	718.64	152.02
2.19	3.57	-0.20	-118.95	418.13	-511.60	2012.28	1075.41	897.86	248.66
2.19	3.32	-0.22	-127.89	441.36	-639.49	2453.64	1570.64	1089.68	374.57
2.19	3.08	-0.24	-135.63	462.45	-775.13	2916.08	2174.49	1294.50	531.95
2.19	2.83	-0.26	-142.33	481.74	-917.46	3397.83	2892.15	1512.76	722.71
2.19	2.58	-0.28	-148.10	499.47	-1065.56	3897.30	3728.36	1744.91	948.50
2.19	2.34	-0.30	-153.05	515.82	-1218.62	4413.11	4687.50	1991.44	1210.74
2.19	2.09	-0.32	-157.26	530.90	-1375.88	4944.01	5773.59	2252.85	1510.65
2.19	1.85	-0.35	-160.78	544.83	-1536.66	5488.84	6990.33	2529.64	1849.25
2.19	1.60	-0.37	-163.67	557.67	-1662.10	5750.26	8288.32	2820.63	2220.61
2.19	1.35	-0.39	-165.98	569.48	-1789.85	6023.49	9652.99	3128.86	2623.15
2.19	1.11	-0.41	-167.74	580.31	-1881.13	6011.30	11076.71	3453.25	3056.06
2.19	0.86	-0.43	-166.81	573.25	-2047.94	6584.55	12556.11	3807.04	3519.02
2.19	0.62	-0.45	-186.05	725.39	-2233.99	7309.95	14176.60	4121.29	4023.02
2.19	0.37	-0.48	-186.89	737.56	-2420.88	8047.51	15975.60	4450.90	4572.82
2.19	0.12	-0.50	-187.28	748.88	-2608.16	8796.38	17956.12	4796.36	5168.60

Table 3.1-37. Case 220 – AC ROLL

CASE 18 – ST ROL C

UNCLASSIFIED

UNCLASSIFIED

X	Y	Z	FX	FZ	SX	SZ	MX	MY	MZ
2.19	4.80	-0.09	-13.14	170.66	-13.14	170.66	0.00	55.61	0.00
2.19	4.55	-0.11	-22.61	219.81	-35.76	390.48	42.00	116.57	3.24
2.19	4.31	-0.13	-29.54	253.80	-65.30	644.28	138.10	182.96	12.04
2.19	4.06	-0.15	-35.17	281.26	-100.46	925.54	296.66	254.90	28.10
2.19	3.81	-0.17	-39.90	304.73	-140.36	1230.27	524.44	332.55	52.83
2.19	3.57	-0.20	-43.94	325.37	-184.31	1555.64	827.21	416.10	87.37
2.19	3.32	-0.22	-47.42	343.84	-231.73	1899.48	1210.06	505.74	132.73
2.19	3.08	-0.24	-50.41	360.55	-282.14	2260.02	1677.53	601.67	189.76
2.19	2.83	-0.26	-52.98	375.76	-335.12	2635.78	2233.73	704.13	259.20
2.19	2.58	-0.28	-55.18	389.68	-390.30	3025.46	2882.40	813.33	341.67
2.19	2.34	-0.30	-57.05	402.44	-447.34	3427.90	3626.98	929.53	437.72
2.19	2.09	-0.32	-58.61	414.16	-505.95	3842.06	4470.60	1052.95	547.81
2.19	1.85	-0.35	-59.91	424.91	-565.87	4266.97	5416.14	1183.87	672.33
2.19	1.60	-0.37	-60.95	434.77	-624.45	4476.66	6426.12	1320.76	811.17
2.19	1.35	-0.39	-61.76	443.78	-683.83	4695.35	7489.48	1465.71	964.44
2.19	1.11	-0.41	-62.35	451.97	-741.44	4697.17	8600.44	1617.23	1132.27
2.19	0.86	-0.43	-62.60	446.52	-804.04	5143.69	9756.43	1786.06	1314.74
2.19	0.62	-0.45	-63.94	561.97	-867.98	5705.65	11022.31	1919.86	1512.62
2.19	0.37	-0.48	-63.98	571.01	-931.96	6276.67	12426.49	2060.45	1726.23
2.19	0.12	-0.50	-63.85	579.36	-995.81	6856.02	13971.20	2208.04	1955.59

Table 3.1-38. Case 18 – ST ROL C

Further on, shear forces, moments and the resultant forces along half span of the wing are plotted on the Figures 125-131, respectively, to illustrate the distribution and to compare the results.

UNCLASSIFIED

UNCLASSIFIED

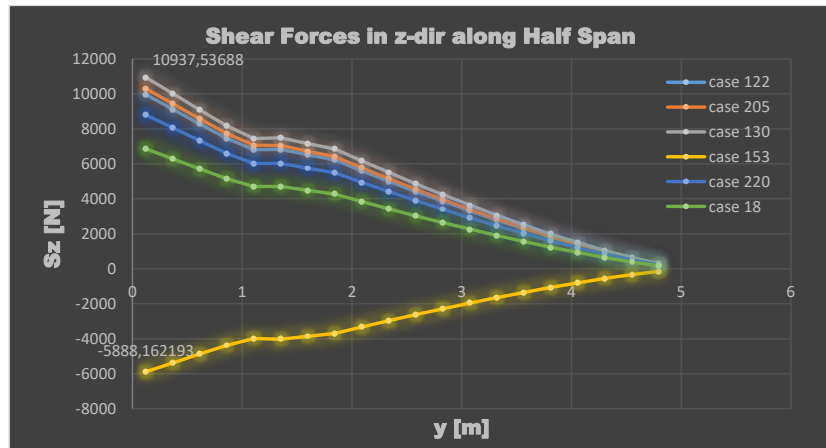


Figure 3.1-125. Shear Forces in z-dir. along Half Span

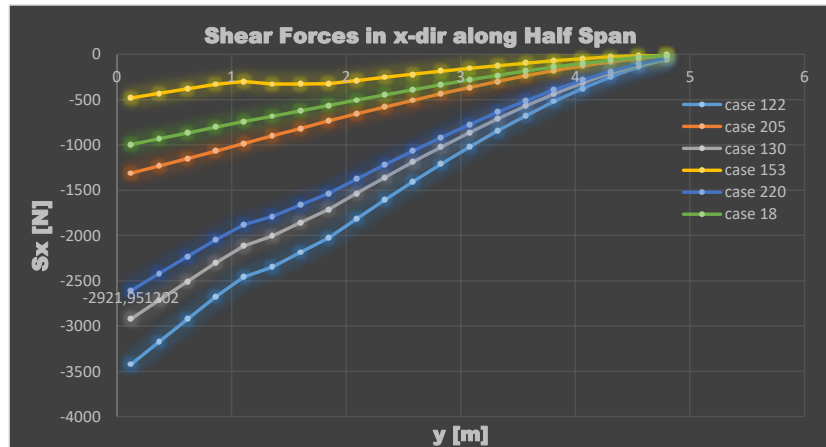


Figure 3.1-126. Shear Forces in x-dir. along Half Span

UNCLASSIFIED

UNCLASSIFIED

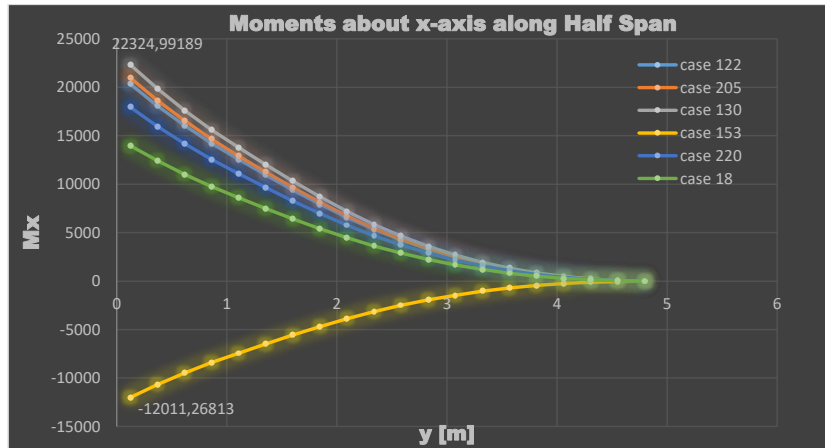


Figure 3.1-127. Moments about x-axis along Half Span

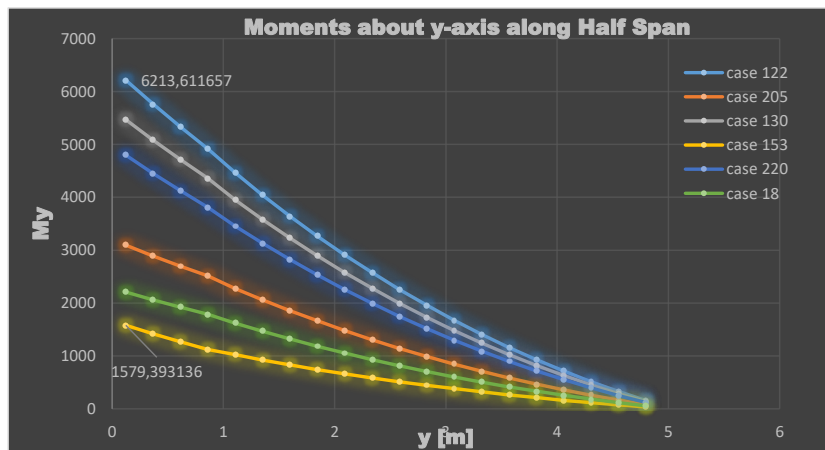


Figure 3.1-128. Moments about y-axis along Half Span

UNCLASSIFIED

UNCLASSIFIED

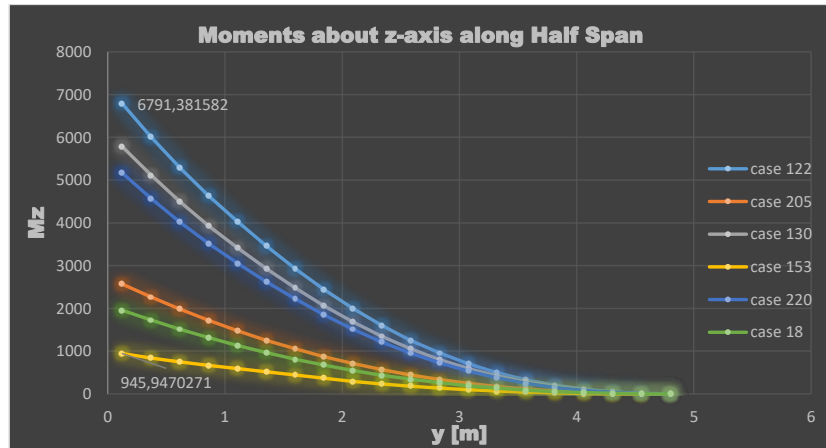


Figure 3.1-129. Moments about z-axis along Half Span

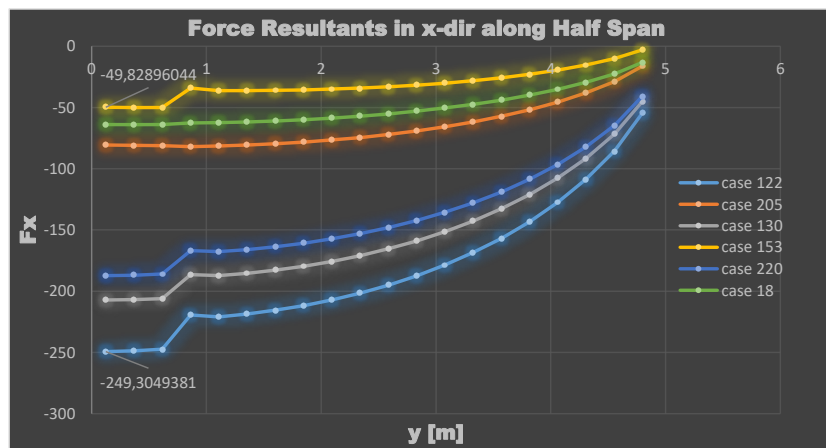


Figure 3.1-130. Force Resultants in z-dir. along Half Span

UNCLASSIFIED

UNCLASSIFIED



Figure 3.1-131. Force Resultants in z-dir. along Half Span

UNCLASSIFIED

UNCLASSIFIED

3.1.4.5.2. HORIZONTAL TAIL

Geometry

The horizontal tail is formed as a rectangle having its long edge as the span of the tail and its short edge as the chord of the tail. The short edge of one of the elevators is chosen to be one fourth of the chord of the tail and the long edge lies along the half span, as illustrated in *Figure 132*.

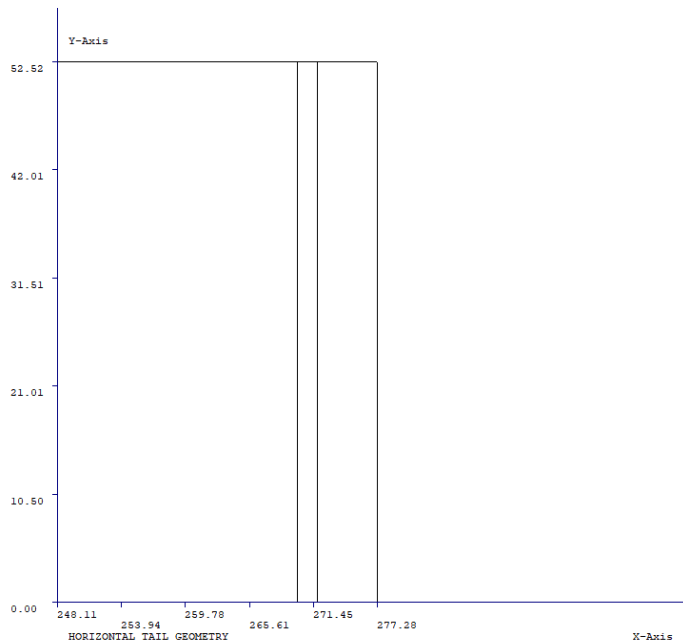


Figure 3.1-132. The Horizontal Tail Geometry along Half Span

UNCLASSIFIED

UNCLASSIFIED

Critical Load Cases

The critical load cases chosen are as follows:

1. UP BALANCING TAIL LOAD FLAPS RETRACTED
2. DOWN BALANCING TAIL LOAD FLAPS RETRACTED
3. UP BALANCING TAIL LOAD FLAPS EXTENDED
4. DOWN BALANCING TAIL LOAD FLAPS EXTENDED
5. UNCHECKED MANEUVER DOWN TAIL LOAD (ELEV TE UP)
6. UNCHECKED MANEUVER UP TAIL LOAD (ELEV TE DN)
7. DOWN LOAD CHECKED MANEUVER TAIL LOAD
8. UP LOAD CHECKED MANEUVER TAIL LOAD
9. UPGUST TAIL LOAD FLAPS RETRACTED
10. DOWN GUST TAIL LOAD FLAPS RETRACTED
11. UP GUST TAIL LOAD FLAPS EXTENDED
12. DOWN GUST TAIL LOAD FLAPS EXTENDED
13. UNSYMMETRICAL TAIL LOAD

Method

Let the following 1-D bar represent the back view of left half of the horizontal tail. FAR23 provides chordwise pressure distribution on chosen locations along the half span as output. The following load distribution is obtained via integrating P vs. Chord diagram. Noting that the directions are arbitrarily chosen for illustration, the distribution would be as follows in *Figure 133*.

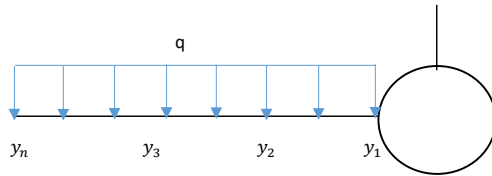


Figure 3.1-133. Back-View Illustration of the Left Half of The Tail of an Aircraft

The shear at the root is calculated via the basic rules of mechanics of materials and the shear at the tip is known to be zero. Furthermore, since the distribution is constant, the shear from the root to tip decreases in magnitude, linearly. As a result, the moment from root to tip also decreases in magnitude. Although the number of spanwise locations, $y_1 \dots y_n$, on which chordwise pressure distributions could be obtained are restricted to 10, since the constant force distribution is rather easy to handle, a quadratic moment vs. half span stations is obtained.

UNCLASSIFIED

UNCLASSIFIED

Results

All the resultant shear forces and moments along the half span of the horizontal tail are compared on the following two figures, *Figures 134 & 135*.

Please refer to Appendix A – Horizontal Tail Shear and Moment Diagrams for Each Critical Case to see detailed V-y and M-y diagrams for each critical case, separately.

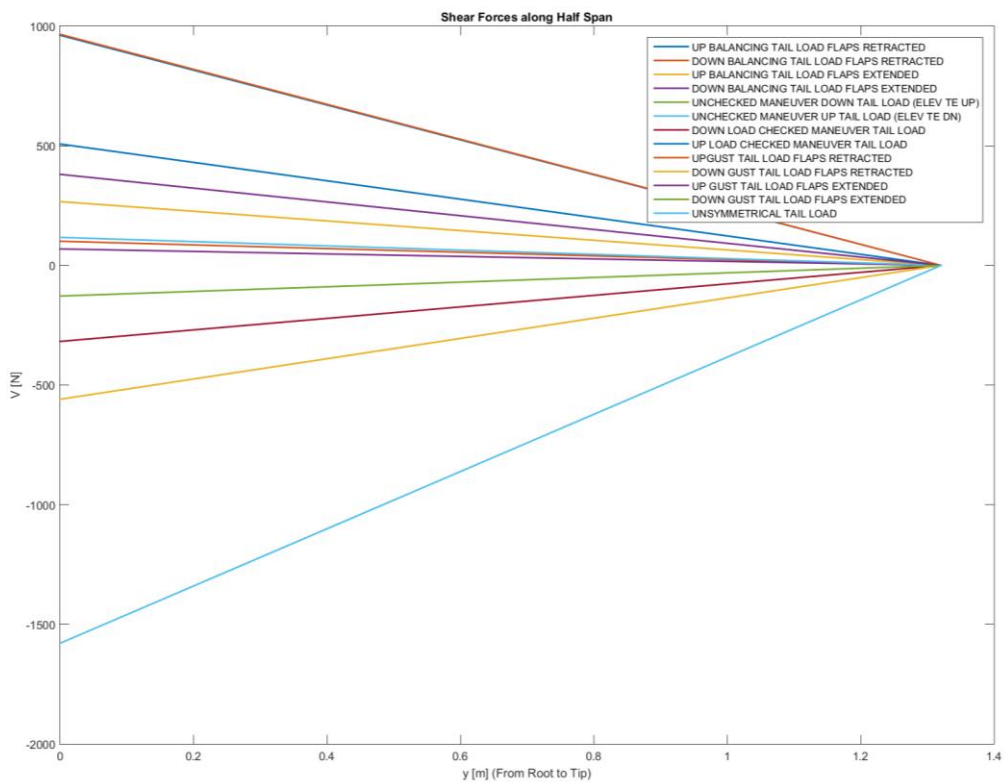


Figure 3.1-134. V-y for all 13 Cases

UNCLASSIFIED

UNCLASSIFIED

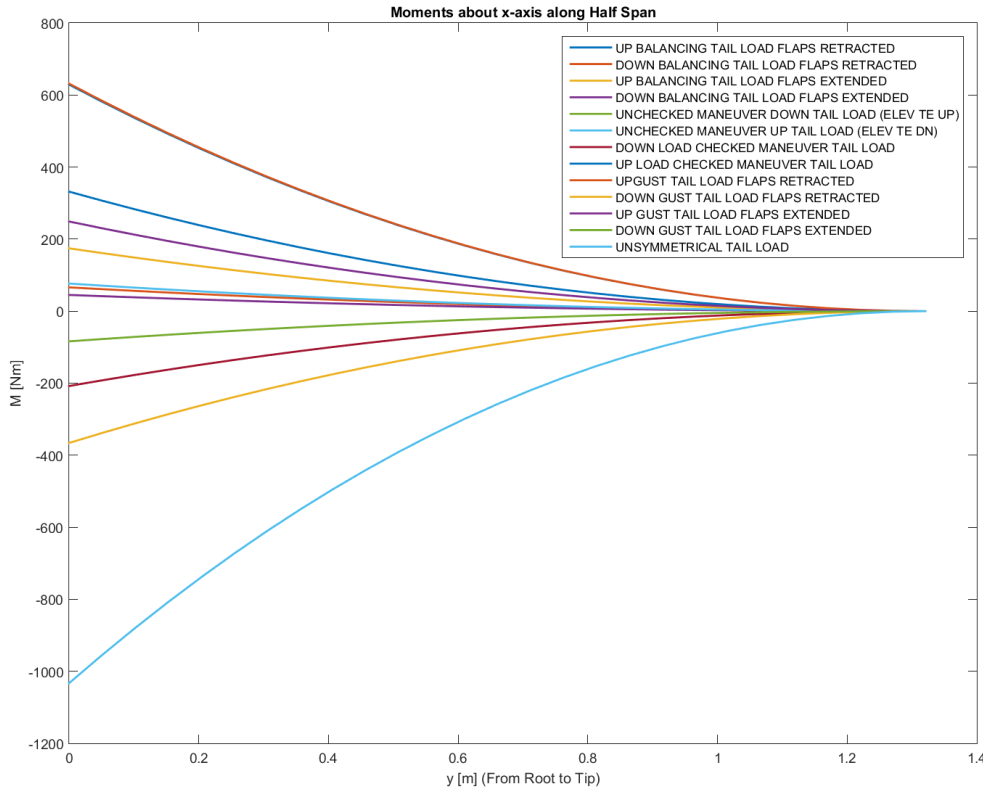


Figure 3.1-135. $M-y$ for all 13 Cases

3.1.4.5.3. VERTICAL TAIL

Geometry

The vertical tail geometry is also obtained from the first sizing process. The dimensions and the location of the rudder, however, is not determined and for the sake of load analyses, its tip chord is one fourth of the tip chord of the tail and its root chord is one fourth of the root chord of the tail, as shown in *Figure 136*.

UNCLASSIFIED

UNCLASSIFIED

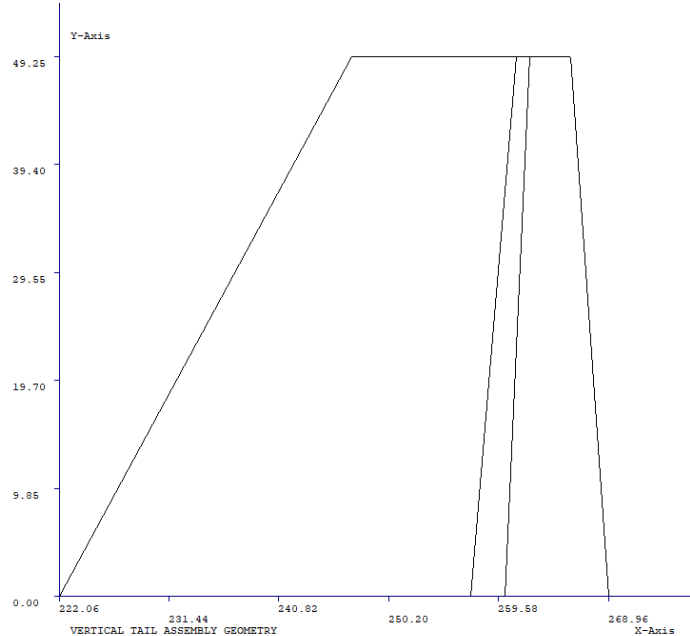


Figure 3.1-136. Vertical Tail Geometry

Critical Load Cases

There are four critical cases selected for vertical tail by FAR23 which are listed as below:

1. MANEUVER LOAD FOR SUDDEN FULL RUDDER DEFLECTION
2. MANEUVER LOAD FOR YAW TO SIDESLIP OF 22.5 DEG WITH RUDDER MAINTAINED AT FULL DEFLECTION
3. MANEUVER LOAD FOR YAW OF 15 DEG WITH RUDDER IN NEUTRAL
4. SIDE GUST LOAD AT VC

Method

Similar to what is done for the horizontal tail, chordwise pressure values are obtained from FAR23 and converted to distributed forces. However, as the tail does not have constant chord length, the force distribution is no longer constant. To overcome this issue and to converge to a result as close to the real load distribution, the tail is divided into five zones via the determination of water line stations and the pressure distributions at those water line stations are converted into the distributed forces (Figure 137). Moving on, the distribution of the distributed forces in between two water line stations are taken to be linearly changing. Finally, application of the rules of mechanics of materials yields the results.

UNCLASSIFIED

UNCLASSIFIED

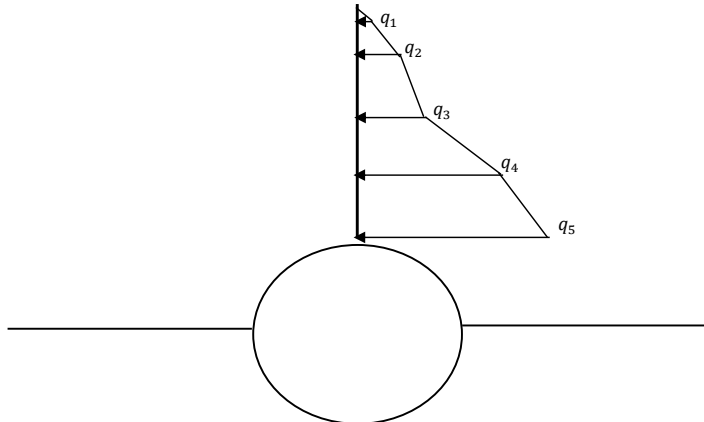


Figure 3.1-137. Sample Force Distribution on the Vertical Tail Shown on the Back-View Illustration of an Aircraft

UNCLASSIFIED

UNCLASSIFIED

1.1.1. Results

The shear and moment diagrams obtained for the load distribution along span for all four cases are given below, in *Figures 138 & 139*.

Please refer to APPENDIX B – Vertical Tail Shear and Moment Diagrams for Each Critical Case to see detailed graphs of each case, separately.

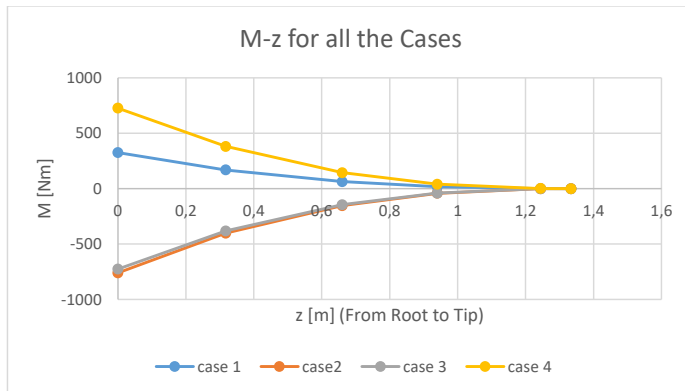


Figure 3.1-138. $V-z$ for all Four Cases

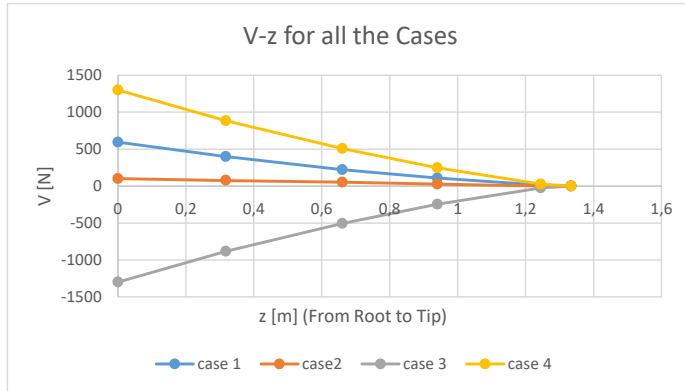


Figure 3.1-139. $M-z$ for all Four Cases

The resultant shear forces and moments at five spanwise locations from root to tip

UNCLASSIFIED

UNCLASSIFIED

m	case 1	case2	case 3	case 4
1.33	0.00	0.00	0.00	0.00
1.25	12.02	0.00	-25.60	25.60
0.94	107.16	25.24	-246.74	246.74
0.66	221.64	50.98	-507.52	507.52
0.32	398.22	75.72	-883.57	883.56
0	593.99	100.96	-1300.47	1300.48

Table 3.1-39. Shear Forces [N] at Spanwise Locations

m	case 1	case2	case 3	case 4
1.33	0	0	0	0
1.25	0.36	-0.78	-0.76	0.76
0.94	17.85	-41.80	-39.90	39.90
0.66	63.08	-153.04	-144.56	144.56
0.32	168.36	-401.15	-380.94	380.94
0	325.02	-760.13	-725.83	725.83

Table 3.1-40. Moments [Nm] at Spanwise Locations

3.1.5. Weight and Balance

3.1.5.1. PURPOSE

This report aims to show the target component weights, empty weight and maximum take-off weight of the aero plane by using different methods from different books. Furthermore, showing the simple C.G. values based on the first simple geometric sizing drawing of the aero plane.

3.1.5.2. NOMENCLATURE

A	= aspect ratio
B _h	= horizontal tail span, ft
B _w	= wing span, ft
D	= fuselage structural depth, ft
D _e	= engine diameter, ft
F _w	= fuselage at horizontal tail intersection, ft
H _t	= horizontal tail height above fuselage, ft
H _t /H _v	= vertical tail height above fuselage, ft
H _v	= vertical tail height above fuselage, ft
I _y	= yawing moment of inertia, lb - ft ²
int	= fuel quantity in integral fuel tank
K _{fsp}	= 5.87 $\frac{\text{lbs}}{\text{gal}}$ for aviation gasoline
L	= fuselage structural length, ft (excludes radome, tail cap)

UNCLASSIFIED

UNCLASSIFIED

L_f	= total fuselage length, ft
L_m	= length of main landing gear, in.
L_n	= nose gear length, ft
M	= Mach Number
N_c	= number of crew
N_{en}	= number of engines
N_l	= ultimate landing load factor; = $N_{gear} \times 1.5$
N_p	= passenger number including crew
N_t	= number of fuel tanks
N_z	= ultimate load factor; = $1.5 \times$ limit load factor
n_{ult}	= N_z
q	= dynamic pressure at cruise, lb/ft ²
S_{ht}	= horizontal tail area, ft ²
S_{vt}	= vertical tail area, ft ²
S_w	= trapezoidal wing area, ft ²
V_{pr}	= volume of pressurized section
W_{dg}	= design gross weight, lb
W_{en}	= engine weight, lb
W_l	= landing design gross weight, lb
W_{press}	= weight penalty due to pressureization,
$= 11.9 + (V_{pr} P_{delta})^{0.271}$, where P_{delta} = cabin pressure differential, psi (typically 8 psi)	
W_{uav}	= uninstalled avionics weight, lb (typically 800 – 1400lb)
Λ	= wing sweep at 25% MAC

3.1.5.3. DEFINITIONS

Empty weight: Empty Weight is an engineering term which is defined as the weight of the complete aircraft as defined in the aircraft specifications, dry, clean, and empty except for fluids in closed systems such as a hydraulic system.

Corresponding CS-VLA article

The empty weight and corresponding center of gravity must be determined by weighing the aeroplane with Fixed ballast; Unusable fuel determined under CS-VLA 959; and Full operating fluids, including Oil; Hydraulic fluid; and Other fluids required for operation of aeroplane systems. The condition of the aeroplane at the time of determining empty weight must be one that is well defined and can be easily repeated.

UNCLASSIFIED

UNCLASSIFIED

Minimum Flight Weight: Minimum Flight Weight is the lowest weight required for flight.

Corresponding CS-VLA article

Minimum weight. The minimum weight (the lowest weight at which compliance with each applicable requirement of this CS-VLA is shown) must be established so that it is not more than the sum of the empty weight determined under CS-VLA 29; the weight of the pilot (assumed as 55 kg); and the fuel necessary for one half hour of operation at maximum continuous power.

Maximum Take-Off Weight: The Maximum Take-Off Weight shall be the highest required weight for flight usage at the time of lift-off.

The Maximum Take-Off Weight is normally defined as the weight of the aircraft with the maximum internal and external loads and full fuel except for fuel used during taxi and warm-up.

Corresponding CS-VLA article

1. Maximum weight. The maximum weight is the highest weight at which compliance with each applicable requirement of this CSVLA is shown. The maximum weight must be established so that it is not more than the highest weight selected by the applicant; the design maximum weight, which is the highest weight at which compliance with each applicable structural loading condition of this CSVLA is shown; or the highest weight at which compliance with each applicable flight requirement of this CS-VLA is shown.
2. Maximum weight. The maximum weight is the highest weight at which compliance with each applicable requirement of this CSVLA is shown. The maximum weight must be established so that it is Assuming a weight of 86 kg for each occupant of each seat, not less than the weight with; Each seat occupied, full quantity of oil, and at least enough fuel for one hour of operation at rated maximum continuous power; or; One pilot, full quantity of oil, and fuel to full tank capacity.

UNCLASSIFIED

UNCLASSIFIED

3.1.5.4. INPUTS

Following input values are listed below are integrated the Design Code and using the input values component weights of the aeroplane are calculated by using the Raymer and Nicolai method.

Inputs		Simge	Birim	Değer
Wing	trapezoidal wing area	S_w	ft ²	137.28
	weight of fuel in wing	W_fw	lbf	159.25
	aspect ratio of wing	AR		7.60
	wing sweep at 25% MGC		rad	0.00
	dynamic pressure at cruise	q	lbf/ft ²	15.76
	wing taper ratio		no unit	0.50
	wing thickness to chord ratio	t/c	no unit	0.15
	wingspan	b	ft	32.30
	Wing Mean Aerodynamic Chord	MAC	ft	4.41
	Wing Density Factor	K_p	no unit	0.0016
	ultimate load factor	n_z	no unit	5.70
	design gross weight	W_0	lbf	1617.35
	maximum level airspeed at sea level	V_H(KEAS)	knot	126.02
Landing Gear	ultimate landing load factor	n_l	no unit	3.00
	design landing weight	W_l	lbf	1478.73
	length of the main landing gear strut	L_m	inc	24.02
	length of the nose landing gear	L_n	inc	24.02
	Landing Place Factor	K_L	no unit	1
	Landing Gear Weight Factor	K_LG	no unit	0.55
	Retract Landing Gear Factor	K_ret	no unit	1
Engine	uninstalled engine weight	W_eng	lbf	124.87
	number of engine	N_eng	no unit	1.00
	Engine Weight Factor	K_E	(lb)	2.6
Fuel System	total fuel quantity	Q_tot	Gallons	14.53
	fuel quantity in integral fuel tanks	Q_int	gallons	14.53
	number of fuel tanks	N_tank		2.00
	Fuel System Density Factor	K_fs	no unit	2.00
	Fuel Density	rho_f	lb/gal	5.87
	Fuel System upper constant	n_fs	no unit	0.667
	weight of the uninstalled avionics	W_uav	lbf	22.06
	number of occupants	N_occ	no unit	2.00
	Mach number	M	no unit	0.150
	number of crew	N_crew	no unit	2.00
	dynamic pressure at max level airspeed	q_H	lb/ft ²	46.41
	rated power of engine	P_rate	BHP	92.73

UNCLASSIFIED

UNCLASSIFIED

Fuselage	length of fuselage structure (forward bulkhead to aft frame)	l_fs	ft	19.64
	depth of fuselage structure	d_fs	ft	0.16
	volume of pressurized cabin section	V_p	ft ³	105.94
	cabin pressure differential	ΔP	psi	0.00
	Fuselage Length	l_f	ft	23.11
	Fuselage Max height	w_f	ft	4.62
	fuselage max width	d_f	ft	4.62
	Fuselage Area	S_fus	ft ²	211.04
	Fuselage Density Factor	Kp_f	no unit	0.00
	Inlet Density Factor	K_inlet	no unit	1.25
Horizontal Tail	trapezoidal HT area	S_HT	ft ²	19.46
	HT sweep at 25% MGC			0.00
	HT taper ratio			1.00
	horizontal tail arm from wing C/4 to HT C/4	l_HT	ft	14.21
	HT span	b_HT	ft	8.75
	max root chord thickness of HT	t_HT_max	inc	4.38
	aspect ratio of horizontal tail	AR_HT	no unit	3.60
	Horizontal Tail Density Factor	KpHT	no unit	0.025
	Horizontal Mean Aerodynamic Chord	MAC_HT	ft	2.432
	0 for conventional tail,=1 for T-tail	F_tail	no unit	0.00
Vertical Tail	VT span	b_VT	ft	4.10
	VT Volume Ratio	Vvt_bar	no unit	0.04
	Rudder chord length	Cr	ft	
	VT chord length	Cvt	ft	3.91
	Vertical Tail Density Factor	KpVT	no unit	0.07
	Vertical Mean Aerodynamic Chord	MAC_VT	ft	2.74
	trapezoidal VT area	S_VT	ft ²	11.23
	VT sweep at 25% MGC		rad	0.35
	VT taper ratio		no unit	0.40
	max root chord thickness of VT	t_VT_max	inc	7.04
	aspect ratio of vertical tail	AR_VT	no unit	1.50
	Aliminium Density	rho_mat	lbs/ft ³	66.54

Table 3.1-41. Iterated Input Values for Empirical Weight Methods

Table 1 includes all the geometric and performance input values that the empirical methods need to calculate the weight of components.

UNCLASSIFIED

UNCLASSIFIED

3.1.5.5. WEIGHT BREAKDOWNS

Iteration in the Design Code excel is done automatically and there is no need extra steps to find the final values of the components.

To catch a more accurate component weights in addition to methods we have used the wing, fuselage, tail and landing gear weight to MTOW ratios according to Ref 6.1.1.

	[kg]	[kg]
	Raymer	Nicolai
Fuselage	58	94
Wing	86	71
Horizontal Tail	4	11
Vertical Tail	1	3
Main Landing gear	36	38
Nose Landing gear	12	-
Installed Engine	100	100
Fuel System	8	7
Flight control-system	9	49
Parachute + Extras	1	-
Avionic System	17	17
Electrical system	46	44
Air conditioning and anti-icing	12	14
Furnishings	10	10
Fuel Weight	77	77
Crew	172	172
Payload	20	20
Wempty	399	458
MTOW	669	728

	[lb]	[kg]
	RESULTANT	
	175	80
	209	95
	23	10
	13	6
	66	30
	28	13
	220	100
	17	8
	79	36
	27	12
	25	11
	94	42
	27	12
	22	10
	170	77
	379	172
	44	20
	1024	465
	1617	734

Table 3.1-42. Weight Breakdown of the Components and Subsystems of the VLA

	Target Weight	Target Percentage
Fusalage	81	11%
Wing	95	13%
Horizontal Tail	15	2%
Vertical Tail		
Main Landing gear	29	4%
Nose Landing gear		

Table 3.1-43. Historical Components' Weight Ratio to MTOW

Table 2 shows the results of 2 different empirical methods Raymer and Nicolai and empyt weight and MTOW . Using the historical ratios in Table 3 target weights of the components are iterated and calculated in table 2. The target weight

UNCLASSIFIED

UNCLASSIFIED

decisions are verified by negotiate with structural designers of the components. Since the results are applicable target weights are defined by combining both empirical methods and historical MTOW ratios.

- Crew weight is taken as 86 kg which is the maximum weight mentioned in CS-VLA 25-a.
- Target weights are found from the target percentages. Target percentages are taken from Sadraey's design book for Single-engine GA category airplanes.
- Values found from empirical methods are converged to target weights in order to have more reasonable weight breakdown.
- In this stage engine is considered to be Rotax 912uls which has a dry weight of 56 kg.
- Installed engine weight includes spinner weight and calculated with the weight approximation methods used in Raymer and Nicolai.

3.1.5.6. C.G. CALCULATIONS

Since the system integration is not done yet, approximate system placements are used in the C.G calculations. Fuselage, wing, tails and landing gears are placed first and they are based on the drawing but the other systems and components are placed approximately. Final total x-direction C.G except fuel weight is calculated as 6.82 feet (2.08 m) from nose and it is %28.8 of total fuselage length which is acceptable.

After system integration is completed, a more accurate C.G. calculation will be done.

	WEIGHT[lb]	WEIGHT[kg]	XCG[feet]	WxXCG	XCG[m]
Fuselage	175	80	8,76	697	2,67
Wing	209	95	7,90	749	2,41
Horizontal Tail	23	10	21,08	217	6,42
Vertical Tail	13	6	20,21	116	6,16
Main Landing gear	66	30	8,69	261	2,65
Nose Landing gear	28	13	1,80	22	0,55
Installed Engine	220	100	1,05	105	0,32
Fuel System	17	8	2,65	20	0,81
Flight control-system	79	36	7,70	277	2,35
Parachute+Extras	27	12	7,70	93	2,35
Avionic System	25	11	3,39	38	1,03
Electricalsystem	94	42	7,70	327	2,35
Air conditioning and anti-icing	27	12	3,39	42	1,03
Furnishings	22	10	7,47	76	2,28
Fuel Weight	170	5	7,90	37	2,41
Crew	379	86	7,47	642	2,28
PayLoad	44	0	7,70	0	2,35
Wempty					0,00
MTOW	1617	734	5,07		1,54
%				0,214	

Table 3.1-44. Most Forward C.G.

UNCLASSIFIED

UNCLASSIFIED

	WEIGHT[lb]	WEIGHT[kg]	XCG[feet]	WxXCG	XCG[m]
Fuselage	175	80	8,76	697	2,67
Wing	209	95	7,90	749	2,41
Horizontal Tail	23	10	21,08	217	6,42
Vertical Tail	13	6	20,21	116	6,16
Main Landing gear	66	30	8,69	261	2,65
Nose Landing gear	28	13	1,80	22	0,55
Installed Engine	220	100	1,05	105	0,32
Fuel System	17	8	2,65	20	0,81
Flight control-system	79	36	7,70	277	2,35
Parachute+Extras	27	12	7,70	93	2,35
Avionic System	25	11	3,39	38	1,03
Electricalsystem	94	42	7,70	327	2,35
Air conditioning and anti-icing	27	12	3,39	42	1,03
Furnishings	22	10	7,47	76	2,28
Fuel Weight	170	77	7,90	611	2,41
Crew	379	172	7,47	1284	2,28
PayLoad	44	20	7,70	154	2,35
Wempty					0,00
MTOW	1617	734	6,93		2,11
%			0,293		

Table 3.1-45. Most Aft C.G.

UNCLASSIFIED

UNCLASSIFIED

	WEIGHT[lb]	WEIGHT[kg]	XCG[feet]	WxXCG	XCG[m]
Fuselage	175	80	8.76	697	2.67
Wing	209	95	7.90	749	2.41
Horizontal Tail	23	10	21.08	217	6.42
Vertical Tail	13	6	20.21	116	6.16
Main Landing gear	66	30	8.69	261	2.65
Nose Landing gear	28	13	1.80	22	0.55
Installed Engine	220	100	1.05	105	0.32
Fuel System	17	8	2.65	20	0.81
Flight control-system	79	36	7.70	277	2.35
Parachute +Extras	27	12	7.70	93	2.35
Avionic System	25	11	3.39	38	1.03
Electrical system	94	42	7.70	327	2.35
Air conditioning and anti-icing	27	12	3.39	42	1.03
Furnishings	22	10	7.47	76	2.28
Fuel Weight	170	77			0.00
Crew	379	172	7.47	1284	2.28
Payload	44	20	7.70	154	2.35
Wempty					0.00
MTOW	1617	734			0.00
MTOW2		656	6.82		2.08
%			0.288		

Table 3.1-46. C.G without fuel

Table 4 shows most forward x-body direction c.g case which includes 1 crew, no payload and trapped fuel. It is at the position which is 21.4% of the fuselage from nose.

Table 5 shows most aft x-body direction c.g case which includes full crew, payload and full fuel. It is at the position which is 29.3% of the fuselage from nose.

Table 5 shows c.g case which includes everything full but excludes the fuel. It is at the position which is 28.8% of the fuselage from nose.

UNCLASSIFIED

UNCLASSIFIED

3.1.5.7. REFERENCES

Books

Mohammad H. Sadraey, Aircraft Design: A Systems Engineering Approach, 2012

Daniel Raymer, Aircraft Design, 1989

Leland M. Nicolai, Grant Carichner, Fundamentals of Aircraft and Airship Design, 2010

Methods

Raymer Method

$$\begin{aligned}
 W_{wing} &= 0.036 S_w^{0.758} W_{fw}^{0.0035} \left(\frac{A}{\cos^2 \Lambda} \right)^{0.6} q^{0.006} \lambda^{0.04} \left(\frac{100 \frac{t}{c}}{\cos \Lambda} \right)^{-0.3} (N_z W_{dg})^{0.49} \\
 W_{horizontal\ tail} &= 0.16 (N_z W_{dg})^{0.414} q^{0.168} S_{ht}^{0.896} \left(\frac{100 \frac{t}{c}}{\cos \Lambda} \right) \left(\frac{A}{\cos^2 \Lambda_{ht}} \right)^{0.043} \lambda_h^{-0.02} \\
 W_{vertical\ tail} &= 0.073 \left(1 + 0.2 \frac{H_i}{H_v} \right) (N_z W_{dg})^{0.376} q^{0.122} S_{vt}^{0.873} \left(\frac{100 \frac{t}{c}}{\cos \Lambda_{vt}} \right)^{-0.49} \left(\frac{A}{\cos^2 \Lambda_{vt}} \right)^{0.357} \lambda_{vt}^{0.039} \\
 W_{fuselage} &= 0.052 S_f^{1.086} (N_z W_{dg})^{0.177} L_f^{-0.051} \left(\frac{L}{D} \right)^{-0.072} q^{0.241} + W_{press} \\
 W_{main\ landing\ gear} &= 0.095 (N_l W_l)^{0.768} \left(\frac{L_m}{12} \right)^{0.409} \\
 W_{nose\ landing\ gear} &= 0.125 (N_l W_l)^{0.566} \left(\frac{L_n}{12} \right)^{0.845} \\
 W_{installed\ engine\ (total)} &= 2.575 W_{en}^{0.922} N_{en}^{0.157} \\
 W_{flight\ controls} &= 0.053 L^{1.536} D_w^{0.371} (N_z W_{dg} \times 10^{-4})^{0.80} \\
 W_{hydraulics} &= 0.001 W_{dg} \\
 W_{electrical} &= 12.57 (W_{fuel\ system} + W_{avionics})^{0.51} \\
 W_{avionics} &= 2.117 W_{uav}^{0.933} \\
 W_{air\ conditioning\ and\ anti-ice} &= 0.265 W_{dg}^{0.52} N_p^{0.68} W_{avionics}^{0.17} M^{0.08} \\
 W_{furnishings} &= 0.0582 W_{dg} - 65
 \end{aligned}$$

UNCLASSIFIED

UNCLASSIFIED

Roskam Method

$$W_{wing} = 96.948 \left[\left(W_{to} \cdot \frac{nult}{10^5} \right)^{0.65} \cdot \left(\frac{A}{\cos(\Lambda)} \right)^{0.57} \left[\frac{S}{100} \right]^{0.61} \cdot \left[\left(\frac{1+\lambda}{2} \right) \cdot M_{wt} \right]^{0.36} \cdot \left(1 + \frac{VH}{500} \right)^{0.5} \right]^{0.993}$$

$$W_{horizontal\ tail} = 127 \left[\left(W_{to} \cdot \frac{nult}{10^5} \right)^{0.87} \left(\frac{SH}{100} \right)^{1.2} \cdot 0.289 \left(\frac{lh}{10} \right)^{0.483} \cdot \left(\frac{bh}{trh} \right)^{0.5} \right]^{0.458}$$

$$W_{vertical\ tail} = 98.5 \left[\left(W_{to} \cdot \frac{nult}{10^5} \right)^{0.87} \left(\frac{SV}{100} \right)^{1.2} \cdot 0.289 \left(\frac{bv}{trv} \right)^{0.5} \right]^{0.458}$$

$$W_{fuselage} = 200 \left[\left(W_{to} \cdot \frac{nult}{10^5} \right)^{0.286} \left(\frac{lf}{10} \right)^{0.857} \left[\frac{bf+hf}{10} \right] \left(\frac{VC}{100} \right)^{0.338} \right]^{1.1}$$

$$W_{landing\ gear\ total} = 0.054 (lsm)^{0.501} [W_{to} \cdot nult]^{0.684}$$

$$W_{fuel\ system} = 2.49 \left[\left(\frac{W_f}{Kfsp} \right)^{0.6} \left[\frac{1}{1 + int} \right]^{0.3} \cdot (N_t)^{0.2} (N_e)^{0.13} \right]^{1.21}$$

$$W_{installed\ engine\ (total)} = 2.575 W_{en}^{0.922} N_{en}$$

$$W_{flight\ controls} = 1.08 (W_{to})^{0.7}$$

$$W_{hydraulics} = 0.012 W_{to}$$

$$W_{electrical} = 426 \left[\frac{(W_{fuel\ system} + W_{avionics})}{1000} \right]^{0.51}$$

$$W_{avionics} = 33. N_{pax}$$

$$W_{air\ conditioning\ and\ anti-ice} = 0.265 W_{to}^{0.52} N_p^{0.68} W_{avionics}^{0.17} M^{0.08}$$

$$W_{furnishings} = 0.412 (N_{pax})^{1.145} (W_{to})^{0.489}$$

UNCLASSIFIED

UNCLASSIFIED

Nicolai Method

$$W_{wing} = 96.948 \left[\left(W_{to} \cdot \frac{nult}{10^5} \right)^{0.65} \cdot \left(\frac{A}{\cos(\Lambda)} \right)^{0.57} \left[\frac{S}{100} \right]^{0.61} \cdot \left[\left(\frac{1+\lambda}{2} \right) \cdot M_{wt} \right]^{0.36} \cdot \left(1 + \frac{VH}{500} \right)^{0.5} \right]^{0.993}$$

$$W_{horizontal\ tail} = 127 \cdot \left[\left(W_{to} \cdot \frac{nult}{10^5} \right)^{0.87} \left(\frac{SH}{100} \right)^{1.2} \cdot \left(\frac{lh}{10} \right)^{0.483} \cdot \left(\frac{bh}{trh} \right)^{0.5} \right]^{0.458}$$

$$W_{vertical\ tail} = 98.5 \cdot \left[\left(W_{to} \cdot \frac{nult}{10^5} \right)^{0.87} \left(\frac{SV}{100} \right)^{1.2} \cdot \left(\frac{bv}{trv} \right)^{0.5} \right]^{0.458}$$

$$W_{fuselage} = 200 \left[\left(W_{to} \cdot \frac{nult}{10^5} \right)^{0.286} \left(\frac{lf}{10} \right)^{0.857} \left[\frac{bf+hf}{10} \right] \left(\frac{VC}{100} \right)^{0.338} \right]^{1.1}$$

$$W_{landing\ gear\ total} = 0.054(lsm)^{0.501}[W_{to}.nult]^{0.684}$$

$$W_{fuel\ system} = 2.49 \left[\left(\frac{W_f}{Kfsp} \right)^{0.6} \left[\frac{1}{1+int} \right]^{0.3} \cdot (N_t)^{0.2} (N_e)^{0.13} \right]^{1.21}$$

$$W_{installed\ engine\ (total)} = 2.575 W_{en}^{0.922} N_{en}$$

$$W_{flight\ controls} = 1.066(W_{to})^{0.626}$$

$$W_{electrical} = 426 \left[\frac{(W_{fuel\ system} + W_{avionics})}{1000} \right]^{0.51}$$

$$W_{avionics} = 2.117(W_{AU})^{0.933}$$

$$W_{air\ conditioning\ and\ anti-ice} = 0.265 W_{to}^{0.52} N_p^{0.68} W_{avionics}^{0.17} M^{0.08}$$

$$W_{furnishings} = 34.5(N_{CR})(q)^{0.25}$$

3.1.6. Cockpit Design & Human Factor

3.1.6.1. INTRODUCTION

This report is written to explain and summarize the trade-off studies about ergonomics and viewpoints at the conceptual design stage within the METU-TAI Very Light Aircraft (VLA) Project. In the content of the report, the criteria considered in cockpit dimensioning will be explained, the importance of these criteria in the conceptual design phase will be mentioned and alternative evaluations will be evaluated.

The report consists of 4 chapters. The first chapter explains the terms that are in the report. Chapter 2 discusses the significance and impact of the points in the cockpit by focusing on the points in the ergonomics. In Chapter 3, details of the alternative cockpit design dimensions are mentioned. Finally, the chapter 4 explains the road map of the cockpit team.

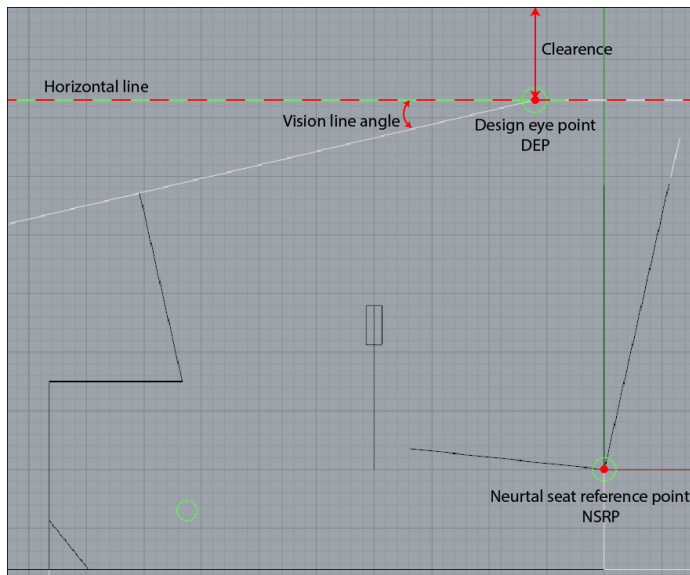
References (MS 33574B, MIL-STD 1333, MIL-STD-850B) are in appendix.

UNCLASSIFIED

UNCLASSIFIED

3.1.6.2. CHAPTER 1:

The terms in the report are:



Neutral seat reference point (NSRP): refers to the position in the x and y axis of the cockpit where the bottom and back surfaces of the seat are joined. Neutral seat reference point is used as a reference in establishing relations with other main members by being determined first when cockpit is measured.

Horizontal line: Horizontal line is the line which is parallel to the cockpit floor and passing through the expected point of view of the pilot.

Design eye point (DEP): It is the expected point of finding the pilot's eye. The design eye point is one of the first reference points that should be determined when dimensioning the cockpit and is critical for the viewpoints.

Vision line angle: Vision line angle refers to the angle formed between the design eye point and the horizontal line drawn at the top point of the front panel. Any change of this angle affects the pilot's view.

Clearence: Clearence is one of the terms used in ergonomics and is a measurement which is used to enhance the comfort of a movement and position. This dimension has some standards in the cockpit. For example, according to military standards, a clearance between the DEP and the canopy is required to be at least 10 inches of radial.

UNCLASSIFIED

UNCLASSIFIED

3.1.6.3. CHAPTER 2

The main instruments in the cockpit that will be studied within the scope of ergonomics are:

1. Seat

a) Connection point: The seat's connecting point is one of the ergonomically important issues, as the cockpit determines the NSRP point while dimensioning the cockpit. The height of the connection point directly determines the vision line angle and the total height of the cockpit. At the same time, this point directly affects the flight dynamics of the aircraft in terms of load distribution. At this point, we are expecting data from the structure team and the load distribution team for the final decision to be made for the joining point of the seat. We expect this point to have a height of 8.5-11 inches when we work independently from this data.

b) Mobility and effectiveness: It is decided to use movable seat in the cockpit as a result of the trade-off studies and interviews made by the teachers. The back and forth motion of the seat is considered to be 3 inches forward and 3 inches back, based on the maximum value observed in equivalent products. In military standards, this measure is 1.5 inches forward and 1.5 inches downwards, which gives us a reference in terms of minimum desired mobility. The up and down movement of the seat directly affects the vision line angle. The 2.5 inch up to 2.5 inch downward movement should be measured by taking military standards into consideration.

c) Seat measurements: The seat measurements are limited to current and available items in the market. As the seat width will directly affect the cockpit width, so we are in search of the seat that matches the aircraft geometry that emerged as the initial sizing result. The seat measurements in the market are not very important to us in the conceptual design phase. But while working on the ability to move the loins may require a space in the middle of the resultant seat. Now we use 18-21 inch for the seat's width.

d) Distance between NSRP and control surfaces: NSRP and control surfaces (panel, lever, throttle, pedals) directly affect the pilot's access to these surfaces. These distances need to be in harmony with each other so that these surfaces can be controlled so as not to cause organizing and faulting.

e) Binding angle: The angle of the seat's connecting point causes changes in the design eye point by affecting the position of the pilot in the cockpit. This angle is considered to be 5 degrees in our configuration considering the military standards, but it can be changed angles if the spar passes through the cockpit.

2. Pedal

a) Distance between the NSRP: The distance between the NSRP and the pedal connection point is calculated by considering the leg length of the pilot and the lowest point of the panel. This measurement directly affects the length of the cockpit. Using military standards and some anthropometric data from reliable sources, we predict that this measurement should be in the range of 33.6-36.9 inches.

b) Movement abilities: After deciding the stability of the pedals, recurrent military standards are taken as reference for calculating how many inches forward and backward from the neutral points of the pedals for rudder movement. Military standards show that this movement should be 3.25 inches forward and 3.25 inches backwards. It is also stated in military standards that after a 3.25 inch forward movement, the foot should brake on the foot pedal and should be at least 1 inch from the firewall in the position it is standing at. This measurement is also effective when determining the cockpit length.

UNCLASSIFIED

UNCLASSIFIED

c) Distance between 2 pedals: The distance between the outer surfaces of 2 pedals will be the maximum seat width, but this measure is not fully specified at this time. Since no standard is found for the distance between the inner surfaces of the 2 pedals, these decisions are made when ergonomics studies are carried out on the mockup. This distance is shared with the relevant team as it will directly affect the flight control team's mechanism.

d) Height from above: This standard is 5 inches in military standards. We will follow this standard.

e) Pedal measurements: The pedal measurements shall be determined by deciding the measurements of the products that can be purchased if the pedals are supplied from the outside. In the case of ourselves, this measurement is made using anthropometric data.

3. Lever

a) Distance from the NSRP: The distance between the lever and the NSRP is the most critical point of access for the pilot. This distance also affects the seat dimensioning, the attachment point of the leopard and the panel position. For the alternatives we use, this distance is 19-20.9 inches considering the military standards of the MS33574B and MIL-STD 1333B.

b) Mobility: The lever must be both accessible and easily capable of providing maximum mobility. For this reason, during use of the lug, consideration must be given to surfaces that restrict movement around the lug. It is expected that these restrictive surfaces, the user's legs, seat and panel. For this reason, the relationship with these surfaces will be studied while determining the mobility. Since we cannot find a value that can be taken as a reference for this measurement, our team will work on mockup tests when this decision is made.

c) Elevation from the ground: elevation of the ground from the ground, affecting the forces required to be applied to the ground by the pilot. At the same time, it is also important in terms of access to lever. Our aim with the flight control team is to bring these forces to the level of applicable forces that will be achieved by utilizing anthropometric studies.

d) Form: Examination of the attachment point and movement ability of the levee will be decided in the form of a final lie. At the same time, the seat to be taken will also be effective. There are currently 2 options available, which are plain and gooseneck types of lows.

4. Panel

a) Panel measurements: For panel measurements, maximum values that can be used in ergonomics are studied. The panel width is important in terms of seeing the entire panel of pilots and also, it affects cockpit width. Panel height will be determined so as not to interfere with pedal access by pilots. At this time values of 15.6-18 inch are foreseen for the height of panel front surface.

b) Distance between NSRP: The NSRP position directly affects the DEP position. The distance between the panel and the DEP can be clearly seen, affecting the vision line angle value and the viewing angle of the entire panel. At this time, the distance between DEP and panel is 26.86-35.21 inch in our alternatives.

c) Panel angle: The panel angle shall be determined from DEP with the aim of making a 90-degree angle where the line drawn to the middle point of the panel intersects the panel.

d) Panel form: If the panel is an obstacle to pedestrian access, the pedestrian access of the pilot can be improved by changing the form.

UNCLASSIFIED

UNCLASSIFIED

e) **Avionic equipment:** Required avionic equipment and dimensions shall be determined by the avionics team and communicated to you. The measurements of these equipment are important in terms of the minimum space that our panel should have.

5. Throttle

a) **Elevation above ground:** Since this is not found by a standard team about the height of the power arm, this decision has been postponed to mockups. This height will be determined by considering the pilot access measures.

b) **Form:** Power cord is ergonomically important because it is a control frequently used by the pilot. For this reason, our team will start working on the form when the power arm becomes more ergonomic.

6. Luggage compartment

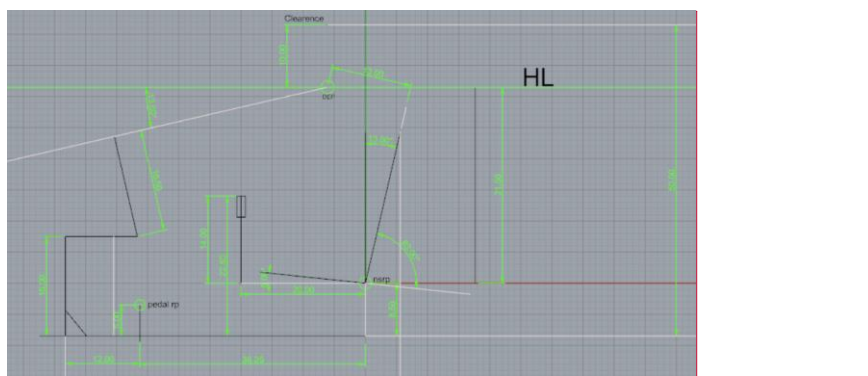
The luggage compartment is expected to be delivered from the load bundle, and it is predicted that if the luggage compartment is located in the cockpit, it will come to the back of the seat. In this case, the total length of the cockpit will vary.

3.1.6.4. CHAPTER 3

Four different alternative measurements for the cockpit design is given for these main instruments. These alternatives are;

Alternative 1

This alternative is based on references to the MS33574B, MIL-STD 1333B and MIL-STD-850B sources. Some information that cannot be obtained from this source is found in "Airplane Design Part 3: Layout design of cockpit, fuselage ..." written by Dr. Jan Roskam. This alternative is the one which requires a minimum height (50 inches).



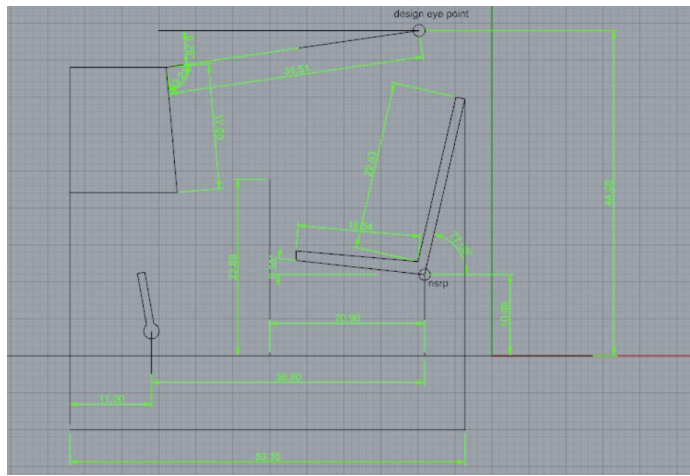
Açıklamalı [k1]: Figure number verelim hepsine

UNCLASSIFIED

UNCLASSIFIED

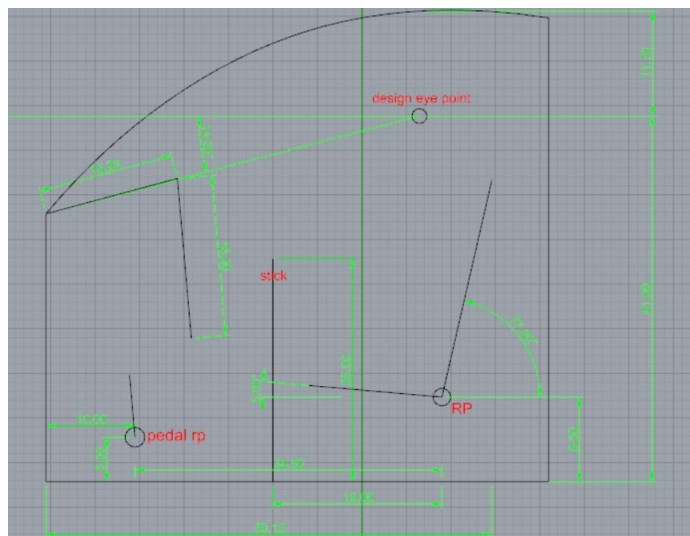
Alternative 2

This alternative is based on the pedestal, panel and stick relationship. In doing so, "Airplane Design Part 3: Layout design of cockpit, fuselage ..." by Dr. Jan Roskam was taken as reference. Military standards and anthropometric data from AGARD are references for some measurement vendors which are not mentioned in the book.



Alternative 3

This alternative is made by taking into consideration the flight team's winter clothes and light helmets which are used in the cockpit. "Airplane Design Part 3: Layout design of cockpit, fuselage ... by Dr. Jan Roskam" is the main reference source.

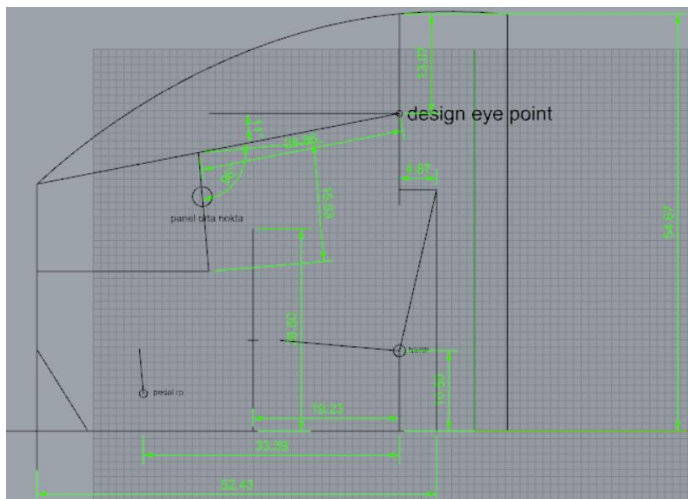


UNCLASSIFIED

UNCLASSIFIED

Alternative 4

This alternative was measured by reference to the anthropometric data of Dutch people aged 20-60 years, published by Delft University. It is intended to be smooth to use by a 95% user group. Also, the military standards are the secondary reference to this measurement.



3.1.6.5. CHAPTER 4

As a result, with these alternatives, a height is measured 50-54.67 inches, which could be updated (reduced) with some data (spar heights and positions) coming from the structure team.

For the length of the cockpit, a value in the range of 50.12-53.87 is predicted, while a value in the range of 42-50 inches is predicted for the width of the cockpit.

As a cockpit team, we are currently working on a 1:1 cockpit mockup to evaluate these alternatives. The results of these studies, we will be hoping to create some new alternatives and increase the reliability of our decisions. Also, by testing the alternative when the mockup is finished could be very helpful for us to see the mobility and positioning of the elements which should be revised again.

3.1.6.6. APPENDIX

MIL-STD 1333
MIL-STD-850B
MS 33574B

UNCLASSIFIED

UNCLASSIFIED

3.2. Airframe

3.2.1. Structural Design

3.2.1.1. Fuselage Configuration

3.2.1.1.1. Truss type construction

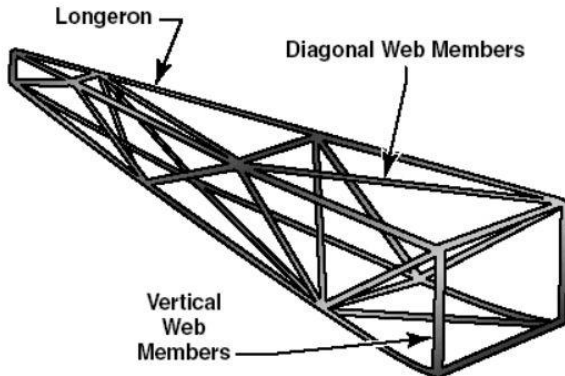


Figure 3.2-1. Truss type construction

A truss is a rigid framework made up of beams, struts and bars to resist deformation by applied loads. Strength and rigidity is attained by welding the tubing together into a series of triangular shapes. Generally, the truss-type fuselage frame is constructed of steel or aluminum tubing and covered with fabric or thin sheet aluminum alloy. When a load on a truss member acts in one direction, every alternate member carries tension while the other members carry compression. When the load is reversed, the members which were carrying compression now are subjected to tension and those which were carrying tension are subjected to compression. The main disadvantage of this configuration is lack of streamlined shape.

Pratt Truss

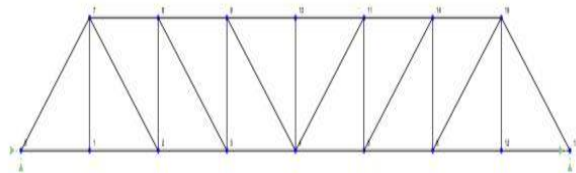


Figure 3.2-2. Pratt truss type construction

A Pratt truss has been used over the last two centuries as an effective truss method. When the vertical members are under compression stress, diagonal members carry tensile stress. This simplifies and produces a more efficient design since diagonal members can be reduced. This situation reduce the cost and weight of the design. Also, it makes the construction of truss is easier. (Airframe Construction p.4)

UNCLASSIFIED

UNCLASSIFIED

Warren Truss

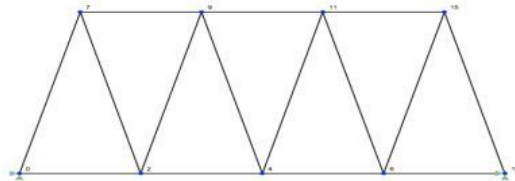


Figure 3.2-3. Warren truss type construction

Warren truss type is another common truss structure and it is constructed by equilateral triangles. This type of truss spread the load evenly across a number of different members, Warren truss is suitable for distributed load but not approvable for concentrated or point load (Airframe Construction pp.5-6).

3.2.1.1.2. Monocoque type construction

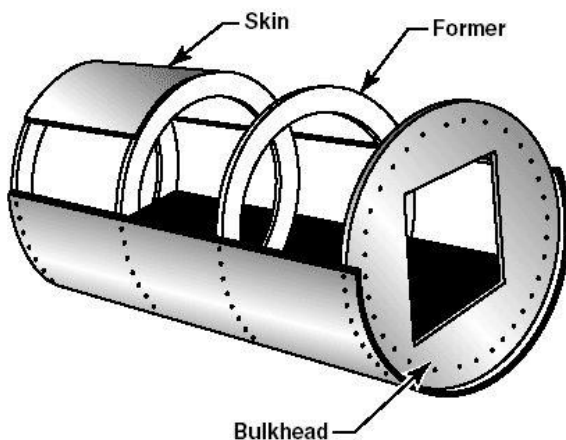


Figure 3.2-4. Monocoque type construction

Monocoque construction is consist of formers, frames and bulkheads. The heaviest of these structural members are located at intervals to carry concentrated loads and fitting points. Skin carry the primary stresses and keep the fuselage rigid since there are no other bracing member .The biggest problem of monocoque construction is maintaining enough strength while keeping weight within allowable limits (Aircraft Structures p.9).

UNCLASSIFIED

UNCLASSIFIED

3.2.1.1.3. Semi-monocoque type construction

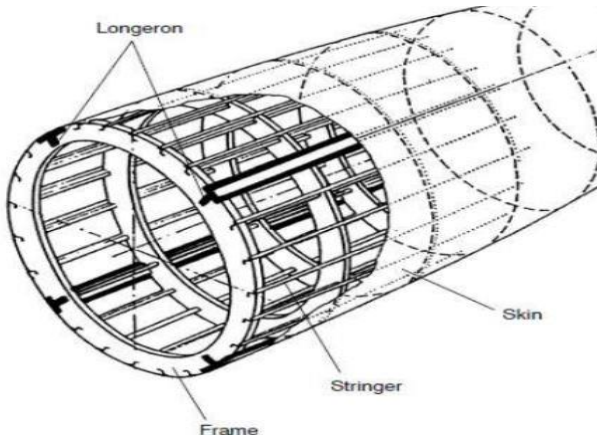


Figure 3.2-5. Semi-monocoque type construction

Semi-monocoque construction is consisting of frames, formers, bulkheads, longerons and stringers. This construction is developed to overcome the strength/weight problem of monocoque construction. Longerons extend across several frame members and help the skin support primary bending loads. Also, stringers are used for giving shape and attachment of the skin. Stringers and longerons together prevent tension and compression from bending the fuselage. Also, at this configuration fuselage skin thickness can vary with load carried and stresses sustained at a particular location. Generally, the semi-monocoque fuselage is constructed aluminum, magnesium, steel and their alloy. Members of the semi-monocoque structure (Bulkheads, frames, longerons and stringers) ease the design and streamlined fuselage construction while keeping the fuselage rigid and strong. They distribute the loads among the structures and skin does not carry only primary loads so there is no single piece which is failure critical. This means is that semi-monocoque fuselage may resist considerable damage and still be strong to hold together (Aircraft Structures pp.9-10).

UNCLASSIFIED

UNCLASSIFIED

3.2.1.2. Competitors' Fuselage Configuration

Some of the VLA and similar aircrafts' (can be defined as a competitor) fuselage structure is investigated and results of this investigation is tabulated at Table 1. Most of the similar aircrafts have semi-monocoque type fuselage structure.

	Truss Construction	Monocoque Construction	Semi-monocoque Construction
AERO AT-3	✓		
BRISTEL			✓
SONACA 200			✓
TECNAM P2002 JF	✓		
EVEKTOR EUROSTAR SL			✓
PIPISTREL			✓
MAGNUS FUSION 212			✓
DIAMOND DA20 C1			✓
SILA 450C			✓
TOTAL	2	0	7

Table 3.2-1. Competitors' fuselage configuration type

	Truss Construction	Monocoque Construction	Semi-monocoque Construction
Percentage of Fuselage Configuration type	% 22.2	% 0	% 77.8

Table 3.2-2. Percentage of competitors' fuselage configuration type

UNCLASSIFIED

UNCLASSIFIED

3.2.1.3. Configuration Choice

Configuration of the fuselage is determined as a semi-monocoque structure. While taking this decision, we consider the TAI requirements and CS-VLA and investigate the fuselage configuration of competitors. We can obtain rigid, strength, streamlined and light enough fuselage by choosing semi-monocoque fuselage. Also, semi-monocoque fuselage relies on many structural members for strength and rigidity so fuselage can withstand damage while is kept together. Semi-monocoque structure eases the design and while keeping the fuselage strong and rigid, it prevents the aircraft from becoming too heavy. Skin form of the important part of the weight of the aircraft and thinner skin and variable skin thickness can be used at this configuration. This means is that we can design lighter fuselage. Investigation of the fuselage structure of competitors showed that %77.8 of the competitors has semi-monocoque structure and modern similar aircrafts choose semi-monocoque configurations. These reasons lead us to choose semi-monocoque and the competitors' fuselage configuration investigation confirms our choice.

UNCLASSIFIED

UNCLASSIFIED

3.2.1.4. REFERENCES

"AIRFRAME CONSTRUCTION." [Online]. Available: <https://soaneemrana.org/onewebmedia/7AN6.3 MAINTENANCE OF AIRFRAME AND SYSTEMS DESIGN UNIT 1 NOTES.pdf>.

"Aircraft Structures." [Online]. Available: https://www.faa.gov/regulations_policies/handbooks_manuals/aircraft/amt_airframe_handbook/media/ama_ch01.pdf.

3.2.1.5. TYPICAL CONFIGURATIONS OF A VLA TAIL

Various possible aircraft configurations and selected base aircraft are compared in feasibility report. Possible configurations and competitors have either T-tail or conventional tail. Therefore, configurations like V-tail, X-tail, Cruciform tail etc. are eliminated. Only T-tail and conventional tail configurations will be examined structurally, based on both competitor analysis and customer requirements.

3.2.1.5.1. Conventional Tail Configuration

The conventional horizontal stabilizer assembly consists of left and right outboard sections attached to a center section or torque box, within the aft fuselage.

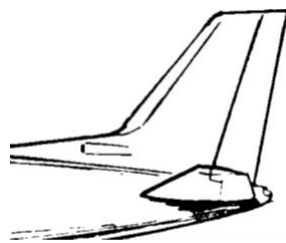


Figure 3.2-6 Conventional Tail

3.2.1.5.2. Horizontal Tail

The horizontal stabilizer is usually a two-spar structure consisting of a center structural box section and two outer sections. The conventional horizontal tail can be categorized into three main group. Categorization is made upon tail box movement and they are listed below.

Permanently Fixed Mount

A pivot bulkhead is located at the juncture of the center box and outer section at each side of the fuselage. Each bulkhead contains a pivot bearing at the aft end and an actuator attach point at the forward end. This provides a four-point, fail-safe support arrangement for the stabilizer assembly.

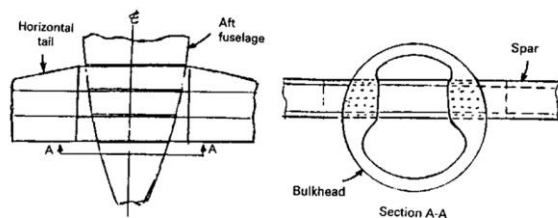


Figure 3.2-7. Permanently fixed mount

UNCLASSIFIED

UNCLASSIFIED

Variable-Incidence Mount

The horizontal stabilizer is designed to pivot on two hinge joints attached to a heavy bulkhead in the fuselage and the angle of attack is adjusted by means of an electrically driven or manually operated ball nut and jackscrew, which is attached to the forward side of the center section. All vertical load distributions on the stabilizer are reacted at the jackscrew at the middle of the front spar and two pivot bearings at each side of the rear spar.

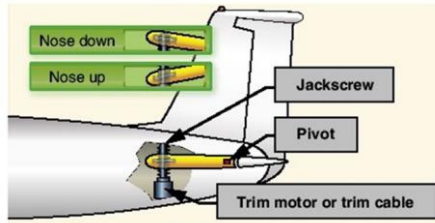


Figure 3.2-8. Jackscrew mechanism

All-Moving Mount

Taileron

Modern air-superiority fighter demands adequate rolling power under all conditions by a taileron (horizontal stabilizer surfaces are moved either together, as pitch control, or independently for additional control in roll). However, it is not recommended on commercial aircrafts due to its complicated design as well as structural weight and cost. Therefore, it is eliminated.

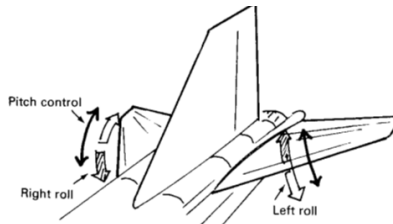


Figure 3.2-9. Taileron movement

Flying Tail

The main advantage of a flying tail is the reduction in tail size and consequent reduction in drag during cruise. However, structural complexity of flight control systems is higher than the permanently fixed one.



Figure 3.2-10. Flying tail of Aero AT-3

UNCLASSIFIED

UNCLASSIFIED

3.2.1.5.3. Vertical Tail

Structural design of vertical stabilizers is essentially the same as for horizontal stabilizers. The vertical stabilizer box is a multi-spar structure with cover panels.

Folding Tail

Folding tail is designed to be folded when it is necessary, for example during transportation. Since there is no request as such, this design is eliminated.

Removable Tail

Removable vertical tail is designed to be removed when it is necessary. Since there is no request as such, removability of the vertical tail will be decided when its fastening type is set.

Fixed Tail

The vertical stabilizer is generally mounted on aft fuselage with joints. The front and rear spars are attached to aft fuselage bulkheads. The vertical tail structure is completely integral with the aft fuselage. The spars enter the fuselage frames and become part of them. Also, skins tie directly to the fuselage skins. A three-spar design is employed on some of the tails to provide fail-safe characteristics.

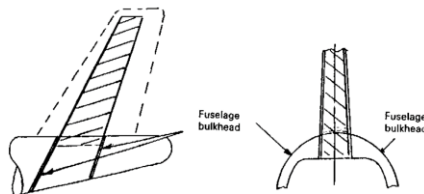


Figure 3.2-11. Fixed vertical tail

3.2.1.5.4. T-Tail Configuration

From a static loads point of view, the design of a T tail is as straightforward as a fuselage-mounted arrangement. However, because of flutter considerations, it is necessary that the vertical fin and the attachment of the horizontal tail to be principally designed to stiffness requirements.

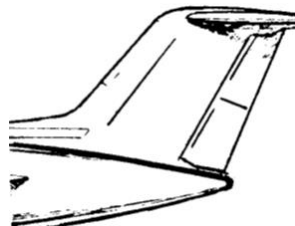


Figure 3.2-12 T-Tail Configuration

The primary parameter for T-tail flutter is the fin torsional stiffness and with this arrangement, the vertical fin stiffness required is heavily dependent on the mass of the horizontal stabilizer. Because of this T-tail characteristic, it is very important to design for minimum horizontal tail size in order to minimize the fin stiffness requirement.

UNCLASSIFIED

UNCLASSIFIED

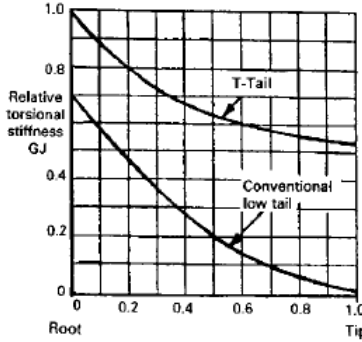


Figure 3.2-13. A comparison of the vertical fin stiffness requirement between a low tail and a T-tail design

The above data shows that the T-tail requires about 1.5 times the stiffness at the vertical fin root and about 40 times the stiffness at the tip than does the low tail arrangement. Obviously, this results in a higher structural weight for the vertical fin for the T-tail.

Therefore, T-tail configuration is eliminated due to its possible higher weight and its sensitive design to the weight of the horizontal stabilizer.

3.3. Propulsion & Fuel Systems

3.3.1. Propulsion

3.3.1.1. Introduction

To begin with, very light aircrafts(VLA) mostly use reciprocating engines i.e. piston-prop engines, since they do not require a lot of power such as commercial aircrafts or military aircrafts. A simple gasoline piston-prop engine is given Figure 1. To find the suitable engine for the VLA making a trade-off is a must since there might be a lot of options. First, trade-off is made according to competitors' engines to see the engine options clearly, and it has to be decided that whether the engine should be gasoline engine or diesel engine, and also it needs to be decided that whether the engine needs to have turbocharger or not. After that cost, fuel consumption, certification and reliability of the engine are considered to find best engines for VLA . After finding a few best engines, their price are compared and then their installation are compared if it will be easy or not, and lastly the performance of the engines are checked in detail. When all these considerations are finished, the most suitable engine for the VLA is found.

UNCLASSIFIED

UNCLASSIFIED

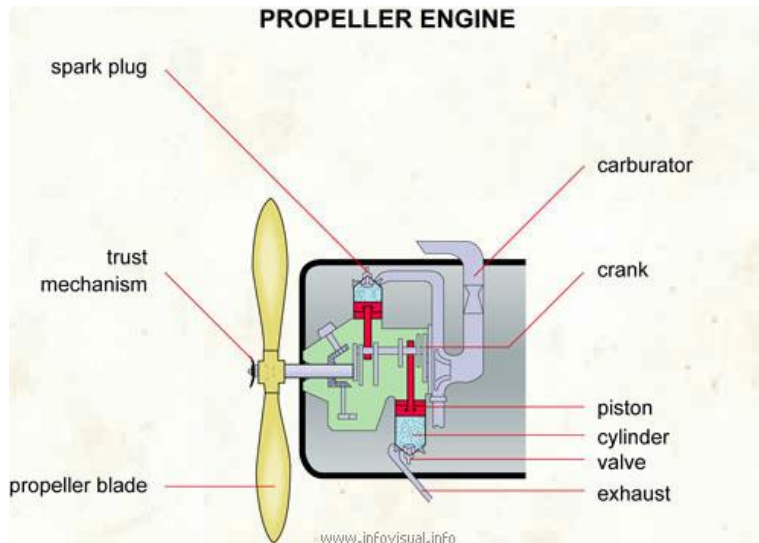


Figure 3.3-1. Piston- Propeller Engine

3.3.1.2. Discussion

3.3.1.2.1. Engine

What do the competitors use?

To start better research, firstly some of the competitors is looked to understand which brand is commonly used and also to see the power of the engine according to the weight of the aircraft. The aircrafts is listed from 550 kg to 750 kg in table and their power ranges from 80 hp to 120 hp, so from the competitors it is understood that engines from 80 hp to around 130 hp have to be listed for finding suitable engine for VLA, which the maximum weight is desired to be 750 kg, until the power required is calculated. When the power required is calculated, the engines which do not have enough power in the list are going to be removed and points will be given according to their other parameters such as fuel consumption, weight, reliability etc.

UNCLASSIFIED

UNCLASSIFIED

Table 3.3-1 Competitors and their engines

Name of Airplane	Engine	Take off	Continuous	Weight of Aircraft
		Power	Power	
Bristel	UL Power 350i	118 hp at 3300 rpm	72 hp at 2500 rpm	560 kg
Aquila A 211	Rotax 912 S3	98.6 hp at 2385 rpm	92.5 hp at 2260 rpm	750 kg
Aero AT-3	Rotax 912 S2/S4	98.5 hp at 5800 rpm	92.5 hp at 5500 rpm	582 kg
Sonaca 200	Rotax 914 F	115 hp at 5800 rpm	100 hp at 5500 rpm	750 kg
Diamond DA20 Katana	Rotax 912 S	100 hp at 2385 rpm	93 hp at 2260 rpm	750 kg
Evektor SportStar	Rotax 912 ULS/S2	100 hp at 5800 rpm	95 hp at 5500 rpm	600 kg
Tecnam P2002 Sierra	Bombardier Rotax 912 S2/ULS	98.5 hp at 5800 rpm	92.5 hp at 5500 rpm	600 kg
Tecnam P2002 JF	Bombardier Rotax 912 S2	98.5 hp at 5800 rpm	92.5 hp at 5500 rpm	620 kg
TECHNAM P2008 JC	Bombardier Rotax 912 S2	98.5 hp at 5800 rpm	92.5 hp at 5500 rpm	630 kg
Skyfox CA 25N	Bombardier Rotax 912 A1/A2	81 hp at 5800 rpm	79 hp at 5500 rpm	550 kg
PS-28 Cruiser	BRP-Powertrain GmbH&Co.KG 912S	100 hp at 5800 rpm	93.8 hp at 5500 rpm	600 kg
APM 20 LIONCEAU	Rotax 912 A	80 hp at 5800 rpm	77 hp at 5500 rpm	634 kg
Airon Aircraft LS-I	Jabiru 3300 120 HP	120 hp at 3300 rpm	107 hp at 2750 RPM	600 kg
Sting Sport TL2000	Rotax 912 UL	80 hp at 5800 rpm	-----	600 kg

Diesel or Gasoline or Hybrid Engine?

It is known that engines for very light aircrafts differ as diesel, gasoline, and hybrid. When these 3 type of engines are considered as our possible candidate, it has to be decided which type will be better for VLA. When weight and noise are taken in account, hybrid engine would be a better choice however, since the hybrid engine is not common in use, finding services, repair centers would be a difficulty for producer, also the reliability and the installation is another major problem that why hybrid engine is not feasible for this application. When diesel or gasoline engines are considered to choose, although it is known that diesel engines are efficient than the gasoline engines [1], they are heavier and nosier than the gasoline engines. In addition, when available diesel engines for VLA are researched , it is seen that their available power is 135 hp and dry weight is 134 kg which is over sized for the VLA in terms of not only required power but also weight. As a results, it is decided that the best choice for the VLA is to use gasoline engines since they are lighter and quieter than diesel engines.

UNCLASSIFIED

UNCLASSIFIED

Turbocharger

A turbocharger ensures the aircraft to climb higher altitudes and as seen in the figure 2 power available for the engine does not reduce until a certain altitude after that it starts to reduce. However, the turbocharger decreases the efficiency of the engine since it causes back-pressure to mount in the exhaust manifold [2]. In addition, engines with turbocharger are heavier and costlier than usual engines. Moreover, the VLA is designed to have a service ceiling at 7500 ft, so just for that altitude buying the engine with turbocharger would be a luxury for the producer, and also for installation it may create a problem that is why an engine without turbocharger is preferred to use unless engine with turbocharger is the only option.

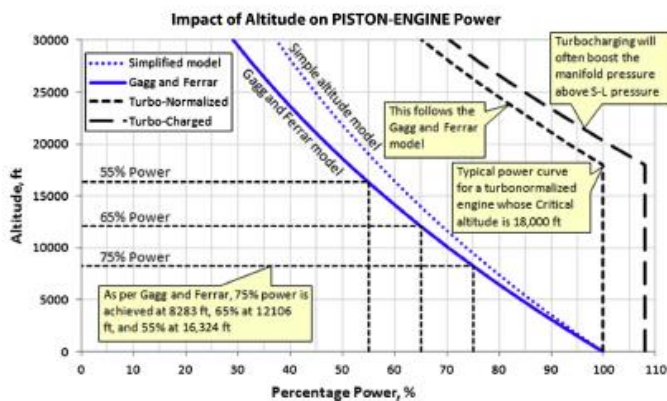


Figure 3.3-2. Change of available power with altitude

Constraint Diagram

To see the power requirement for VLA, the constraint diagram is plotted, after that $\frac{T}{W}$ (Thrust to Weight) vs $\frac{W}{S}$ (Wing Loading) is converted to P (Power) vs $\frac{W}{S}$ (Wing Loading) and plotted.

In the constraint diagram cruise speed, constant velocity turn, rate of climb, take off distance and service ceiling are plotted. Constant velocity turn was the one which requires most power in the calculation. As seen from the figure, required Thrust-to-Weight ratio is 0.19 since rate of climb constrains it and above that point can be taken as desired Thrust-to-Weight ratio. For the VLA 0.21 is selected considering %10 of safety.

UNCLASSIFIED

UNCLASSIFIED

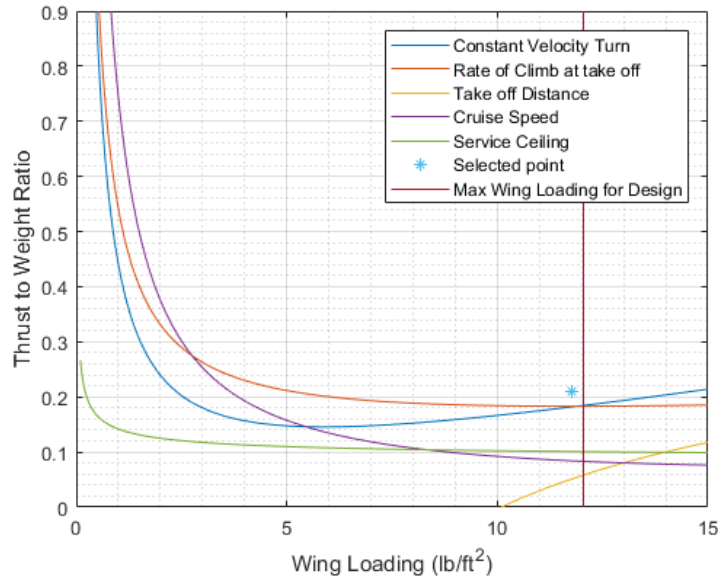


Figure 3.3-3. Thrust to Weight ratio vs Wing Loading

After plotting Thrust-to-Weight ratio, it is converted to Power vs Wing Loading to find available power for our aircraft. Actually, required power for our engine is 92 hp but since 92 hp engines are usually not available in the market, and most of the engine start from 100 hp and with the safety consideration, design requirement is taken as 100 hp at least.

UNCLASSIFIED

UNCLASSIFIED

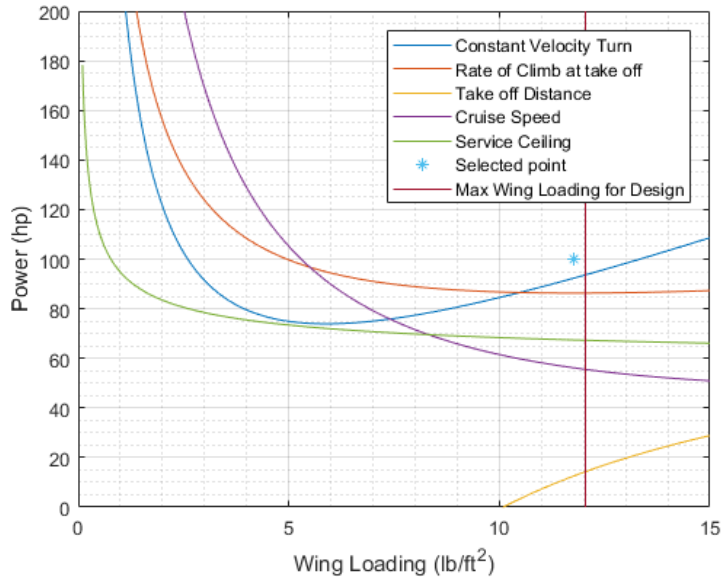
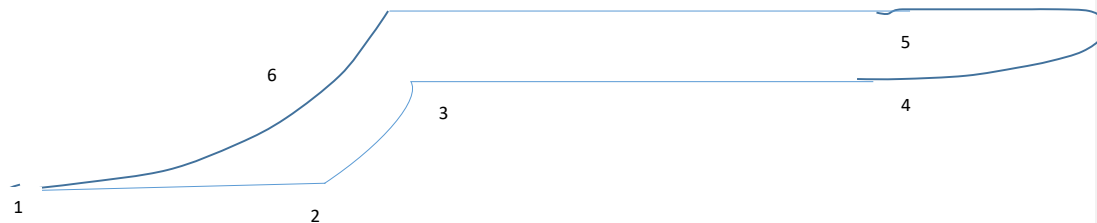


Figure 3.3-4. Power vs Wing Loading



1-2 Warm up and take-off, at sea level and standard day conditions (59 °F),the desired take-off distance is smaller than 1000 ft, ground friction coefficient is $\mu = 0.3$, desired stall velocity is $V_{stall} = 45 \text{ knots}$, and take off velocity is $V_{to} = \frac{1.1 + V_{stall}}{\sqrt{2}}$ [2] .

Açıklamalı [k2]: Buradaki [2] nedir

2-3 Climbing to best cruise altitude with desired $V_y=13 \text{ ft/s}$ at sea level and performing a minimum time climb

3-4 Subsonic cruise flight at 5000 ft with Carson speed which is the fastest efficient airspeed [2], $V_c=98 \text{ knots}$

4-5 Sustained-turn flight with a bank angle of 60 degrees by using $\max(P_{available} - P_{required})$ at 5000 ft.

5-6 Subsonic cruise flight at 5000 ft with Carson speed which is the fastest efficient airspeed

6-1 Landing, at at sea level and standard day conditions (59 °F),the desired take-off distance is 3280 ft.

UNCLASSIFIED

UNCLASSIFIED

Selecting the Engine

After looking competitors' engines, the engines from Rotax, UL Power, Limbach, Lycoming, Jabiru from 80 hp to 130 hp are listed. Also, properties of the engines in table 2 fuel consumption, weight, TBO hours, rate of accidents etc. are listed. After plotting the constraint diagram the power requirement is seen and the engines below 100 hp from the table is removed. After that grading the remaining engines is started.

To explain how an engine is graded, a part of the table is given below as an example. So, for grading maximum fuel consumption, it is considered that how much it consumes less fuel it is better, so least consumer engine took the highest grade in the calculation as seen in the table, which is Rotax 912 iSc Sport with 25 L/h consumption took the 100 points. After that, to make a fair grading a linear function is set;

$$f(\text{fuel consumption}) = -3 * (\text{fuel consumption}) + 175$$

In this formula when someone puts 25, 100 points will be got, or when we put 47 we got 34 points which is the lowest grade in the table. Thus, that formula is arranged in a way that the best option takes the 100 point, and the worst point takes the around 30 points and the rest of the engines ranges between them linearly.

Table 3.3-2 Candidate Engines and Fuel Consumption Data and Grading

Engine Brand	Type	Take off	
		Max Fuel Consumption (L/h)	Max Fuel Consumption (grade)
Rotax	Rotax 914 F	33	76
	Rotax 912 iSC Sport	25	100
UL power	UL 260iF	26	97
	UL350iS	36	67
Limbach	Limbach L 2400 DF/EF	27.2	93.4
	Limbach L 2400 DFi/Efi	27.2	93.4
Continental Motors	O-200-D	33	76
	IOF-240-B	41.5	50.5
Lycoming	O-290-D Series	47	34
Jabiru	Jabiru 3300 A/L	35	70

This was just an example to explain how grading is made, if you want to see the all grading you can just look file [VLA Motor.xlsb.xlsx](#). And press [alt+f11](#) to see the functions in visual basic for each parameter.

After grading fuel consumption, weight, TBO hours, service, certification, and reliability, overall point of the engines is needed to find and from those overall points the best five engine is selected. Overall grading is calculated as follows;

UNCLASSIFIED

UNCLASSIFIED

$$\begin{aligned} \text{Overall} = & 0.15 * (\text{Fuel consumption}) + 0.25 * (\text{Weight}) + 0.05 * (\text{TBO hours}) + 0.05 * (\text{service}) + \\ & 0.25 * (\text{Certification}) + 0.25 * (\text{Reliability}) \end{aligned}$$

By this way the overall grading is made out of 100, and the coefficients are given according to requirements, also the opinion of other teams is asked to give the points and coefficients. So, as seen in the table there are five engines better than the others, and those five engines (Rotax 914F, 912 iSc Sport, 912 iS, 912S and Limbach 2400 DF/EF) will be considered to make a final comparison. Since in those calculation installation and cost of the engines are not included, it is a better way to make a decision between these five engines according to installation, cost and detailed performance to find best one. The main purpose is not to jump an engine directly and trying to be sure that the best engines is chosen in all way.

Engine Brand	Type	Max Fuel Consumption (grade)	Weight (grade)	TBO (grade)	Service(grade)	Certification (grade)	Rate of Accidents (grade)	Overall Rate
Rotax	Rotax 914 F	76	84.05	90	100	100	91	89.6625
	Rotax 914 UL	76	84.05	90	100	20	91	69.6625
	Rotax 912 iSc Sport	100	90.5	90	100	100	91	94.875
	Rotax 912 iS	92.5	90.5	90	100	100	91	93.75
	Rotax 912 S	94	93.65	90	100	100	91	94.7625
UL power	Rotax 912 ULS	94	93.65	90	100	20	91	74.7625
	UL260iF	97	99.65	80	50	20		50.9625
	UL260iS(K)	97	99.65	80	50	20		50.9625
	UL260iSA	97	93.56	55	50	20		48.19
	UL350i	77.5	90.65	80	50	20		45.7875
	UL350iS	67	90.65	80	50	20		44.2125
	UL350iSA	67	84.5	55	50	20		41.425
Limbach	Limbach L 2400 DF/EF	93.4	89	82	50	100	100	92.86
	Limbach L 2400 DF/Efi	93.4	89	50	50	100		66.26
	Limbach L 2400 DT/ET	72.25	80	82	50	100		62.4375
	Limbach L 2400 DS	82.24		50	50			17.336
Continental Motors	O-200-A		62	94	50	100	99.75	72.6375
	O-200-D	76	79.85	98	50	100	99.75	88.7
	IO-240-B		41.6	98	50	100	99.75	67.7375
	IOF-240-B	50.5	35.45	90	50	100	99.75	73.375
	O-235-C*	53.5	45.5	98	65	100	98.25	77.1125
Lycoming	O-235-E	53.5	39.5	98	65	100	98.25	75.6125
	O-235-F, -G, -J	53.5	38	90	65	100	98.25	74.8375
	O-235-K, -L, -M	67.15	36.5	98	65	100	98.25	76.91
	O-235-K2C	67.15	40.25	98	65	100	98.25	77.8475
	O-235-H Series	53.5	43.25	98	65	100	98.25	76.55
	O-235-N, -P Series	67.15	35.75	98	65	100	98.25	76.7225
	O-290-D Series	34	32	90	65	100	98.25	70.4125
Jabiru	Jabiru 3300 A/L	70	83.75	90	50	100	49.75	75.875

Figure 3.3-5.Engines and their overall grading

UNCLASSIFIED

UNCLASSIFIED

Table 3.3-3 The table is put to show the comments about the selected five engines compared to each other.

	Rotax 912 S	Rotax 912 iS	Rotax 912 iSc Sport	Rotax 914 F	Limbach 2400 DF/EF
Performance	Max cont. Power 90 hp and at 5000 rpm it provides 68 hp.	Max cont. Power 92 hp and at 5000 rpm it provides 69 hp.	Max Cont. Power is 97 hp and with rpm reduction it does not reduce a lot, e.g. at 5000 rpm it provides 73.4 hp.	Its max. Cont. Power is 100 hp at 5000 rpm it provides 74 hp and max take of power is 115 hp since it has turbocharger.	Better than 912 iS and 912 S but, not good as much as 912 iSc Sport and 914 F
Fuel Consumption	Higher fuel consumption than 912 iS series.	It has Eco mode but not good as much as 912 iSc Sport.	Best one, and it also has Eco mode at lower rpm.	Higher fuel consumption than 912 Series.	It is good as much as 912 iS.
Ease of Installation	Clear and understandable installation manuals, but exhaust system is not tested.	Very clear and understandable installation manuals	Very clear and understandable Installation manuals	It has turbocharger a little bit harder than Rotax series, but it is good that it includes more parts than other Rotax series in the kit.	Installation manuals are not clear as much as Rotax engines.
Weight	Estimated weight 76.9 with accessories.	Estimated weight 79 with accessories.	Estimated weight 79 with accessories.	Estimated weight 83.3 with accessories.	Dry weight 76, Estimated weight 80 with accessories.
Average Cost (\$)	21200	24780	25000	33035	27450

The selected engines are evaluated according to their performance, and fuel consumption in detail since maximum values of those parameters were considered before. The other important parameters were the ease of installation of the engines, weight, and cost of the engines. Rotax 914 F seems best when the performance is considered, and if there would be a higher rate of climb requirement and service ceiling at a higher altitude than 7500 ft this engine could have been selected. However, Rotax 912 iSc Sport ensure a good enough performance and less fuel consumption together with the price compared to 914 F. Also, Rotax 912 iSc has acceptable weight when its performance is considered compared to 912 S engine. Also, 912 S has one disadvantage that its exhaust system is not tested. As a result, when the overall advantages and disadvantages of these engines is considered and evaluated, the best option seems to be Rotax 912 iSc Sport.



Figure 3.3-6. Rotax 912 iSc Sport

UNCLASSIFIED

UNCLASSIFIED

Bill of Materials

An example of bill of materials is put below, although most of the parts are included this table might be updated later in the case of existing of missing parts.

Table 3.3-4 Bill of Materials

Accessories	
Rotax 912 iSc Sport Engine	1
Propeller Flange	1
Propeller Gearbox	1
Throttle Valve Support Assy.	1
Airbox	1
Fuel Rails	2
Engine Suspension Frame (Ring Mount)	1
Fuel Pump Assembly	2
Oil Filter	1
Oil Cooler	1
Oil Tank	1
Oil Pump	1
Pressure Gauge	1
Exhaust Flange	4
EGT Temperature Sensor	4
Tension Spring	8
Muffler Assy.	1
Expansion Tank Assy.	1
Temperature Sensor for Radiator	1
Radiator	1
Overflow Bottle	1
Water Pump Housing	1
Fuse Box Assembly	1
Control Unit Assembly (ECU)	1
Dual Ignition Coils	4
Stator	1
Fly wheel	1
Crankshaft position sensors	2
Starter Relay	1
Electric Starter	1
EMS ground	1

UNCLASSIFIED

UNCLASSIFIED

Engine System Architecture

Engine system architecture is drawn for our selected engine, Rotax 912 iSc Sport as you can see below.

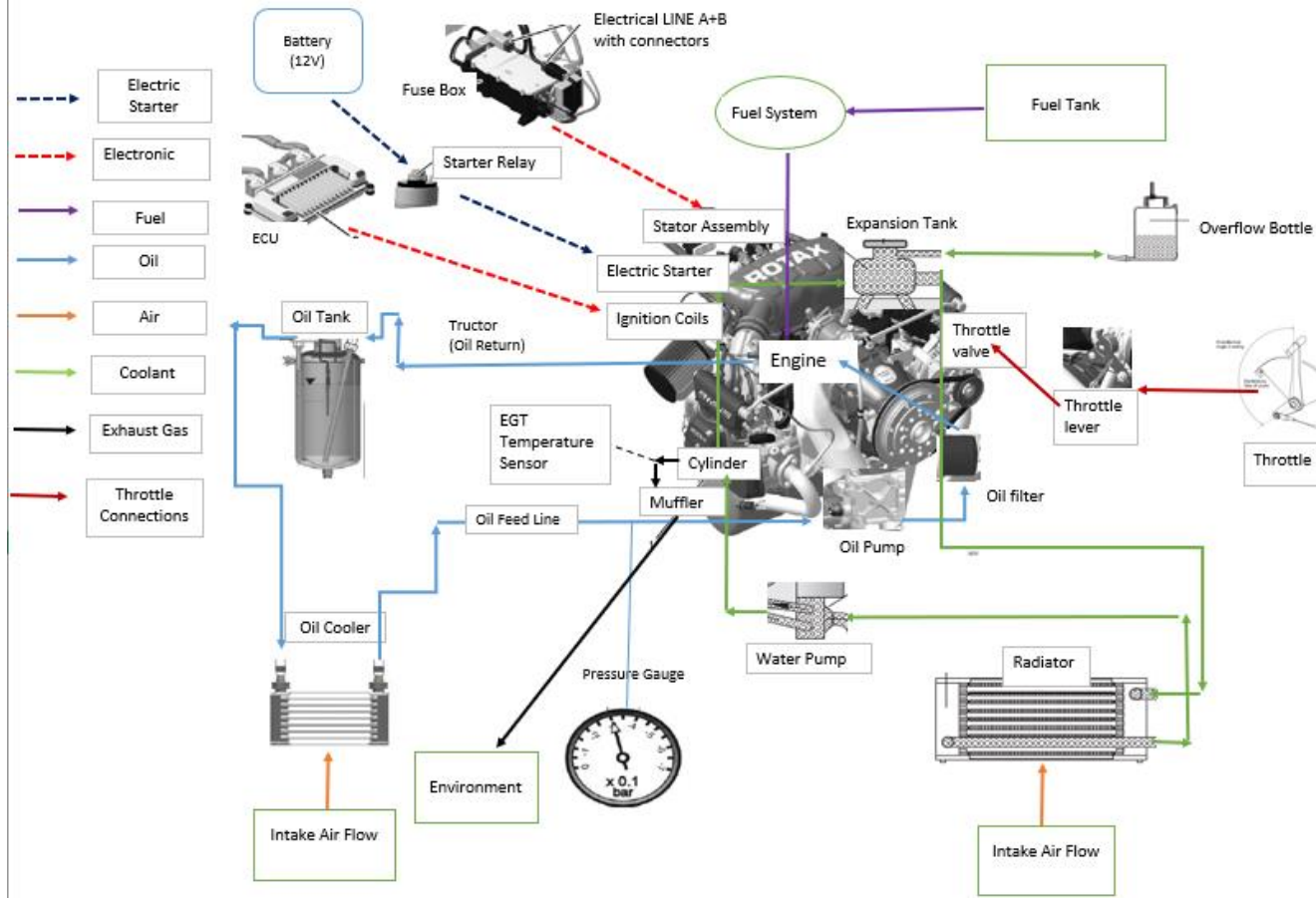


Figure 3.3-7. Engine System Architecture for Rotax 912 iSc Sport

UNCLASSIFIED

UNCLASSIFIED

3.3.1.3. Propeller

Number of Blades

The number of blades is fundamental to how the engine power is converted into propulsive power. Therefore, choosing suitable blade number is very important and while doing so, parameters like engine power, operating RPM for the propeller, diameter limitations, aircraft performance requirements have to be considered.

In general, VLA competitors have used 2 or 3-blades for a propeller. Because of this, 2 and 3 blades are considered. Both blades have pros and cons in terms of performance, cost etc.



Figure 3.3-8.2 and 3-blade propellers

Generally, 2-blade propellers are noisier and has more vibration than 3-blades because 2-blade propellers larger diameter causing more tip speed however, having larger diameter leads to produce more thrust which is needed. With regards to cost, 2-blades are cheaper since the cost of blade is usually proportional to the number of blades. In other words, while the number increases, the cost increases. Weight is also significant parameter. The point here is the lighter aircraft has better performance and a lighter propeller has less vibration meaning less damage caused by fatigue. When other parameters assume constant, propeller with 2-blade is more advantageous in terms of weight. Apart from all of these, the most important among these parameters is efficiency. When considering thrust per number of blades, the fewer the blades the more efficient is the propeller and the more blades, the more aerodynamic interference will happen. As mentioned above, larger diameter results in more thrust. As a consequence, the required diameter and tip speed for the propeller is determined and it is observed that the obtained value for tip speed will not reach speed of sound and therefore, it will not cause any loss in efficiency and thrust. the choice of propeller with two blades might be better for the VLA.

Table 3.3-5 Showing Trade-off for Number of Blades

Parameters	Number of Blades	
	2	3
Noise and Vibration	-1	1
Weight	1	-1
Cost	1	-1
Thrust/Blade	1	-1
Efficiency	1	-1

UNCLASSIFIED

UNCLASSIFIED

Pitch Mechanism

There are three types of pitch mechanism: fixed-pitch, constant-speed and variable-pitch.

A fixed-pitch propeller is a propeller whose pitch angle (the incidence of the blades with respect to the plane of rotation) cannot be changed. Such propellers are comparatively inexpensive, light, and require very little maintenance. A ground-adjustable propeller is a propeller whose pitch angle can be adjusted using simple tools while stopped on the ground only. Thus, the operator can change the pitch from, say, a "climb" to a "cruise" style propeller between flights.

A constant-speed propeller is a propeller that will automatically adjust its pitch to maintain a preset RPM, which otherwise is highly affected by airspeed. It does this through the use of a controlling mechanism attached to the engine, called a governor, which balances centripetal and hydraulic forces. Controllable-pitch is same as constant-speed in terms of mechanism but in the former, a pilot changes the setting of pitch position of the blades during flight.

Double click on the picture below to see how constant-speed(hydraulic) propeller works.

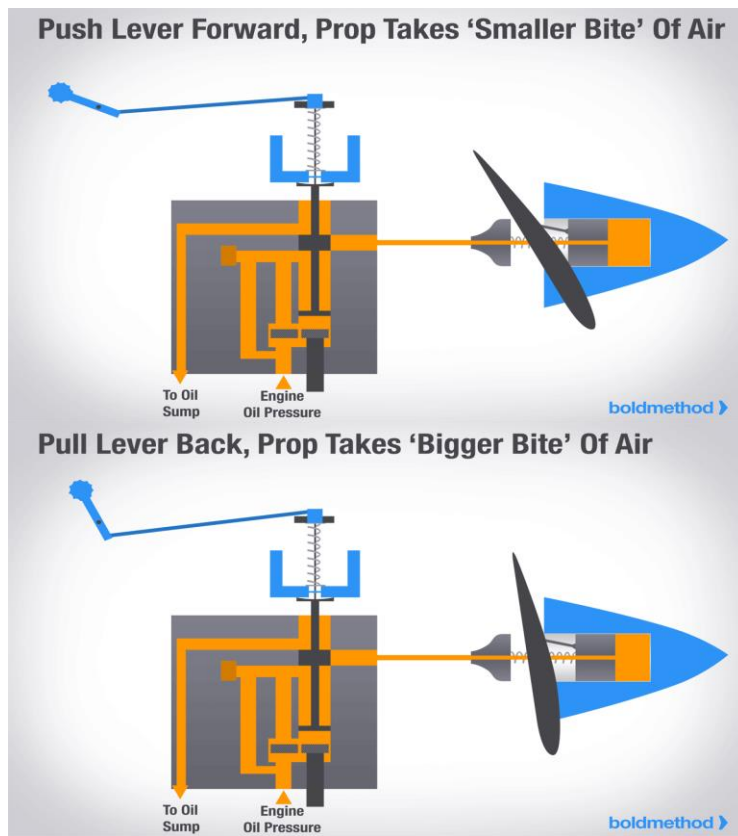


Figure 3.3-9. Showing how constant speed propeller Works

UNCLASSIFIED

UNCLASSIFIED

Fixed-Pitch vs. Constant-Speed

As mentioned above, fixed-pitch is cheaper, lighter and its maintenance is easy due to having less complexity. However, considerable difference between fixed-pitch and constant-speed will occur during flight with respect to performance and efficiency. As opposed to fixed-pitch propellers, which only operate at their optimal efficiency in one stage of flight, constant speed propellers can provide peak performance at each phase of flight, from takeoff to landing. With a constant speed propeller, pilots can select the revolutions per minute (RPM) that provide the most suitable power for every given situation. For

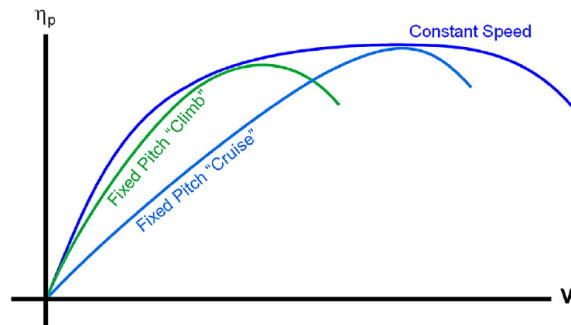


Figure 3.3-10. Showing the difference between fixed propeller and constant speed propeller [2]

example, you may want a higher RPM for increased takeoff power and a lower RPM for cruise flight. By automatically adjusting the angle of the blades, constant speed propellers can better control the RPM levels and provide the appropriate amount of power for each stage of flight. Today's constant speed propellers adjust automatically many times throughout flight to take a greater or lesser "bite" of air depending on the aircraft's speed. In cruise flight, increasing the angle-of-attack of the prop also increases the engine's torque. This increase in torque effectively slows down the engine, resulting in improved fuel efficiency. Constant speed propellers may also prevent damage to the aircraft's engine. For example, if an engine is operated at an RPM setting that is too high or too low, the engine can become damaged or worn out. Constant speed propellers are commonly found on today's high-performance aircraft to protect their powerful engines while providing pilots with increased control throughout flight. To conclude, constant speed propeller for the VLA is much better than fixed-pitch propeller.

Table 3.3-6 Trade-off for Pitch mechanism

Parameters	Pitch Mechanisms		
	Fixed-Pitch	Constant-Speed	Variable-Pitch
Cost	1	-1	
Weight	1	-1	
Efficiency	-1	1	
Fuel Consumption	-1	1	
Complexity	1	-1	

UNCLASSIFIED

UNCLASSIFIED

Selection of Material

The modern propellers are composed of three different materials: wood, metal, or composites. They have good and bad aspects compared to each other.

The first thing is that wooden and composite propellers dampen the engine vibration much better which may lead to reduce blade failures and noise [2]. Moreover, wood propellers are probably cheapest, composite can be more expensive than wood as layers of carbon or glass and epoxy are used to re-enforce the wood inside the blades. Furthermore, wooden propellers are often the lightest one however, some composite propellers are lighter than wood depending on how they are processed and material they contain. Also, composite and metal propeller have higher tip speed limit than wooden one since both are extremely durable. Composites and metal retain their shape and size when they are hot or cool, wet or dry. In addition, while rotational tip speed for composite and metal propeller have to be in interval of 0.75-0.8 Mach, it is 0.6 Mach for wooden propeller [2]. In summary, Composite blades has more advantageous in terms of weight, vibration and noise, durability and dimensional stability and composite material meets requirements for computed tip speed limit and high-performance VLA.

No.	Tip speed limit (m/s)	Propeller type
1	310	Metal high-performance prop
2	270	Metal regular prop
3	250	Composite prop
4	210	Wooden prop
5	150	Plastic prop for RC model aircraft

Figure 3.3-11. Showing tip speed limits for different materials[2]

Table 3.3-7 Material trade-off

Characteristic	Material		
	Wood	Composite	Metal
Noise and Vibration	1	1	-1
Cost	1	-1	-1
Weight	1	1	-1
Tip Speed Limit	-1	1	1
Durable	-1	1	1
Dimensional Stability	-1	1	1

UNCLASSIFIED

UNCLASSIFIED

Rapid Estimation of Propeller Diameter

According to Gudmunsson [2]:

→ For 2-blade wooden propeller

$$D_1 = 10000 * \sqrt[4]{\frac{P_{BHP}}{53.5 * RPM^2 * V_{TAS}}}$$

where V_{TAS} : Cruise Speed, $RPM = 1852$ for a propeller, P_{BHP} : Cruise Power

Substituting the values,

$$D = 10000 * \sqrt[4]{\frac{60}{53.5 * 1852^2 * 98}}$$

$$D_1 \cong 76'' \cong 193 \text{ cm}$$

→ Determination of D_{MAX} from V_{tipMAX} formula

$$D_{MAX} = \frac{60 * \sqrt{V_{tipcruise_{MAX}}^2 - V_{cruise}^2}}{\pi * RPM} \quad \text{where } V_{tipcruise_{MAX}} = 250 \text{ m/s and } V_{cruise} = 50 \text{ m/s}$$

$$D_{MAX} = 76.72'' = 194.87 \text{ cm}$$

→ For 2-blade metal propeller

$$D = 22 \sqrt[4]{P_{BHP}}$$

$$D_2 = 69.57'' = 176.71 \text{ cm}$$

According to Raymer [11]:

Being independent of material:

$$D = K_p \sqrt[4]{P_{BHP}} , \quad \text{where } K_p = 20.4 \text{ for 2 blade}$$

$$D_3 = 64.51'' \cong 164 \text{ cm}$$

By taking the average of these three values, optimum diameter for composite propeller might be obtained.

$$\frac{D_1 + D_2 + D_3}{3} = \frac{193 + 176.71 + 164}{3}$$

$$D_{optimum} = 177.90 \text{ cm}$$

UNCLASSIFIED

UNCLASSIFIED

It can be concluded that diameter of the propeller can be taken in interval 170 – 180 cm. In addition, the similar VLA has propeller whose diameter is around 170 cm.

Governor Type

Constant speed propellers are driven by oil pressure or electric power and need control unit(governor) to maintain preset RPM by varying blade angle.

Hydraulic Governor

Also called constant speed unit, it contains a governor which uses engine oil pressure to control a hydraulic operated piston (in the propeller) and changes the propeller blade angle in order to keep RPM constant. The governors consist of flyweights which senses engine RPM and change position in relation to change in RPM, thus changing oil pressure to the propeller and moving blade pitch and keeping that preset RPM constant.

The blades themselves contains flyweights which compensate aerodynamic forces so that oil pressure only needs a little bit of effort to change blade angle. This means that oil pressure will remain constant and engine lubrication is guaranteed during blade angle movement.

Electric Governor

Detection of propeller RPM can be done in several ways: by optical(light), magnetic fields(flux) or sensing the engine RPM by connecting into the ignition or RPM indicator. This signal is then fed to a controller which calculates any change in RPM and drives an electric motor inside a propeller to keep the preset RPM constant.

When comparison is made between these two governor types, although the hydraulic constant speed is expensive, it responds faster than electric types to changes in pitch angle and risk of engine overrun reduces minimal. Hydraulic governor is suitable for the selected engine ROTAX 912 iSc sport.

Selecting propeller

After specifying the propeller our candidate propellers are listed below in Table 8. The propeller will be selected from that table afterwards.

UNCLASSIFIED

UNCLASSIFIED

Table 3.3-8 Candidate Propellers

Company	Propeller System	Number of Blade	Max Power (hp)	Max Speed (rpm)	Total Weight (kg)	Diameter (cm)	Engine Type	Pitch Mechanism	Certification	Distributor and Maintenance	Material	TBO		
Airmaster	AP420	2	120	3300	9,20	162,5\172,7\177,8	Rotax 912, 912S, 914 Jabiru 2200 and 3300	Constant Speed Propeller(electric)						
Hoffman	HO-V 62	2	100	3600	11	170	Rotax 912(), 914()	Mechanical variable pitch propeller	EASA and FAA	Wood-Composite	1500			
	HO-V 352	2	122,37	2700	11,18	180,34		Constant Speed Propeller				2000		
Woodcomp	SR 3000	2	115	2600	9,4	160-174	Rotax	Constant Speed Propeller(electric)	Turkey, Asia, Europe Africa and USA	Composite	1200			
	KW-20W	2	2550	7,4	170,9	160\ 170		Constant Speed (hydraulic)				1200		
MT	VAR 2	2	100	4,9	160\ 170	150-178	Rotax 912(), 914()	Constant Speed (mechanic or electric)	Europe, USA, Canada, Asia, South Africa and Australia	Wood-Composite	1000			
	MTV-33	2	115					Constant Speed (hydraulic)				1000		
FP	MTV-21	2	114	10	145-180	8,4	175	Rotax 912(), 914()	Constant Speed (hydraulic)	ASTM	Italy, France and Norway	Wood-Composite		
	VPH3-BHS-HHS	2	100											
	KA-3	2	7,3			168	Rotax 912()	Constant Speed Propeller (hydraulic or electric)	Europe	Composite				
Kasparaero	KA-2	2	7,2			172								
	KA-4	2	5,7			170								

UNCLASSIFIED

UNCLASSIFIED



TECHNICAL DOCUMENT
DOCUMENT NO: XXXXXXXXXX

CAGE Code: T0544
Issue No: 1

3.3.1.4. Conclusion

To conclude, it is decided whether the engine should be gasoline, diesel or hybrid and it is discussed that whether turbocharger is a requirement or not in our aircraft. Then, to select the engine possible engines are listed and according to the constraint diagram, some of the engines which they are not enough to meet the power requirement of aircraft are eliminated. After that, rest of the engines is graded considering weight, fuel consumption, service and reliability. Finally, five best engines are compared and the best one is tried to be chosen according to their detailed performance, and also their price and installation. After that evaluation, Rotax 912 iSc Sport engine is chosen as the best option for the very light aircraft. When the engine is selected, the engine system architecture is drawn, and bill of materials is listed . For the propeller, 2 blades propeller is decided to use, and also a trade-off is made whether fixed pitch propeller or constant speed propeller should be used, and it is understood that for the performance requirement, constant speed propeller is suitable for our VLA. In addition, composite material is decided to be used in our aircraft and hydraulic governor is planned to be used since it response faster than electrical governor. As a result, in conceptual design phase the engine is chosen and which type propeller should be used in our VLA is specified, and candidate propellers are listed.

3.3.1.5. References

- [1] "3.6 Diesel Cycle," *jon.* [Online]. Available: <http://web.mit.edu/16.unified/www/SPRING/propulsion/notes/node26.html>. [Accessed: 12-Sep-2018].
- [2] S. N. O. R. R. I. GUDMUNDSSON, *GENERAL AVIATION AIRCRAFT DESIGN*. S.l.: BUTTERWORTH-HEINEMANN LTD, 2016.
- [3] "Rotax 912 i series Operator's Manual," *Manuals Library*. [Online]. Available: <https://www.manualslib.com/manual/957345/Rotax-912-i-Series.html>. [Accessed: 6-Sep-2018].
- [4] "Operators Manual 912S - US Sport Aircraft." [Online]. Available: https://www.usportaircraft.com/documents/Rotax_Operators_Manual_912.pdf. [Accessed: 6-Sep-2018].
- [5] "Rotax 914 Series Operator's Manual," *Manuals Library*. [Online]. Available: <https://www.manualslib.com/manual/929250/Rotax-914-Series.html>. [Accessed: 6-Sep-2018].
- [6] "Rotax 912 i Series Installation Manual," *Manuals Library*. [Online]. Available: <https://www.manualslib.com/manual/1368458/Rotax-912-i-Series.html>. [Accessed: 6-Sep-2018].
- [7] "Rotax 912 Series Installation Manual," *Manuals Library*. [Online]. Available: <https://www.manualslib.com/manual/847567/Rotax-912-Series.html>. [Accessed: 6-Sep-2018].
- [8] "Rotax 914 series Installation Manual," *Manuals Library*. [Online]. Available: <https://www.manualslib.com/manual/846548/Rotax-914-Series.html>. [Accessed: 6-Sep-2018].
- [9] "Engines," *Aircraft engines from 56 kW to 75 kW. Fuel-efficient powerhouses.* [Online]. Available: <http://limflug.de/en/products/engines-56kw-75kw.php>. [Accessed: 6-Sep-2018].
- [10] "Downloads," *Aircraft engines from 56 kW to 75 kW. Fuel-efficient powerhouses.* [Online]. Available: <http://limflug.de/en/support/downloads.php?prod=L2400&subprod=DF/EF>. [Accessed: 6-Sep-2018].
- [11] D. P. Raymer, *Aircraft design: a conceptual approach*. Reston, VA: American Institute of Aeronautics and Astronautics, 2012.

Açıklamalı [k3]: Tüm rapordaki referanslar bu formatta olmasında yarar var.. aralarda referanslar verilmiş ama ref listesinde yoklar.

3.3.2. Fuel System

3.3.2.1. Chapter 1: Fuel Tank Trade-Off Study

Fuel Tank Types

There are three different fuel tank options. Each of them explained briefly below.

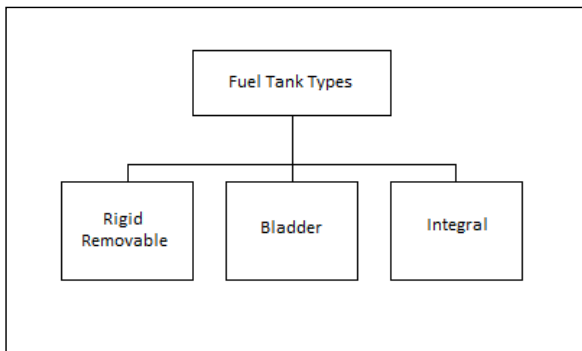


Figure 3.3-12: Fuel Tank Types

Rigid Removable Type Fuel Tanks

A rigid tank is a simple fuel storage box. It can be made from a various material such as aluminum alloy, stainless steel. Also, resin and composite can be used as a tank material. This type tanks are placed into the aircraft structure.

Remove, repair and replace of the rigid removable fuel tanks can be great convenience if a leak or malfunction. Once repaired, fuel tanks need to be pressure checked, usually while installed in the airframe, to prevent distortion while under pressure.



Figure 3.3-13. Rigid Removable Tank

Bladder Type Fuel Tanks

A fuel tank is made out a reinforced flexible material called a bladder tank can be used instead of a rigid tank. A bladder tank contains most of the features of a rigid tank but does not require as large an opening in the aircraft skin to install. The fuel or fuel cell as it is sometimes called, can be rolled up and put into a specially prepared structural bay or cavity through a small opening, such as an inspection opening. The soft flexible nature of bladder fuel tanks requires that they remain wet.

Bladder tanks are made by stuffing a shaped rubber bag into a cavity in the structure. The rubber bag is thick, causing the loss of about 10% of the available fuel volume.



Figure 3.3-14. Bladder Tank

This offers a major improvement in aircraft survivability. Their advantages are ease of installation through access doors, ease of repair by turning the tanks inside out, self-sealing, crash and vibration resistance. However, their high cost and additional weight are their major disadvantages.

Integral Type Fuel Tanks

On many aircraft, part of the structure of the wings or fuselage can be used as a fuel tank. This type tank is called an integral fuel tank since it forms a tank as a unit within the aircraft structure. Integral tanks are cavities within the airframe structure that are sealed to form a fuel tank. Ideally, an integral tank would be created simply by sealing existing structures such as wing boxes.

The sealed skin and structural members provide the highest volume of space available with the lowest weight. Integral fuel tanks can be located in the unused space of the wings and/or fuselage. Since integral fuel tanks can get the complex shape of where it is integrated, and they have an advantage of increasing fuel capacity by 10 or 15%. Also, aircraft with integral fuel tanks in the wings are called as "wet wings"

3.3.2.1.2. Fuel Tank Type Selection

In order to select the most suitable type of tank for that aircraft, a trade-off study is needed to be done. In the trade-off study, the most important criteria are listed. Then their multipliers are defined by several project members, who are studying on different working group, in order to get objective and healthy trade-off study. Fuel tank options can be poor, average or good aspect for a criterion then, it gets -1, 0 or 1 point relatively.

Fuel tank type trade-off table is given below.

Evaluation Criteria	Multiplier	Fuel Tank Types		
		Rigid Removable Tank	Bladder Tank	Integral Tank
Safety/Reliability	15	-1	0	1
Maintenance/Ease of Repair	5	1	-1	0
Endurance	10	0	1	1
Weight	25	-1	0	1
Cost	20	0	-1	1
Accessibility	10	0	1	-1
Available Fuel Capacity	15	-1	0	1
TOTAL	100	-50	-5	75

Table 3.3-9. Fuel Tank Type Trade-Off Study

At the end of the fuel tank trade-off study, integral type fuel tank gets highest grade. It means that, for VLA project, the most suitable type is integral fuel tank. Main advantages of the integral type fuel tanks are weight and cost effectiveness. Since the aircraft structure is used as fuel storage, there is no need extra closed construction as a tank and known that weight is very important for very light category aircrafts. At the same time, no extra component means is cost advantages. It is another important criterion for VLA.

3.3.2.1.3. Fuel Tank Locations

There are three possible locations in order to place fuel tanks in the aircraft. Also, possible places for fuel tanks are shown on an aircraft below.

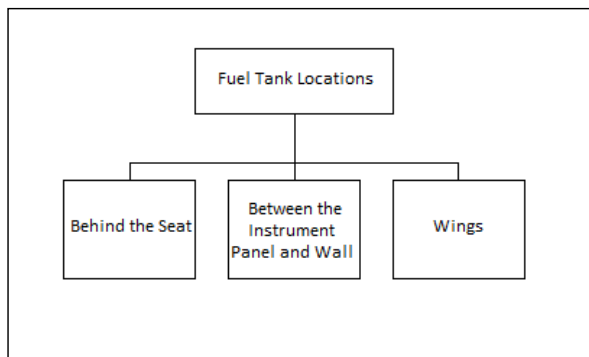


Figure 3.3-15. Fuel Tank Locations

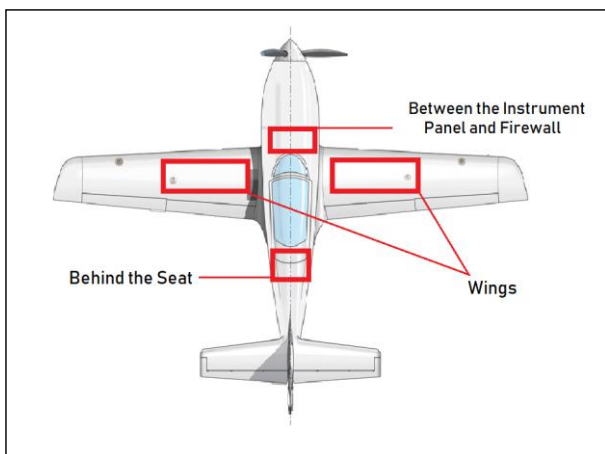


Figure 3.3-16. Fuel Tank Locations on an Aircraft

3.3.2.1.4. Fuel Tank Location Selection

In order to select the most suitable tank location, a trade-off study is needed to be done. In the trade-off study, the most important criteria are listed. Then their multipliers are defined by several project members, who are study on different working group, in order to get objective and healthy trade-off study. Fuel tank location options can be poor, average or good aspect for a criterion then, it gets -1, 0 or 1 point relatively.

Fuel tank location trade-off table is given below.

This document is the property of TAI, no part of it shall be reproduced or transmitted without written authorization of TAI, and its contents shall not be disclosed. All rights reserved. A hard copy of this technical document may not be the current issue. Check always with EDMS.

Evaluation Criteria	Multiplier	Fuel Tank Location		
		Behind the Seat	Between the Instrument Panel and Firewall	Wing
Fire Danger	25	1	-1	0
Impact Damage Resistance	20	0	-1	-1
Accessibility/Ease of Repair	10	0	-1	1
Available Space	10	0	-1	1
Effect on CG	35	-1	1	1
TOTAL	100	-10	-30	35

Table 3.3-10. Fuel Tank Location Trade-Off Study

At the end of the trade-off study, wings get highest grade in order to store the fuel. Therefore, wings are selected to locate the fuel tanks. One of the advantages storing the fuel inside the wings is that wing structure becomes stiffer. Also, when the fuel tanks are placed inside the wings, location of CG is preserved in front of the aircraft.

3.3.2.1.5. Result of Fuel Tank Trade-Off Study

After two different trade-off studies are done, suitable type of fuel tank for this project is integral type of fuel tank and the suitable location is wings.

3.3.2.2. Chapter 2: Conceptual Fuel System Architecture**3.3.2.2.1. Fuel System Schematic**

For VLA project, selected engine model is ROTAX 912 iSc Sport. Therefore, fuel system schematic is constructed according to technical document of the engine model and CS-VLA Technical Requirement document.

Constructed fuel system schematic is given below.

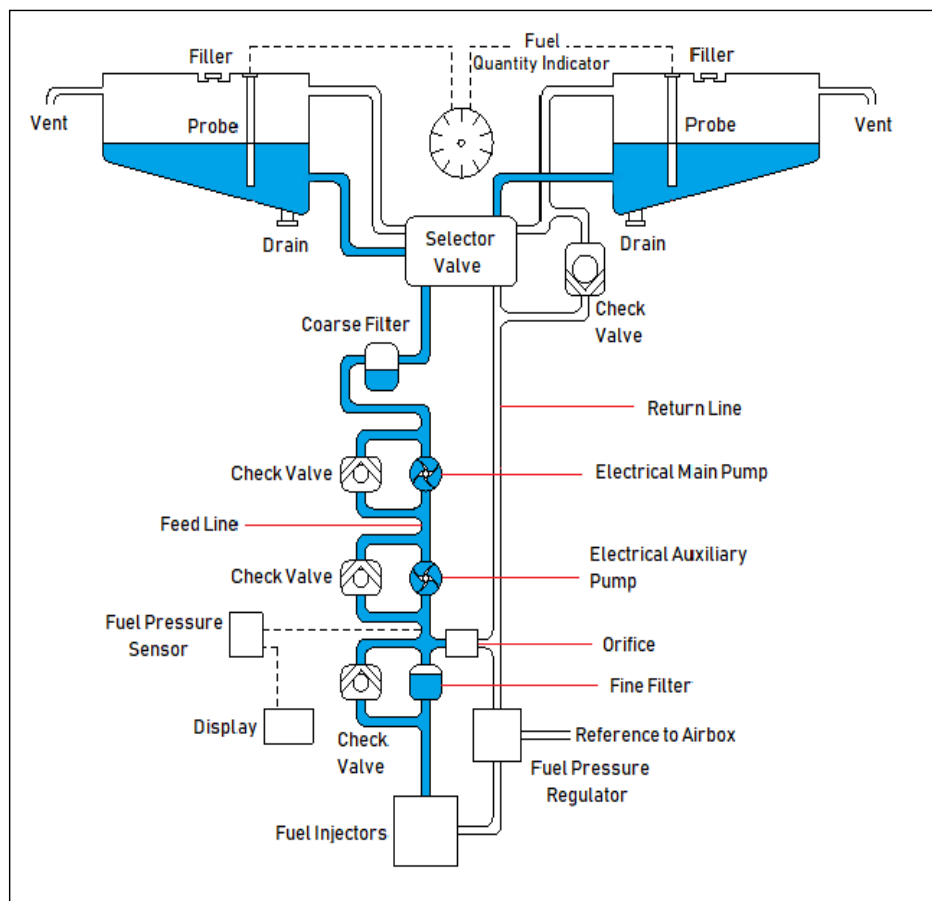


Figure 3.3-17. Fuel System Schematic

3.3.2.2. Fuel System Description

The fuel system operates with the AVGAS and MOGAS. All materials used in the fuel system are compatible with these fuels.

- Three fluid networks are employed in the fuel system; main feed line, return line and by-pass line.
- Main feed line is composed of functional equipment, pipes and carrying fuel from tanks to the engine. Electrical fuel pumps deliver the fuel from fuel tank to the engine.
- Return line carries air/fuel from the engine. The trapped air in the engine feed line is directed to the return line via the orifice.
- Double Valve is used as a fuel selector. Also, there is "off" function in order to shut off the fuel. Double main valve is pretty useful selector valve since it directs the excess fuel from the return line. When the engine is fed from the right or left tank also excess fuel returns the same tank which is used to engine feed via double main valve.
- Vent lines are routed from top part of the each wing tank expansion space. Each tank has own vent line and they are not connected.
- Fuel balancing is important issue for an aircraft whose fuel tanks are located inside the wings. In this schematic, there is no collector tank or connection between the fuel tanks in order to balance fuel. Fuel balancing is responsibility of pilot. There can be a timer which reminds the change of selected fuel tank to retain stability of the aircraft.
- Fuel Quantity is measured by probes. Each tanks has own probe. Therefore, fuel quantity is displayed for each tank separately.

3.3.2.2.3. Fuel System Components

The components shown in the schematic are listed below, and each of them is briefly explained.

1. Electrical Main Fuel Pump
2. Electrical Auxiliary Fuel Pump
3. Fine Fuel Filter
4. Coarse Fuel Filter
5. Check Valve (X4)
6. Selector Valve (Double Main Valve)
7. Probe (X2)
8. Fuel Pressure Regulator
9. Fuel Pressure Sensor
10. Drain Valve (X2)
11. Fuel Quantity Indicator
12. Orifice
13. Fuel Filler (X2)
14. Vent Line
15. Feed Line
16. Return Line

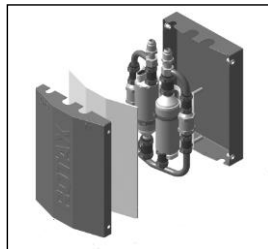
Electrical Main and Auxiliary Fuel Pumps

Figure 3.3-18. Electrical Fuel Pump Set

In order to feed the engine, there are two separate electrical fuel pumps. They are powered from two different generators in order to safety. There is a by-pass line in case of malfunction of a pump. Fuel pumps set is provided by the engine manufacturer.

Fine and Coarse Fuel Filter

Main purpose of the fuel filters is to separate the foreign particles from the fuel. Therefore engine is fed up with the clean fuel. Additionally, other components of the fuel system are protected.

In the fuel system schematic, there are two fuel filters. First one is close to the fuel tanks and its mesh size is great, called "coarse fuel filter". Second one is "fine fuel filter" and close to the engine and it has smaller mesh size. Engine manufacturer suggests 50-60 micron for coarse fuel filter and 8-12 micron for fine fuel filter.

Check Valves

Check valves allow flow in one direction and it automatically prevents reverse flow. They are self-automated valves does not require open and close. In addition to that, they prevent reverse rotation of the pumps. In the fuel system schematic, there are 4 check valves on the by-pass lines.

Selector Valve (Double Main Valve)

Figure 3.3-19. Selector Valve

Main Double Valve is used to control the direction of the fuel flow. Right or left fuel tank can be selected in order to feed the engine. There is also "OFF" position to shut off the fuel. In the schematic, it is located between the fuel tanks.

Main Double Valve has two separate compartments so that two independent fuel lines (feed and return) can be switched simultaneously. Fuel can be returned to the same tank from which it is drawn, thus it prevents dumping fuel overboard.

Probes

Fuel probes are used to measure the fuel quantity inside the fuel tanks. They operate according to the capacitance principle. Probe contains two concentric plates that are fixed distance apart. Therefore, the capacitance of a unit can change if the dielectric constant of the material separating the plate varies. The units are open at the top and bottom so they can assume the same level of fuel as is in the tanks. Therefore, the material between the plates is either fuel (if the tank is full), air (if the tank is empty), or some ratio of fuel and air depending on how much fuel remains in the tank.

In the fuel schematic, there are probes for each tank. Number of them can be increase depending of the tank geometry later.

Fuel Pressure Regulator

Injectors require a certain pressure to operate correctly. When the pressure is too low, the fuel does not spray out and will mix poorly with the air. If the pressure is too high, the components, which are located in the fuel system, could become damaged.

Therefore, fuel pressure regulator is used to ensure that constant fuel pressure is fed to injectors of the engine. In addition, each cylinder gets same mass flow rate of the fuel and air.

Drain Valves

Drain valves are used to take sample fuel and dump the tank. The drain valves are located lowest points of the fuel tanks. In the constructed fuel system, there are two drain valves for each fuel tank.

Orifice

An orifice is used for reducing pressure or restricting flow. In the fuel system schematic, there is an orifice between the feed and return line. The orifice helps the distribution subsystem to provide clean fuel to the engine since the air bubbles pass through the orifice from the feeding line to the return line.

Feed, Return and By-Pass Lines

Fuel is delivered from tank to the engine by feed lines.

Return line regulates pressure in a fluid system. It provides nearly constant pressure to the injectors. Therefore, excess fuel can be transferred back to the tanks by return line.

By-pass lines are essential in case of that some components which are by-passed are fail. This precaution has to be taken to prevent interruption of engine feeding.

In the fuel system schematic, there are by-pass lines for four different components which are selector valve, electrical main fuel pump, electrical auxiliary fuel pump and fine filter.

3.3.2.3. CONCLUSION

Fuel system involves three main parts. These are fuel storage, distribution and fuel indication. In conceptual design report, two of them are studied which are storage and distribution. In the first place, fuel tank type and fuel tank location is selected according to trade-off studies. After grading is done, integral type fuel tank is selected. Also, fuel tanks are located inside the wings.

In the second chapter of the conceptual design report, fuel system schematic is constructed according to engine which is ROTAX 912iSc Sport, then components of the fuel system is listed and briefly explained.

3.3.2.4. REFERENCES

- [1] R.Langton, C.Clark, M.Hewitt, L.Richards, Aircraft Fuel Systems. John Wiley & Sons, 2009.
- [2] D. Raymer-Aircraft Design. A Conceptual Approach.
- [3] Sadraey, Mohammad H. Aircraft design: A systems engineering approach. John Wiley & Sons, 2013.
- [4] Z.Goraj, P.Zakrzewski, Aircraft Fuel Systems and Their Influence on Stability Margin.
- [5] ROTAX 912iSc Sport Installation Manual.

3.4. Air Vehicle Systems**3.4.1. Flight Control****3.4.1.1. Purpose**

This report is prepared by METU-VLA Project Flight Control Students in order to show trade-off study & conceptual designs of flight control systems.

3.4.1.2. Trade-Off Study**3.4.1.2.1. Cable-Push Rod Selection**

There are two basic alternative mechanical systems which are cable-pulley systems and push-pull rod systems while designing mechanisms between cockpit and flight surfaces. While deciding which one is best for different mechanisms some factors need to be considered so that the mechanisms are light, safe and they can endure the loads.

Cable:

Steel cables and pulleys are used. Since the steel cable is elastic, some elongation can be observed; hence, while designing the cable system, the diameters of cable and dimensions of pulleys must be chosen, so the system do not fail under given loads. Before flight, pretensions must be given properly in order not to release cable itself. Also, since the cable cannot be under compression, they are used as pairs.

- It is relatively lighter than "push-pull rod"
- It eases to change direction or plane in mechanisms
- Backlash is not observed and it is strong and flexible choice

Push Rod:

Hollow aluminum cylinders are used because of being light. Although push-rods are stronger, they can fail under bending and torsion. Thus, strength of materials must be calculated carefully during design step, so the mechanisms do not fail under maximum static loads.

- It can withstand to higher loads than cable.
- Necessity of maintenance is less than cable and its periods are much more longer. Elongation due to temperature change is negligible. If the rods are designed to withstand maximum static load, maintenance is necessary only for fatigue failure.
- Since there is not additional friction forces as in cable-pulley systems.

3.4.1.2.2. Primary Control Mechanisms

Stick Type and Mechanism

To control aileron and elevator movement, center stick type controller is chosen because of experiences of the company with it. When stick mechanisms used by the competitors are considered, one stick concept that resembled Aquila A210 and Diamond D20 is decided to be used. The reason why this concept is chosen is that stick movement in the direction of aileron control is not affected by the movement in the elevator or vice versa.

Ailerons & Elevator:

Since the plane will be a low-wing plane, it was decided to use push-rods to connect center stick with ailerons. Since their maintenance is easier and it is easier to hold the given loads in CS VLA 397.b, use of push-rods would be more advantageous. For the cables to satisfy the tension of loads, they have to be connected to each other at a distance, which may not fit in the space provided behind the spar of the wings; therefore, it was decided to use push-rods to connect center stick with ailerons.

Since the distance between center stick and elevator is greater than distance between center stick and ailerons, it was first decided to use cable to connect center stick and elevator, but if the given hinge moment at elevator is greater than that cable can stand, push-rods can be a secondary option.

To control aileron and elevator movement, centre stick type controller is chosen because of experiences of the company with it. When stick mechanisms used by the competitors are considered, one stick concept that resembled Aquila A210 and Diamond DA20 is decided to be used. The reason why this concept is chosen is that stick movement in the direction of aileron control is not affected by the movement in the elevator or vice versa.

Rudder:

Studies about rudder up to now were progressed as lower and fixed pedals. A fixed pedal design used by most of the side-by-side planes was used. Since hinge moment on rudder is not high and distance between pedals and rudder is long, it was decided to connect pedals and rudder with cables.

3.4.1.2.3. Secondary Control Mechanisms

Flaps:

Mechanism to control flaps is going to be similar to mechanism used in Hürkuş since it will be easier to manufacture such system by the company. Using a rotational motion to control flaps would be more convenient since push rods are more resistant to torsion than they are to bending or tension/compression, and a lighter mechanism would be obtained. Two rotating rods to control flaps will be rotated by a single linear actuator located in the empennage, since there will be enough space behind pilots' seats and it will have less vibration than rotational actuator. A convenient actuator will be selected once hinge moments at flaps and time ratio to open the flaps are given.

Trims:

Since trim tab is a requirement to control trims, linear trim actuators can be placed in control surfaces and simple four-bar mechanism can be used to control them. If required, gear tabs can be designed too.

3.4.1.3. Conceptual Designs
3.4.1.3.1. Primary Control Mechanisms

According to this trade-off study, following designs are chosen to work on at this moment.

Stick, Aileron & Elevator

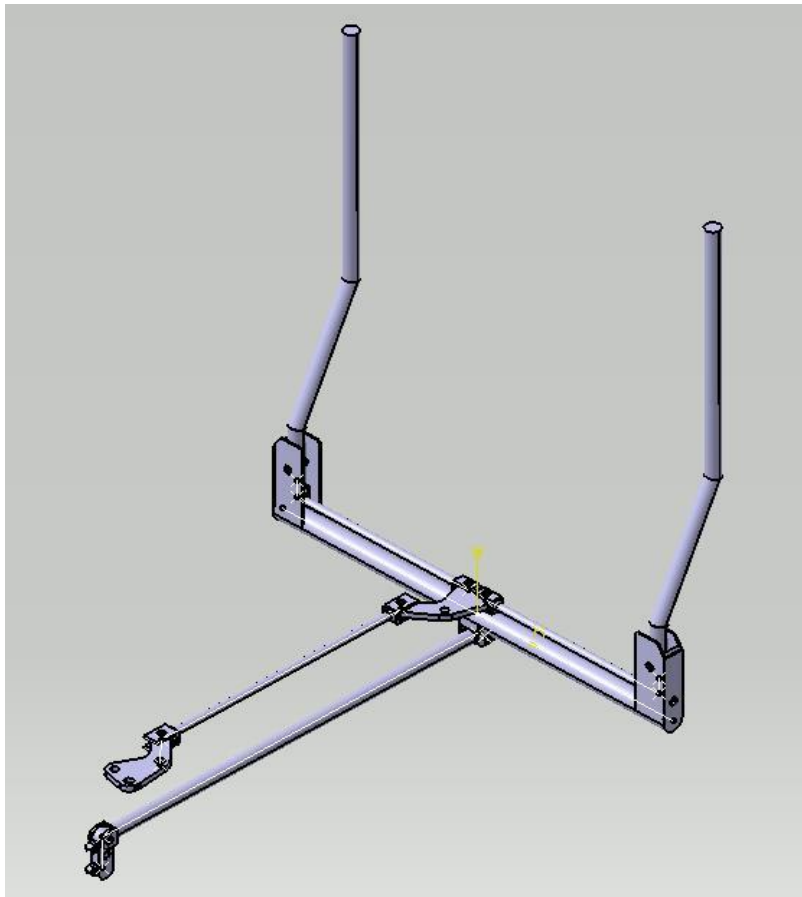


Figure 3.4-1: Isometric View of the Stick

The mechanism of the stick until the wings is shown above. According to trade-off study, aileron is decided to move by push-pull rods while elevator motion is obtained by cable-pulley system. For elevator motion, before cables one short push-rod has been used in order not to affect the aileron mechanism. The kinematic analysis is done and the demanded motions are obtained.

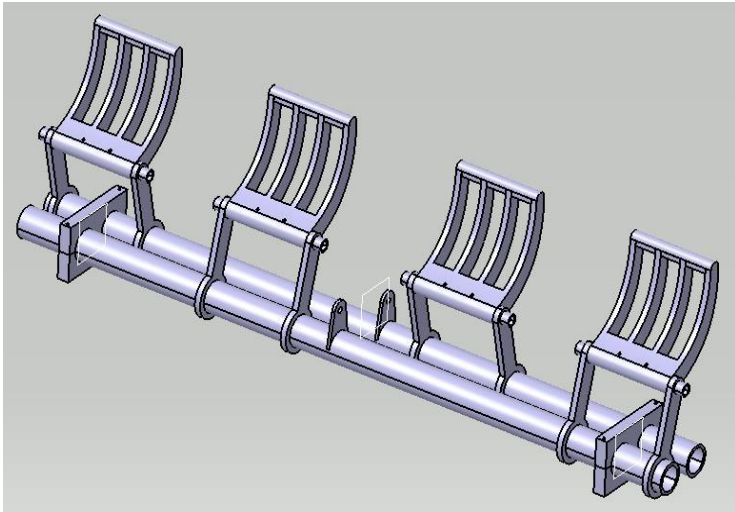
Pedal & Rudder

Figure 3.4-2: Isometric View of the Pedal

The mechanism of the pedal is shown above. For this mechanism, the pedal is mounted from the bottom. However, if the situation changes, we have another design where pedal mounted from the top as well. For rudder motion, cables will be used. The kinematic analysis is done and the demanded motions are obtained.

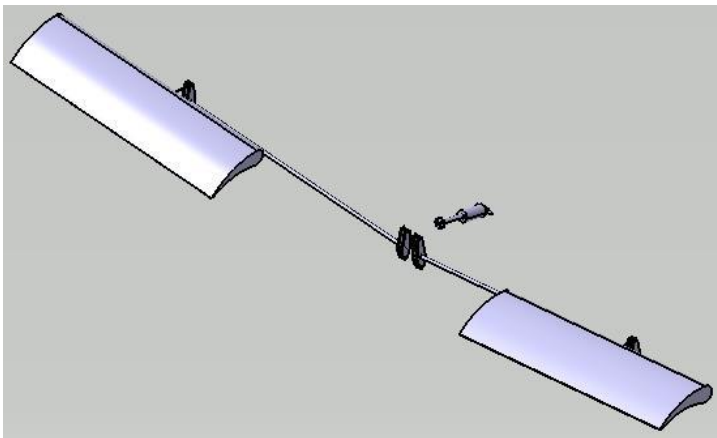
Secondary Control Mechanisms

Figure 3.4-3: Isometric View of Flap System

The mechanism of the flap is shown above, with a linear actuator. The kinematic analysis is done and the demanded motions are obtained.

3.4.1.4. Conceptual Design Assembly

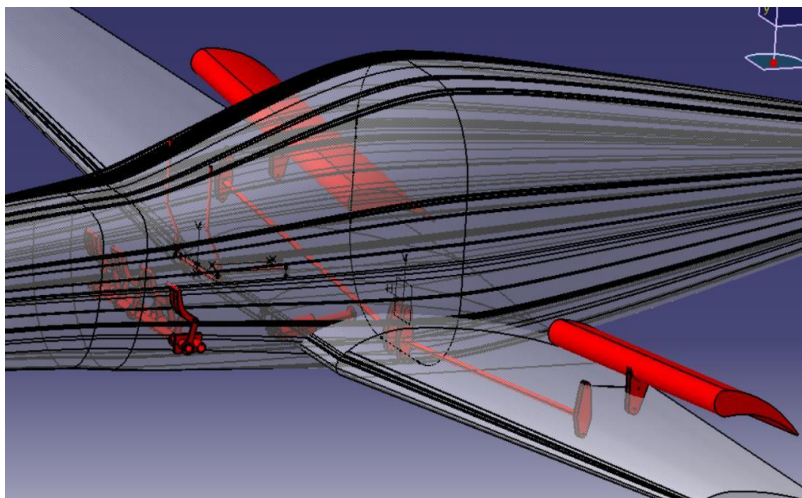


Figure 3.4-4: Final Assembly

The conceptual designs are assembled together and put into the given aircraft, for the upcoming studies. Cables and pushrods will take place at the critical design phase.

3.4.2. Landing Gear System**3.4.2.1. Fork Design****Force calculation****Vertical Load**

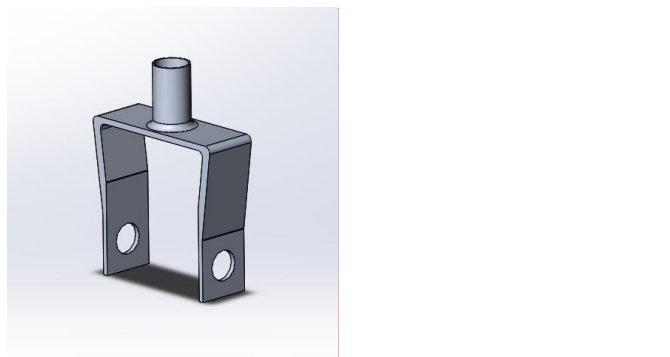
The maximum load on the NLG is 20% of the total aircraft load. The default Load Factor 3 is received for problematic descents
(The highest value in this category will be re-evaluated later)

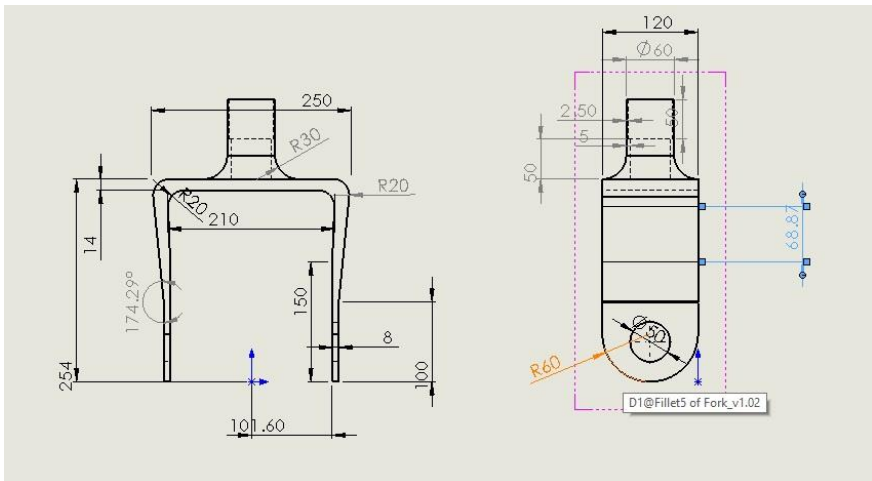
$$750 \text{ kg} * 0.2 * 9.81 \frac{\text{m}}{\text{s}^2} * 3 = 4415 \text{ N} \cong 4500 \text{ N}$$

Lateral Load

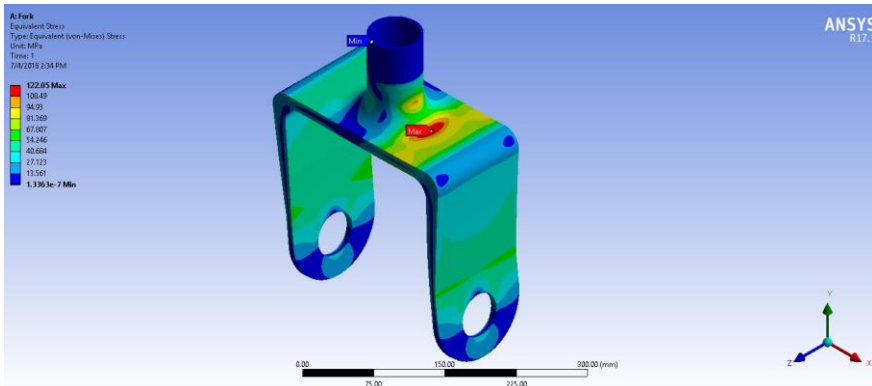
The flight was calculated at a speed of approximately 72 mph (20 m / s) and a turning radius of 15 mph. The coefficient of friction was taken as 0.7 . Load distribution : NLG:20% Each MLG Wheels :40%

$$750 \text{ kg} * \frac{\left(\frac{20 \text{ m}}{\text{s}}\right)^2}{15 \text{ m}} * 0.2 * 0.7 = 2800 \text{ N}$$

**Açıklamalı [k4]:** Figure ismi verelim



- max equivalent stress :122 Mpa
- min safety factor:2.65
- Material: Al 2024



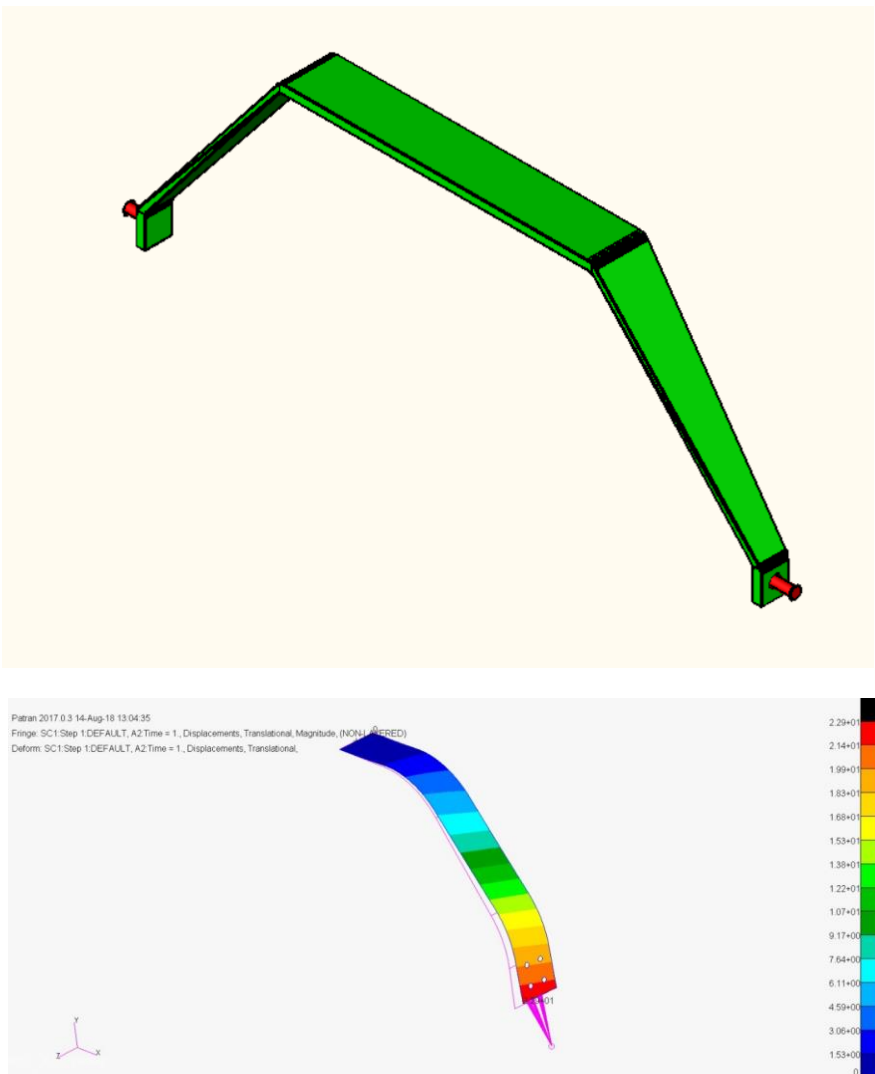
3.4.2.2. Main Landing

This report contains information about choosing main landing gear type for a via class. Firstly, the number of choice is reduced to three as bungee cord, leaf spring and shock strut with the help of literature researches. Among those three choices, leaf spring is the most suitable landing gear type for a very light aircraft's main landing. Detailed scoring table can be seen at the end of the report. Although bungee cord and leaf spring is so similar, bungee cord is disadvantageous in terms of maintainability.

This document is the property of TAI, no part of it shall be reproduced or transmitted without written authorization of TAI, and its contents shall not be disclosed. All rights reserved. A hard copy of this technical document may not be the current issue. Check always with EDMS.

because after each flight or operation bungee cord need to be inspected carefully in terms of elasticity and integrity of the cord. The comparison between leaf spring and shock struts is different than the previous one. Although shock struts efficiency per weight is higher than the leaf spring, leaf spring is much more ideal from standpoints of simplicity, reliability, and maintainability. Moreover, aircraft companies mostly use leaf spring type gear in main landing gears in VLA class. When that information is considered leaf spring is the most suitable choice for main landing gear.

3.4.2.3. Sample Drawing and Procedure of Design



This document is the property of TAI, no part of it shall be reproduced or transmitted without written authorization of TAI, and its contents shall not be disclosed. All rights reserved. A hard copy of this technical document may not be the current issue. Check always with EDMS.

While designing the leaf spring gear procedure described in Ladislao Pazmany books, Landing Gear Design for Light Aircraft and PL-8 Main Gear Design and Trade Offs, will be followed. As a first step a sample geometry for iterative calculations will be decided by measuring the details of a similar airplanes main landing gear. Also, the main landing gear designer of ANKA advised us to use computer program, 'Adams Aircraft', for drop tests and check the results with hand calculations.

3.5. Avionics, Missions & Electrical System

Our intention in this report is to present our ideas for the electrical and avionic architecture of our VLA

3.5.1. Avionics and BFI

3.5.1.1. Choosing the Avionics

As choosing the necessary avionic devices for the aircraft, the requirements specified by the TAI is considered. Corresponding requirements considered in this process can be seen at Table 3.5.1.

G5 ve GTX345 tablolarda yok.

Requirement	Definition	Chosen Avonic	Bağlantı
<u>ODTÜ-VLA-SRD-017</u>		<u>Garmin G500-Garmin GTN 750</u>	
<u>ODTÜ-VLA-SRD-018</u>		<u>Garmin G500-Garmin GTN 750</u>	
<u>ODTÜ-VLA-SRD-019</u>		<u>Garmin G500-Garmin GTN 750</u>	
<u>ODTÜ-VLA-SRD-020</u>		<u>Garmin G500-Garmin GTN 750</u>	
<u>ODTÜ-VLA-SRD-021</u>		<u>Garmin G500-Garmin GTN 750</u>	
<u>ODTÜ-VLA-SRD-022</u>		<u>Garmin GTN 750</u>	
<u>ODTÜ-VLA-SRD-023</u>		<u>Garmin GTN 750-Garmin GTX 335</u>	
<u>ODTÜ-VLA-SRD-024</u>		<u>Garmin GMA 340</u>	
<u>ODTÜ-VLA-SRD-026</u>		<u>Garmin GTN 750</u>	
<u>ODTÜ-VLA-SRD-027</u>		<u>Garmin GTN 750</u>	
<u>ODTÜ-VLA-SRD-028</u>		<u>Garmin GTN 750</u>	
<u>ODTÜ-VLA-SRD-029</u>		<u>Artex ME406 ELT</u>	
<u>ODTÜ-VLA-SRD-030</u>		<u>Garmin GTX 335</u>	
<u>ODTÜ-VLA-SRD-025</u>		<u>Garmin GMA 340</u>	

Table 3.5.1 Table

Bağlantı: Bağlantı

Bağlantı: Sonraki ile birlikte tut

Bağlantı: Konum: Yatay: 9,81 cm, Bağıntı: Sayfa, Dikey: 10,45 cm, Bağıntı: Paragraf, Yatay: 0,32 cm, Metin Çevresinde Kaydırır

<u>Required Equipment</u>	<u>Chosen Avionic</u>	Biçimlendirilmiş Tablo
<u>Seyrüsefer Ekipmanı</u>	<u>Garmin GTN 750</u>	
<u>Transponder</u>	<u>Garmin GTX 335</u>	
<u>Hız/İrtifa Göstergesi</u>	<u>Garmin G500</u>	
<u>Motor & Yakıt Kontrol Paneli</u>	<u>Garmin G500</u>	
<u>Elektrik Kontrol Paneli</u>	<u>Garmin G500</u>	
<u>Saat</u>	<u>Garmin G500</u>	
<u>ELT (Emergency Locator Transmitter)</u>	<u>Artex ME 406 ELT</u>	
<u>Magnetic Compass</u>	<u>Garmin G500</u>	
<u>Statik Port</u>	<u>Garmin G500</u>	
<u>Pitot Tube</u>	<u>Garmin G500</u>	
<u>Stall Uyarısı</u>	<u>Garmin G500?</u>	
<u>Haberleşme Sistemi</u>	<u>Garmin GMA 340</u>	

*Table 3.5_2 Table***Biçimlendirilmiş:** Sonraki ile birlikte tut**Biçimlendirilmiş:** Resim Yazısı, Ortadan, Girinti: Sol: 0 cm

<u>Requirement</u>	<u>Chosen Avionics</u>
<u>ODTÜ-VLA-SRD-017</u>	<u>Garmin GTN 750-Garmin G500</u>
<u>ODTÜ-VLA-SRD-018</u>	<u>Garmin G500-Garmin GTN 750</u>
<u>ODTÜ-VLA-SRD-019</u>	<u>Garmin G500-Garmin GTN 750</u>
<u>ODTÜ-VLA-SRD-020</u>	<u>Garmin G500-Garmin GTN 750</u>
<u>ODTÜ-VLA-SRD-021</u>	<u>Garmin G500-Garmin GTN 750</u>
<u>ODTÜ-VLA-SRD-022</u>	<u>Garmin GTN 750</u>
<u>ODTÜ-VLA-SRD-023</u>	<u>Garmin GTN 750-Garmin GTX 335</u>
<u>ODTÜ-VLA-SRD-024</u>	<u>Garmin GMA 340</u>
<u>ODTÜ-VLA-SRD-026</u>	<u>Garmin GTN 750</u>
<u>ODTÜ-VLA-SRD-027</u>	<u>Garmin GTN 750</u>
<u>ODTÜ-VLA-SRD-028</u>	<u>Garmin GTN 750</u>

<u>ODTÜ VLA SRD-029</u>	<u>Arteq ME406 ELT</u>
<u>ODTÜ VLA SRD-030</u>	<u>Garmin GTX 335</u>
<u>ODTÜ VLA SRD-025</u>	<u>Garmin GMA 340</u>

Table 3.5.1 Corresponding Requirements for Avionics

3.5.

3.5.1.1. Avionic and Electrical Architecture Proposal Report

Our intention in this report is to present our ideas for the electrical and avionic architecture of our VLA. This is a draft document and therefore should not be regarded as the final proposal.

On Figure 1, you can observe the crude electrical architecture. Two busses — main and essential — are used on the architecture, typical for such aircraft. The generator relies on the engine to provide power while battery is used to provide a steady and safe source of energy in the case of a discrepancy.

GMFD stands for the control panels.

CVR is the black box.

The rest is given below.

Figure 2 shows our design for the avionic architecture. The avionic architecture relies mainly on ARINC 429 standard, which is well known to be wide spread in non-military avionic applications. However, the system also employs discrete and Ethernet connections. To denote briefly the individual components on the architecture:

CV / FDR stands for “Cockpit Voice / Flight Data Recorder”, is the black box of the aircraft.

G500 represents Garmin G500 dual screen electronic display.

BFI or more commonly BFS is the “Backup Flight System”.

ADC is the air data computer.

INS / GPS stands for the Inertial Navigation System and the Global Positioning System.

ELT is the Emergency Locator Transmitter.

ICS is the Intercom equipment.

V/UHF is the Very High and Ultra High Frequency Radio.

Mode S is the Mode S Transponder.

Biçimlendirilmiş: Yazı tipi:

Biçimlendirilmiş: Normal

Biçimlendirilmiş: Level 3 Heading, Numaralandırılmış ana hat + Düzey: 4 + Numaralandırma Stili: 1, 2, 3, ... + Başlangıç: 1 + Hızalama: Soldan + Hizalandığı yer: 1,9 cm + Girinti yeri: 3,05 cm

Biçimlendirilmiş: Başlık 4

1.3.5.1.2. Avionics

Avionic	Configuration	Functionality	Width	Height	Dept
G500 TXI	10.6"	Display	11.4"	7.25"	3"
G500 TXI	7"	EIS	5.5"	7.25"	3"
GTN 750	-	GPS/NAV/COMM/MFD	6.25" (159 mm)	6.00" (152 mm)	11.25 (286 mm)
GTX 345	-	ADS-B & Transponder	6.30" (160 mm)	1.65" (42 m)	10.07" (256 mm)
GMA 345	-	Audio Panel	6.30" (160 mm)	1.33" (34 mm)	8.09" (205 mm)
G5	-	Attitude Indicator	3.4" (86.4 mm)	3.6" (91.4 mm)	3.0" (76.2 mm)

Table 3.5_3

Biçimlendirilmiş: Sonraki ile birlikte tut

Biçimlendirilmiş: Resim Yazısı, Ortadan

Avionic	Configuration	Functionality	Weight	Weight with Additions
G500 TXI	10.6"	Display	6.49 lbs.	7.25 lbs. (with integral ADAHRS)
G500 TXI	7"	EIS	3.99 lbs.	4.45 lbs. (with integral ADAHRS)
GTN 750	-	GPS/NAV/COMM/MFD	9.3 lbs. (4.24 kg)	
GTX 345	-	ADS-B & Transponder	3.1 lbs. (1.41 kg)	
GMA 345	-	Audio Panel	1.78 lbs. (807.4 g)	
G5	-	Attitude Indicator	13.3 oz (377.0 g)	

Table 3.5_4

Biçimlendirilmiş: Sonraki ile birlikte tut

Biçimlendirilmiş: Resim Yazısı, Ortadan

Biçimlendirilmiş: Başlık 5, Aralık Önce: 0 nk, Satır aralığı: tek, Madde işaretleri veya numaralandırma yok

1.1.1.3.5.1.2.1. Garmin G500 TXI

The G500 TXI is a display and sensor system available in three display options:

- o GDU 1060 – 10" display
- o GDU 700P – 7" portrait display
- o GDU 700L – 7" landscape display

Display options can be seen at Figure 8. Depending on system specifics one or more of the following functions may apply:

1. **Primary Flight Display (PFD)** – provides attitude, heading, air data, and navigation information to the pilot
2. **Multi-Function Display (MFD)** – provides pilot awareness of factors that may affect the overall conduct of a flight

This document is the property of TAI, no part of it shall be reproduced or transmitted without written authorization of TAI, and its contents shall not be disclosed. All rights reserved. A hard copy of this technical document may not be the current issue. Check always with EDMS.

3. Engine Indicating System (EIS) – provides engine and airframe operating parameters to the pilot

Due to its natural support to EIS, we decided to use G500 TXI over G500. With an integrated EIS at Figure 9, G500 TXI can simply display any vital engine information on its screen. Considering the display configurations for the 1060, ~~700P~~ and ~~700L~~ ~~700P~~ at Figures [40](#), [11176](#) and [1772](#) respectively, we decided to use 10" configuration and 7" configuration of the G500 TXI instead of dual 7" option. Using MFD/PFD configuration of 10" configuration and EIS only mode of 7" configuration, pilots can be informed about the plane from two screen.



Figure 51 GDU 1060 Display Configuration



Figure 62 GDU 700P Display Configuration

This document is the property of TAI, no part of it shall be reproduced or transmitted without written authorization of TAI, and its contents shall not be disclosed. All rights reserved. A hard copy of this technical document may not be the current issue. Check always with EDMS.

PFD	MFD	EIS [2]
GDU 700()/1060	GDU 700P/1060 [3]	GDU 700()/1060 [3]
<ul style="list-style-type: none"> • Attitude • Airspeed • Altitude • Vertical Speed • Turn Coordinator • HSI • HSI Map [4] • Clock • Lateral and Vertical Deviation Indicators • Datalink Weather Display [1] • Radar Altimeter [1] • Autopilot Annunciations [1] • Flight Director [1] • Synthetic Vision [1] • Flight Path Marker [1] • System Advisories • Safety Monitors [1] • GPS NAV Status • Display Backup [1] [4] • Terrain Avoidance [1] 	<ul style="list-style-type: none"> • Navigation Map • Traffic [1] • Terrain • Charts • Flight Plan • Weather [1] • Waypoint Information • Music Services [1] • Terrain Avoidance [1] • Engine Data [1] • System Advisories • Video [1] 	<ul style="list-style-type: none"> • Fuel Qty (Main, Aux) • RPM/Tach • Propeller Sync Display • Manifold Pressure • Oil Pressure • Oil Temperature • Fuel Flow • Fuel Pressure • Fuel Calculations • Cylinder Operating Temperatures (CHT, EGT) • TIT • Lean Assist Mode • Carburetor Air Temperature • Intercooler Temperatures (IAT, CDT, Difference) • Amps/Volts • User Selectable Fields • User Adjustable Advisories

[1] Function availability dependent upon aircraft interfaces or enablement.

[2] Displayed engine operating parameters dependent upon configuration.

[3] GDU 700() MFD/EIS provides the same MFD and EIS functionality listed with the exception of weather radar and multi-engine.

[4] Not available for GDU 700L.

Figure 7-3 System Functions

System functions of G500 TXI can be seen at Figure 1-783 while electrical loads of subsystems of G500 TXI can be seen at Figure 4-4179.

UNCLASSIFIED

DOCUMENT NO:[XXXXXXXXXX](#)

Issue No: [1](#)

LRU	14 Volt Current Draw		28 Volt Current Draw	
	Typical	Maximum	Typical	Maximum
GDU 700()	3.0 A	6.0 A	1.5 A	3.0 A
GDU 1060	5.0 A	8.0 A	2.5 A	4.0 A
GRS 79/GMU 44	480 mA	958 mA	240 mA	479 mA
GRS 77/GMU 44	600 mA	1.0 A	300 mA	1.0 A
GSU 75()/GMU 44/GTP 59	760 mA	958 mA	380 mA	479 mA
GDC 72/GTP 59	420 mA	958 mA	210 mA	479 mA
GDC 74()/GTP 59	410 mA	480 mA	200 mA	235 mA
GAD 43	410 mA	720 mA	210 mA	350 mA
GAD 43e	790 mA	1.22 A	390 mA	590 mA
GCU 485	120 mA	357 mA	64 mA	179 mA
GEA 110	0.30 A	0.60 A	0.15 A	0.30 A

Figure 84 Electrical Load of Subsystems of G500 TXI

1.1.2.3.5.1.2.2. [Garmin GTN750](#)



Figure 95 [Garmin GTN750](#)

UNCLASSIFIED

DOCUMENT NO:XXXXXXXXXX

Issue No: 1

1.1.3.3.5.1.2.3. Garmin GMA345



Figure 106 Garmin GMA 345

1.1.4.3.5.1.2.4. Garmin GTX345



Figure 117 Garmin GTX 335/345

1.1.5.3.5.1.2.5. Garmin G5



Figure 128 Garmin G5

This document is the property of TAI, no part of it shall be reproduced or transmitted without written authorization of TAI, and its contents shall not be disclosed. All rights reserved. A hard copy of this technical document may not be the current issue. Check always with EDMS.

UNCLASSIFIED

2.3.5.1.3_ Proposed Avionic Architecture

Figure [2.2-184](#) shows our design for the avionic architecture. The avionic architecture relies mainly on ARINC-429 standard, which is well known to be wide spread in non-military avionic applications. However, the system also employs discrete and Ethernet connections. To denote briefly the individual components on the architecture:

- **CV / FDR** stands for "Cockpit Voice / Flight Data Recorder", is the black box of the aircraft.
- **G500** represents Garmin G500 dual screen electronic display.
- **BFI** or more commonly BFS is the "Backup Flight System".
- **ADC** is the air data computer.
- **INS / GPS** stands for the Inertial Navigation System and the Global Positioning System.
- **ELT** is the Emergency Locator Transmitter.
- **ICS** is the Intercom equipment.
- **V/UHF** is the Very High and Ultra High Frequency Radio.
- **Mode-S** is the Mode-S Transponder.

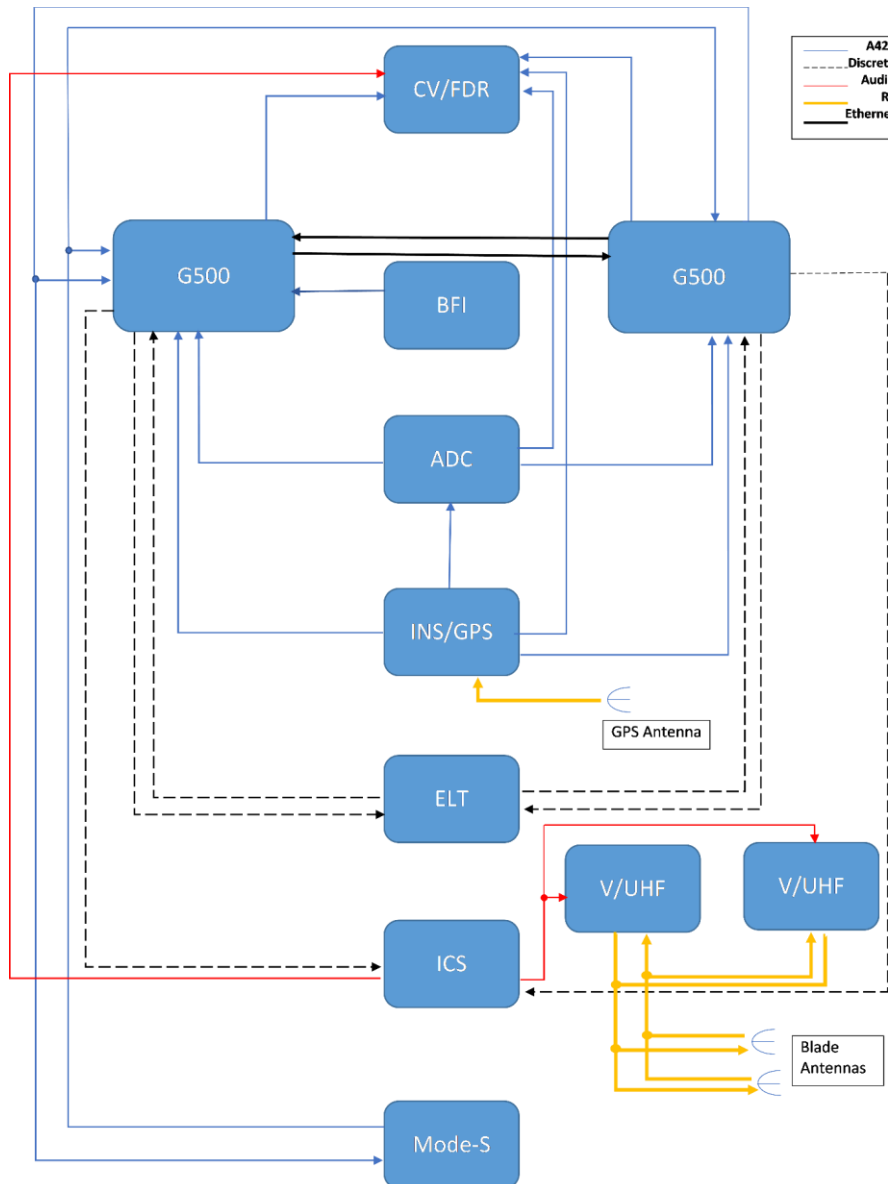


Figure 139 : The proposed avionic architecture. Notice the legend.

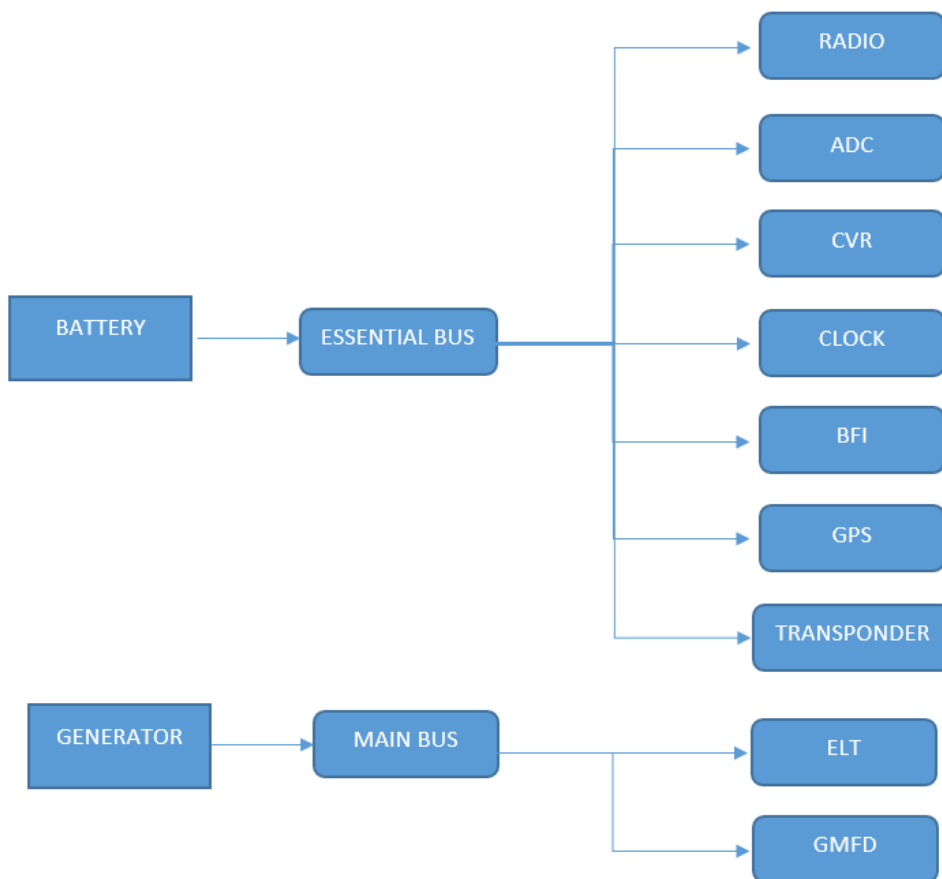
BİÇİMLENİRLİMİŞ: Başlık 3

Figure 3.5.1 : The crude electrical architecture

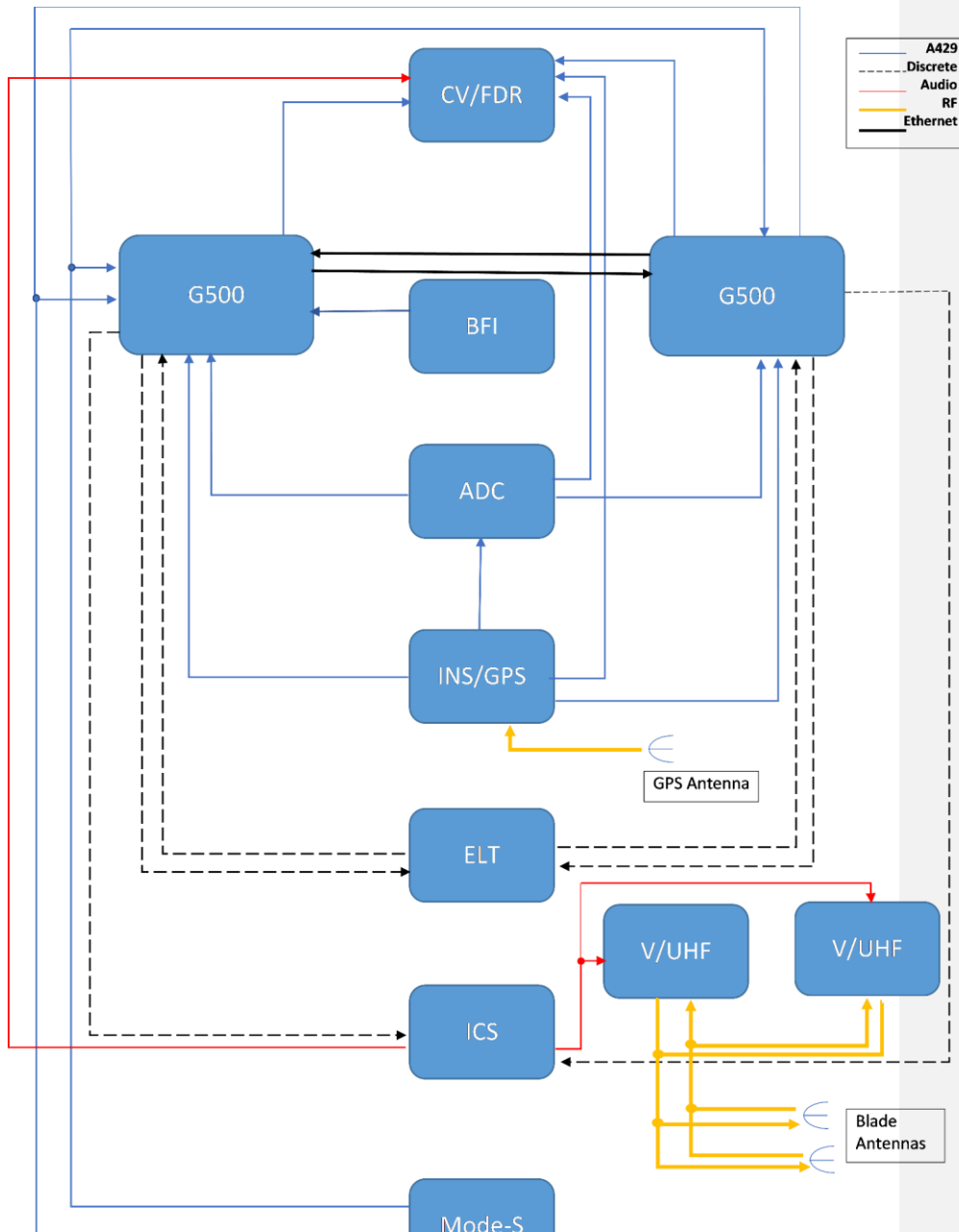


Figure 3.5.2 : The proposed avionic architecture. Notice the legend.

This document is the property of TAI, no part of it shall be reproduced or transmitted without written authorization of TAI, and its contents shall not be disclosed.
All rights reserved. A hard copy of this technical document may not be the current issue. Check always with EDMS.

Choosing the Necessary Lighting ~~Equipments~~

According to CS-VLA 1384, external lights must be installed with regard to CS-23 23.2530. These sub-paragraphs mention that any position lights must include a red light on the left wing, a green light on the right wing and a white light facing aft. Also any position or anti-collision lights must have proper features to provide sufficient time for another aircraft to avoid a collision. Therefore, we deduced that we should have 3 position lights, as red, green and white, and 2 anti-collision lights.



Figure 1.3.5-3 Anti-collision LED light – Red or White

Figure 14185 Anti-collision LED light – Red or White

Since those lighting systems are very common, companies like AVEO Engineering are building compact systems. AVEO's Ultra DayLite and Andromeda DayLite products are two examples of that. They both have navigation (red and green lights), position (white light) and strobe (anti-collision light) systems built in. When compared in terms of weight and power usage, they do not have an important difference. Main reason to choose one to other can be the design. Their prices are same, \$769.00. However, these products are not TSO certified. If a TSO certified product is necessary, TSO certified Ultra Galactica can be used, priced at \$1099.00. An example for Anti-collision LED light from AVEO can be seen from Figure 3-185 while an example for Navigation / Position / Strobe LED light can be seen at Figure 4186.



Figure 3.5-4186 Navigation / Position / Strobe LED light

Bağlantılı: Sonraki ile birlikte tut

Bağlantılı: İki Yana Yasla

2.3.5.3. Preliminary Electrical Architecture

On Figure 32187, you can observe the preliminary electrical architecture. Two busses – main and essential- are used on the architecture, typical for such aircraft. The generator relies on the engine to provide power while battery is used to provide a steady and safe source of energy in the case of a discrepancy.

- GMFD stands for the control panels.
- CVR is the black box.
- The rest is given below.

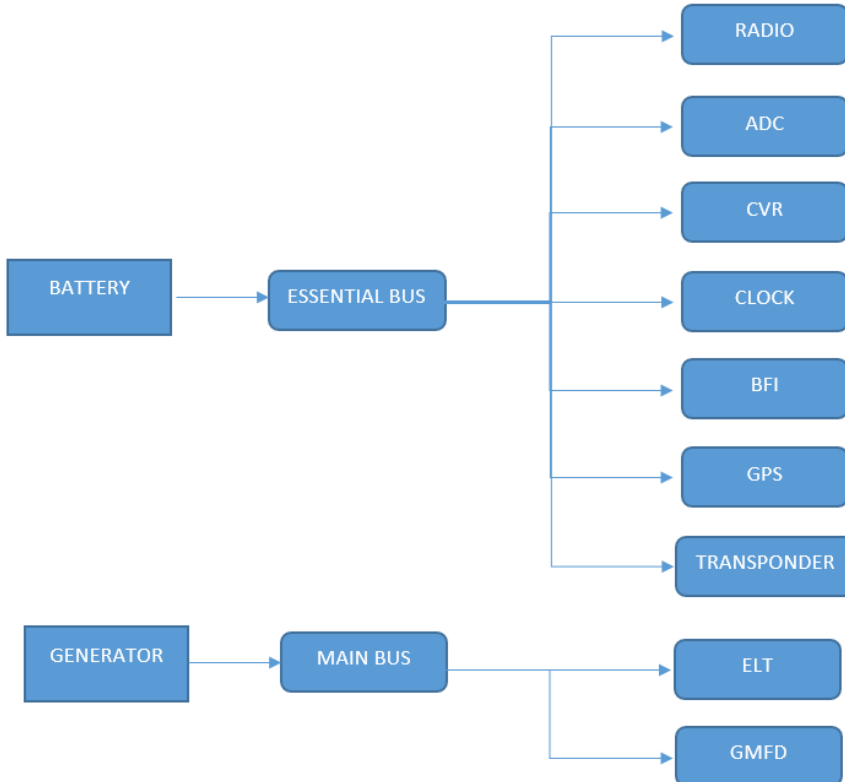


Figure 1518728 : Preliminary Electrical Architecture

2.5.1.3.1.1.1. Choosing the Avionics

Biçimlendirilmiş: Level 3 Heading

As choosing the necessary avionic devices for the aircraft, the requirements specified by the TAI is considered. Corresponding requirements considered in this process can be seen at Table 1.

Requirement	Chosen Avionics
<u>ODTÜ VLA SRD-017</u>	Garmin GTN 750 Garmin G500
<u>ODTÜ VLA SRD-018</u>	Garmin G500 Garmin GTN 750
<u>ODTÜ VLA SRD-019</u>	Garmin G500 Garmin GTN 750
<u>ODTÜ VLA SRD-020</u>	Garmin G500 Garmin GTN 750
<u>ODTÜ VLA SRD-021</u>	Garmin G500 Garmin GTN 750
<u>ODTÜ VLA SRD-022</u>	Garmin GTN 750
<u>ODTÜ VLA SRD-023</u>	Garmin GTN 750 Garmin CTX 335
<u>ODTÜ VLA SRD-024</u>	Garmin GMA 340
<u>ODTÜ VLA SRD-026</u>	Garmin GTN 750
<u>ODTÜ VLA SRD-027</u>	Garmin GTN 750
<u>ODTÜ VLA SRD-028</u>	Garmin GTN 750
<u>ODTÜ VLA SRD-029</u>	Arteox ME406 ELT
<u>ODTÜ VLA SRD-030</u>	Garmin CTX 335
<u>ODTÜ VLA SRD-025</u>	Garmin GMA 340

Table 3.5.1 Corresponding Requirements for Avionics

4. APPENDIX (AERODYNAMICS, FLIGHT MECHANICS, FLIGHT PERFORMANCE)

4.1. APPENDIX A

Results of the analysis of SD 7062 Airfoil with 0 degrees of flap deflections at 5000 ft.

Airfoil	Axial	Normal		AOA	C _L	C _D	C _M

This document is the property of TAI, no part of it shall be reproduced or transmitted without written authorization of TAI, and its contents shall not be disclosed. All rights reserved. A hard copy of this technical document may not be the current issue. Check always with EDMS.

UNCLASSIFIED

DOCUMENT NO:[XXXXXXXXXX](#)

Issue No: [1](#)

-6	-0,01482	-0,24036		-6	-0,24059	0,01039	-0,08135
-5	-0,00127	-0,12775		-5	-0,12737	0,00987	-0,08156
-4	0,00851	-0,01426		-4	-0,01363	0,00948	-0,08176
-3	0,01452	0,09941		-3	0,10004	0,00930	-0,08193
-2	0,01671	0,21363		-2	0,21408	0,00924	-0,08213
-1	0,01502	0,32757		-1	0,32778	0,00930	-0,08228
0	0,00946	0,44075		0	0,44075	0,00946	-0,08232
1	0,00014	0,55242		1	0,55233	0,00978	-0,08233
2	-0,01293	0,66303		2	0,66308	0,01022	-0,08228
3	-0,02965	0,77216		3	0,77265	0,01081	-0,08217
4	-0,04994	0,87935		4	0,88069	0,01152	-0,08192
5	-0,07358	0,98301		5	0,98568	0,01238	-0,08139
6	-0,10022	1,08232		6	1,08687	0,01346	-0,08052
7	-0,12978	1,17768		7	1,18472	0,01471	-0,07943
8	-0,16157	1,26678		8	1,27694	0,01631	-0,07796
9	-0,19535	1,35020		9	1,36414	0,01827	-0,07627
10	-0,23063	1,42711		10	1,44548	0,02069	-0,07447
11	-0,26589	1,49326		11	1,51656	0,02392	-0,07246
12	-0,29928	1,54403		12	1,57251	0,02828	-0,07020
13	-0,32799	1,57421		13	1,60764	0,03453	-0,06811
14	-0,34993	1,58225		14	1,61991	0,04324	-0,06662
15	-0,36118	1,56089		15	1,60118	0,05512	-0,06576
16	-0,35796	1,50884		16	1,54906	0,07180	-0,06731
17	-0,33880	1,43094		17	1,46747	0,09437	-0,07234

4.2. APPENDIX B

Results of the analysis of 3D wing with 0 flap deflections at 5000 ft.

AOA	Axial	Normal		AOA	CL	CD	CM
0	0,0164	0,3197		0	0,3197	0,0164	-0,1300

This document is the property of TAI, no part of it shall be reproduced or transmitted without written authorization of TAI, and its contents shall not be disclosed.
All rights reserved. A hard copy of this technical document may not be the current issue. Check always with EDMS.

UNCLASSIFIED

UNCLASSIFIEDDOCUMENT NO:[XXXXXXXXXX](#)Issue No: [1](#)

2	0,0046	0,4851		2	0,4846	0,0215	-0,1433
3	-0,0046	0,5681		3	0,5676	0,0251	-0,1500
4	-0,0158	0,6493		4	0,6488	0,0295	-0,1562
6	-0,0445	0,8084		6	0,8086	0,0402	-0,1677
8	-0,0809	0,9578		8	0,9598	0,0532	-0,1770
10	-0,1233	1,0921		10	1,0970	0,0682	-0,1836
12	-0,1682	1,1997		12	1,2085	0,0849	-0,1861
14	-0,2116	1,2791		14	1,2923	0,1042	-0,1875
15	-0,2344	1,3213		15	1,3369	0,1155	-0,1904
16	-0,2549	1,3500		16	1,3680	0,1271	-0,1912
17	-0,2702	1,3599		17	1,3795	0,1392	-0,1903
18	-0,2774	1,3557		18	1,3750	0,1551	-0,1925

4.3. APPENDIX C

Results of the analysis of 3D wing with 10 degrees of deflections at 0 ft.

AOA	Axial	Normal	AOA	CL	CD	CM	Force
12	-0,2004	1,5540	12	1,5617	0,1270	-0,3147	3966 N
13	-0,2322	1,6218	13	1,6325	0,1386	-0,3192	4139 N
14	-0,2638	1,6773	14	1,6913	0,1499	-0,3199	4281 N
15	-0,2967	1,7331	15	1,7509	0,1620	-0,3224	4350 N
16	-0,3304	1,7826	16	1,8046	0,1737	-0,3225	4550 N
17	-0,3572	1,8080	17	1,8334	0,1870	-0,3228	4615 N

4.4. APPENDIX D

Results of the analysis of 3D wing with 15 degrees of deflections at 0 ft.

AOA	Axial	Normal	AOA	CL	CD	CM	Normal Force
12	-0,2129	1,7375	12	1,7438	0,1530	-0,3824	4433 N
13	-0,2443	1,8115	13	1,8200	0,1695	-0,3856	4624 N
14	-0,2785	1,8677	14	1,8796	0,1816	-0,3861	4767 N
15	-0,3070	1,9044	15	1,9190	0,1964	-0,3749	4810 N
16	-0,3428	1,9339	16	1,9535	0,2035	-0,3756	4936 N
17	-0,3635	1,9546	16	1,9755	0,2238	-0,3748	5011 N

This document is the property of TAI, no part of it shall be reproduced or transmitted without written authorization of TAI, and its contents shall not be disclosed.
All rights reserved. A hard copy of this technical document may not be the current issue. Check always with EDMS.

UNCLASSIFIED

DOCUMENT NO:[XXXXXXXXXX](#)

Issue No: [1](#)

4.5. APPENDIX E

Results of the analysis of 3D wing with 30 degrees of deflections at 0 ft.

AOA	Axial	Normal	AOA	CL	CD	CM	Normal Force
12	-0,1520	1,5669	12	1,5642	0,1771	-0,3257	3999 N
13	-0,1783	1,6230	13	1,6215	0,1913	-0,3303	4142 N
14	-0,2121	1,6717	14	1,6734	0,1986	-0,3293	4267 N
15	-0,2388	1,7115	15	1,7150	0,2123	-0,3310	4368 N
16	-0,2539	1,7490	16	1,7512	0,2380	-0,3408	4464 N
17	-0,2599	1,7583	17	1,7574	0,2655	-0,3398	4588 N

4.6. APPENDIX F

Results of the analysis of SD 7062 Airfoil with 0 degrees of flap deflections at 7500 ft.

AOA	C _I	C _d	C _m	C _I /C _d	C _I ^{3/2} /C _d
-6	-0,24059	0,01039	-0,08135	-23,15591915	0
-5	-0,12737	0,00987	-0,08156	-12,9047619	0
-4	-0,01363	0,00948	-0,08176	-1,437763713	0
-3	0,10004	0,0093	-0,08193	10,75698925	3,402338942
-2	0,21408	0,00924	-0,08213	23,16883117	10,71993552
-1	0,32778	0,0093	-0,08228	35,24516129	20,17858589
0	0,44075	0,00946	-0,08232	46,59090909	30,93124102
1	0,55233	0,00978	-0,08233	56,47546012	41,97194492
2	0,66308	0,01022	-0,08228	64,88062622	52,83211506
3	0,77265	0,01081	-0,08217	71,47548566	62,82731781
4	0,88069	0,01152	-0,08192	76,44878472	71,74342709
5	0,98568	0,01238	-0,08139	79,6187399	79,04661413
6	1,08687	0,01346	-0,08052	80,74814264	84,18240759
7	1,18472	0,01471	-0,07943	80,53840925	87,66190566
8	1,27694	0,01631	-0,07796	78,29184549	88,47117109
9	1,36414	0,01827	-0,07627	74,66557198	87,20670313
10	1,44548	0,02069	-0,07447	69,86370227	83,99581337
11	1,51656	0,02392	-0,07246	63,40133779	78,07791732
12	1,57251	0,02828	-0,0702	55,60502122	69,72856358
13	1,60764	0,03453	-0,06811	46,55777585	59,03188167
14	1,61991	0,04324	-0,06662	37,46322849	47,6815807
15	1,60118	0,05512	-0,06576	29,04898403	36,7579283

This document is the property of TAI, no part of it shall be reproduced or transmitted without written authorization of TAI, and its contents shall not be disclosed.
All rights reserved. A hard copy of this technical document may not be the current issue. Check always with EDMS.

UNCLASSIFIED

UNCLASSIFIED

DOCUMENT NO:[XXXXXXXXXX](#)

Issue No: [1](#)

16		1,54906	0,0718	-0,06731	21,57465181	26,85207894
17		1,46747	0,09437	-0,07234	15,55017484	18,8373537

4.7. APPENDIX G

Results of the analysis of Rhodes St. 32 Airfoil with 0 degrees of flap deflections at 7500 ft.

AOA		Cl	Cd	Cm	Cl/Cd	Cl(3/2)/Cd
-6		-0,0883	0,0181	0,0733	-4,8712	0,0000
-5		0,0153	0,0174	0,0723	0,8793	0,1087
-4		0,1196	0,0169	0,0713	7,0634	2,4426
-3		0,2242	0,0168	0,0705	13,3638	6,3275
-2		0,3286	0,0169	0,0697	19,4531	11,1518
-1		0,4327	0,0172	0,0689	25,0989	16,5103
0		0,5359	0,0178	0,0682	30,1220	22,0517
1		0,6382	0,0186	0,0675	34,4003	27,4816
2		0,7391	0,0195	0,0667	37,8708	32,5577
3		0,8376	0,0207	0,0658	40,4609	37,0301
4		0,9344	0,0221	0,0649	42,2490	40,8397
5		1,0280	0,0238	0,0638	43,2004	43,8007
6		1,1178	0,0258	0,0625	43,3899	45,8747
7		1,2034	0,0281	0,0610	42,8589	47,0159
8		1,2833	0,0308	0,0591	41,7067	47,2462
9		1,3565	0,0339	0,0568	39,9612	46,5424
10		1,4210	0,0377	0,0542	37,7098	44,9523
11		1,4748	0,0422	0,0512	34,9842	42,4856
12		1,5141	0,0475	0,0478	31,8485	39,1894
13		1,5335	0,0543	0,0441	28,2666	35,0038
14		1,5233	0,0629	0,0402	24,2092	29,8790
15		1,4705	0,0746	0,0368	19,7119	23,9039
16		1,3669	0,0907	0,0359	15,0645	17,6127

This document is the property of TAI, no part of it shall be reproduced or transmitted without written authorization of TAI, and its contents shall not be disclosed.
All rights reserved. A hard copy of this technical document may not be the current issue. Check always with EDMS.

UNCLASSIFIED

4.8. APPENDIX H

Results of the analysis of Rhodes St. 32 Airfoil with 15 degrees of flap deflections at 0 ft.

AOA	Cl	Cd	Cm
0	1,2577	0,0249	0,2179
1	1,3573	0,0265	0,2193
2	1,4523	0,0285	0,2199
3	1,5422	0,0309	0,2199
4	1,6261	0,0339	0,2190
5	1,7015	0,0373	0,2168
6	1,7680	0,0414	0,2136
7	1,8264	0,0462	0,2095
8	1,8739	0,0519	0,2043
9	1,9093	0,0587	0,1981
10	1,9268	0,0669	0,1906
11	1,9222	0,0773	0,1823
12	1,8866	0,0909	0,1738
13	1,8071	0,1096	0,1663

4.9. APPENDIX I

Results of the analysis of Rhodes St. 32 Airfoil with 30 degrees of flap deflections at 0 ft.

AOA	Cl	Cd	Cm
0	1,7004	0,0437	0,1913
1	1,8178	0,0451	0,1889
2	1,9426	0,0471	0,1864
3	2,0779	0,0502	0,1840
4	2,1539	0,0547	0,1811
5	2,1911	0,0603	0,1778
6	2,2150	0,0670	0,1744
7	2,2194	0,0743	0,1701
8	2,2218	0,0843	0,1654
9	2,2228	0,0985	0,1605
10	2,1639	0,1091	0,1558
11	2,0903	0,1273	0,1518

4.10. APPENDIX J

Results of the analysis of SD7062 airfoil with sharp TE using SU2. Mach = 0.129, Re=2.9M

alpha	CD	CM	CL/CD	CL
-6.00	0.0137	-0.0809	-16.6105	-0.2280
-3.00	0.0107	-0.0823	9.6453	0.1031
0.00	0.0107	-0.0834	40.8064	0.4385

This document is the property of TAI, no part of it shall be reproduced or transmitted without written authorization of TAI, and its contents shall not be disclosed. All rights reserved. A hard copy of this technical document may not be the current issue. Check always with EDMS.

UNCLASSIFIED

DOCUMENT NO:[XXXXXXXXXX](#)

Issue No: [1](#)

3.00	0.0129	-0.0839	59.5002	0.7688
6.00	0.0171	-0.0829	63.2064	1.0826
7.50	0.0201	-0.0814	61.1785	1.2284
9.00	0.0237	-0.0790	57.4878	1.3634
10.50	0.0282	-0.0757	52.7020	1.4841
12.00	0.0357	-0.0700	43.6112	1.5556
13.50	0.0438	-0.0662	36.9923	1.6217
15.00	0.0589	-0.0713	28.6811	1.4669

4.11. APPENDIX K

Results of the analysis of SD7062 airfoil with blunt TE using SU2. Mach = 0.129, Re=2.9M

alpha	C _I	C _d	C _I /C _d	C _m
-6	-0.23794	0.014517	-17.6033	-0.07797
-5	-0.16371	0.013974	-11.7154	-0.07185
-4	-0.05597	0.012911	-4.33525	-0.07166
-3	0.052823	0.012226	4.320409	-0.07147
-2	0.162214	0.011875	13.65995	-0.07128
-1	0.271868	0.011805	23.02997	-0.07111
0	0.381391	0.011964	31.87854	-0.07094
1	0.490326	0.012263	39.98302	-0.07064
2	0.599274	0.012917	46.39584	-0.0705
3	0.706741	0.013669	51.70424	-0.07017
4	0.832624	0.013415	62.06492	-0.07413
5	0.936096	0.014614	64.05592	-0.07331
6	1.030699	0.016255	63.4089	-0.07157
7	1.129136	0.017745	63.63063	-0.07023
8	1.244349	0.019633	63.38207	-0.07181
9	1.310971	0.021538	60.8689	-0.06625
10	1.384207	0.024329	56.89566	-0.06273
11	1.449491	0.027576	52.56338	-0.05898
12	1.505668	0.031408	47.9396	-0.05521
13	1.619707	0.035348	46.50369	-0.05856
14	1.653319	0.041733	36.25619	-0.0558
15	1.642769	0.051588	31.84432	-0.05276
16	1.497497	0.064201	23.32497	-0.04401

This document is the property of TAI, no part of it shall be reproduced or transmitted without written authorization of TAI, and its contents shall not be disclosed.
All rights reserved. A hard copy of this technical document may not be the current issue. Check always with EDMS.

UNCLASSIFIED

UNCLASSIFIED

DOCUMENT NO:~~XXXXXXXXXX~~

Issue No: 1

This document is the property of TAI, no part of it shall be reproduced or transmitted without written authorization of TAI, and its contents shall not be disclosed.
All rights reserved. A hard copy of this technical document may not be the current issue. Check always with EDMS.

40 | P a g e

UNCLASSIFIED

4.12. APPENDIX L

Results of the analysis of SD7062 airfoil with sharp TE using XFOIL 6.99.

alpha	C _L	C _D	C _{Dp}	CM	Top_Xtr	Bot_Xtr
-1	0.3605	0.00687	0.00112	-0.0872	0.4749	0.0209
0	0.4764	0.00685	0.0011	-0.0873	0.432	0.0495
1	0.5912	0.00668	0.00115	-0.0874	0.3882	0.1904
2	0.7051	0.00623	0.00136	-0.0878	0.36	0.4908
3	0.8189	0.00613	0.00171	-0.0878	0.3293	0.7086
4	0.9306	0.00639	0.00209	-0.0874	0.2947	0.8321
5	1.0399	0.00677	0.00255	-0.0864	0.2548	1
6	1.1512	0.00738	0.00305	-0.0862	0.2357	1
7	1.2601	0.0081	0.00363	-0.0856	0.2065	1
8	1.3586	0.00949	0.00463	-0.0836	0.1522	1
9	1.4664	0.01005	0.0053	-0.0829	0.153	1
10	1.5653	0.01104	0.00625	-0.0809	0.1353	1
11	1.6527	0.01244	0.00753	-0.0773	0.1104	1
12	1.716	0.01421	0.00919	-0.0697	0.089	1
13	1.7567	0.01709	0.01198	-0.0604	0.0645	1
14	1.7974	0.02069	0.01563	-0.0535	0.0546	1
15	1.8227	0.02623	0.02123	-0.0476	0.0415	1
16	1.8251	0.03468	0.02979	-0.0432	0.0337	1
17	1.8289	0.04455	0.03982	-0.0415	0.0256	1
18	1.8192	0.05693	0.05253	-0.0424	0.025	1
19	1.7909	0.07281	0.06867	-0.0456	0.022	1

Mach = 0.129 , Re = 2.900E6 Ncrit = 9.000

4.13. APPENDIX M

Results of the analysis of SD7062 airfoil with sharp TE using Fluent, Mach = 0.129, Re=2.9M.

alpha	CL	CD	CM
-6	-0,24059	0,01039	-0,08135
-5	-0,12737	0,00987	-0,08156
-4	-0,01363	0,00948	-0,08176
-3	0,10004	0,0093	-0,08193
-2	0,21408	0,00924	-0,08213
-1	0,32778	0,0093	-0,08228
0	0,44075	0,00946	-0,08232
1	0,55233	0,00978	-0,08233
2	0,66308	0,01022	-0,08228
3	0,77265	0,01081	-0,08217
4	0,88069	0,01152	-0,08192
5	0,98568	0,01238	-0,08139
6	108,687	0,01346	-0,08052
7	118,472	0,01471	-0,07943
8	127,694	0,01631	-0,07796
9	136,414	0,01827	-0,07627
10	144,548	0,02069	-0,07447
11	151,656	0,02392	-0,07246
12	157,251	0,02828	-0,0702
13	160,764	0,03453	-0,06811
14	161,991	0,04324	-0,06662
15	160,118	0,05512	-0,06576
16	154,906	0,0718	-0,06731
17	146,747	0,09437	-0,07234

UNCLASSIFIEDDOCUMENT NO:~~XXXXXXXXXX~~Issue No: [1](#)**4.14. APPENDIX N****DATCOM Outputs**

Characteristics at Angle of Attack and in Side Slip												
ALPHA	CD	CL	CM	CN	CA	XCP	CLA	CMA	CYB	CNB	CLB	L/D
-8,0	0,028	-0,199	0,2098	-0,201	0,000	-1,046	9,424E-02	-4,112E-02	-8,640E-03	7,885E-04	-1,030E-03	-7,107
-6,0	0,025	-0,006	0,1339	-0,008	0,024	*****	9,838E-02	-3,892E-02			-1,005E-03	-0,240
-4,0	0,026	0,195	0,0541	0,193	0,040	0,281	1,026E-01	-4,038E-02			-9,817E-04	7,500
-2,0	0,031	0,405	-0,0276	0,403	0,045	-0,069	1,065E-01	-4,114E-02			-9,587E-04	13,065
-1,0	0,036	0,512	-0,0689	0,511	0,045	-0,135	1,083E-01	-4,126E-02			-9,472E-04	14,222
0,0	0,041	0,621	-0,1102	0,621	0,041	-0,177	1,099E-01	-4,126E-02			-9,358E-04	15,146
1,0	0,048	0,732	-0,1514	0,733	0,035	-0,207	1,111E-01	-4,128E-02			-9,243E-04	15,250
2,0	0,056	0,843	-0,1927	0,845	0,027	-0,228	1,121E-01	-4,128E-02			-9,129E-04	15,054
3,0	0,066	0,956	-0,2340	0,958	0,015	-0,244	1,132E-01	-4,139E-02			-9,014E-04	14,485
4,0	0,076	1,070	-0,2755	1,073	0,001	-0,257	1,144E-01	-4,170E-02			-8,899E-04	14,079
6,0	0,102	1,301	-0,3596	1,304	-0,035	-0,276	1,087E-01	-3,999E-02			-8,667E-04	12,755
8,0	0,127	1,505	-0,4355	1,508	-0,083	-0,289	9,357E-02	-3,622E-02			-8,414E-04	11,850
10,0	0,152	1,675	-0,5045	1,676	-0,141	-0,301	7,888E-02	-3,291E-02			-8,122E-04	11,020
11,0	0,165	1,751	-0,5366	1,750	-0,173	-0,307	7,061E-02	-3,127E-02			-7,959E-04	10,612
12,0	0,176	1,816	-0,5671	1,813	-0,205	-0,313	6,107E-02	-2,954E-02			-7,783E-04	10,318
13,0	0,187	1,873	-0,5957	1,867	-0,239	-0,319	5,163E-02	-2,751E-02			-7,593E-04	10,016
14,0	0,197	1,920	-0,6221	1,910	-0,273	-0,326	3,684E-02	-2,526E-02			-7,390E-04	9,746
15,0	0,203	1,947	NA	1,933	-0,308	NA	-6,073E-03	NA			-7,165E-04	9,591
16,0	0,195	1,908	NA	1,887	-0,338	NA	-1,039E-01	NA			-6,890E-04	9,785
18,0	0,140	1,440	NA	1,413	-0,312	NA	-3,631E-01	NA			-6,119E-04	10,286

Dynamic Derivatives									
ALPHA	CLQ	CMQ	CLAD	CMAD	CLP	CYP	CNP	CNR	CLR
-8,0	1,397E-01	-1,923E-01	1,894E-02	-6,179E-02	-8,099E-03	-2,462E-03	2,132E-04	-1,246E-03	2,932E-04
-6,0			1,894E-02	-6,179E-02	-8,508E-03	-2,607E-03	1,241E-05	-1,275E-03	8,110E-04
-4,0			1,894E-02	-6,179E-02	-8,901E-03	-2,761E-03	-1,903E-04	-1,301E-03	1,356E-03
-2,0			1,894E-02	-6,179E-02	-9,245E-03	-2,922E-03	-3,941E-04	-1,324E-03	1,924E-03
-1,0			1,894E-02	-6,179E-02	-9,390E-03	-3,004E-03	-4,966E-04	-1,334E-03	2,216E-03
0,0			1,894E-02	-6,179E-02	-9,513E-03	-3,089E-03	-5,998E-04	-1,344E-03	2,513E-03
1,0			1,894E-02	-6,179E-02	-9,617E-03	-3,174E-03	-7,042E-04	-1,353E-03	2,812E-03
2,0			1,894E-02	-6,179E-02	-9,702E-03	-3,261E-03	-8,099E-04	-1,360E-03	3,115E-03
3,0			1,894E-02	-6,179E-02	-9,767E-03	-3,349E-03	-9,173E-04	-1,367E-03	3,419E-03
4,0			1,894E-02	-6,179E-02	-9,808E-03	-3,439E-03	-1,027E-03	-1,373E-03	3,725E-03
6,0			1,894E-02	-6,179E-02	-8,896E-03	-3,649E-03	-1,343E-03	-1,383E-03	4,339E-03
8,0			1,894E-02	-6,179E-02	-7,146E-03	-3,841E-03	-1,719E-03	-1,389E-03	4,823E-03
10,0			1,894E-02	-6,179E-02	-5,558E-03	-3,998E-03	-2,067E-03	-1,392E-03	5,196E-03
11,0			1,894E-02	-6,179E-02	-4,735E-03	-4,065E-03	-2,235E-03	-1,393E-03	5,342E-03
12,0			1,894E-02	-6,179E-02	-3,832E-03	-4,128E-03	-2,402E-03	-1,392E-03	5,459E-03
13,0			1,894E-02	-6,179E-02	-2,864E-03	-4,184E-03	-2,561E-03	-1,392E-03	5,544E-03
14,0			1,894E-02	-6,179E-02	-1,047E-03	-4,286E-03	-2,772E-03	-1,390E-03	5,594E-03
15,0			1,894E-02	-6,179E-02	4,970E-03	-5,072E-03	-2,968E-03	-1,388E-03	5,556E-03
16,0			1,894E-02	-6,179E-02	1,574E-02	-2,555E-03	-5,165E-03	-1,386E-03	5,199E-03
18,0			1,892E-02	-6,170E-02	4,004E-02	-2,480E-03	-6,629E-03	-1,383E-03	3,254E-03

This document is the property of TAI, no part of it shall be reproduced or transmitted without written authorization of TAI, and its contents shall not be disclosed. All rights reserved. A hard copy of this technical document may not be the current issue. Check always with EDMS.

5. APPENDIX (LOADS)

5.1. APPENDIX A– HORIZONTAL TAIL SHEAR AND MOMENT DIAGRAMS FOR EACH CRITICAL CASE

Figures 18-43 show distribution of shear forces and moments along half span of the horizontal tail for each critical case, respectively.

Açıklamalı [k5]: Figure number control edilsin Figure 18 den başlış

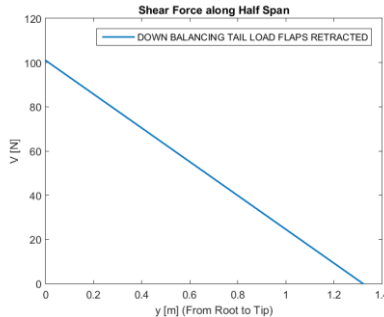
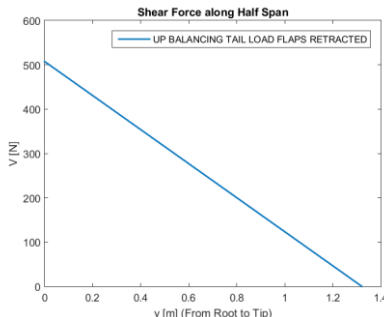


Figure 18. V-y for UP BALANCING TAIL LOAD FLAPS RETRACTED Figure 19. V-y for DOWN BALANCING TAIL LOAD FLAPS RETRACTED

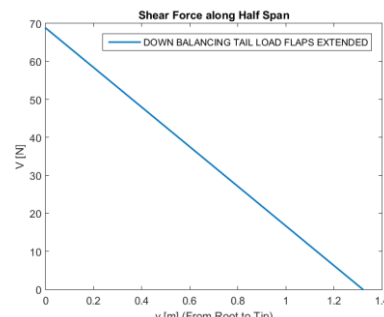
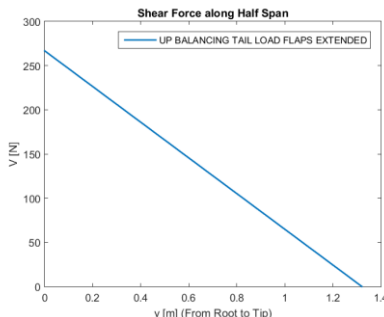


Figure 20. V-y for UP BALANCING TAIL LOAD FLAPS EXTENDED

Figure 21. V-y for DOWN BALANCING TAIL LOAD FLAPS EXTENDED

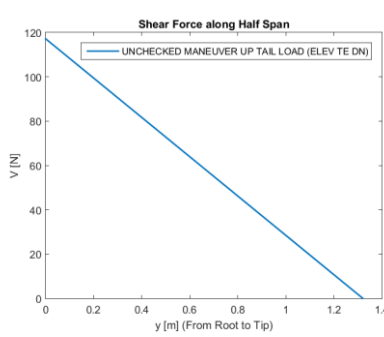
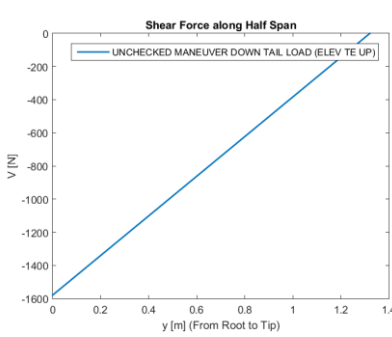


Figure 22. V-y for UNCHECKED MANEUVER DOWN TAIL LOAD (ELEV TE UP)

Figure 23. V-y for UNCHECKED MANEUVER UP TAIL LOAD (ELEV TE DN)

UNCLASSIFIED

DOCUMENT NO:XXXXXX

Issue No: 1

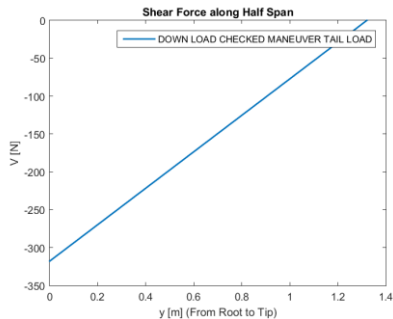


Figure 24. V-y for DOWN LOAD CHECKED MANEUVER TAIL LOAD

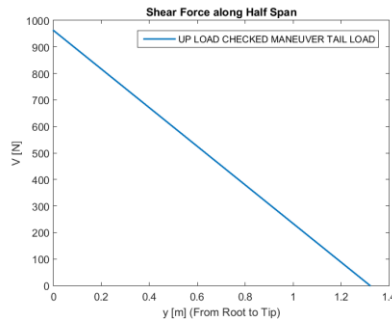


Figure 25. V-y for UP LOAD CHECKED MANEUVER TAIL LOAD

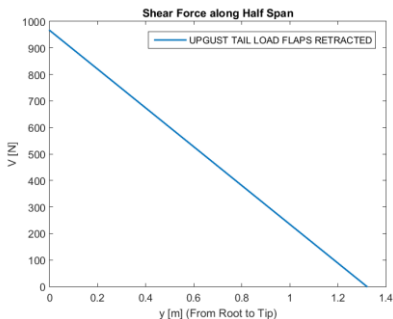


Figure 26. V-y for UPGUST TAIL LOAD FLAPS RETRACTED

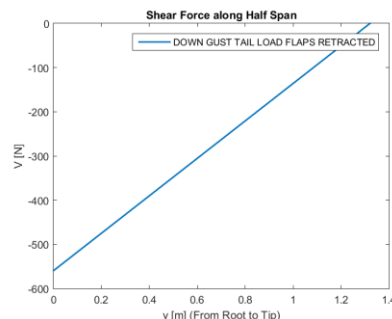


Figure 27. V-y for DOWN GUST TAIL LOAD FLAPS RETRACTED

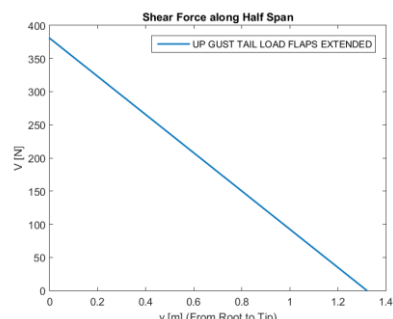


Figure 28. V-y for UP GUST TAIL LOAD FLAPS EXTENDED

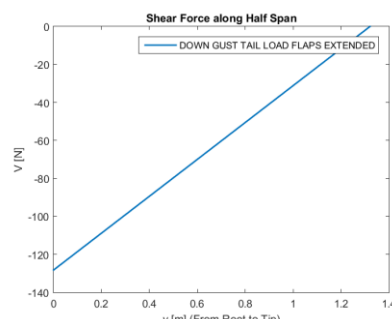


Figure 29. V-y for DOWN GUST TAIL LOAD FLAPS EXTENDED

This document is the property of TAI, no part of it shall be reproduced or transmitted without written authorization of TAI, and its contents shall not be disclosed. All rights reserved. A hard copy of this technical document may not be the current issue. Check always with EDMS.

UNCLASSIFIED

UNCLASSIFIED

DOCUMENT NO:XXXXXX

Issue No: 1

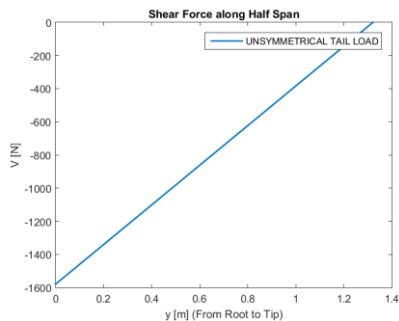


Figure 30. V - y for UNSYMMETRICAL TAIL LOAD

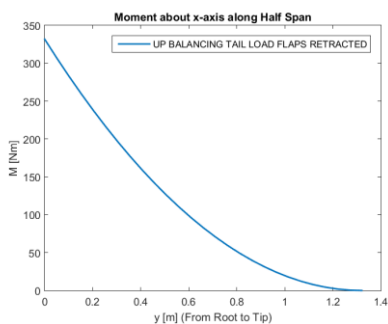


Figure 31. M - y for UP BALANCING TAIL LOAD
FLAPS RETRACTED

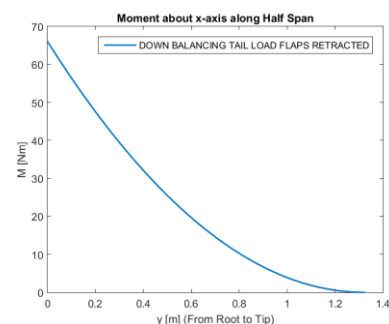


Figure 32. M - y for DOWN BALANCING TAIL LOAD
FLAPS RETRACTED

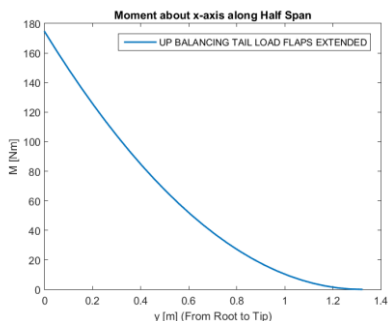


Figure 33. M - y for UP BALANCING TAIL LOAD
FLAPS EXTENDED

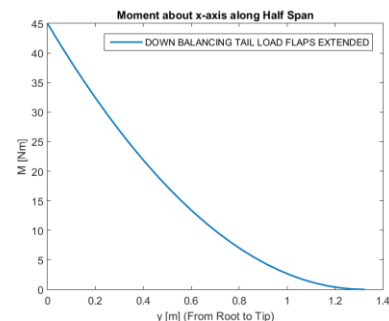


Figure 34. M - y for DOWN BALANCING TAIL LOAD
FLAPS EXTENDED

This document is the property of TAI, no part of it shall be reproduced or transmitted without written authorization of TAI, and its contents shall not be disclosed. All rights reserved. A hard copy of this technical document may not be the current issue. Check always with EDMS.

UNCLASSIFIED

UNCLASSIFIED

DOCUMENT NO:[XXXXXXXXXX](#)

Issue No: 1

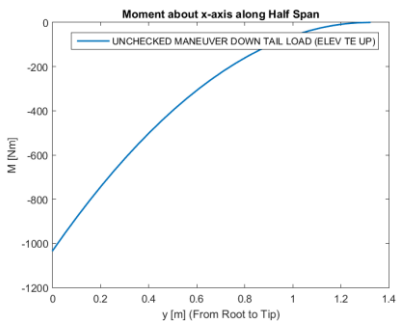


Figure 35. $M-y$ for UNCHECKED MANEUVER DOWN TAIL LOAD (ELEV TE UP)

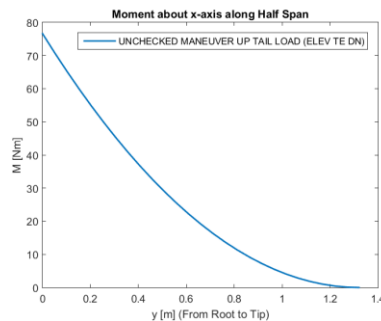


Figure 36. $M-y$ for UNCHECKED MANEUVER UP TAIL LOAD (ELEV TE DN)

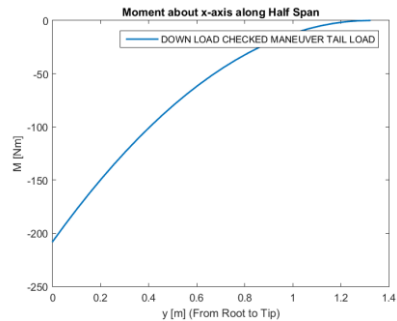


Figure 37. $M-y$ for DOWN LOAD CHECKED MANEUVER TAIL LOAD

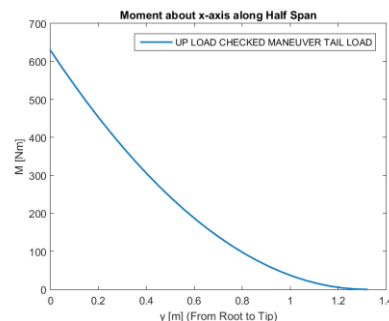


Figure 38. $M-y$ for UP LOAD CHECKED MANEUVER TAIL LOAD

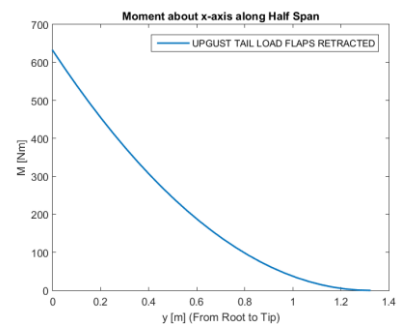


Figure 39. $M-y$ for UPGUST TAIL LOAD FLAPS RETRACTED

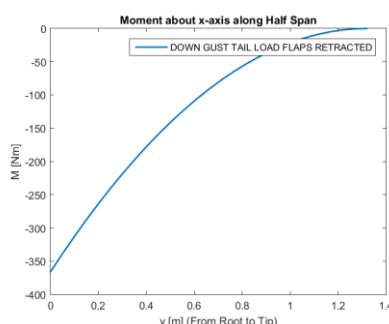


Figure 40. $M-y$ for DOWN GUST TAIL LOAD FLAPS RETRACTED

This document is the property of TAI, no part of it shall be reproduced or transmitted without written authorization of TAI, and its contents shall not be disclosed. All rights reserved. A hard copy of this technical document may not be the current issue. Check always with EDMS.

U N C L A S S I F I E D

UNCLASSIFIED

DOCUMENT NO:[XXXXXXXXXX](#)

Issue No: [1](#)

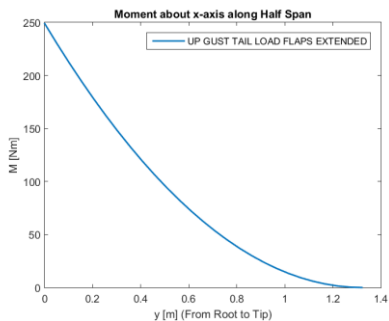


Figure 41. M-y for UP GUST TAIL LOAD FLAPS EXTENDED

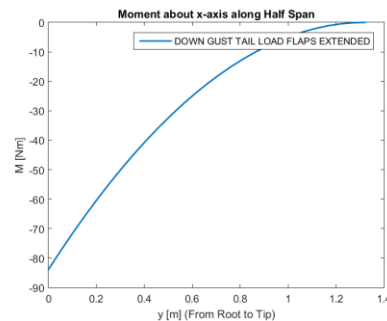


Figure 42. M-y for DOWN GUST TAIL LOAD FLAPS EXTENDED

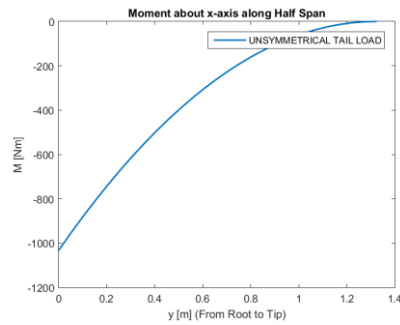


Figure 43. M-y for UNSYMMETRICAL TAIL LOAD

5.2. APPENDIX B – VERTICAL TAIL SHEAR AND MOMENT DIAGRAMS FOR EACH CRITICAL CASE

MANEUVER LOAD FOR SUDDEN FULL RUDDER DEFLECTION

Figures 44-45 show the shear force and moment distribution along the vertical tail span, respectively.

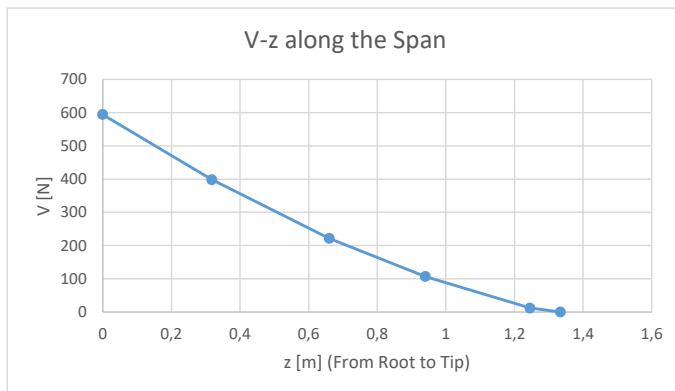


Figure 44. V - z for MANEUVER LOAD FOR SUDDEN FULL RUDDER DEFLECTION

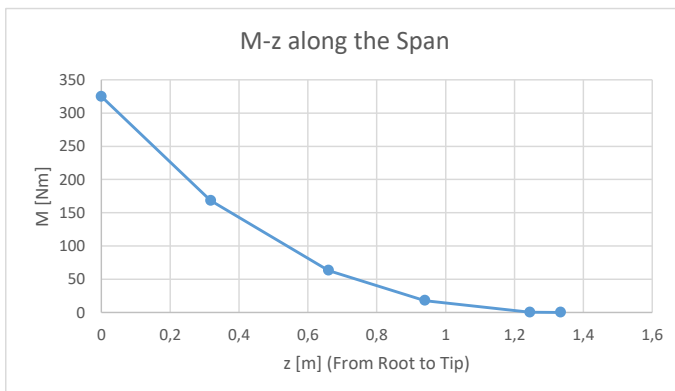


Figure 45. M - z for MANEUVER LOAD FOR SUDDEN FULL RUDDER DEFLECTION

MANEUVER LOAD FOR YAW TO SIDESLIP OF 22.5 DEG WITH RUDDER MAINTAINED AT FULL DEFLECTION

Figures 46-47 show the shear force and moment distribution along the vertical tail span, respectively.

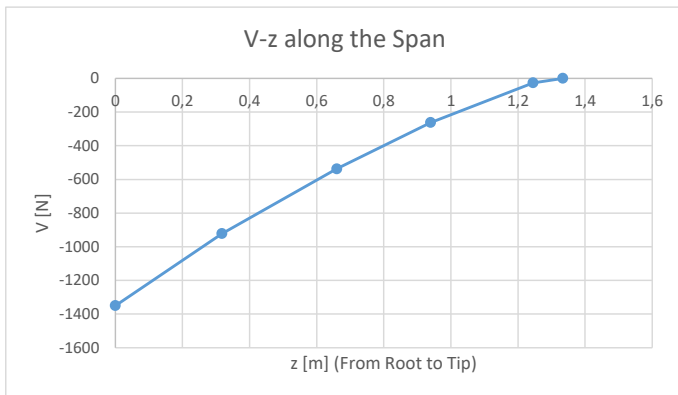


Figure 46. V-z for MANEUVER LOAD FOR YAW TO SIDESLIP OF 22.5 DEG WITH RUDDER MAINTAINED AT FULL DEFLECTION

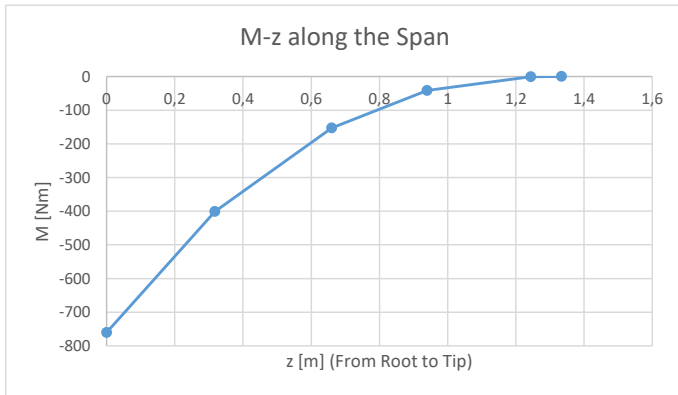


Figure 47. M-z for MANEUVER LOAD FOR YAW TO SIDESLIP OF 22.5 DEG WITH RUDDER MAINTAINED AT FULL DEFLECTION

MANEUVER LOAD FOR YAW OF 15 DEG WITH RUDDER IN NEUTRAL

Figures 48-49 show the shear force and moment distribution along the vertical tail span, respectively.

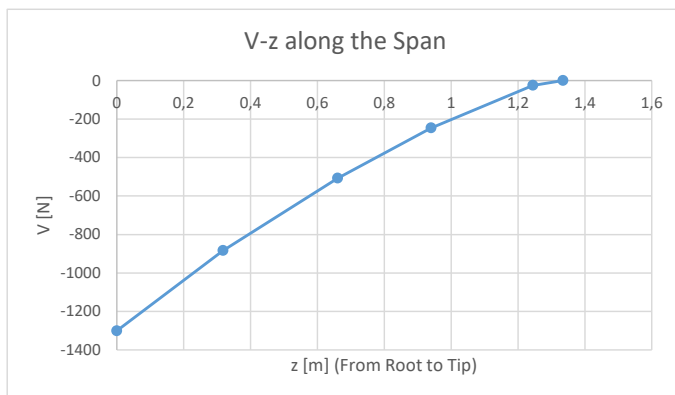


Figure 48. V-z for MANEUVER LOAD FOR YAW OF 15 DEG WITH RUDDER IN NEUTRAL

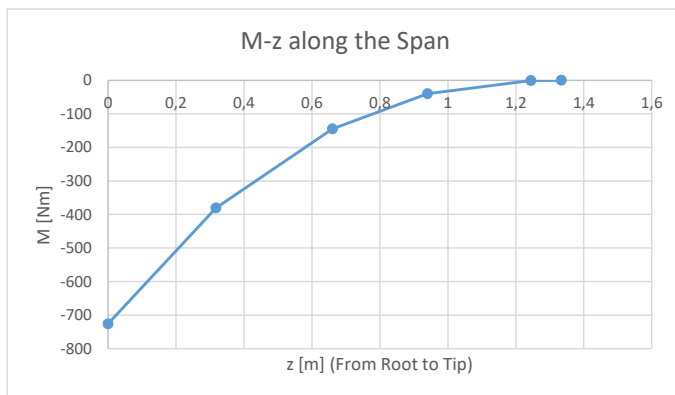


Figure 49. M-z for MANEUVER LOAD FOR YAW OF 15 DEG WITH RUDDER IN NEUTRAL

SIDE GUST LOAD AT VC

Figures 50-51 show the shear force and moment distribution along the vertical tail span, respectively.

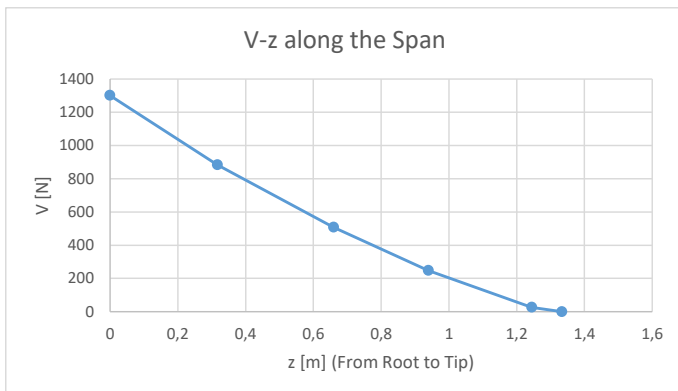


Figure 50. V-z for SIDE GUST LOAD AT VC

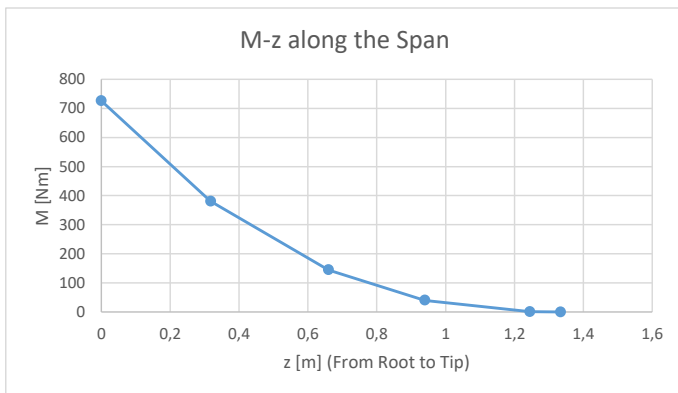


Figure 51. M-z for SIDE GUST LOAD AT VC